



The University of
Nottingham



Nottingham Centre
for Geomechanics

Numerical Modelling of Shaft Lining Stability

Prepared by

Yudan Jia

BEng in Civil Engineering

MSc in Structural Engineering

Thesis submitted to The University of Nottingham

for the degree of Doctor of Philosophy

October 2010

This thesis is dedicated
to my parents, sisters, brother, my husband and our baby.

ABSTRACT

This research project focuses on the application of numerical modelling methods to rock mechanics problems, combining theoretical, experimental and numerical modelling work. Specifically, practical finite difference modelling approach for analysing shaft lining stability through the Marl and Potash strata at Boulby mine UK has been developed using the commercially available software FLAC^{2D}/FLAC^{3D} (ITASCA, 2008).

A soft rock Marl occurs close to the bottom of the two deep shafts at the mine. Both shafts concrete linings through this stratum have suffered considerable pressure, which has caused gradual failure of the shaft lining. So far, both shaft linings through the Marl stratum have been restored twice after sunk in 1970s and a further third relining is now required and being planned. The in situ observations, the rock engineers' experience, and the available in situ measurements at the mine have been significantly helpful in the validation of the numerical modelling. Many factors at the mine site have, however, made this numerical modelling research challenging, including complicated lining structures, complex lining failure conditions and the scarcity of laboratory test data for the weakest rock material - the Marl, which easily weathers on exposure.

Based on a comprehensive literature review, a database of materials properties relevant to this research has been produced. The methodology of obtaining appropriate rock mass input material properties to use in numerical modelling based on laboratory test data has been studied. In three-dimensional models in this research, two modelling methods have been developed to simulate each stage in the shaft linings: the continuous model for all shaft linings and independent models for each shaft lining. The numerical modelling results imply that:

Firstly, in the independent three-dimensional models, the modelling results were difficult to understand due to the complexity of the structures

representing the shaft relining systems and difficulty in defining appropriate properties for the interface elements. Therefore, the continuous three-dimensional model that gives the analysable modelling results is recommended by the author for this research. By this method, the effect of the historic changes in the stress field on each shaft lining's stability can be investigated from initial shaft construction to subsequent relining phases.

Secondly, the weak rock Marl should not be the only reason for the shaft linings' failure through this stratum. The roadway approximately 10 m beneath the Marl stratum was also a key factor for the stability of the shaft linings. The weak Marl cannot carry the stress redistribution around the shaft caused by the roadway excavation, which was an uneven loading acting on the circular shaft linings. This uneven loading introduced high shear and tensile stresses which threatened the stability of the circular concrete structures.

Thirdly, the interface materials between high strength concrete blocks in shaft relinings improved the flexibility of the lining systems successfully, but decreased the strength of the whole lining systems as weak "joints". In addition, the single ring concrete blocks (the first and third relinings) are a more effective lining than the double rings (the second relining), and the third relining would perform better than the previous ones.

As a recommendation for the further simulation, it is worth attempting to simulate the longer term deformation and stress conditions of the shaft concrete lining systems using the Creep model built in FLAC^{2D}/FLAC^{3D} codes. Additionally, deeper research work combined with in situ investigation can be done to decrease the uncertainty of the input material properties to make the numerical models as close to the real engineering situation as possible.

ACKNOWLEDGEMENTS

First of all I would like to express my sincere thanks and gratitude to my supervisors Dr. David Reddish and Dr. Rod Stace for their academic guidance, encouragement and financial support throughout the PhD course.

I would also like to thank Prof. Hai-Sui Yu and Prof. Yang Ju for their supervisions, help and encouragement during this research.

Acknowledgements are also given to Mr. Allan Williams and Mr. Mike Keen, the rock engineers of Boulby mine, Cleveland Potash Ltd for their support during the progress of the research project.

Thanks must go to Dr. Philip Rowsell, Mr. Mark Dale and Mr. Craig Cox for their generous help and collaboration during the laboratory tests for this research.

I am thankful to all friends at the Nottingham Centre for Geomechanics with whom I have had a wonderful time throughout three years' PhD study.

Sincerely thanks must go to my parents, my husband Yate, my sisters and brother without whose support and encouragement I would not have been what I am now; especially to my husband Yate, who I believe is a great husband and will be a great father.

The research work outlined in this thesis was largely funded by Cleveland Potash Ltd. Part-funding was also gratefully received from the National Basic Research Project of China (Grant No. 2010CB226804, 2002CB412705), the New Century Excellent Talents Program of the Ministry of Education of China (Grant No. NCET-05-0215) and Beijing Key Laboratory Research Project (Grant No. JD102900671), who have provided financial support with part of the tuition fees.

Finally, I would like to thank the Institute of Materials, Minerals and Mining (IOM³) and South Midlands Mining and Minerals Institute (SMMMI) for the awards that provided part of my research and living expenses.

LIST OF CONTENTS

Abstract.....	i
Acknowledgements.....	iii
List of Contents.....	iv
List of Figures.....	viii
List of Tables.....	xiv
Notation.....	xvi

CHAPTER 1 INTRODUCTION

1.1 Introduction.....	1
1.2 Problem Definition.....	2
1.3 Aims and Objectives.....	6
1.4 Technical Challenges.....	7
1.5 Research Outline.....	9

CHAPTER 2 GENERAL LITERATURE REVIEW

2.1 In Situ State of Ground Stress.....	12
2.2 Stress Distribution around Excavations.....	20
2.3 Rock Mass Classification Systems.....	23
2.3.1 Introduction.....	23
2.3.2 Rock Quality Designation (RQD).....	25
2.3.3 Rock Mass Rating (RMR) System.....	26
2.3.4 Coal Mine Classification Rating (CMCR).....	29
2.3.5 Rock Tunnelling Quality Index, Q.....	32
2.3.6 Conclusions.....	37
2.4 Shaft Stability Problems.....	38
2.5 Previous Rock Mechanics Research at Boulby Mine.....	42
2.6 History of Shafts at Boulby Mine.....	48
2.6.1 The Design for the Original Lining of the Shafts.....	48
2.6.2 The Design for the First Relining of the Shafts.....	51
2.6.3 The Design for the Second Relining of the Shafts.....	54
2.6.4 The Design for the Third Relining of the Shafts.....	58
2.6.5 Conclusions and Assumptions.....	60
2.7 In Situ Stress Measurements at Boulby Mine.....	65

2.8	In Situ Deformation Measurements at Boulby Mine.....	67
2.9	Chapter Summary.....	69

CHAPTER 3 LABORATORY DETERMINATION OF GEOTECHNICAL PARAMETERS

3.1	Determination of Rock Mass Strength.....	70
3.1.1	Introduction.....	70
3.1.2	Geological Strength Index (GSI).....	71
3.1.3	Hoek-Brown Failure Criterion.....	75
3.1.4	RocLab Software.....	76
3.2	Rock Materials from Boulby Mine.....	82
3.2.1	Laboratory Tests Data Collection.....	82
3.2.2	Materials Properties Used in Modelling.....	85
3.3	Laboratory Tests for Concretes used at Boulby Mine.....	85
3.3.1	Introduction.....	85
3.3.2	Laboratory Tests Results and Analysis.....	88
3.3.3	Material Properties Used in Modelling.....	90
3.4	Interface Problems in the Shaft Lining Modelling.....	93
3.4.1	Introduction.....	93
3.4.2	Interfaces between Epoxy Resin and Concrete.....	96
3.4.3	Interfaces between Cement Mortar and Concrete.....	98
3.4.4	Interfaces between Plywood Pack and Concrete.....	100
3.5	Other Parameters used in the Shaft Lining Modelling.....	107
3.5.1	Material Properties of Polyurethane and Vermiculite.....	107
3.5.2	Material Properties of Cement Grout.....	108
3.6	Chapter Summary.....	109

CHAPTER 4 INTRODUCTION OF FLAC^{2D}/FLAC^{3D}

4.1	Introduction.....	110
4.2	Fields of Application.....	110
4.3	Fundamental Components of a Problem.....	112
4.3.1	Finite Difference Grid.....	113
4.3.2	Boundary Conditions.....	117
4.3.3	Initial Stress Conditions.....	119
4.3.4	Constitutive Models.....	119

4.3.5	Material Properties.....	122
4.4	Chapter Summary.....	123

CHAPTER 5 TWO-DIMENSIONAL NUMERICAL

MODELLING OF SHAFTS' LINING SYSTEMS

5.1	Introduction.....	124
5.2	Parametric Study.....	126
5.2.1	Geometry of the Model and Mesh Definition.....	126
5.2.2	Boundary and Initial Stress Conditions.....	128
5.2.3	Material Properties.....	131
5.2.4	Stress Relaxation and Modelling Sequence.....	135
5.3	Modelling Results of the Parametric Study.....	138
5.3.1	The Effect of the Properties of the Marl.....	139
5.3.2	The Effect of the Extent of the Weathered Marl.....	142
5.3.3	The Effect of the Ground Stress Field.....	143
5.4	The Possible "Point" Loading on the Original Lining.....	145
5.4.1	Model Configurations.....	146
5.4.2	Modelling Results and Discussion.....	147
5.5	Modelling for the Shaft Original Lining and Relinings.....	149
5.5.1	Model Configurations.....	149
5.5.2	Interfaces between Concrete Blocks.....	151
5.5.3	Modelling Results and Discussion.....	152
5.6	Conclusions.....	159

CHAPTER 6 THREE-DIMENSIONAL NUMERICAL

MODELLING OF SHAFTS' LINING SYSTEMS

6.1	Introduction.....	162
6.2	Modelling Methodology - A Continuous Model for the Original Lining and All Relining Systems.....	163
6.3	Modelling Methodology - Independent Models for the Original Lining and All Relining Systems.....	168
6.4	Modelling Methodology - Excavation and Relining Sequences.....	171
6.5	Model Configurations.....	174
6.5.1	Domain and Mesh Design.....	174
6.5.2	Dimensions Used in the Models.....	176

6.5.3	Support for the Roadway.....	177
6.5.4	Detailed Engineering Design Modelling.....	178
6.6	Boundary and Initial Stress Conditions.....	183
6.7	Material Properties.....	185
6.7.1	Surrounding Rock.....	185
6.7.2	Concrete and Cement Grout.....	189
6.7.3	Interfaces.....	189
6.7.4	Polyurethane and Vermiculite.....	190
6.8	Modelling Results.....	191
6.8.1	Results of the Continuous Model.....	192
6.8.2	Results of the Independent Models.....	214
6.9	Conclusions.....	225

CHAPTER 7 CONCLUSIONS AND RECOMMENDATIONS

7.1	Conclusions.....	230
7.2	Recommendations.....	236

REFERENCES	238
-------------------------	------------

APPENDIX

I	Summary of Boulby Mine Rock Materials Laboratory Tests Data
II	Mohr-Coulomb/Hoek-Brown Properties of Rock Materials at Boulby Mine
III	Laboratory Tests Data of the Concrete Segmental Linings from Boulby Mine

LIST OF FIGURES

Figure 1.1	Location of Boulby mine.....	3
Figure 1.2	Stratigraphic section.....	5
Figure 2.1	Results of stress measurements: vertical stress (1973)....	14
Figure 2.2	Results of stress measurements: average horizontal stress.....	15
Figure 2.3	Results of stress measurements: vertical stress (1978)....	17
Figure 2.4	Variation of ratio of average horizontal stresses to vertical stress.....	18
Figure 2.5	Equations for the stresses in the material surrounding a circular hole in a stressed elastic body.....	21
Figure 2.6	Variation in ratio of tangential stress σ_{θ} to vertical applied stress σ_z with radial distance r along horizontal axis for $k_0=0$	22
Figure 2.7	Estimated support categories based on the Tunnelling Quality Index Q	37
Figure 2.8	Strata sequence of Boulby potash mine.....	43
Figure 2.9	Detailed geology of the Permian strata at Boulby mine....	44
Figure 2.10	Indicative longitudinal section through original rock-shaft lining.....	49
Figure 2.11	First relining for the man shaft, section.....	52
Figure 2.12	First relining, plan.....	53
Figure 2.13	Damaged manshaft before the second relining.....	54
Figure 2.14	Second relining, plan.....	55
Figure 2.15	Second relining, section.....	56
Figure 2.16	Damaged manshaft before the third relining.....	59
Figure 2.17	Third relining, plan.....	60
Figure 2.18	Plastic zone becoming bigger with relining.....	61
Figure 2.19	Conceptual relationship between strength of lining required and practical concrete lining.....	64
Figure 2.20	Recorded stress in row 7 in the second relining.....	67

Figure 2.21	Instrumentation layouts at man shaft through Upper Halite stratum.....	68
Figure 3.1	RocLab software user interface.....	77
Figure 3.2	Mohr-Coulomb strength envelopes for the Marl obtained from tests data.....	84
Figure 3.3	Samples of concrete from Boulby mine.....	86
Figure 3.4	Test set up for UCS and Young's modulus.....	87
Figure 3.5	Test set up for triaxial compressive tests.....	87
Figure 3.6	Zone dimension used in stiffness calculation.....	95
Figure 3.7	Diagram of direct shear test.....	101
Figure 3.8	Marine plywood and concrete samples used in direct shear test.....	102
Figure 3.9	$\sigma - \tau$ curves obtained from the direct shear tests: shear force perpendicular to the texture of the plywood surface.....	103
Figure 3.10	$\sigma - \tau$ curves obtained from the direct shear tests: shear force parallel to the texture of the plywood surface.....	103
Figure 3.11	Stress-strain curve for the plywood pack used in relining systems.....	105
Figure 4.1	General solution procedure.....	113
Figure 4.2	Gradually changed mesh: fine mesh in the vicinity of excavation (inside red dashed line), coarse mesh in other parts of the model.....	114
Figure 4.3	Sudden changes in neighbour zone size.....	115
Figure 4.4	Geometry for an example water tunnel.....	116
Figure 4.5	Example of boundary conditions.....	118
Figure 4.6	Determination of material properties for Mohr-Coulomb model.....	123
Figure 5.1	Deformed shape of 25 mm diameter rockbolt following rupture at end of shear test.....	125
Figure 5.2	A horizontal slice in Marl in the two-dimensional model (not to scale).....	127

Figure 5.3	Finite difference grid used in the two-dimensional models.....	128
Figure 5.4	Boundary and initial stress conditions of the two-dimensional numerical model.....	130
Figure 5.5	Conceptual plastic zone around the shaft.....	133
Figure 5.6	Weathered Marl simulated in the two-dimensional models.....	133
Figure 5.7	Mohr-Coulomb strength envelopes for the Marl.....	135
Figure 5.8	Radial convergence and tangential stress in vicinity of tunnel face.....	137
Figure 5.9	Modelling sequence flow chart in the two-dimensional models.....	138
Figure 5.10	Shaft lining closure vs. the properties of the Marl.....	139
Figure 5.11	Max. σ_1 in shaft lining vs. the properties of the Marl.....	140
Figure 5.12	Shaft lining closure vs. the thickness of the weathered Marl.....	142
Figure 5.13	Max. σ_1 in shaft lining vs. the thickness of the weathered Marl.....	142
Figure 5.14	Shaft lining closure vs. background stress ratio λ	144
Figure 5.15	Max. σ_1 in lining vs. background stress ratio λ	144
Figure 5.16	Failure state of the original shaft lining under background stress ratio $\lambda = 0.5$	145
Figure 5.17	FLAC ^{2D} mesh for possible "point" loading model (not full window).....	147
Figure 5.18	Failure state and schematic shape change of the original shaft lining under possible "point" loading.....	148
Figure 5.19	Lateral movement of the original lining.....	148
Figure 5.20	Detailed finite difference mesh of the shaft linings.....	152
Figure 5.21	Shaft linings' closure from the two-dimensional models.....	153
Figure 5.22	Ratio of lining's closure with inner radius of each lining.....	153
Figure 5.23	Principal stress tensors in the first relining.....	155
Figure 5.24	Mohr circles and strength envelop in the Mohr-Coulomb failure criteria.....	156

Figure 5.25	Maximum major principal stress and maximum deviator stress in shaft linings.....	156
Figure 5.26	The ratio of the max. deviator stress in shaft linings with the corresponding HSC strength.....	157
Figure 5.27	Major principal stress contour and direction of displacement in the first relining.....	158
Figure 6.1	Schematic inset of the shaft and the roadway.....	162
Figure 6.2	Mesh in the dimensions of the first relining system.....	165
Figure 6.3	Curves obtained in the process of calculating equivalent properties for the shaft's first HSC relining system.....	166
Figure 6.4	Mesh in the dimensions of the original shaft lining.....	167
Figure 6.5	Consistent mesh for the original lining (part of vertical section)	169
Figure 6.6	Non-consistent mesh for the first relining (part of vertical section)	169
Figure 6.7	Interfaces in the relining systems in the numerical models.....	170
Figure 6.8	Excavation steps flow chart in numerical modelling.....	172
Figure 6.9	Schematic shaft relining sequences in the continuous model.....	173
Figure 6.10	Geological stratigraphy in the study.....	175
Figure 6.11	Numerical model domain and mesh in the study.....	176
Figure 6.12	Foundation of the intermediate tower - vertical section.....	179
Figure 6.13	Foundation of the Manshaft - vertical section.....	180
Figure 6.14	Vertical section of the whole model mesh for this study (through X-Z plane).....	181
Figure 6.15	Plan of shaft inset level at -1108 m below shaft collar (BSC), the inset of the roadway and the shaft.....	182
Figure 6.16	Plan view of wing walls modelled in this study (through X-Y plane).....	183
Figure 6.17	Boundary conditions in the three-dimensional models in this study.....	184

Figure 6.18	Conceptual graded plastic zone around the shaft.....	186
Figure 6.19	Plan view of graded weathered Marl simulated in the three-dimensional models.....	187
Figure 6.20	Mohr-Coulomb strength envelopes for the Marl in the three-dimensional models.....	189
Figure 6.21	Displacement measure points in the three-dimensional models (not to scale).....	193
Figure 6.22	Horizontal displacements of the original lining's inner surface.....	194
Figure 6.23	Horizontal displacement contour of the original shaft lining before the roadway excavation (Roadway direction: Y).....	194
Figure 6.24	Horizontal displacement contour of the original shaft lining after the roadway excavation (Roadway direction: Y).....	195
Figure 6.25	Horizontal displacement vectors of the original shaft lining before the roadway excavation.....	196
Figure 6.26	Horizontal displacement vectors of the original shaft lining after the roadway excavation.....	197
Figure 6.27	Horizontal displacements of the shaft relinings' inner surface.....	197
Figure 6.28	Horizontal displacement contour of the first relining (Roadway direction: Y).....	198
Figure 6.29	Horizontal displacement contour of the second relining (Roadway direction: Y).....	199
Figure 6.30	Horizontal displacement contour of the third relining (Roadway direction: Y).....	199
Figure 6.31	Vertical stress σ_z in the original lining after the shaft excavation.....	202
Figure 6.32	Vertical stress σ_z in the original lining after the roadway excavation.....	203
Figure 6.33	Vertical stress σ_z in the first relining.....	204
Figure 6.34	Vertical stress σ_z in the second relining.....	205

Figure 6.35	Vertical stress σ_z in the third relining.....	206
Figure 6.36	Principal stress contours for the original lining: 9.8 m above the roadway roof in the Marl stratum, before the roadway excavation.....	208
Figure 6.37	Minor principal stresses σ_3 contour of the shaft linings: 9.8 m above the roadway roof in the Marl stratum.....	210
Figure 6.38	Schematic horizontal closure of the shaft lining through the Marl and Potash strata in the model.....	212
Figure 6.39	Plastic states of the shaft linings at 7 m above the roadway roof in the Potash stratum (the inside two rings are the shaft linings)	213
Figure 6.40	Displacement vectors of the first relining in the independent model (Roadway direction: Y).....	214
Figure 6.41	Interface normal stress in the second relining in the independent model (Roadway direction: Y).....	215
Figure 6.42	Interface shear stress in the second relining in the independent model (Roadway direction: Y).....	216
Figure 6.43	Interface shear failure in the first relining in the independent model (Roadway direction: Y).....	217
Figure 6.44	Interface shear failure in the second relining in the independent model (Roadway direction: Y).....	218
Figure 6.45	Interface shear failure in the third relining in the independent model (Roadway direction: Y).....	218
Figure 6.46	Vertical stress σ_z in the first relining in the independent model.....	220
Figure 6.47	Vertical stress σ_z in the second relining in the independent model.....	221
Figure 6.48	Vertical stress σ_z in the third relining in the independent model.....	222

LIST OF TABLES

Table 2.1	Major engineering rock mass classifications.....	24
Table 2.2	Rock Mass Rating System.....	28
Table 2.3	Classification of individual parameters used in the Tunnelling Quality Index Q.....	33
Table 2.4	ESR values suggested by Barton et al.....	36
Table 2.5	Boulby mine shaft lining sequence and information (through the Marl zone).....	62
Table 2.6	Actual support load capacity of the concrete lining systems at Boulby mine.....	63
Table 3.1	Characterisation of rock masses on the basis of interlocking and joint alteration.....	73
Table 3.2	Estimate of Geological Strength Index GSI based on geological descriptions.....	74
Table 3.3	Guidelines for estimating disturbance factor D.....	79
Table 3.4	Average UCS and Young's modulus of HSC used at Boulby mine.....	88
Table 3.5	Average tensile strength of HSC used at Boulby mine.....	88
Table 3.6	Mohr-Coulomb properties for HSC used at Boulby mine.....	89
Table 3.7	Young's modulus of NSC.....	91
Table 3.8	Poisson's ratio of NSC.....	91
Table 3.9	Tensile strength of NSC.....	92
Table 3.10	Input properties for all concrete materials in the numerical modelling.....	92
Table 3.11	Physical properties – a comparison of typical products.....	97
Table 3.12	Input properties for the interfaces elements representing the epoxy resin between concrete blocks.....	98
Table 3.13	Compressive strength requirements given as characteristic values for masonry cement.....	98
Table 3.14	Input properties for the interfaces elements representing the cement mortar between concrete blocks.....	100
Table 3.15	Mohr-Coulomb properties obtained from the plywood-concrete direct shear test.....	104
Table 3.16	Compression test data on plywood sample.....	105

Table 3.17	Input properties for the interfaces elements representing the plywood pack between concrete blocks.....	106
Table 3.18	The stiffness measured in the compression and nano-indentation tests.....	107
Table 3.19	Input properties for polyurethane and vermiculite in the numerical modelling.....	108
Table 3.20	Input properties of the cement grout used in the numerical modelling.....	109
Table 4.1	FLAC ^{2D} /FLAC ^{3D} constitutive models.....	121
Table 5.1	Background stress ratio λ used in the models.....	131
Table 5.2	Input properties for the Marl in parametric studies on the effect of its properties on the stability of the linings.....	132
Table 5.3	Input properties for the weathered and un-weathered Marl in parametric studies on the effect of the extent of weathered Marl on the stability of the original shaft lining.....	134
Table 5.4	Dimensions of shaft linings through the Marl zone at Boulby mine.....	150
Table 5.5	Dimensions used for the weathered Marl zone in the two-dimensional models.....	151
Table 6.1	Equivalent input properties for the HSC used in shaft's relining systems at Boulby mine.....	168
Table 6.2	Shaft excavation sequences used in the models.....	171
Table 6.3	Dimensions used for the weathered Marl zone in the three-dimensional models.....	188
Table 6.4	Input properties for the Marl used in the models.....	188
Table 6.5	Stiffness comparison between rocks and backfill materials.....	190
Table 6.6	Major principal stress σ_1 of the shaft linings' inner surface.....	207
Table 6.7	Minor principal stress σ_3 of the shaft linings' inner surface.....	207
Table 6.8	Major principal stress σ_1 of the first relining's inner surface.....	223
Table 6.9	Minor principal stress σ_3 of the first relining's inner surface.....	223

NOTATION

σ	Normal stress
$\Delta\sigma$	Normal stress difference
σ_{θ}	Tangential stress
σ_r	Radial stress
σ_c	Uniaxial compressive strength of rock mass
σ_{ci}	Uniaxial compressive strength of intact rock
σ_h	The horizontal component of ground stress
σ_{hav}	The average horizontal component of ground stress
σ_t	Tensile strength
σ_x	The horizontal ground stress in x direction
σ_y	The horizontal ground stress in y direction
σ_z	The vertical component of ground stress
σ_1	Major principal stress
σ_2	Intermediate principal stress
σ_3	Minor principal stress
σ_1'	Maximum effective stress at failure
σ_3'	Minimum effective stress at failure
$\sigma_{3\max}'$	The upper limit of confining stress over which the relationship between the Hoek-Brown and the Mohr-Coulomb criteria is considered
τ	Shear stress
$\tau_{r\theta}$	Shear stress in polar coordinates system
$\Delta\tau_c$	Shear stress difference caused by Δc

$\Delta\tau_\varphi$	Shear stress difference caused by $\Delta\varphi$
φ	Friction angle
$\Delta\varphi$	Friction angle difference
$\Delta\varepsilon$	Strain difference
λ	The background stress ratio, σ_x / σ_y
ν	Poisson's ratio
a_1	Excavation radius
B	Bulk modulus
c	Cohesion
Δc	Cohesion difference
CMC	The Coal Mine Classification
D	The disturbance factor
D_e	The equivalent dimension of the excavation
E	Young's modulus
E_i	Young's modulus of the intact rock
E_{rm}	Young's modulus of the rock mass
ESR	Excavation support ratio
f_c	Concrete cube compressive strength
f_{ck}	Characteristic cylinder compressive strength
f_{cm}	Mean value of concrete cylinder compressive strength
f_t, f_{sp}	Tensile strength of concrete
GSI	Geological Strength Index
h	The depth
HSC	High strength concrete
J_a	The joint alteration number
J_n	The joint set number

J_r	The joint roughness number
J_w	The joint water reduction factor
K_n	Normal stiffness
K_s	Shear stiffness
k_0	The ratio of the average horizontal component of ground stress to the vertical component of ground stress
m_i	The intact rock parameter (constant)
m_b, s and a	The Generalized Hoek-Brown strength parameters
NSC	Normal strength concrete
P	Normal force
Q	The Rock Tunnelling Quality Index
r	The distance from the excavation face
RQD	The Rock Quality Designation Index
RMR	The Rock Mass Rating
$\Delta r/r$	Concrete lining's inner radius decreasing ratio
S	Shear modulus
SRF	A stress reduction factor
T	Shear force
UCS	Uniaxial compressive strength
UTS	Uniaxial tensile strength
Δz_{\min}	The smallest width of an adjoining zone in the normal direction in FLAC ^{2D} /FLAC ^{3D} mesh

CHAPTER 1

INTRODUCTION

1.1 Introduction

Geotechnical engineers always face a dilemma when a structure, e.g. an underground excavation, is required to be designed and constructed in a rock mass in mining, petroleum or civil engineering. It is well known that a rock mass with its heterogeneous nature is inherently very complex in its structure and mechanical behaviour. This means that many influential parameters cannot be precisely determined and this factor alone makes design very difficult.

Before the advent of computers, structures in rock masses were designed mainly based on rules of thumb and experience. They usually tended to be over-designed with excessive safety factors and the design was based on situations similar to the one for which the new design was being developed. This raises the question however, what should the geotechnical engineers do with problems for which no past experience is available? They have to seek more rational solutions for these rock mechanics problems, taking both the safety factor and economic cost of the design into account.

A wide variety of techniques have been developed to deal with complex rock mechanics problems, such as limit equilibrium methods, photo-elastic techniques and the use of physical models. At present, computer based numerical modelling methods are very popular for solving rock mechanics problems due to rapid advancements in computer technology and its availability to engineers. A number of numerical methods of analysis have been developed over the past thirty years, for example the Finite Element

Method (FEM), the Boundary Element Method (BEM), the Discrete Element Method (DEM), the Finite Difference Method (FDM) and so on.

This thesis is based on research into numerical modelling application of FDM to a particular rock mechanics problem, combining theoretical, experimental and numerical modelling works. In this research, the shaft lining stability at Boulby mine has been investigated as a practical engineering example using commercial FDM codes - FLAC^{2D}/FLAC^{3D}. There are many advantages to using a practical engineering example for this research. The most important one is that the in situ observations, the rock engineers' experience at Boulby mine, and the available in situ measurements provide validation of the numerical modelling.

However, many factors at the Boulby mine site have made this numerical modelling research challenging, including low strength rock strata, a high ground stress field, complicated shaft lining structures, complex failure and yield conditions of the shaft lining and the scarcity of laboratory test data for the weakest rock material. It is recognised that the usefulness of powerful numerical analysis programs is greatly limited if the analyst does not have reliable input data for rock mass properties. Therefore, the methodology of obtaining appropriate material properties for rock mass in numerical modelling from laboratory tests data has also been studied.

1.2 Problem Definition

Boulby mine (Cleveland Potash Ltd.) is located on the North-East coast of England in the county of Cleveland and lies within the North Yorkshire Moors National Park (Figure 1.1). The mine produces a million tonnes of potash product in various grades annually, primarily to be used as a fertilizer. In addition, about 750,000 tonnes of rock salt is produced for

road de-icing (Williams and Auld 2002). The potash seam mined is about 7 m thick on average and approximately in a horizontal plane however with a shallow dip from northwest to southeast (average gradient is 1: 33). The complete workings of the Boulby mine lie approximately 800~1150 m below sea-level. The potash is generally mined where the seam is more than 4 m thick (Williams and Auld 2002).

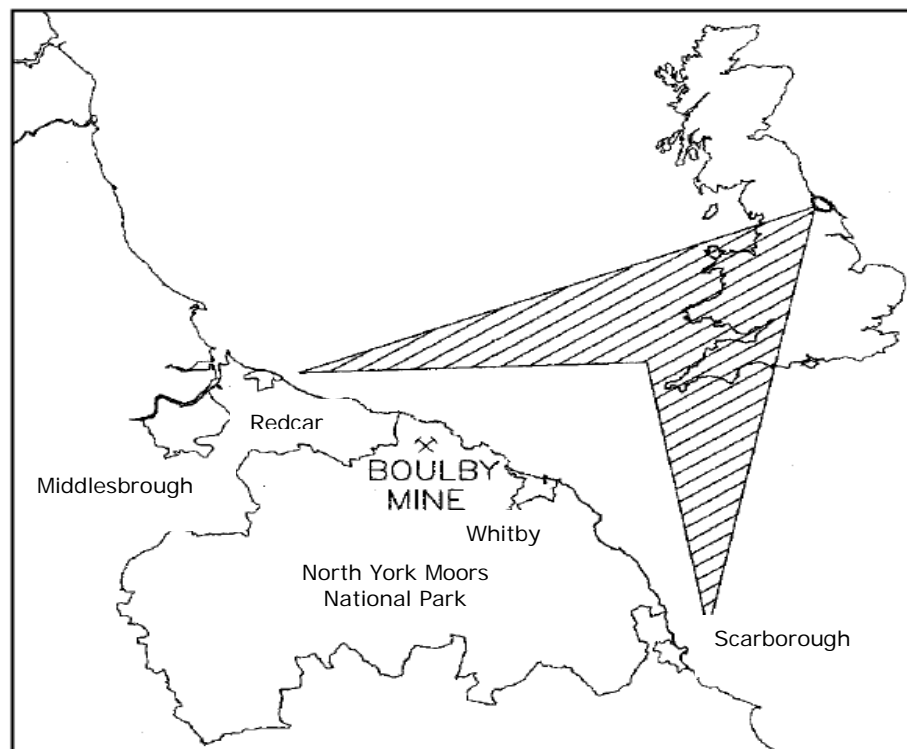


Figure 1.1 Location of Boulby mine (Williams and Auld 2002)

There are two shafts at Boulby mine, No. 1 shaft (rock shaft) and No. 2 shaft (man shaft), both of which were sunk during the period 1968 to 1974. Both shafts are around 5.5 m finished diameter and approximately 1150 m in depth, making them the deepest in the United Kingdom at that time. The upcast of rock shaft is used primarily for mineral winding and the manwinding-shaft is the downcast situated 91 m away, in which men

and materials are wound in two cages that use rope guides (Williams and Auld 2002).

The geological strata, through which the Boulby twin shafts are sunk is shown in Figure 1.2. At a depth of approximately 1100 m, close to the bottom of the shafts, a layer of Carnallitic Marl (about 9 m thick, Marl for short in later chapters) overlies the potash seam. The Marl, a reddish-brown saliferous clay, is often wet and poorly consolidated with frequent slicken sides and veins of halite and sylvinite (Williams and Auld 2002). The permanent support of the twin shafts through the zone of Marl stratum has proven difficult and now consists of a segmental concrete lining. Both shaft linings have suffered considerable radial pressure from the Marl stratum together with vertical compression from the upper part of the shafts resulting from subsidence of the host surrounding rock. This subsidence likely resulted from large numbers of roadway excavation in shafts pillar area. These pressures caused gradual failure of the concrete lining of the shafts in the Marl zone and failure of the relatively weak unsupported wing walls at the bottom of the shafts at the inset level (Chilton and Maxwell 1989).

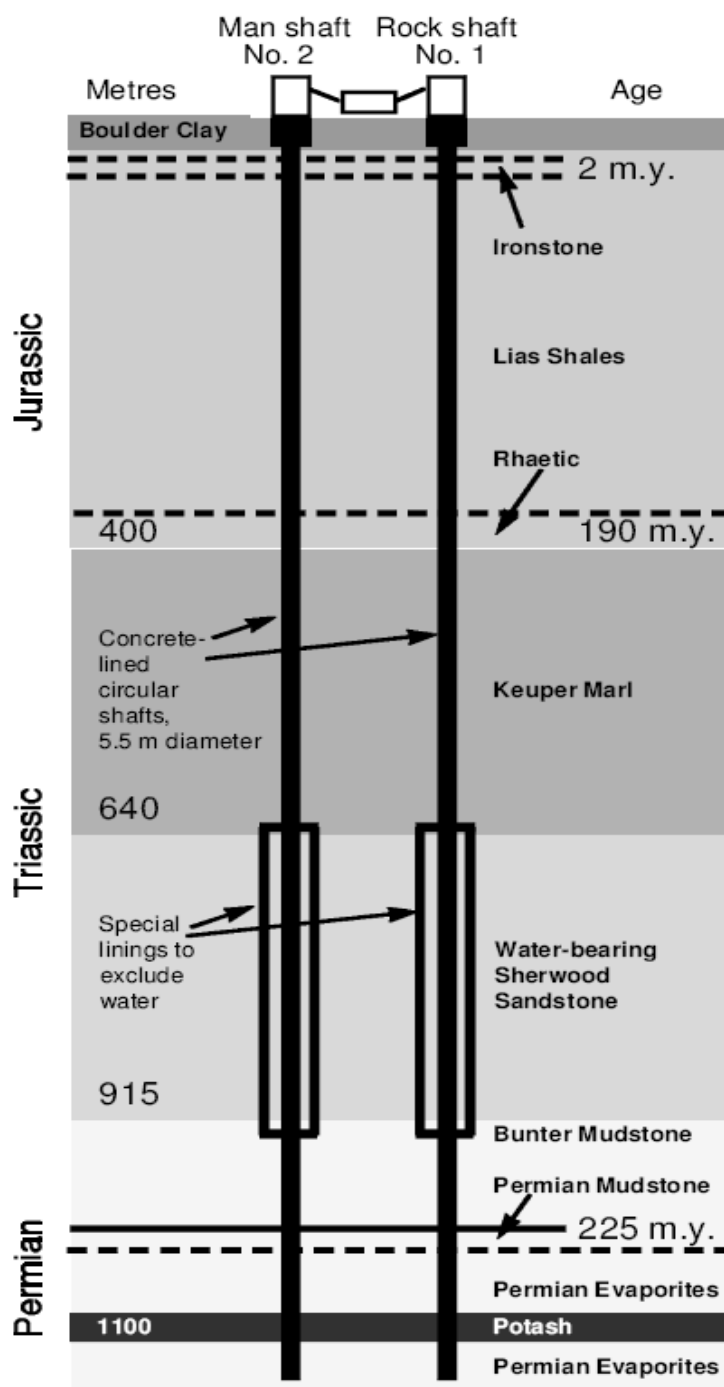


Figure 1.2 Stratigraphic section (Williams and Auld 2002)

After several years, the deterioration of the shafts concrete lining walls was so extensive that replacement of the lining became necessary through this zone. Repair work on two shafts has been carried out twice so far. The first relining of both shafts through the Marl zone took place during

1983~1986, and they were again relined (second relining) through the same zone during 1997~2001. At present, damage to the shafts' concrete lining (second relining) is again becoming severe, and a further repair (third relining) is now required and being planned. The shaft relinings through the Marl zone have always been started with the man shaft each time. To date, the design of the third relining and some preparation work for reconstruction has been completed for the man shaft.

1.3 Aims and Objectives

The main aim of this research project was the application of numerical modelling methods to rock mechanics problems in complicated rock strata under high stress field, combining theoretical, experimental and numerical modelling work. Specifically, a practical finite difference modelling approach for simulating the shaft lining stability in the shaft bottom area of the mine has been developed using the commercial software FLAC^{2D}/FLAC^{3D} (Itasca, 2008). The specific aims and objectives can be summarized as follows:

- 1) To develop the methodology of obtaining appropriate rock mass input material properties to use in numerical modelling based on laboratory test data, to make the numerical models more reliable.
- 2) To undertake parametric studies of different rock materials properties to determine their potential effects on the shaft lining stability.
- 3) To numerically simulate all the Boulby historical cases of shaft concrete linings, and to analyze the modelling results and compare them with the available measured data to determine the shaft lining probable failure mechanism.
- 4) To predict, using the numerical models, the long-term stress and deformation conditions for the latest newly designed shaft lining

system under the severe ground loading in particular strata zones. This will supply important reference data for Boulby mine shaft engineers (especially for the design and construction of the third relining of the rock shaft).

1.4 Technical Challenges

The structures of shaft lining systems at Boulby mine are very complex and the behaviour of the Marl is not well understood. The main components of the shaft lining systems are in situ cast concrete or concrete blocks. In addition, some special yielding designs have been introduced and implemented to obtain 'ideal' shaft lining systems at Boulby mine, which were expected to resist severe ground stress effectively over time. In this research, an attempt has been made to develop numerical models as close to the actual engineering structure as possible although there were some simplifications that had to be made. There were many technical difficulties encountered during this study, the most problematic of which are discussed as follows:

- 1) It has been difficult to determine the final strength and stiffness properties for the Marl used in the numerical models. The Marl is a weak rock and has a tendency to squeeze, which has been demonstrated by the gripping of the drill rods during boring (Squirrell 1992). This weak rock easily weathers on exposure. It is not normally exposed during mining operations, except during shaft lining restoration work. Therefore it is difficult to obtain and preserve the samples of this rock for laboratory tests, which are a significant and reliable data source for determining the material properties. Only two limited sets of test data have been available and utilised for the Marl in this research.

- 2) There has also been some difficult problem in numerical modelling of the original shaft lining system. In the original lining system at Boulby mine, vermiculite and polyurethane foams were used to backfill the gap (around 0.4 m thick) between the concrete lining and excavation face through the Marl stratum and the stratum above it. These materials are very soft compared with the surrounding rock and concrete used in the original shaft lining at Boulby mine, and their stiffnesses are several thousandths of those of the lining and the rock. When these materials were included in the numerical models, it resulted in many problems, especially in three dimensional modelling, such as unrealistic deformation of the original concrete lining and a dramatic increase in the program run time. The solutions adopted to deal with this problem are discussed in detail in a later chapter.
- 3) The problem of modelling of joints between concrete blocks also caused difficulties. For all the shaft relining systems at Boulby mine, high strength concrete (HSC) blocks were employed, with different materials filled between the concrete blocks each time, including epoxy resin, cement mortar and plywood packs. All these "joints" are very thin (12~18 mm) compared to the concrete blocks (around 0.5 m × 0.5 m) but are important to the mechanical behaviour of the whole concrete lining systems. Therefore interface elements have been built in FLAC^{2D}/FLAC^{3D} to be used to represent their behaviour in numerical models. However, it is very difficult to determine the appropriate mechanical properties for the interface elements for each relining model in the absence of laboratory test data. In order to solve this problem, some laboratory tests have been conducted, but most properties for the interface elements have been assumed based on

some reference papers, British Standards and available test data from Boulby mine.

- 4) The dimensions of the shaft concrete lining through the Marl stratum changed every time it was replaced. The expected ideal numerical modelling in this research is to try to simulate all the historical cases of the shaft lining systems in their real dimensions continuously in a single model. In this way, the effect of the historic changes in the stress field on each shaft lining stability could be investigated from the shaft's initial construction, original lining installation, the construction of the inset and the roadway leading from the shaft, and subsequent relining phases. However, the changing dimensions of the restored shaft lining makes this impossible since the finite difference mesh cannot be changed once the modelling of the original shaft excavation is started. Equivalent material properties for the shaft relining systems have been developed in this research to solve this problem.

1.5 Research Outline

The first stage of the study was a comprehensive literature review which concentrated on the following fields and is described in Chapter 2:

- 1) The virgin ground stress state and its influence on underground excavations
- 2) Rock mass classification systems and methods to determine rock mass strength and stiffness for numerical models
- 3) Rock mechanics influences on general shaft stability problems
- 4) Previous rock mechanics research at Boulby mine
- 5) The history of shafts at Boulby mine, including construction and restorations and available in situ measurements of stress and displacements of shaft linings

Following the literature review, a methodology for the laboratory determination of geotechnical parameters for the rock and other support materials used in this research is described in Chapter 3. This allowed a database of reliable rock and material properties for this research to be developed. New laboratory tests have been conducted and previously conducted testing data integrated into the database. Additionally, time-dependent (creep) tests on some rock materials and laboratory tests (uniaxial and triaxial compression tests and Brazilian Disc tests) on samples of the concrete from the shaft linings at Boulby mine were conducted in the Nottingham Centre for Geomechanics (NCG).

For the second and third shaft relining, HSC concrete blocks were employed and squeezable plywood packs were inserted between the blocks. To make the numerical modelling closer to the real situation, the properties of the interfaces between the concrete block and the plywood pack were needed. Therefore, shear box tests between the concrete and the plywood packs were also carried out in the laboratory at the NCG.

The database of material properties from Boulby mine comprises all the above laboratory tests data and the laboratory tests data from previous rock mechanics research at Boulby mine, including Patchet's tests (1970), Cook's tests (1974) (both from the University of Newcastle upon Tyne) and tests conducted at the Royal School of Mine Imperial College (2000). The materials' mechanical properties used in later numerical modelling were based on this database. In addition, several field visits to the Boulby mine were arranged, which were helpful to promote numerical modelling, modelling results analysis and comparison with in situ measurements.

Numerical modelling has then been conducted following these preparatory works, including an analysis of all the historical cases of the shaft concrete

relining systems. The content of this part of the research is produced in Chapters 5 and 6 after a brief overview of the numerical software used in Chapter 4. The potential effect of uneven loading on the original concrete lining and the effect of weathering on the surrounding rock (Marl) were also taken into account. Numerical modelling results were analyzed and compared with in situ measurements and an attempt was made to find the probable failure mechanisms of the concrete linings.

Based on all the numerical modelling results and available in situ measurements, the long-term stress and deformation conditions of the third shaft relining system under severe ground loading was predicted. Additionally, the effect of time dependent (creep) behaviour of related rocks on the shaft lining systems at Boulby mine is discussed.

This thesis ends with conclusions and recommendation in Chapter 7 and four appendix files:

- 1) *Summary of Boulby Mine Rock Materials Laboratory Tests Data*, which were collected from several PhD theses and test reports, which supplied important raw data of the rock materials properties for this research.
- 2) *Mohr-Coulomb/Hoek-Brown Properties of the Rock Materials at Boulby Mine*, which were based on the appendix above and were used with mass reductions in all the numerical models presented in this research.
- 3) *Laboratory Uniaxial and Triaxial Strength Test and Brazilian Disc Test Data of the Concrete Segmental Linings from Boulby Mine*.

CHAPTER 2

GENERAL LITERATURE REVIEW

2.1 In situ State of Ground Stress

In situ pre-existing ground stresses in the rock mass prior to any artificial disturbance (such as an excavation or construction work) are referred to as the initial stresses. The initial stresses are disturbed and re-distributed due to man-made excavations especially in the domain immediately surrounding the excavation. The new ground stresses after the disturbance are called induced stresses. The in situ state of ground stress is a fundamental concern not only for the design and construction of civil and mining engineering structures in rock, but also for numerical simulations of any geomechanics problems. It is an essential component to be considered in setting up numerical models.

The initial in situ stresses are highly variable natural phenomena which are related to the weight of the overlying materials, the geological history, tectonic movements and structural geological features (Whittaker and Frith, 1990). Usually, ground stresses represent three-dimensional quantities which are mathematically described as tensors. In many cases the principal directions of the ground stress tensors are parallel and perpendicular to the earth's surface. These are called horizontal and vertical stresses. The vertical and horizontal stresses can be treated separately to describe the change of stress magnitudes with depth (Herget, 1988).

In the stress field close to the surface in the depth range, the horizontal stresses are generally governed by the Poisson's effect in conjunction with

the vertical stress, which is commonly calculated from the gravity loads due to the weight of the overlying materials (Whittaker and Frith, 1990).

The ratio of $\sigma_h : \sigma_z$ is given as k_0 , whereby:

$$\frac{\sigma_h}{\sigma_z} = k_0 = \frac{\nu}{1 - \nu} \quad (2.1)$$

Where, σ_h , the horizontal component of ground stress

σ_z , the vertical component of ground stress

k_0 , the Earth Pressure Coefficient

ν , Poisson's ratio

Terzaghi and Richart (1952) also suggested that in the case of sedimentary rocks in geologically undisturbed regions where the strata were built up in horizontal layers in such a way that there was no lateral strain, the horizontal stresses are equal and are given by the Equation (2.1). This equation derives from the symmetry of one-dimensional loading of an elastic material over a continuous plane surface which infers a condition of no horizontal strain (Goodman, 1980). However, the basic assumptions used in Equation (2.1) do not apply to the real geological situations where the rock mass has experienced a complex geological history and contains many discontinuities (joints, cracks, bedding planes and so on). To understand the ground stress condition or stress fields around mine sites and in different geological environments, in situ stress measurements will supply significant information. Figures 2.1 and 2.2 show vertical stress and average horizontal stress with depth based on world stress measurements data (Herget, 1973).

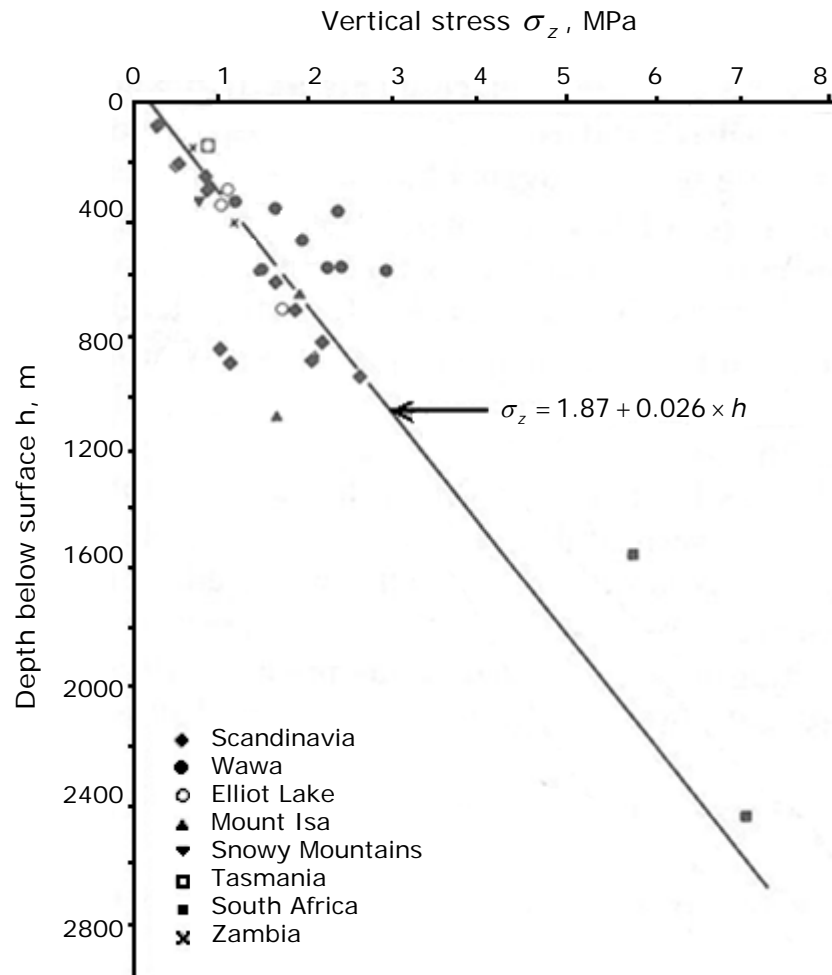


Figure 2.1 Results of stress measurements: vertical stress (Herget, 1973)

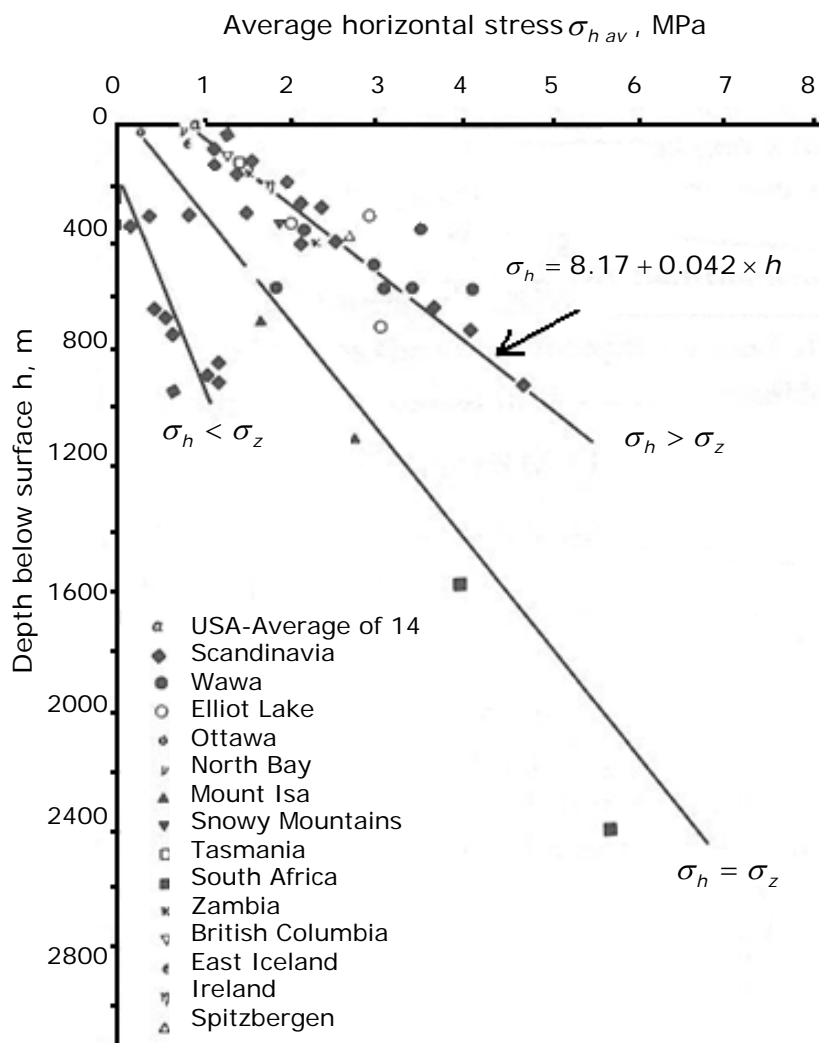


Figure 2.2 Results of stress measurements: average horizontal stress
(Herget, 1973)

Based on the stress measurement results shown in Figure 2.1, Herget (1973) suggested the average relationship between the vertical stress and the depth follows the equation:

$$\sigma_z = 1.87 + 0.026 \times h \quad (2.2)$$

Where, σ_z , the vertical ground stress, MPa

h , depth, m

At the same time, the horizontal stress measurements in Figure 2.2 have been separated into various populations using their relationships with the vertical stress:

1) $\sigma_h < \sigma_v$, e.g. Scandinavia (2.3)

2) $\sigma_h = \sigma_v$, e.g. South Africa (2.4)

3) $\sigma_h > \sigma_v$, prevailing (2.5)

$$\sigma_h = 8.17 + 0.042 \times h \quad (2.6)$$

Where, σ_h , the horizontal ground stress, MPa

σ_v , the vertical ground stress, MPa

h , depth, m

It can be seen from Figure 2.2 that the horizontal stresses were higher than the vertical stress in most cases of Herget's in situ stress measurements collection where the depth was between 0 m and 1000 m (Herget 1973).

Brown and Hoek (1978) also collated the published results of stress measurements made around the world and selected the data presented in Figures 2.3 and 2.4.

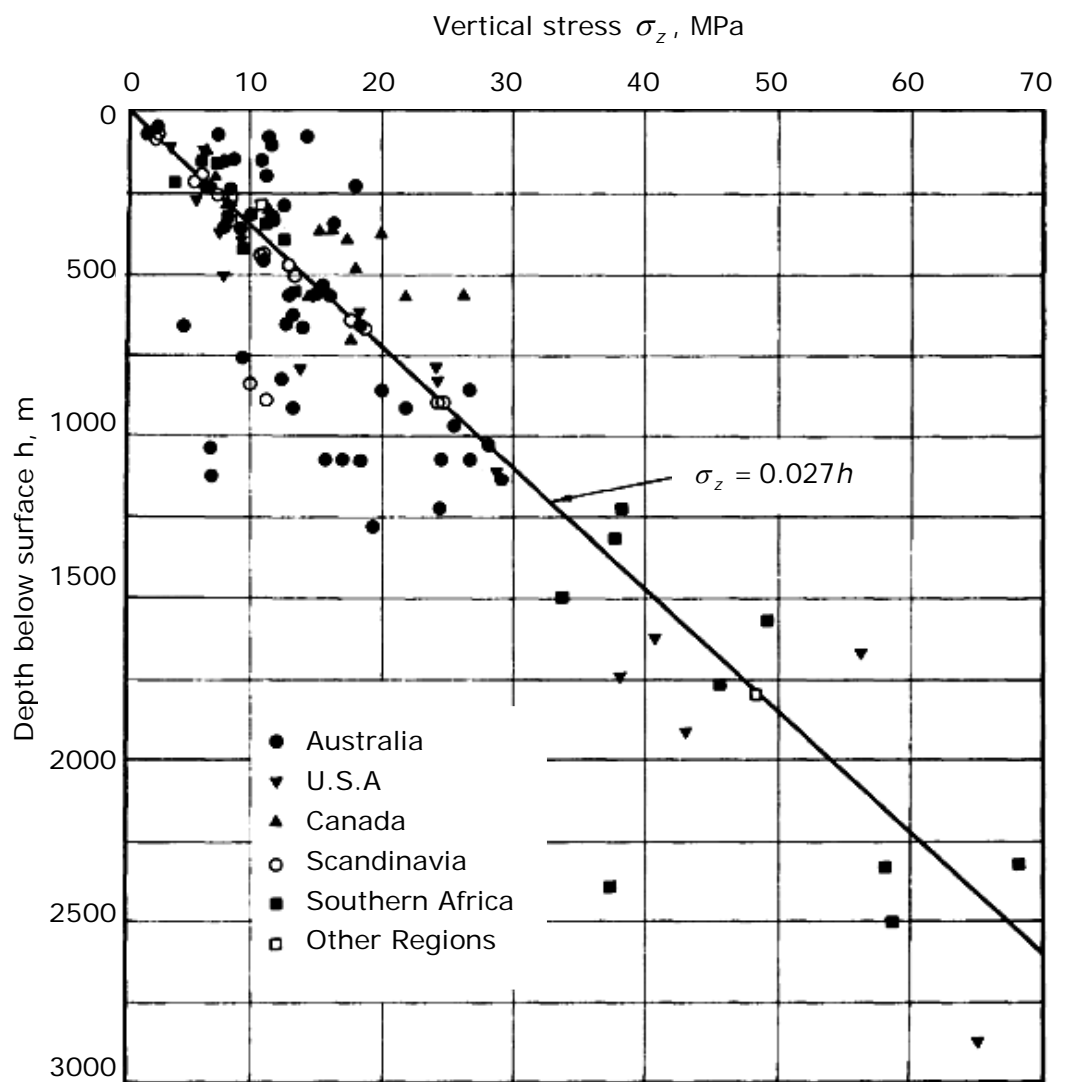


Figure 2.3 Results of stress measurements: vertical stress (Brown and Hoek, 1978)

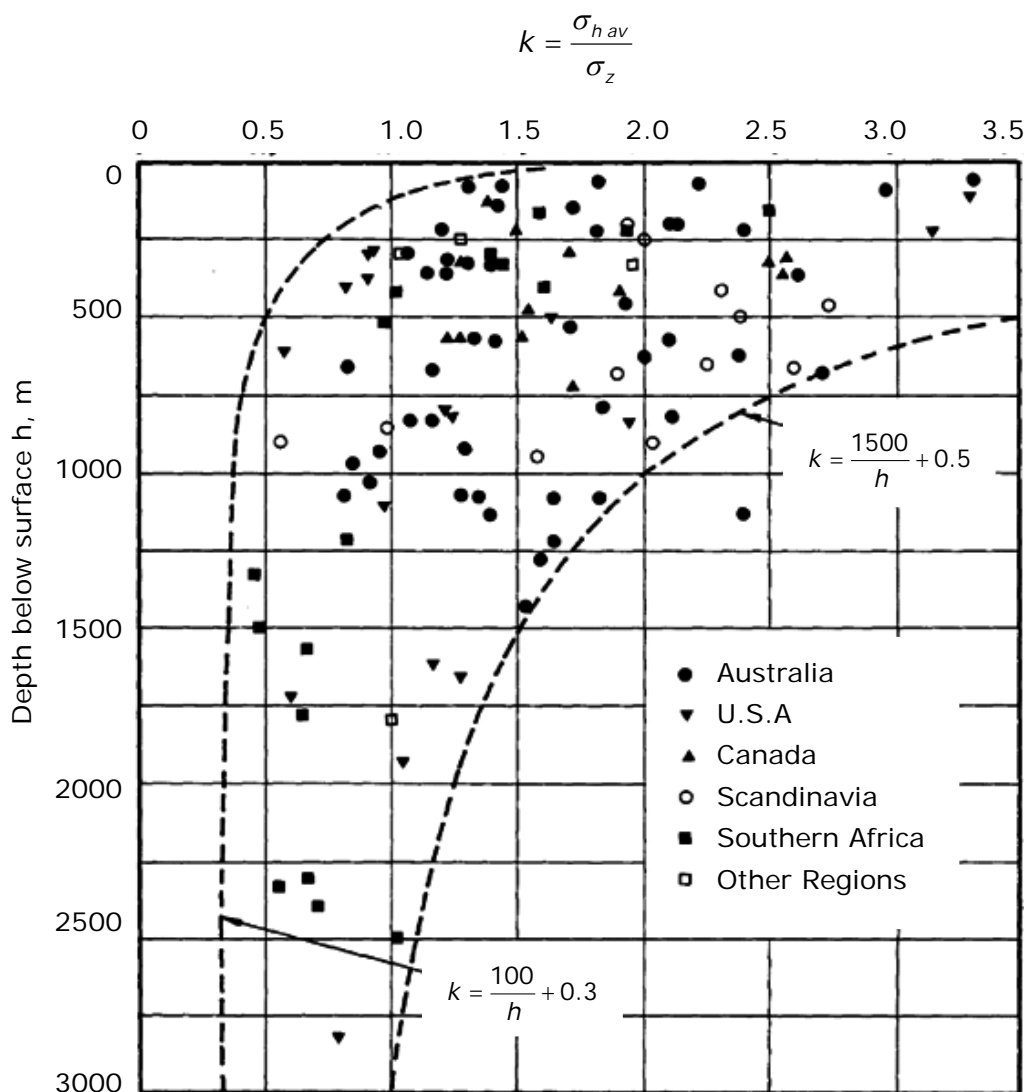


Figure 2.4 Variation of ratio of average horizontal stresses to vertical stress (Brown and Hoek, 1978)

They found that the measured vertical stresses were in fair agreement with the prediction that the vertical component of stress was simply a function of depth and cover rock density (usually in the range of 20 to 30 kN/m^3). Based on those measured results, they obtained the following Equation (2.7) which gives the average relationship for the vertical stress in relation to depth:

$$\sigma_z = 0.027 \times h \quad (2.7)$$

Where, σ_z , the vertical ground stress, MPa and

h, depth, m

It can be seen that the Equation (2.2) gives higher vertical stress predictions compared with the Equation (2.7) when the depth is lower than 1870 m. Stress measurement results collected by Brown and Hoek (1978) also show that the average horizontal stress ($\sigma_{h\ av}$) and the vertical stress (σ_z) tend to equalise (i.e. hydrostatic stress conditions) when the depth increases towards and beyond 1000 m as shown in Figures 2.2 and 2.4. As reported by Hoek and Brown (1980), this phenomenon confirms the suggestion by Heim (1912) and Talobre (1957): the inability of rock to support high stresses with large magnitudes differences together with the effects of time-dependent deformation of the rock mass can cause lateral and vertical stresses to equalise over periods of geological time. Heim's rule (1912) is widely used in weak rocks (e.g. coal measures and evaporites) and it has been found to give a good approximation of the in situ stress field in these materials (Hoek and Brown, 1980).

It should be remembered that only the average horizontal stress is plotted in Figure 2.4 and in many cases there is a significant difference between the horizontal stresses in different directions. For practical engineering problems, it may be useful to consider the significance of the individual stresses rather than the average (Hoek and Brown, 1980).

However, in both Mohr-Coulomb and Hoek-Brown failure criteria, the influence of the intermediate principal stress σ_2 is not taken into account. This assumption appears to be justified by both the results of tests by

Hojem and Cook (1968) and the investigations by Brace (1964). Hojem and Cook (1968) investigated intact rock samples in triaxial tests with states of stress $\sigma_1 \neq \sigma_2 \neq \sigma_3$. They concluded that the strength of rock increases with increasing intermediate principal stress σ_2 level but that increase is small enough to ignore for most practical application. Brace (1964) carried out so-called triaxial extension tests with $\sigma_1 = \sigma_2 > \sigma_3$ (where σ_3 is the axial stress in the specimen) as well as the usual triaxial tests with $\sigma_1 > \sigma_2 = \sigma_3$. Brace found no significant variation between the results obtained when $\sigma_1 = \sigma_2 > \sigma_3$ and when $\sigma_1 > \sigma_2 = \sigma_3$. He concluded that the intermediate principal stress σ_2 has a negligible influence upon the failure of the rocks which he tested.

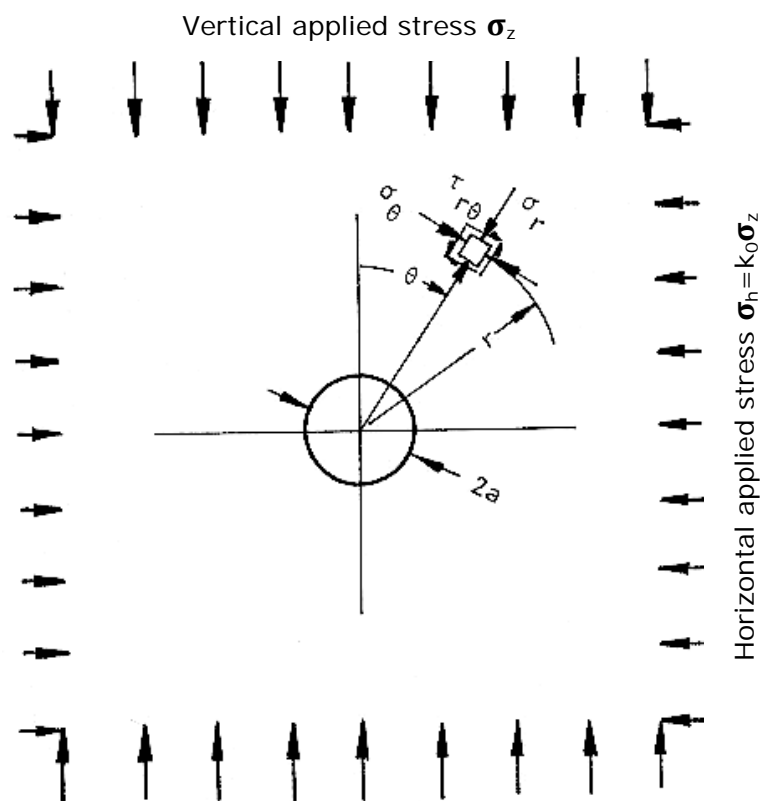
Based on these available evidences, Hoek and Brown (1980) suggested that it is admissible to ignore the influence of the intermediate principal stress σ_2 upon the failure of brittle rock. This assumption is important in keeping the failure criterion as simple as possible in order that it can be extended to include the effects of joints and pre-existing fractures (Hoek and Brown, 1980).

2.2 Stress Distribution around Excavations

The creation of an underground excavation will alter the in situ stress field in close proximity according to the size and shape of the excavation and the nature of the rock mass in terms of its failure characteristics. The rock left standing has to take more loading because the original support provided by the rock within the excavation has been removed. In some cases, the induced stresses by the disturbance are high enough to exceed the strength of the rock, leading to failure of the rock adjacent to the

excavation boundary. This instability may be in the form of gradual closure of the excavation, roof falls and slabbing of sidewalls or even rock bursts.

One of the earliest solutions for the two-dimensional distribution of stresses around an opening in an elastic body was published by Kirsch (1898) for the simplest cross-sectional shape, the circular hole, using mathematical theory of linear elasticity, illustrated in Figure 2.5.



Stress components at point (r, θ)

$$\text{Radial: } \sigma_r = \frac{1}{2} \sigma_z \left[(1 + k_0) \left(1 - \frac{a_1^2}{r^2} \right) + (1 - k_0) \left(1 - 4 \frac{a_1^2}{r^2} + 3 \frac{a_1^4}{r^4} \right) \cos 2\theta \right] \quad (2.8)$$

$$\text{Tangential: } \sigma_\theta = \frac{1}{2} \sigma_z \left[(1 + k_0) \left(1 + \frac{a_1^2}{r^2} \right) - (1 - k_0) \left(1 + 3 \frac{a_1^4}{r^4} \right) \cos 2\theta \right] \quad (2.9)$$

$$\text{Shear: } \tau_{r\theta} = \frac{1}{2} \sigma_z \left[-(1 - k_0) \left(1 + 2 \frac{a_1^2}{r^2} - 3 \frac{a_1^4}{r^4} \right) \sin 2\theta \right] \quad (2.10)$$

Figure 2.5 Equations for the stresses in the material surrounding a circular hole in a stressed elastic body (Hoek and Brown, 1980)

As the distance r from the excavation increases, the influence of the excavation on the stresses in the rock decreases. Based on Kirsch's equations, a plot of the ratio of $\sigma_{\theta} / \sigma_z$ against the distance r along the horizontal axis of the stressed model is given in Figure 2.6.

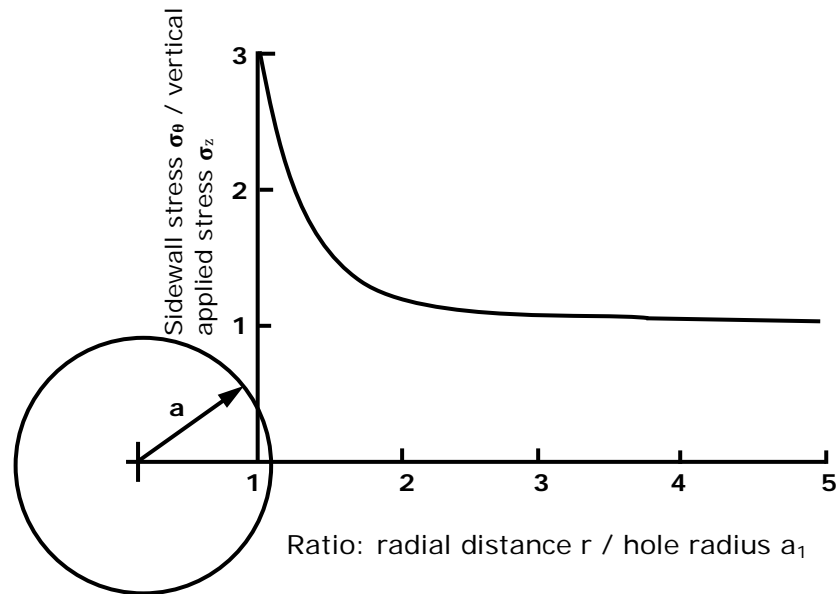


Figure 2.6 Variation in ratio of tangential stress σ_{θ} to vertical applied stress σ_z with radial distance r along horizontal axis for $k_0=0$ (Hoek and Brown, 1980)

Figure 2.6 shows that the stress concentration effect of the hole dies away fairly rapidly and that, at $r=3a_1$, the ratio of induced to applied stress is very close to unity, which means the excavation only creates a local disturbance. According to this fact, the general rule in model studies of stresses around underground excavations is that the minimum size of the model should be 3 to 4 times the maximum dimension of the excavation in the model (Hoek and Brown, 1980). However, it should be noted that the model in Figure 2.5 is an elastic model under compressive stress. The model size suggestion above may be only suitable for hard rock, but tends

to underestimate the model size for the problems in soft (weak) rock in a high hydrostatic ground stress field.

Stress distribution around different shape excavations or multiple underground excavations is more complicated as it is influenced by several other factors. For example, the orientation of the rectangular excavation plays an important role in the induced stresses distribution in surrounding rock. Furthermore, for multiple excavations, the distance between excavations will significantly influence the induced stresses distribution in surrounding rock.

2.3 Rock Mass Classification Systems

2.3.1 Introduction

Creating underground excavations and installing support are extremely complex engineering activities. Prediction of virgin rock mass behaviour, support pressure and tunnel closure is always one of the most difficult problems in rock engineering although much research has been focused on this area over many years. At the same time, large amounts of numerical modelling software has been developed to simulate and help solve geological and geotechnical problems. In order to obtain a good simulation, the input data must be of high quality, which mainly comprises of mechanical and physical properties of the rock mass. The rock mass usually contains a lot of irregular discontinuities, e.g. joints, bedding planes and faults. It is practically impossible to obtain all the properties of the rock mass by direct tests or measurements.

It has been recognized for a long time that a system was needed to classify the strength of a rock mass including its discontinuities as a whole

rather than just the strength of a piece of the intact rock. This classification system should be based on a sufficient number of in situ experiences (geological surveys, observations or measurements in the rock mass). Such a classification system acts as a vehicle which enables a designer to relate the experience of rock conditions and support requirements gained on other sites to the conditions anticipated on his own site (Hoek and Brown, 1980). This is more realistic and useful for the practical mining or civil engineering situation.

Bieniawski (1989) reviewed the development of rock mass classification systems, the most common of which are summarized in Table 2.1. The following section after Table 2.1 briefly summarizes some of the more important classification systems.

Name of Classifications	Originator and date	Country of origin	Applications
Rock load	Terzaghi, 1946	USA	Tunnels with steel support
Stand-up time	Lauffer, 1958	Austria	Tunnelling
New Austrian Tunnelling Method (NATM)	Rabcewicz, 1964	Austria	Tunnelling
Rock quality designation	Deere et al., 1964	USA	Core logging, tunnelling
RSR concept	Wickham et al., 1972	USA	Tunnelling
RMR system (Modified)	Bieniawski, 1973 Bieniawski, 1989	South Africa	Tunnels, mines, slopes, foundations
Q-system	Barton et al., 1974	Norway	Tunnels, Chambers
Strength-size	Franklin, 1975	Canada	Tunnelling
Basic geotechnical description	ISRM, 1981		General, communication
Unified classification	Williamson, 1984	USA	General, communication

Table 2.1 Major engineering rock mass classifications (Bieniawski, 1989)

2.3.2 Rock Quality Designation (RQD)

The Rock Quality Designation index (RQD), which has played an important role in the development of rock mass classification schemes, was proposed based on core recovery by diamond drilling by Deere in 1964. This index provides the first method to quantitatively classify rock masses. RQD is defined as the percentage of intact rock pieces (longer than 100 mm) within a total length of borehole, as follows:

$$RQD(\%) = 100 \times \frac{\sum \text{Length of Intact Rock Pieces } (> 100 \text{ mm})}{\text{Total Length of Borehole}} \quad (2.11)$$

To accurately present the quality of the rock mass, only the core broken by joints or other naturally occurring discontinuities are considered. Drill induced breaks must be ignored. Deere proposed the following relationship between the RQD values and the engineering quality of the rock mass:

RQD	Rock Quality
<25%	Very poor
25 – 50%	Poor
50 – 75%	Fair
75 – 90%	Good
90 – 100%	Very good

RQD can also be obtained from measurements of fracture spacings in excavation walls (Priest and Hudson, 1976). Obviously, RQD is a simple and quick practical index used to describe rock quality. However, the value of RQD is very sensitive to a change of borehole orientation. At the same time, RQD's definition shows that some important factors were not taken into account, such as rock strength, discontinuities character, discontinuities orientation and environment factors, which have great

influence on the behaviour of a rock mass surrounding an underground opening. Therefore, RQD on its own is not comprehensive enough as a method to classify rock masses. But as a component in other systems, e.g. RMR (Bieniawski 1974), it can be a very valuable single parameter to help classify rock masses.

2.3.3 Rock Mass Rating (RMR) System

The rock mass is composed of intact rock blocks with various geological discontinuities between them and therefore the properties of both intact rock and the discontinuities should be taken into account. The Rock Mass Rating (RMR) system is this kind of rock mass classification system, combining several factors such as RQD, uniaxial compressive strength of intact rock and the condition of discontinuities. It was proposed by Bieniawski (1974) of the South African Council for Scientific and Industrial Research (CSIR). This system is called the CSIR Geomechanics Classification or the Rock Mass Rating (RMR) system, and is based upon case histories drawn from civil engineering. Over the years, this system has been successively refined as more case records have been examined. After modification based on its application experience by Bieniawski (1989), this system has six parameters listed below:

- Uniaxial compressive strength of rock material
- Rock Quality Designation (RQD)
- Spacing of discontinuities
- Condition of discontinuities
- Groundwater conditions
- Orientation of discontinuities

The RMR system is presented in Table 2.2, giving the ratings for each of the six parameters listed above. Different ratings are assigned to each parameter according to its degree of importance and a higher overall rating indicates a better rock mass condition (Part A in Table 2.2). The RMR rating is adjusted according to the specific engineering application (Part B in Table 2.2). The final RMR rating is divided into five groups indicating the rock mass conditions (Part C in Table 2.2) and the practical meaning of each group is described in Part D in Table 2.2. This classification is one of the two classifications recommended by Hoek and Brown (1980) for general use in the preliminary design of underground excavations.

A. CLASSIFICATION PARAMETERS AND THEIR RATINGS									
Parameter			Range of values						
1	Strength of intact rock material	Point-load strength index	>10 MPa	4 - 10 MPa	2 - 4 MPa	1 - 2 MPa	For this low range - uniaxial compressive test is preferred		
		Uniaxial comp. strength	>250 MPa	100 - 250 MPa	50 - 100 MPa	25 - 50 MPa	5 - 25 MPa	1 - 5 MPa	< 1 MPa
	Rating	15	12	7	4	2	1	0	
2	Drill core Quality RQD		90% - 100%	75% - 90%	50% - 75%	25% - 50%	< 25%		
	Rating		20	17	13	8	3		
3	Spacing of discontinuities		> 2 m	0.6 - 2 . m	200 - 600 mm	60 - 200 mm	< 60 mm		
	Rating		20	15	10	8	5		
4	Condition of discontinuities (See E)		Very rough surfaces Not continuous No separation Unweathered wall rock	Slightly rough surfaces Separation < 1 mm Slightly weathered walls	Slightly rough surfaces Separation < 1 mm Highly weathered walls	Slicksided surfaces or Gouge < 5 mm thick or Separation 1-5 mm Continuous	Soft gouge >5 mm thick or Separation > 5 mm Continuous		
	Rating		30	25	20	10	0		
5	Ground water	Inflow per 10 m tunnel length (l/m)	None	< 10	10 - 25	25 - 125	> 125		
		(Joint water press)/ (Major principal σ)	0	< 0.1	0.1 - 0.2	0.2 - 0.5	> 0.5		
		General conditions	Completely dry	Damp	Wet	Dripping	Flowing		
	Rating		15	10	7	4	0		
B. RATING ADJUSTMENT FOR DISCONTINUITY ORIENTATIONS (See F)									
Strike and dip orientations			Very favourable	Favourable	Fair	Unfavourable	Very Unfavourable		
Ratings	Tunnels & mines		0	-2	-5	-10	-12		
	Foundations		0	-2	-7	-15	-25		
	Slopes		0	-5	-25	-60			
C. ROCK MASS CLASSES DETERMINED FROM TOTAL RATINGS									
Rating			100 ← 81	80 ← 61	60 ← 41	40 ← 21	< 21		
Class number			I	II	III	IV	V		
Description			Very good rock	Good rock	Fair rock	Poor rock	Very poor rock		
D. MEANING OF ROCK CLASSES									
Class number			I	II	III	IV	V		
Average stand-up time			20 yrs for 15 m span	1 year for 10 m span	1 week for 5 m span	10 hrs for 2.5 m span	30 min for 1 m span		
Cohesion of rock mass (kPa)			> 400	300 - 400	200 - 300	100 - 200	< 100		
Friction angle of rock mass (deg)			> 45	35 - 45	25 - 35	15 - 25	< 15		
E. GUIDELINES FOR CLASSIFICATION OF DISCONTINUITY conditions									
Discontinuity length (persistence)			< 1 m	1 - 3 m	3 - 10 m	10 - 20 m	> 20 m		
Rating			8	4	2	1	0		
Separation (aperture)			None	< 0.1 mm	0.1 - 1.0 mm	1 - 5 mm	> 5 mm		
Rating			8	5	4	1	0		
Roughness			Very rough	Rough	Slightly rough	Smooth	Slicksided		
Rating			8	5	3	1	0		
Infilling (gouge)			None	Hard filling < 5 mm	Hard filling > 5 mm	Soft filling < 5 mm	Soft filling > 5 mm		
Rating			8	4	2	2	0		
Weathering			Unweathered	Slightly weathered	Moderately weathered	Highly weathered	Decomposed		
Ratings			8	5	3	1	0		
F. EFFECT OF DISCONTINUITY STRIKE AND DIP ORIENTATION IN TUNNELLING**									
Strike perpendicular to tunnel axis				Strike parallel to tunnel axis					
Drive with dip - Dip 45 - 90°			Drive with dip - Dip 20 - 45°		Dip 45 - 90°		Dip 20 - 45°		
Very favourable			Favourable		Very unfavourable		Fair		
Drive against dip - Dip 45-90°			Drive against dip - Dip 20-45°		Dip 0-20 - Irrespective of strike°				
Fair			Unfavourable		Fair				

*Some conditions are mutually exclusive. For example, if infilling is present, the roughness of the surface will be overshadowed by the influence of the gouge. In such cases use A.4 directly.

**Modified after Wickham et al (1972).

Table 2.2 Rock Mass Rating System (Bieniawski 1989)

So far, several modifications have been proposed in the worldwide based upon Bieniawski's RMR system in order to make the classification more relevant to mining and civil engineering applications (Whittles 1999). Empirical relationships have been established between the RMR value and design parameters such as rock mass strength and stiffness, tunnel support requirements, factors of safety, stand-up times and support loads (Whittles 1999). In this way, the RMR system can be used in the design of a structure.

Laubscher (1977, 1984), Laubscher and Taylor (1976) and Laubscher and Page (1990) have described a Modified Rock Mass Rating (MRMR) system for mining. This system took the basic RMR value, and adjusted it to account for the in situ and induced stresses, stress changes and the effects of blasting and weathering. It should be noted that Laubscher's MRMR system was mainly based upon cases from caving operations.

The structure of the RMR system has been successfully used as a basis for most of the rock mass classifications in use today (Whittles 1999). A rock mass classification system specifically for UK Coal Measure strata was proposed and developed by Whittles (1999), which is similar in structure to Bieniawski's RMR system. It is called the Coal Mine Classification rating (CMC) and is introduced in the following section.

2.3.4 Coal Mine Classification (CMC)

In most empirical equations proposed for estimating the strength and stiffness properties, the rock mass is assumed isotropic (Whittles et al 2007). Within UK coal mines, the geological strata conditions are usually weak stratified rock masses in a high stress environment. It is known that the strength and deformation of a stratified rock mass varies depending on

the loading direction in relation to the orientation of the lamination planes. It was thought by Whittles (1999) that the existing rock mass classifications have limited applicability for the anisotropy within UK coal mines. Therefore, a rock mass classification system specifically for UK coal mines, named the Coal Mine Classification (CMC), was proposed and developed (Whittles 1999), based on the existing established classifications and the unique properties to the UK coal mining environment. By this specific classification, the strength and stiffness properties of rock strata encountered within UK coal mines can be predicted. CMC's output can be useful in determining representative engineering properties of rock strata used in numerical modelling techniques for underground roadway design in retreat face longwall mining.

Based on a database of information obtained from 118 different rock mass classifications, the CMC's parameters have been identified, which was thought by Whittles to have the greatest influence on the typical strata deformation mechanisms that occur within UK coal mines. The identified parameters were synthesized and listed as follows:

- Unconfined Compressive Strength
- Bedding/ Lamination Properties
 - ❖ Spacing
 - ❖ Strength
- Joint Properties
 - ❖ Set Number
 - ❖ Spacing
 - ❖ Orientation
 - ❖ Strength
- Fissility

- Water Flow
- Moisture Sensitivity

The selected parameters do not all have the same degree of influence on the strength and stiffness properties of the rock strata. Therefore, a relative importance weighting and rating scale for each individual parameter on the mechanism of strata deformation has been proposed. The basic CMC for a stratum unit is derived as a summation of the ratings attributed to each measured parameter. The rating can vary between 0 with extremely poor rock mass conditions and 100 suggesting a very strong rock mass with no weakness planes.

When applying the CMC, adjustments can be made where required to the basic rating to account for the effect of joint/cleat orientation relative to the orientation of the rib sides or coal face. The anisotropic nature of the UK coal measures strata was characterized within the CMC by the calculation of separate ratings for directions parallel to and perpendicular to bedding. The lithological and structural characteristics of the rock strata were also taken into consideration which may be significant to the engineering properties of the strata but not previously identified.

To validate the CMC system as a means of predicting the strength and stiffness properties of the rock mass, the CMC was applied to the strata at case study localities within rock bolted roadways within three UK mine sites. At the same time, numerical modelling of the case study localities were developed using the finite difference code FLAC^{2D} to simulate strata behaviour. The input mechanical properties of the rock strata were determined from the CMC. The results of the numerical modelling indicated that the predictions produced by the numerical models reflected the pattern and scale of deformations actually measured in-situ within the

coal mine roadways, thus indicating that the CMC system provides a means of predicatively determining the engineering properties of the in-situ UK Coal Measure strata.

2.3.5 Rock Tunnelling Quality Index, Q

This classification was proposed in 1974 by Barton et al of the Norwegian Geotechnical Institute (NGI) on the basis of evaluating a large number of case histories of underground excavation stability. The value of this index Q is defined by:

$$Q = \frac{RQD}{J_n} \times \frac{J_r}{J_a} \times \frac{J_w}{SRF} \quad (2.12)$$

Where RQD is Deere's Rock Quality Designation defined by Equation 2.11, J_n is the joint set number, J_r is the joint roughness number, J_a is the joint alteration number, J_w is the joint water reduction factor, and SRF is a stress reduction factor.

The first quotient (RQD/J_n) represents the structure of the rock mass, a crude measure of the block or particle size. The second quotient (J_r/J_a) represents the shear strength of the inter-block. The third quotient (J_w/SRF) is a complicated empirical factor describing the 'active stress'. SRF can be regarded as a total stress parameter. The parameter J_w is a measure of water pressure, which has an adverse effect on the shear strength of joints due to a reduction in effective normal stress. The values for single parameter are obtained from the very comprehensive Table 2.3.

DESCRIPTION	VALUE	NOTES
1. ROCK QUALITY DESIGNATION	<i>RQD</i>	
A. Very poor	0 - 25	1. Where <i>RQD</i> is reported or measured as ≤ 10 (including 0), a nominal value of 10 is used to evaluate <i>Q</i> .
B. Poor	25 - 50	
C. Fair	50 - 75	
D. Good	75 - 90	2. <i>RQD</i> intervals of 5, i.e. 100, 95, 90 etc. are sufficiently accurate.
E. Excellent	90 - 100	
2. JOINT SET NUMBER	J_n	
A. Massive, no or few joints	0.5 - 1.0	
B. One joint set	2	
C. One joint set plus random	3	
D. Two joint sets	4	
E. Two joint sets plus random	6	
F. Three joint sets	9	1. For intersections use $(3.0 \times J_n)$
G. Three joint sets plus random	12	
H. Four or more joint sets, random, heavily jointed, 'sugar cube', etc.	15	2. For portals use $(2.0 \times J_n)$
J. Crushed rock, earthlike	20	
3. JOINT ROUGHNESS NUMBER	J_r	
<i>a. Rock wall contact</i>		
<i>b. Rock wall contact before 10 cm shear</i>		
A. Discontinuous joints	4	
B. Rough and irregular, undulating	3	
C. Smooth undulating	2	
D. Slickensided undulating	1.5	1. Add 1.0 if the mean spacing of the relevant joint set is greater than 3 m.
E. Rough or irregular, planar	1.5	
F. Smooth, planar	1.0	
G. Slickensided, planar	0.5	2. $J_r = 0.5$ can be used for planar, slickensided joints having lineations, provided that the lineations are oriented for minimum strength.
<i>c. No rock wall contact when sheared</i>		
H. Zones containing clay minerals thick enough to prevent rock wall contact	1.0 (nominal)	
J. Sandy, gravely or crushed zone thick enough to prevent rock wall contact	1.0 (nominal)	
4. JOINT ALTERATION NUMBER	J_a	ϕ r degrees (approx.)
<i>a. Rock wall contact</i>		
A. Tightly healed, hard, non-softening, impermeable filling	0.75	1. Values of ϕ r, the residual friction angle, are intended as an approximate guide to the mineralogical properties of the alteration products, if present.
B. Unaltered joint walls, surface staining only	1.0	25 - 35
C. Slightly altered joint walls, non-softening mineral coatings, sandy particles, clay-free disintegrated rock, etc.	2.0	25 - 30
D. Silty-, or sandy-clay coatings, small clay-fraction (non-softening)	3.0	20 - 25
E. Softening or low-friction clay mineral coatings, i.e. kaolinite, mica. Also chlorite, talc, gypsum and graphite etc., and small quantities of swelling clays. (Discontinuous coatings, 1 - 2 mm or less)	4.0	8 - 16

Table 2.3 Classification of individual parameters used in the Tunnelling Quality Index Q (Barton et al 1974)

DESCRIPTION	VALUE	NOTES
4. JOINT ALTERATION NUMBER	J_a	ϕ r degrees (approx.)
<i>b. Rock wall contact before 10 cm shear</i>		
F. Sandy particles, clay-free, disintegrating rock etc.	4.0	25 - 30
G. Strongly over-consolidated, non-softening clay mineral fillings (continuous < 5 mm thick)	6.0	16 - 24
H. Medium or low over-consolidation, softening clay mineral fillings (continuous < 5 mm thick)	8.0	12 - 16
J. Swelling clay fillings, i.e. montmorillonite, (continuous < 5 mm thick). Values of J_a depend on percent of swelling clay-size particles, and access to water.	8.0 - 12.0	6 - 12
<i>c. No rock wall contact when sheared</i>		
K. Zones or bands of disintegrated or crushed	6.0	
L. rock and clay (see G, H and J for clay	8.0	
M. conditions)	8.0 - 12.0	6 - 24
N. Zones or bands of silty- or sandy-clay, small clay fraction, non-softening	5.0	
O. Thick continuous zones or bands of clay	10.0 - 13.0	
P. & R. (see G.H and J for clay conditions)	6.0 - 24.0	
5. JOINT WATER REDUCTION	J_w	approx. water pressure (kgf/cm ²)
A. Dry excavation or minor inflow i.e. < 5 l/m locally	1.0	< 1.0
B. Medium inflow or pressure, occasional outwash of joint fillings	0.66	1.0 - 2.5
C. Large inflow or high pressure in competent rock with unfilled joints	0.5	2.5 - 10.0
D. Large inflow or high pressure	0.33	2.5 - 10.0
E. Exceptionally high inflow or pressure at blasting, decaying with time	0.2 - 0.1	> 10
F. Exceptionally high inflow or pressure	0.1 - 0.05	> 10
1. Factors C to F are crude estimates; increase J_w if drainage installed.		
2. Special problems caused by ice formation are not considered.		
6. STRESS REDUCTION FACTOR		SRF
<i>a. Weakness zones intersecting excavation, which may cause loosening of rock mass when tunnel is excavated</i>		
A. Multiple occurrences of weakness zones containing clay or chemically disintegrated rock, very loose surrounding rock any depth)	10.0	1. Reduce these values of <i>SRF</i> by 25 - 60% but only if the relevant shear zones influence do not intersect the excavation
B. Single weakness zones containing clay, or chemically disintegrated rock (excavation depth < 50 m)	5.0	
C. Single weakness zones containing clay, or chemically disintegrated rock (excavation depth > 50 m)	2.5	
D. Multiple shear zones in competent rock (clay free), loose surrounding rock (any depth)	7.5	
E. Single shear zone in competent rock (clay free). (depth of excavation < 50 m)	5.0	
F. Single shear zone in competent rock (clay free). (depth of excavation > 50 m)	2.5	
G. Loose open joints, heavily jointed or 'sugar cube', (any depth)	5.0	

Table 2.3 (cont'd) Classification of individual parameters used in the Tunnelling Quality Index Q (Barton et al 1974)

DESCRIPTION	VALUE		NOTES
6. STRESS REDUCTION FACTOR			SRF
<i>b. Competent rock, rock stress problems</i>			
	σ_c/σ_1	$\alpha_t\sigma_1$	
H. Low stress, near surface	> 200	> 13	2.5
J. Medium stress	200 - 10	13 - 0.66	1.0
K. High stress, very tight structure (usually favourable to stability, may be unfavourable to wall stability)	10 - 5	0.66 - 0.33	0.5 - 2
L. Mild rockburst (massive rock)	5 - 2.5	0.33 - 0.16	5 - 10
M. Heavy rockburst (massive rock)	< 2.5	< 0.16	10 - 20
<i>c. Squeezing rock, plastic flow of incompetent rock under influence of high rock pressure</i>			
N. Mild squeezing rock pressure			5 - 10
O. Heavy squeezing rock pressure			10 - 20
<i>d. Swelling rock, chemical swelling activity depending on presence of water</i>			
P. Mild swelling rock pressure			5 - 10
R. Heavy swelling rock pressure			10 - 15
ADDITIONAL NOTES ON THE USE OF THESE TABLES			
When making estimates of the rock mass Quality (Q), the following guidelines should be followed in addition to the notes listed in the tables:			
1. When borehole core is unavailable, RQD can be estimated from the number of joints per unit volume, in which the number of joints per metre for each joint set are added. A simple relationship can be used to convert this number to RQD for the case of clay free rock masses: $RQD = 115 - 3.3 J_v$ (approx.), where J_v = total number of joints per m^3 ($0 < RQD < 100$ for $35 > J_v > 4.5$).			
2. The parameter J_n representing the number of joint sets will often be affected by foliation, schistosity, slaty cleavage or bedding etc. If strongly developed, these parallel 'joints' should obviously be counted as a complete joint set. However, if there are few 'joints' visible, or if only occasional breaks in the core are due to these features, then it will be more appropriate to count them as 'random' joints when evaluating J_n .			
3. The parameters J_r and J_a (representing shear strength) should be relevant to the weakest significant joint set or clay filled discontinuity in the given zone. However, if the joint set or discontinuity with the minimum value of J_r/J_a is favourably oriented for stability, then a second, less favourably oriented joint set or discontinuity may sometimes be more significant, and its higher value of J_r/J_a should be used when evaluating Q. The value of J_r/J_a should in fact relate to the surface most likely to allow failure to initiate.			
4. When a rock mass contains clay, the factor SRF appropriate to loosening loads should be evaluated. In such cases the strength of the intact rock is of little interest. However, when jointing is minimal and clay is completely absent, the strength of the intact rock may become the weakest link, and the stability will then depend on the ratio rock-stress/rock-strength. A strongly anisotropic stress field is unfavourable for stability and is roughly accounted for as in note 2 in the table for stress reduction factor evaluation.			
5. The compressive and tensile strengths (σ_c and α_t) of the intact rock should be evaluated in the saturated condition if this is appropriate to the present and future in situ conditions. A very conservative estimate of the strength should be made for those rocks that deteriorate when exposed to moist or saturated conditions.			

Table 2.3 (cont'd) Classification of individual parameters used in the Tunnelling Quality Index Q (Barton et al 1974)

In order to relate the Q value to the stability and support requirements of underground excavations, Barton et al (1974) defined an additional parameter called the Equivalent Dimension, D_e , of the excavation. This dimension is defined as:

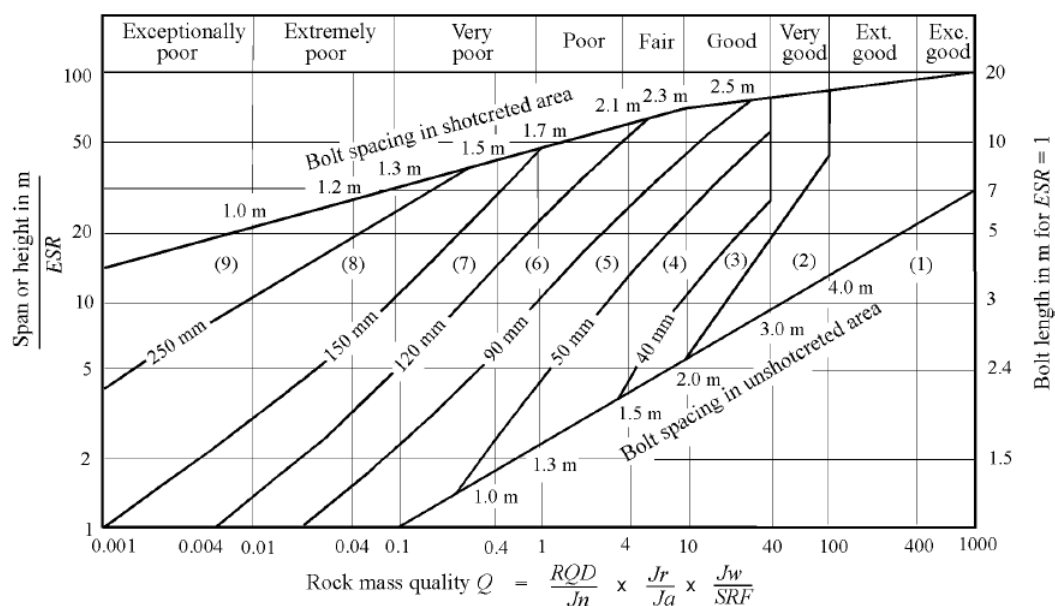
$$D_e = \frac{\text{Excavation Span, Diameter or Height (m)}}{\text{Excavation Support Ratio (ESR)}} \quad (2.13)$$

The value of ESR is a quantity, related to the use of the excavation and to the degree of safety which is demanded of the support system installed to maintain the stability of the excavation. Barton et al (1974) suggested the following values in Table 2.4:

Excavation Category	ESR
Temporary mine openings.	3-5
Permanent mine openings, water tunnels for hydro power (excluding high pressure penstocks), pilot tunnels, drifts and headings for large excavations.	1.6
Storage rooms, water treatment plants, minor road and railway tunnels, surge chambers, access tunnels.	1.3
Power stations, major road and railway tunnels, civil defence chambers, portal intersections.	1.0
Underground nuclear power stations, railway stations, sports and public facilities, factories.	0.8

Table 2.4 ESR values suggested by Barton et al (1974)

Figure 2.7 shows the relationship between the Tunnelling Quality Index Q and the Equivalent Dimension D_e of an excavation which will stand unsupported. Figure 2.7 can also be utilized to determine the support categories required to maintain excavation stability.



REINFORCEMENT CATEGORIES

- | | |
|---|---|
| <ul style="list-style-type: none"> 1) Unsupported 2) Spot bolting 3) Systematic bolting 4) Systematic bolting with 40-100 mm unreinforced shotcrete | <ul style="list-style-type: none"> 5) Fibre reinforced shotcrete, 50 - 90 mm, and bolting 6) Fibre reinforced shotcrete, 90 - 120 mm, and bolting 7) Fibre reinforced shotcrete, 120 - 150 mm, and bolting 8) Fibre reinforced shotcrete, > 150 mm, with reinforced ribs of shotcrete and bolting 9) Cast concrete lining |
|---|---|

Figure 2.7 Estimated support categories based on the Tunnelling Quality Index Q (Grimstad and Barton 1993)

2.3.6 Conclusions

Prediction of virgin rock mass behaviour, support pressure and underground excavation closure requires an estimation of the mechanical properties of the rock mass. The mechanical properties of the in situ rock mass are influenced by many factors, such as intact rock strength, the nature and orientation of planes of discontinuities, weathering and ground water conditions. Laboratory tests can provide mechanical properties for intact rock, which can supply some information for the upper limit of the rock mass mechanical properties, but cannot provide those for the in situ rock mass. However, by means of the rock mass classification, the mechanical properties of the rock mass may be estimated. Many rock mass classifications have been developed over the last sixty years.

Most of the multi-parameter rock mass classifications (RQD, RMR and Q systems) were developed from civil engineering case histories and have been widely utilized in the civil engineering industry to assist with the assessment of rock support requirements. However, there are obvious differences between mining and civil engineering design approaches to rock mass classification. One of the fundamental differences is higher ground stress condition (at deeper position) and bigger opening's dimension (some mine roadways) in mining industry. As there are often many kinds of discontinuities surrounding a mine roadway, such as bedding planes, joints and faults. These classifications are somewhat conservative if used directly in the mining industry.

2.4 Shaft Stability Problems

In a mine environment, many factors will influence the stability of underground excavations. These factors include the size and shape of the excavations, the magnitude of the existing stress regime, geological structures, such as faults, folds and altered zones occurring in the strata. Failure frequency also is increased by the presence of ground water (Bruneau et al 2003).

Shafts are examples of permanent mining excavations. Because of the frequent use of such excavations by mine personnel, a significantly higher degree of security is required than for other mine openings (Vandewalle 1998). It is reported by Beus and Board (1984) that secondary excavation, such as inset and roadway construction leading from the shaft, station, etc., can be expected to influence rock movement and shaft lining pressure at least as much as does shaft sinking. In mature mines, the influence of geological structural features and the modified stress regimes,

which may be caused by some underground excavation very close to the shafts, on the stability of shafts is even more dominant (Bruneau et al 2003).

Groundwater inflow is also a serious problem for shafts stability. Two examples are presented in this section. In October 1998, consultants were called in, after a serious water ingress, to investigate the feasibility of pre-cementation to control groundwater inflow into the proposed ventilation shaft No.1A at Impala Platinum mine (Bothma 2001). South Deep's main shaft at Western Areas Gold mine was flooded by an inrush of water at about 450 m below collar (the uppermost portion of the shaft and acting as a protective barrier to prevent water and soil from entering the shaft) in May 1996, leading to a tactical withdrawal up the shaft.

A survey on shaft wall failures showed that 90% of all the shaft walls that failed were in shale, coal and marls (Herget 1988). Most shafts in medium strength rock without geological failure surfaces are self supporting. In these cases linings are often installed for other than structural reason, e.g. control of water and weathering. However, if shafts reach great depths, in situ stresses might exceed in situ material strength. If the material is weak, this critical depth is reached sooner (Herget 1988).

In unfavourable ground conditions, the construction of circular shafts is required. The most commonly used shaft design in modern day mining is actually of circular or elliptical shape which in itself is self-supporting and accommodating if a concrete lining is being utilized. The circular shafts avoid stress concentrations in corners and benefit from arching action in the supported material. Based on a field experiment involving the sinking of two full-size test shafts to directly compare the deformational behaviour of circular and rectangular shapes, Beus and Chan (1985) concluded that:

- 1) The circular shape is less sensitive to geologic discontinuities and applied stress field.
- 2) The rectangular shape is subject to a variety of behavioural modes, including beam bending and buckling.
- 3) Regardless of shaft shape and in situ stress field, shaft wall displacement is significantly affected by rock mass anisotropy and geologic discontinuities.

Design and construction of permanent mine workings, especially their shafts, faces the task of their reliable support for the whole service life period of the mine (Olovyanny and Kozel 2005). Shafts, which are heavily trafficked openings, should have rockbolts and/or reinforced shotcrete installed to protect personnel and equipment from rockfalls (Vandewalle 1998). The experience gained in operation of shafts indicates that when the shafts intersect the salt layers at a depth more than 300 m, damages of a concrete or ferroconcrete support sharply intensify (Kozel 2001).

For supporting shafts, rockbolts, steel-fibre reinforced shotcrete lining and mesh reinforced shotcrete lining are often utilized (Vandewalle 1998, Bothma 2001 and Erasmus et al 2001). In Nikolaichuk's paper (1978), a two-layer support with a yielding external layer was offered for the use in salt rocks for making permanent workings, vertical shaft in particular, safe. When this support was applied, the radial displacements of the rock surrounding the vertical shaft compact the yielding layer of the support, and the pressure on its rigid (internal) concrete layer was zero until a certain time when the rigid layer intervened in the joint action with the salt rocks. The radial displacements of the unsupported rock intensified with time due to continuous creep of rocks so that pressure on the concrete support grew as well.

Combining mature numerical simulation techniques and field observation is a very popular, helpful and rational option for researchers of rock mechanics problems at present. Two practical examples relating to shafts are briefly discussed in this section. One is that there has been observed evidence of degradation of the shaft concrete lining in the early 1990s at the Copper Mine, at Mount Isa, Australia. The shaft degradation has been attributed to the presence of two major geological structures (two faults), which intersect the shaft in two distinct locations. To gain a better understanding of the mechanisms inducing damage to the shaft, the influence of faulting and mining sequence on the stability of the main mine shaft were investigated by means of field investigations and numerical modelling. The numerical modelling results have a fairly good agreement with the recorded field observation (Bruneau et al 2003).

The other example is from a large gold mine in South Africa, East Rand Proprietary Mines Ltd. The lower levels of this mine were exploited by means of inclined shafts. Below 3000 m, failure of the monolithic concrete linings characteristically occurred when mining work came near to the shaft. It appeared that failure did not occur as a result of an increasing stress field but from a general reduction in stress. The marked relaxation of the high stress in the rock sidewall induced a high tensile stress in the adjacent lining. This somewhat paradoxical suggestion was confirmed quantitatively by finite element analysis and qualitatively by in situ deformation measurements. The method of support has consequently been changed completely to one using reinforced shotcrete and rockbolts (Ortlepp 1974).

2.5 Previous Rock Mechanics Research at Boulby Mine

The geology overlying the Potash seam at Boulby is a mixture of marine sediments and evaporites. Figure 2.8 shows the general sequence of strata based on the information obtained by Boulby mine. The detailed geology near the working seam (Potash) is shown in Figure 2.9. The strata are generally flat while the thickness of various beds varies considerably within the area of Boulby mine. Details of the whole geology have been described previously by Patchet (1970) and Cook (1974). The laboratory test data have been collected from these two PhD theses and some other laboratory test reports are shown in the Appendix I of this thesis for all the rock types in this geology. However, only part of the geology has been included in the numerical modelling in this thesis to save on the models' size and numerical calculation time. This is mainly the Middle Evaporites in the Permian strata shown in Figure 2.9.

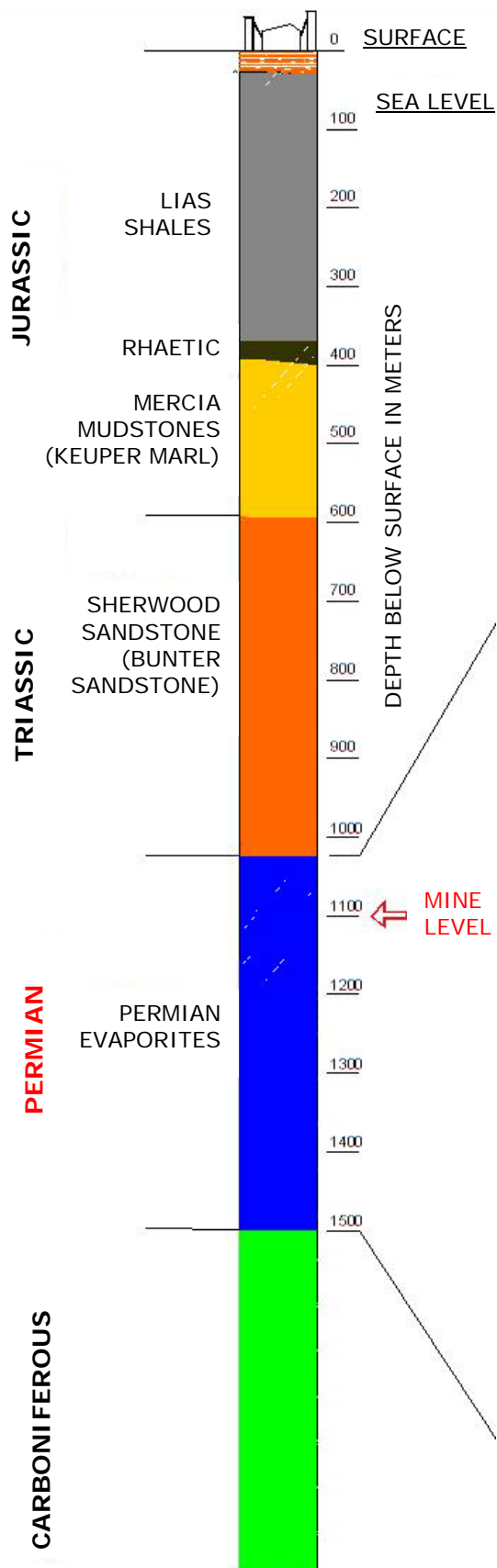


Figure 2.8 Strata sequence of Boulby potash mine (Boulby mine)

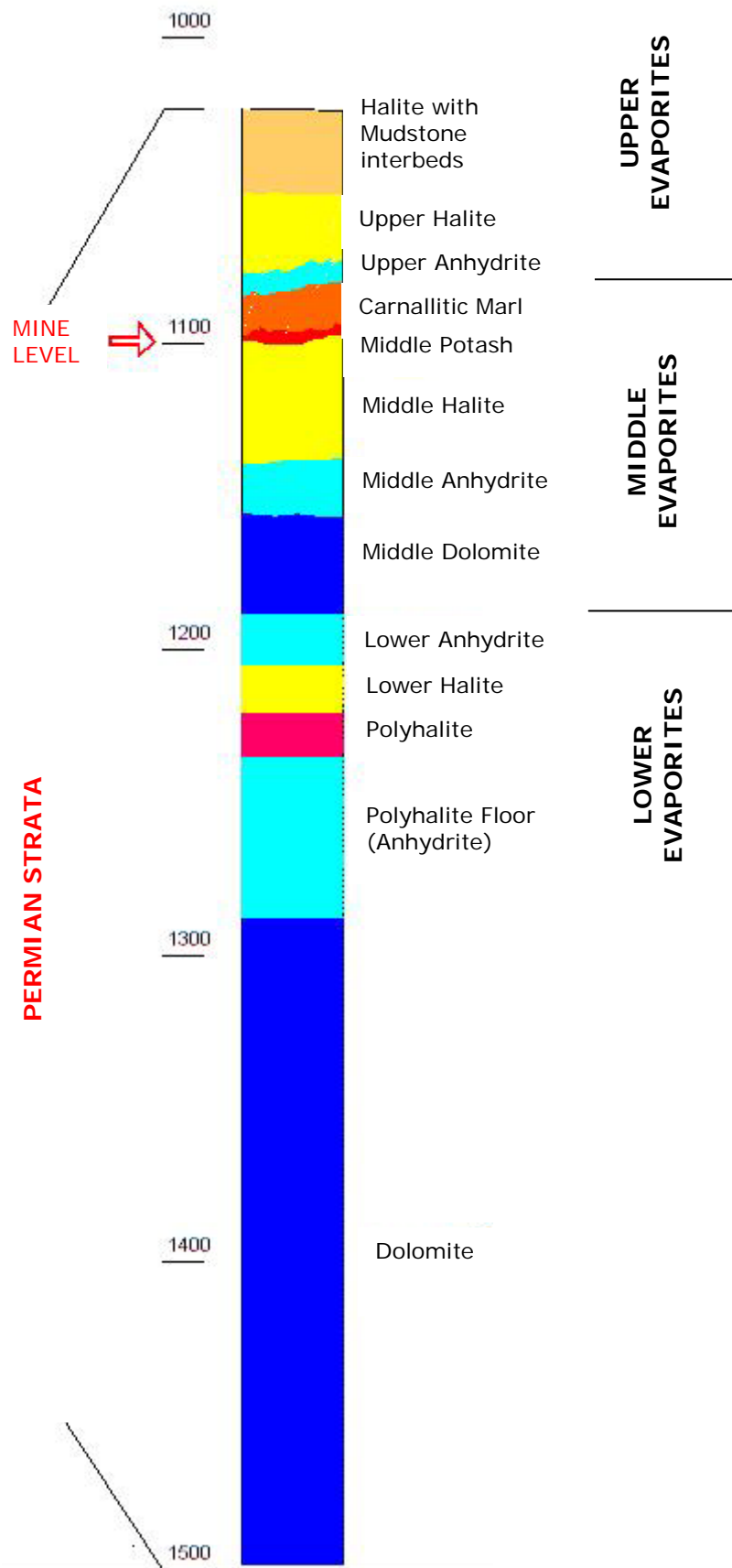


Figure 2.9 Detailed geology of the Permian strata at Boulby mine

During the past forty years, much rock mechanics research has been carried out at Boulby mine, some of which supplied important reference for this research and is briefly summarized as follows:

- 1) The laboratory tests initiated by Buzdar (1968) and carried out by Patchet (1970)

In Patchet's thesis, the mechanical properties and strengths of the complete geological succession at Boulby were studied. Patchet defined all strata from surface to Upper Halite shown in Figure 2.9 as Upper Strata, and strata from Upper Anhydrite to Middle Halite shown in Figure 2.9 as Near-seam Strata. His laboratory tests of the near-seam rocks included the uniaxial and triaxial compressive tests, tensile tests and uniaxial time-dependent (creep) tests.

Some of the basic conclusions from Patchet's work were as follows:

- Neither all the upper strata nor the stratum of Middle Potash nor the other near-seam strata should offer any problems to the underground stability. Near-seam beds dip gently and this factor can be neglected as influencing underground stability. Extensive shaft stability problems will occur in the weakest near-seam rock – the Marl.
- Except for the Upper Anhydrite shown in Figure 2.9, all other near-seam rock materials have low compressive and tensile strength, failures of which were very slow and explosive failures were rarely found. The Marl can be considered as plastic under most conditions and as a stratum, it probably has no tensile strength.
- With regard to the possible effect of the time dependent behaviour of the Middle Potash: for long term stability of pillared mine workings it was essential for a triaxially confined core of rock to exist within the pillar and remain confined, even though slightly diminished with time.

2) The research by Cook (1974)

Cook continued Patchet's research project and focused on the stability of the shaft excavations through the Upper Evaporites strata in Figure 2.9. Cook extended the laboratory testing programme to triaxial time dependent (creep) testing in order to analyse the time dependent properties of the evaporites, both in the laboratory and in the field. Model work had been undertaken in the laboratory in order to demonstrate the deformation of openings in time dependent material and dimensional analysis has been used to relate this behaviour to the deformation of large underground excavations. The man shaft at Boulby mine was instrumented in order to monitor the in situ behaviour and compare the obtained movements with these predicted from laboratory experiments when it was sunk through the Upper Halite stratum, which possesses time dependent properties. Based on Cook's tests, a gap (0.46 m) was left between the surrounding rock and the shaft lining through the Upper Halite to allow for time-dependent radial closure of the excavation.

3) Hebblewhite's work (1977)

Hebblewhite put emphasis on establishing the design criteria for underground Potash workings based on rock mechanics principles and measurements taken in the field. Hebblewhite agreed with Patchet and also stated in his PhD thesis that the Marl was the weakest rock in the sequence and provided a major problem of stability both in the underground workings and in the shaft.

Hebblewhite analyzed the possible water problem during the mining in the Potash seam which could have very serious consequences. The only water-bearing stratum in the sequence was the massive Bunter Sandstone

(Figure 2.8), which consists of fine grained, red sandstones grading into mudstones. The sandstone stratum has low permeability under high hydrostatic pressure. During shaft-sinking there was evidence of fissures containing water from the sandstone occurring in the stratum between the Bunter Sandstone (Figure 2.8) and the Upper Evaporites (Figure 2.9). This stratum can approach to within 70m above the Potash seam and form the only low permeability bed of significant thickness between the saturated Bunter Sandstone beds (Figure 2.8) and the evaporites below (Figure 2.9). A thin band of Anhydrite occurs above the Upper Evaporites (Figure 2.9) and is also relatively impermeable. This combination of beds composes the main barrier preventing possible inflow of water into the mine workings in the Potash.

4) Research by Golder Associates (1997)

Golder Associates have undertaken research for Boulby mine to optimise the extraction ratio across the mine, particularly at the south end of the mine and revise the primary panel and pillar layouts using numerical modelling. FLAC^{2D} was utilized in the modelling for the extraction ratio and panel layout review. Meanwhile, the stresses and displacements around mine openings were simulated using VNFOLD (3D), a displacement discontinuity program. Time-dependent (creep) curves and parameters of Middle Halite and Middle Potash were discussed in this research.

5) Laboratory tests at the Royal School of Mines, Imperial College (2000)

A series of laboratory tests on several rock materials (some near-seam rocks and Polyhalite) were conducted by the Royal School of Mines, Imperial College (RSM) in July 2000. The tests included uniaxial compression tests, single stage and 5-stage triaxial compression tests and

Brazilian Disc tensile strength tests. The following data were obtained from these tests and have been included in Appendix I in this thesis:

- Dynamic and static Young's modulus (E)
 - Poisson's ratio (ν)
 - Mohr-Coulomb strength properties (cohesion c and friction angle ϕ)
 - Tensile strength
 - Uniaxial compressive strength (UCS)
- 6) Laboratory tests at the Nottingham Centre for Geomechanics in the University of Nottingham (2007~2009)

During 2007 and 2009, a series of laboratory tests on the rock materials from Boulby mine, mainly from Middle Evaporites and Lower Evaporites in the Permian Strata (Figure 2.9), were carried out at the Nottingham Centre for Geomechanics (NCG) in the University of Nottingham. The tests included uniaxial compression tests, single stage and 5-stage triaxial compression tests, and Brazilian Disc tensile strength tests, following the methodology outlined in "Rock Characterisation Testing and Monitoring – ISRM suggested methods" (Pergamon Press 1981). All the data have been collected from these tests and shown in Appendix I in this thesis. Uniaxial time-dependent (creep) tests under different temperatures on some rock types from Boulby mine have also been conducted at the NCG.

2.6 History of the Shafts at Boulby Mine

2.6.1 The Design for the Original Lining of the Shafts

The two shafts at Boulby mine were originally constructed during 1968~1974. They were approximately 5.5 m finished internal diameter and approximately 1150 m deep. Figure 2.10 is an indicative longitudinal

section through the rock shaft as originally constructed (Williams and Auld 2002).

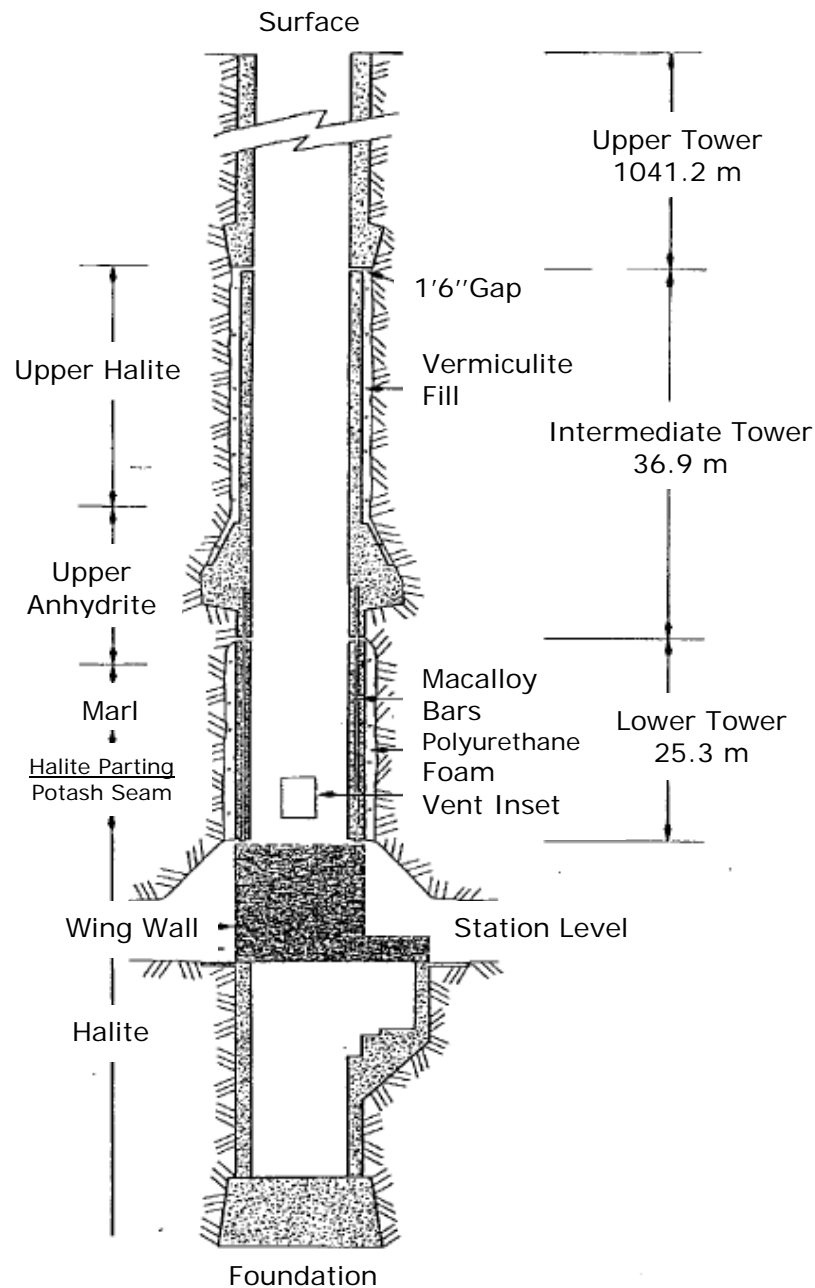


Figure 2.10 Indicative longitudinal section through original rock-shaft lining (Williams and Auld 2002)

As shown in Figure 2.10, both of the shafts were composed of three sections: the upper towers, the intermediate towers and the lower towers.

The upper tower is by far the longest, approximately 1040 m down from the surface. They were mostly lined in unreinforced concrete that was cast in situ directly against the host rock. The section in the rock shaft through the Bunter Sandstone zone (610~914 m) was sunk using ground freezing as a temporary support and then a combined concrete and steel lining as a permanent support. For the same section in the man shaft, sinking was carried out using grouting for groundwater control and a permanent lining of cast-iron tubing was installed. Below the upper towers, the intermediate towers are about 37 m long with their foundations in the Upper Anhydrite. The lower towers are beneath the intermediate towers and 25.3 m in height. They are suspended by Macalloy bars embedded in the lining and also attachments to the thrust rings associated with the foundations of the intermediate towers. Both intermediate and lower towers are lined with reinforced concrete. A gap of 0.46 m (Figure 2.10, 1'6" gap) was left between the intermediate and upper towers to absorb any relative movement (Chilton and Maxwell 1989).

Cleasby et al. (1975) referred to extensive rock mechanics studies at the University of Newcastle upon Tyne that showed that the Halite would exhibit creep properties and it was expected that the shaft walls would converge some 150 mm in diameter within two months of excavation. So, the compressible materials, vermiculite fill for intermediate towers and polyurethane fill for lower towers, were placed in the 0.46 m gaps between the reinforced concrete shaft lining and the surrounding rock intending to absorb ground radial movement due to the creep of the Halite and Potash beds and relieve the pressure on the lining. It was considered that several years would elapse before the Marl would move far enough to exert high pressure upon the shaft walls. However, cracks appeared in the walls of both shafts after only two years (Chilton and Maxwell 1989) and within a

decade of their completion the lower towers in the shafts were so severely distressed that they both had to be replaced.

Because of different construction methods for the intermediate and lower towers, different compressible materials were chosen for them. The intermediate towers were constructed from the bottom foundation upwards and the concrete was cast against bags of vermiculite placed against the excavation face. However, the lower towers were lined from the top downwards in stages, suspended on hanging rods. The polyurethane foam, with its poorer squeezable properties, had to be sprayed on to the excavation face first as the backing to the concrete lining in the lower towers through the Marl (Williams and Auld 2002).

2.6.2 The Design for the First Relining of the Shafts

Rock bolts, weld mesh, shotcrete and combinations of these had been used in an attempt to maintain the shafts in a reasonable state of repair (Chilton and Maxwell 1989), but by 1983 it was obvious that the shaft lining was too badly damaged to offer resistance to the movements of the Marl. The shaft lining throughout the Marl zone had to be removed and replaced.

The first relining design was based on uniform geostatic pressure in the order of 16.55 N/mm^2 acting on a circular shaft (Chilton and Maxwell 1989). The first relining design for the man shaft is illustrated in section and plan in Figures 2.11 and 2.12. The design for the rock shaft's lining was similar. It comprised rings of precast high strength concrete (HSC) blocks, with a guaranteed compressive strength of over 100 N/mm^2 , supported on steel decks suspended by Macalloy-bar hanging rods. The blocks were 610 mm high and 1067 mm thick. Each block weighed

approximately 1 tonne, which was considered the limit for safe handling in the shaft (Williams and Auld 2002).

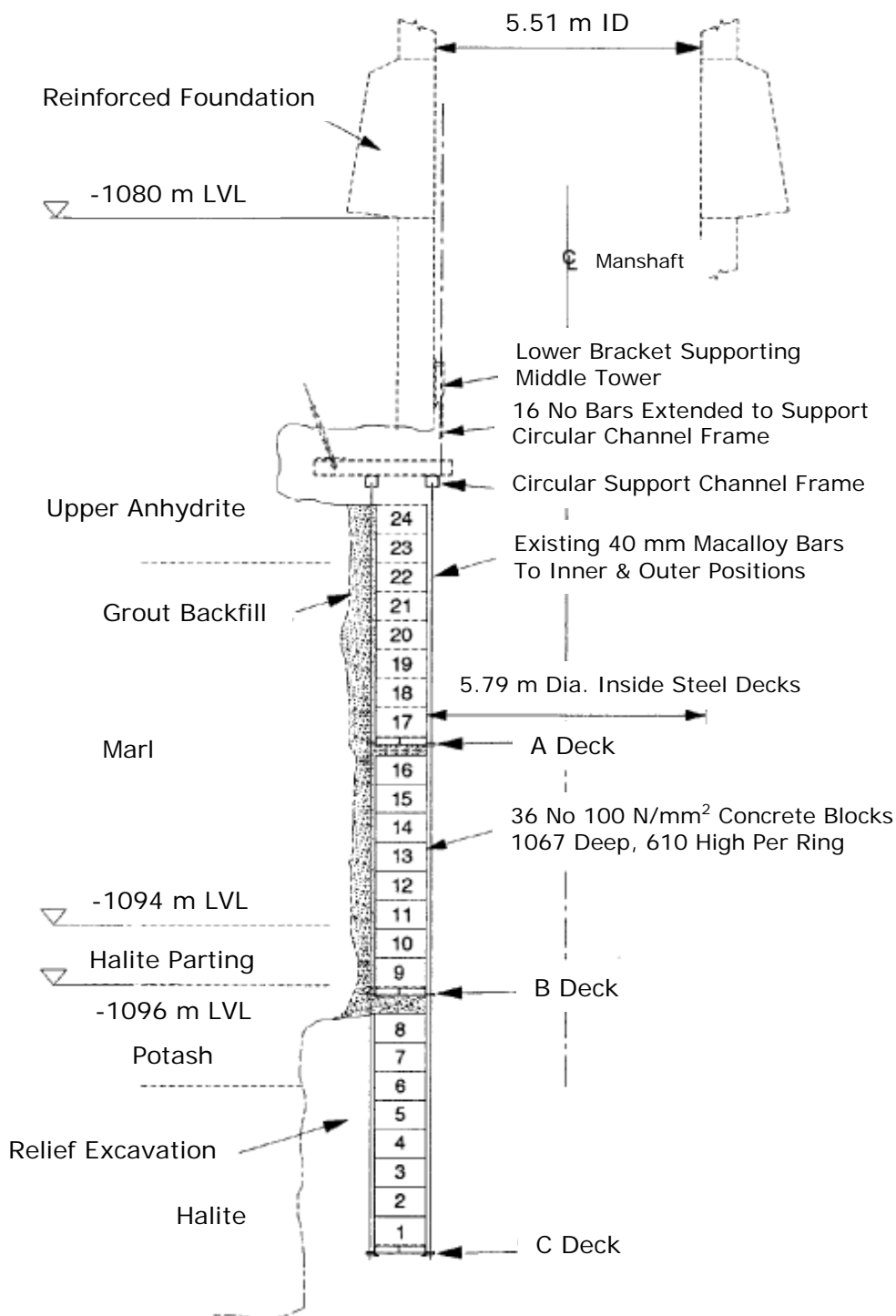


Figure 2.11 First relining for the man shaft, section (Williams and Auld 2002)

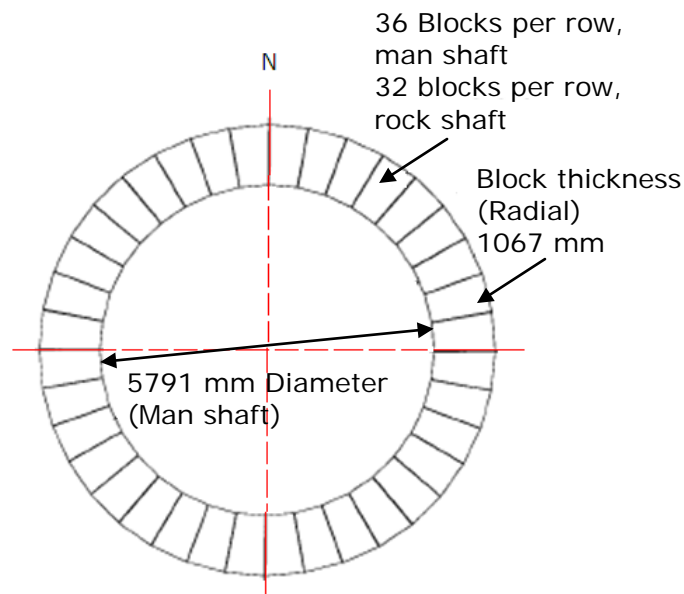


Figure 2.12 First relining, plan (Williams and Auld 2002)

Because of the failure of the original concrete lining with the compressible backfill, a rigid lining system was adopted for the first relining to resist full geostatic pressure from the Marl. Epoxy resin was placed between the vertical joints and cement mortar was employed in the horizontal joints to achieve a bond between concrete blocks. Cement was pumped into the gap between the back of the blocks and the excavation face to form an incompressible fill, so that any horizontal pressure would be transferred via the blocks around the shaft in the form of hoop stress. The gap between each deck and the row of blocks immediately below was about 0.23 m. This gap was filled with cement (Chilton and Maxwell 1989). In addition, the new lining would have to cope with vertical movement of the shafts.

This new lining, although regarded as temporary, was expected to last for 5–10 years before a more effective lining would be installed based on a better understanding of the behaviour of the surrounding strata. However,

minor deterioration had taken place in both shaft linings after nearly three years in the rock shaft and only approximately two years in the man shaft.

2.6.3 The Design for the Second Relining of the Shafts

At the beginning of 1996, deterioration of the first relining through the Marl zone in both shafts was so severe (Figure 2.13) that replacements were once again necessary.



Figure 2.13 Damaged manshaft before the second relining (Williams and Auld 2002)

In fact, work had commenced on the man shaft several years before to relieve the distress in its lining by partial excavation (left bottom in Figure 2.11) behind the lining to reduce ground pressure. Contrary to the original aim, this exercise exacerbated the lining's damage by translating and accelerating deterioration further up the lining. New linings (second relining) were again designed and installed through the Marl zone in the twin shafts during 1998–2001.

The second relining design shown in Figures 2.14 and 2.15 was similar to that for the first relining, but based on the consideration of compatibility of deformations between the surrounding Marl and the shaft lining. The major difference was that the second relining system included a flexibility which was introduced into the rigid concrete lining to allow the surrounding host rock time-dependent (creep) inward movements. This was achieved by using double rings of blocks with squeezable plywood packs in all horizontal and vertical joints between blocks and rings. At the same time, it can be seen from Figure 2.15 that gaps left between the top rows of blocks and the deck immediately above severed the lining's continuity. These gaps also acted as a flexible coupling between adjacent deck and block sections in addition to facilitating the construction process.

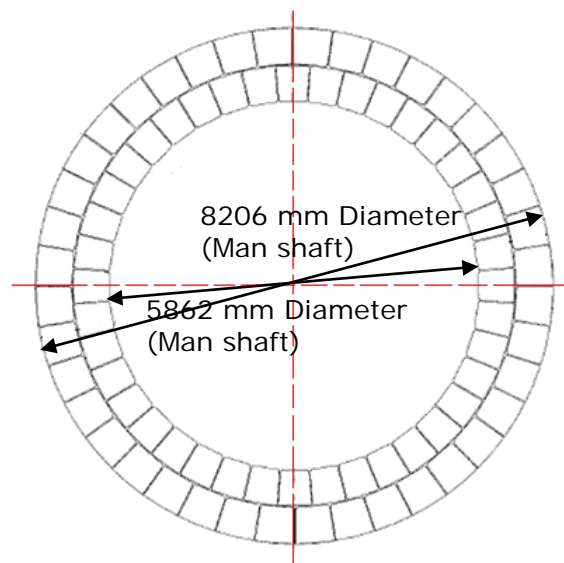


Figure 2.14 Second relining, plan (Williams and Auld 2002)

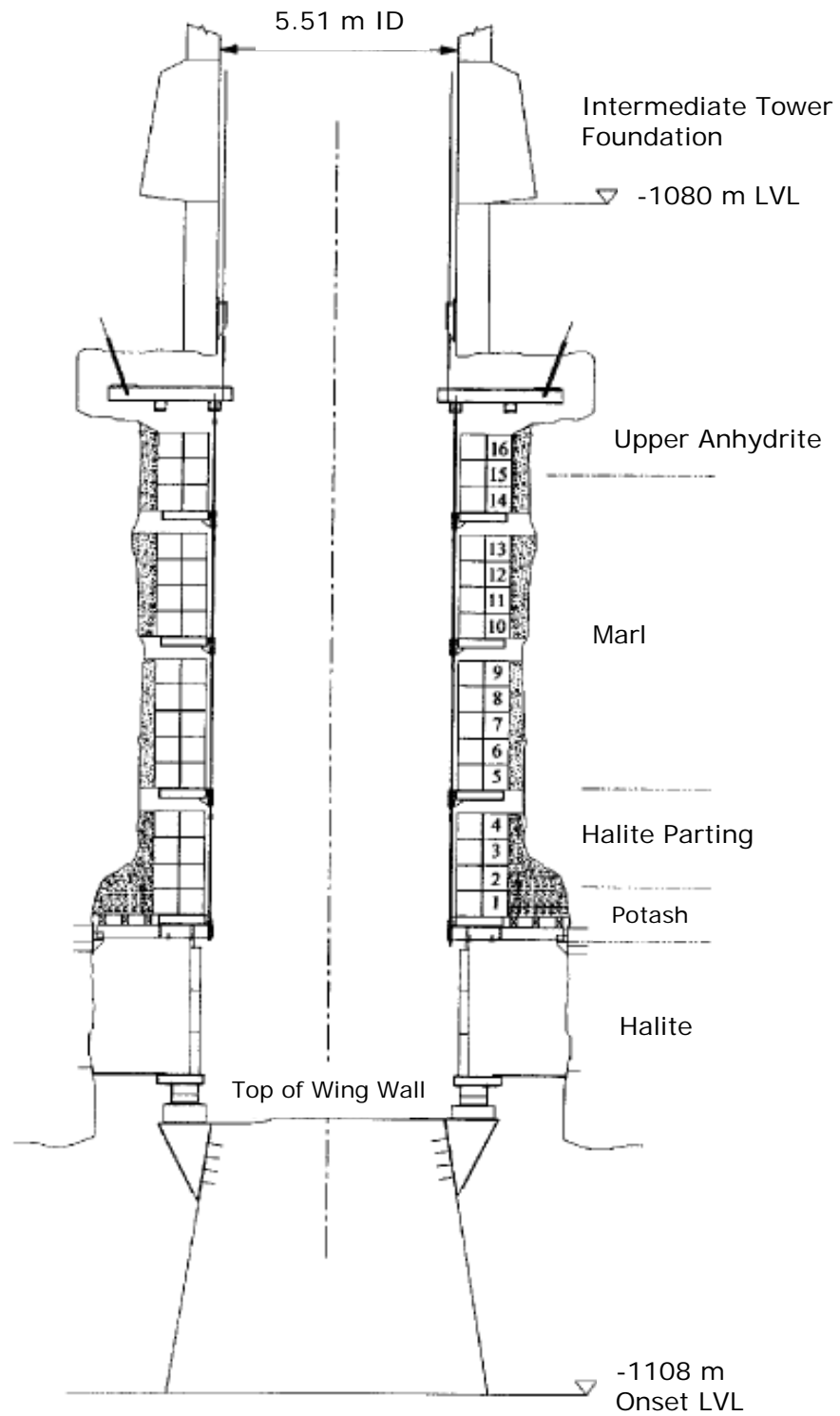


Figure 2.15 Second relining, section (Williams and Auld 2002)

Chilton and Maxwell (1989) recorded that the original shaft lining had failed in an elliptical manner, with tensile cracking on the minor axis and spalling on the major axis. The first relining failed in exactly the same manner. This failure condition should be kept in mind when any relining design is carried out. During the second relining design, some errors that had been made in the first design were realized and corrected for in the second relining design (Williams and Auld 2002), including:

- Higher assumed lining factor of safety.
- A value of full geostatic pressure of 31.01 N/mm^2 was adopted for the second relining design. The first relining was designed for a lower geostatic pressure (16.55 N/mm^2).
- The first relining design was only based on uniform geostatic pressure with the concept of the 1:2 horizontal to vertical stress ratio. The new design included a non-uniform loading condition due to the observed ovality failure and a horizontal to vertical stress ratio approaching 1:1 as full geostatic pressure was expected to be subsequently imposed on the lining with time because of time-dependent (creep) behaviour of Middle Halite and Potash.
- The lining design for the second shaft relining was based on the compatibility of deformations between the surrounding rock and the shaft lining, which had not been taken into account for the first relining design.

Precast microsilica HSC with a 28-day cube test compressive strength of 120 N/mm^2 was utilized in the form of 16 double rings of 40 blocks (Williams et al. 2001) shown in Figure 2.15. The blocks were 0.6 m high with a thickness of 0.55 m and the weight of each single block was approximately half tonne. Macalloy-bar hanging rods, attached to pile

beams located below the thrust rings associated with the foundations of the intermediate towers, supported the steel decks carrying the rings of precast concrete blocks.

Marine grade plywood squeeze packs (BS 1088: 1966), 18 mm thick, separated the blocks vertically, both in the radial direction between each block and circumferentially in the gap between the double rings. Horizontally, between each double ring, 12-mm marine-grade plywood was used as a levelling layer. Pozament GP2.5 (ordinary Portland cement–pulverized fuel ash) grout with a characteristic strength of 15 N/mm^2 (based on cubes tested at 28 days) was pumped into the gap between the back of the blocks and the excavation face to form a fill of a similar strength to the Marl (Williams and Auld 2002).

Theoretically, this new second relining had a factor of safety of 1.47 after 30 years to the lining failure stress of 18.73 N/mm^2 with a deformation capability of 33 mm, which was determined by finite-element analysis (Williams and Auld 2002).

2.6.4 The Design for the Third Relining of the Shafts

During recent years, damage to the shaft lining was increasing (Figure 2.16) and a further third relining is required. Plywood pack joints highlighted in red in Figure 2.16 show massive shear failure in the concrete lining system.

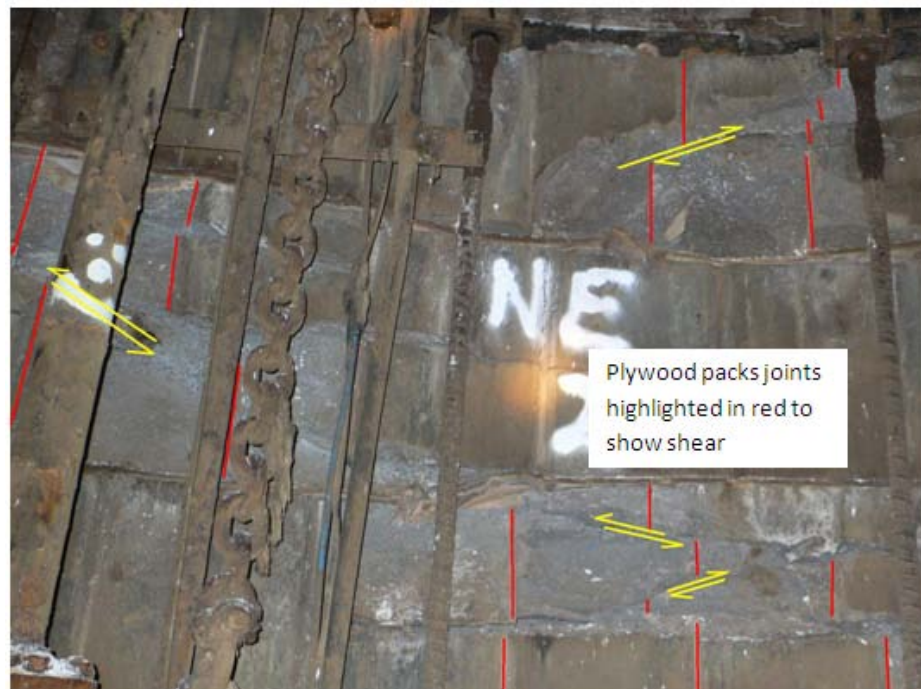


Figure 2.16 Damaged manshaft before the third relining (Boulby mine 2009)

The Boulby mine has been working on the third relining design in recent years, which combines features of the design for the first relining with those for the second relining. The third relining will be firstly started in the man shaft again in the 'bottom-up' direction. The new third relining system mainly comprises of a single ring of HSC blocks (shown in Figure 2.17) with 12 mm thick plywood packs (BS 1088: 1966) located vertically (radially) and horizontally between blocks. There will be 18 rows vertically and no construction gaps will be required, as were adopted in the first and second relining.

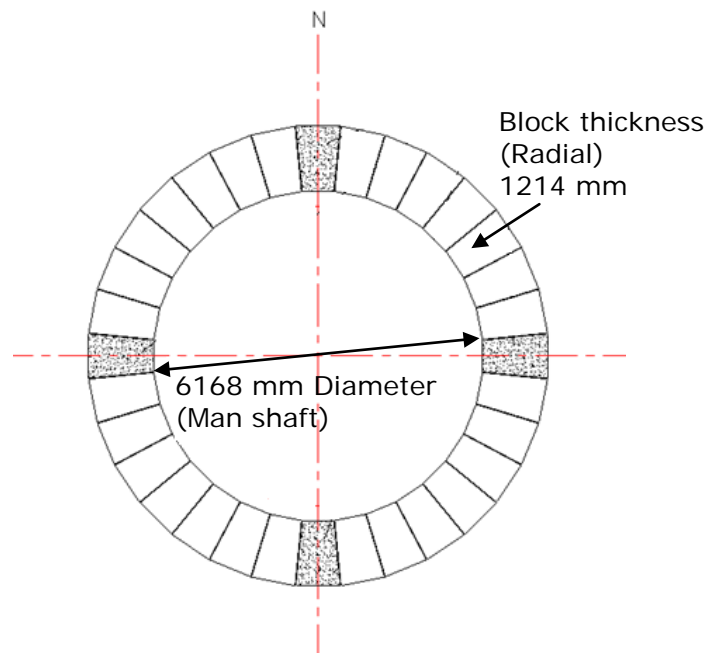


Figure 2.17 Third relining, plan (Boulby mine 2009)

Precast HSC with a 28-day cube test compressive strength of 120 N/mm^2 will be used. The blocks are 600 mm high with a thickness of 1214 mm. Each block weighs approximately 1.3 tonnes. For the backfill material in the gap between the back of the blocks and the excavation face, the cement grout used in the second relining will again be adopted. This is Pozament GP2.5 (ordinary Portland cement–pulverized fuel ash) grout with a characteristic strength of 15 N/mm^2 (based on cubes tested at 28 days).

2.6.5 Conclusions

The collected detailed data about the original shaft construction and all relinings are shown in Table 2.5. In the last four decades, the shaft linings at Boulby mine have experienced two relinings through the Marl zone and each relining has lasted less than 15 years. It has been hypothesized by the author that there was a plastic zone at the shaft periphery due to the

shaft excavation disturbance to the confined surrounding rock mass and this zone would become bigger (Figure 2.18) as the relinings were carried out. So a stronger support was required. The characteristic compressive strength of concrete used in the original shaft lining system, and the first and second shaft relinings through the Marl zone were 34.5 MPa, 100 MPa and 120 MPa, respectively. But actually the strength of the whole shaft lining system had not achieved those high values since they were not intact concrete but were discontinuous with some joints (described in section 2.6) between the concrete blocks.

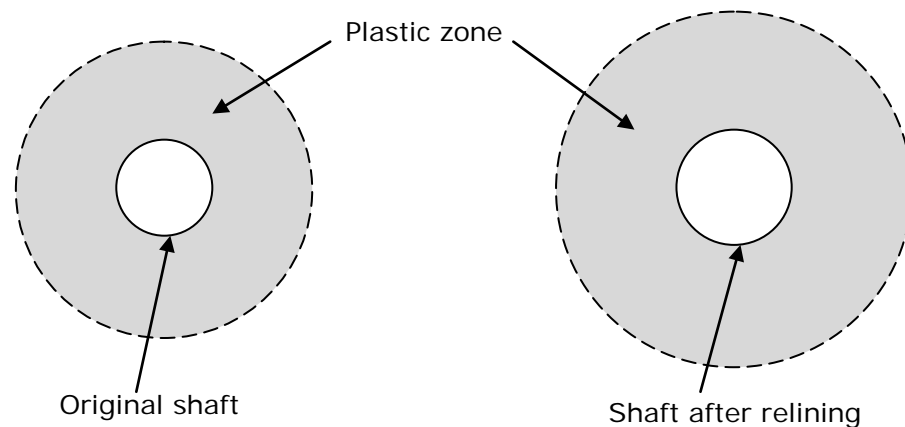


Figure 2.18 Plastic zone becoming bigger with relining (not to scale)

	Concrete lining			Backfill between the liner and excavation face	Excavation diameter	Lining inner diameter
Original lining	In situ cast concrete, 34.5 MPa;	0.75 m thick, continuous in vertical direction.		Polyurethane fill; 457 mm thick.	7.89 m	5.49 m
1st relining	Precast HSC blocks; 28 days cube compressive strength, 100 MPa;	24 levels, 36 rings in rock shaft, 32 rings in man shaft, discontinuous in vertical direction;	Blocks 610 mm high, 1067 mm thick; Rigid lining system, epoxy resin between the vertical joints and cement mortar in the horizontal joints.	Cement	Rock shaft: 7.80 m + backfill thickness Man shaft: 7.93 m + backfill thickness	Rock shaft: 5.66 m Man shaft: 5.79 m
2nd relining	Precast HSC blocks, microsilica concrete CRC; 28 days cube compressive strength, 120 MPa;	16 levels, double rings, 40 blocks in each ring, discontinuous in vertical direction;	Blocks 600 mm high, 577 mm thick; Flexible lining system, squeezable plywood packs in all joints between concrete blocks, 12 ~ 18 mm thick.	Pozament GP2.5 (OPC/PFA) grout; 28 days cube compressive strength 15MPa.	Rock shaft: similar design as man shaft Man shaft: 8.21 m + backfill thickness	Rock shaft: similar design as man shaft Man shaft: 5.86 m
3rd relining	Precast HSC blocks, microsilica concrete CRC; 28 days cube compressive strength, 120 MPa;	18 levels, single ring, 32 blocks in each ring, continuous in vertical direction;	Blocks 600 mm high, 1214 mm thick; Flexible lining system, squeezable plywood packs in all joints between concrete blocks, 12 ~ 18 mm thick.	Pozament GP2.5 (OPC/PFA) grout; 28 days cube compressive strength 15MPa.	Man shaft: 8.60 m + backfill thickness	Man shaft: 6.17m

Table 2.5 Boulby mine shaft lining sequence and information (through the Marl zone)

Based on the literature review of shaft lining and relining history at Boulby mine, another assumption has been postulated by the author in this research, with regard to the passive support load capacity of the concrete lining system involved in the shaft relining through the Marl zone. In this assumption, the actual support load capacity of each concrete lining system is supposed to be given by the thickness of concrete lining multiplied by the characteristic compressive strength of concrete, shown in Table 2.6.

Concrete lining system	Thickness of concrete lining × characteristic compressive strength of concrete (MN/m)
Original one	$34.5 \times 0.75 = 25.9$
1 st relining	$110 \times 1.07 = 107$
2 nd relining	$120 \times 1.17 = 140.4$
3 rd relining	$140 \times 1.21 = 169.4$

Table 2.6 Actual support load capacity of the concrete lining systems at Boulby mine

This conceptual assumption is illustrated in Figure 2.19. Although the actual support load capacity of the concrete lining system in history (black line in Figure 2.19) has been improved, it was still not big enough to resist increasing severe ground stress from surrounding strata (in Figure 2.19, the black line is lower than the other three lines, which represents trends of the required support load capacity of the lining system).

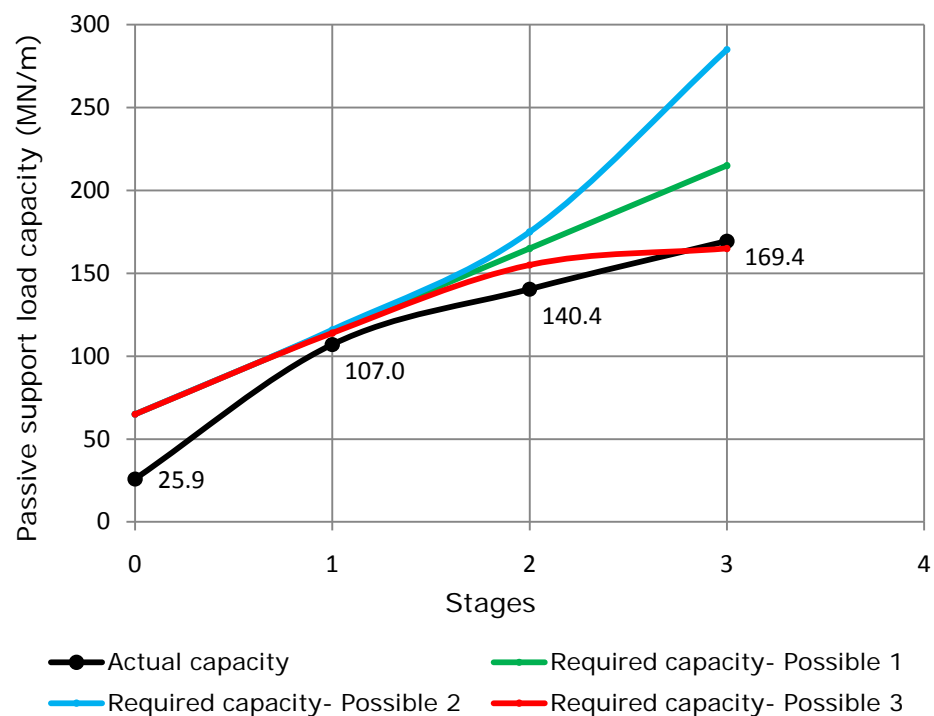


Figure 2.19 Conceptual relationship between strength of lining required and actual strength of lining

Theoretically, there are three possible trends of the required support load capacity of the concrete lining system with time (relining stages):

- In the first possible trend (green line in Figure 2.19), there is a linear relationship between the required support load capacity of the shaft lining system and time.
- In the second possible trend (blue line in Figure 2.19), the required support load capacity of the shaft lining system increases with time linearly after the shaft excavation and lining's installation. However, after some period of work time, the required capacity increases with time dramatically.
- In the third possible trend (red line in Figure 2.19), the required support load capacity of the shaft lining system increases with time

linearly after the shaft excavation and lining's installation. After some period of work time, the trend of the required capacity tends to be steady, and no big enhancement is needed for the support load capacity of the further relining system.

In the first and second trends (especially in the second trend), the lining system with ultra high support load capacity is required for the further relining system, which may be impossible to achieve in terms of design and cost in practice. On the other hand, it is thought by the author that the third trend is more likely to occur in reality because the ground stress condition in the surrounding strata will finally achieve a steady state. For the actual support load capacity of the further third shaft relining system at Boulby mine, it should be big enough to exceed the required support load capacity of the lining system to resist increasing severe pressure from surrounding strata for a much longer time.

2.7 In situ Stress Measurements at Boulby Mine

Some in situ stress measurement data of the Potash and Marl strata at Boulby mine were presented in a previous report by Potts et al (1976). Some conclusions in this report follow:

- The vertical stress in the Potash seam was $31.01 \text{ N/mm}^2 \pm 18\%$ ($25.43 \sim 36.59 \text{ N/mm}^2$);
- The horizontal stresses were $14.24 \text{ N/mm}^2 \pm 18\%$ ($11.68 \sim 16.80 \text{ N/mm}^2$) and $16.51 \text{ N/mm}^2 \pm 18\%$ ($13.54 \sim 19.48 \text{ N/mm}^2$);
- Within the tolerance of 18% the horizontal stress field in the Potash seam was uniform in all directions;
- The horizontal to vertical stress ratio, k_0 , measured in the Potash seam was approximately 1:2;

The horizontal-to-vertical stress ratio as measured in the Potash seam was approximately 1:2 (Potts et al 1976), and this led to the adoption of the design pressure of 16.55 N/mm² for the first relining design (Clifton and Maxwell 1989). However, this is only suitable for undisturbed ground conditions.

For the weak rock after the disturbance due to excavation and installation of lining, hydrostatic stresses are expected to subsequently act on the lining with time. In other words, the horizontal ground stress tends to be equal to the vertical ground stress in a weak rock mass with time. This agrees with the phenomenon and the suggestion (Heim 1912, Talobre 1957) about the in situ ground stresses described in Section 2.1: the inability of rock to support high stresses with large magnitudes differences together with the effects of time-dependent deformation of the rock mass can cause lateral and vertical stresses to equalise over periods of geological time.

The first shaft relining at Boulby mine was instrumented. Readings taken up to 750 days from installation showed a steadily increasing, uniform, horizontal stress field in the Marl section. Unfortunately, the instruments failed through corrosion (Williams and Auld 2002). During the second shaft relining, monitoring was also included in the form of 48 vibrating wire 'flat jacks' cast into and affixed to certain blocks (in rows 2, 7, 11 and 15 only in Figure 2.14). Three years after the man shaft was relined, the recorded highest tangential stress (hoop stress) was some 34 N/mm² (Figure 2.20) in the inner course of blocks in row 7 (Williams and Auld 2002) in Figure 2.14.

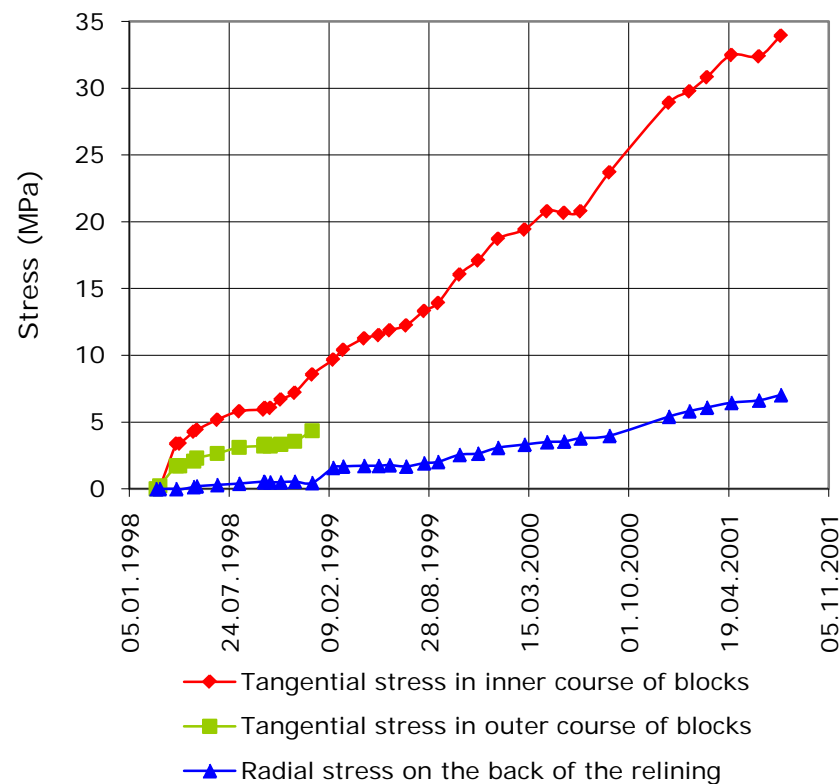


Figure 2.20 Recorded stress in row 7 in the second relining (man shaft, Williams and Auld 2002)

The extent of movement occurring in the lining exceeded that of the design and ultimately caused breaks in the cable-runs that rendered the instruments unreadable. However, up to six years of data has been collected (Boulby mine). After that, the movement occurring in the lining was too big and caused the monitoring instruments to become unreadable.

2.8 In situ Deformation Measurements at Boulby Mine

When the man shaft at Boulby mine was sunk through the Upper Halite stratum (Figure 2.9), it was instrumented in order to monitor the in situ behaviour of the rock mass around the shaft, which has been described in Cook's thesis (1974). The instrumentation consisted of four radial borehole extensometer systems installed at various orientations about the circular shaft excavation (Figure 2.21). Within each borehole, mechanical anchors

were established at distances of 0.6 m, 1.5 m, 3.0 m and 4.5 m respectively and movements were transferred to a mouth station located within the permanent concrete lining.

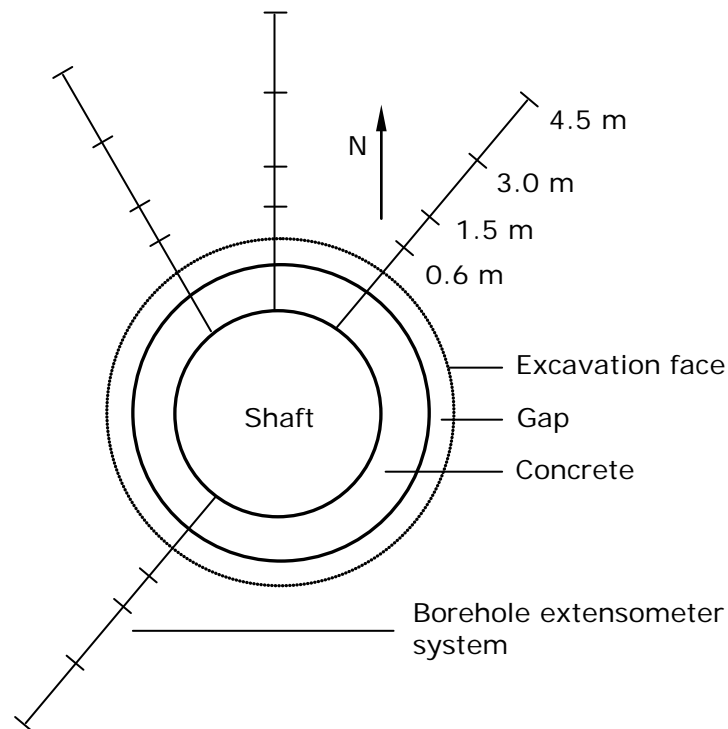


Figure 2.21 Instrumentation layouts at man shaft through Upper Halite stratum (Cook 1983)

The measured radial creep of the surrounding rock mass in the instrumented level in the Upper Halite stratum was approximately 70 mm (Cook 1983). This value included an estimate of creep during the initial 24 hours period before measurements were started, based on the initial measured rate of creep. The in situ investigation results show that:

- The movement of the surrounding rock mass was time dependent towards the shaft axis, and occurred at a distance of 4.5 m from the excavation face, which is approximately equal to one radius into the solid.

- The rock displacements at any particular radius were uniform for different orientations around the shaft which indicated that the excavation was subjected to a uniform compressive stress field and that the rock was acting as an isotropic and homogeneous material.
- Lateral movement of the permanent shaft lining through the evaporites has occurred at the instrumented level. This was probably caused by a differential settlement of the foundation crib formed in the Upper Anhydrite. The rate of the lateral movement of the lining decreased with time and after 300 days became negligible.

All these in situ stress and deformation measurements supply significant reference data for validation of numerical modelling and back-analysis research.

2.9 Chapter Summary

This chapter comprises the general literature review required for this research. The in situ ground stress state and induced stress distribution around excavations were firstly reviewed. Then, the development history of rock mass classification systems was introduced, followed by a brief summary of some of the more important classification systems. Some possible factors influencing shaft stability and two brief practical examples were then described. At the end of this chapter, all the designs for the original shaft lining and the historical relinings at Boulby mine were described in detail. This is the data on which all numerical modelling in this research were based. Some available in situ stress and deformation measurements at Boulby mine were also included. Chapter 3 focuses on the methodology of laboratory determination of input material geotechnical properties for the later numerical modelling.

CHAPTER 3

LABORATORY DETERMINATION OF GEOTECHNICAL PARAMETERS

3.1 Determination of Rock Mass Strength

3.1.1 Introduction

Reliable estimates of the strength and deformation characteristics of rock masses are required for almost any form of analysis used for the design of slopes, foundations and underground excavations. One of the major obstacles which are encountered in numerical modelling for rock mechanics problems is how to choose the appropriate input data for rock mass properties. The usefulness of elaborate constitutive models, and powerful numerical analysis programs, is greatly limited, if the analyst does not have reliable input data for rock mass properties.

As is well known, there are usually some joints and weakness planes in rock masses which act in reducing the strength of the rock mass to some value less than that of the intact rock. It is impossible in most cases to characterize the deformability and strength of rock masses using laboratory tests, because to be representative of the discontinuity and heterogeneity usually occurring in rock masses, the specimens would have to be excessively large. Even the usual in situ tests cannot supply satisfactory results in most cases, because the rock mass zone under test has been already disturbed by the excavation and the tested volumes are not yet representative of the rock mass.

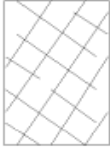
However, the laboratory tests results based on small scale rock specimens are very helpful for estimating the deformability and strength characteristics of the rock masses. The deformability and strength characteristics of the rock specimens can be obtained from the laboratory tests, the results of which are usually higher in magnitude than those of the rock masses because of fewer discontinuities in small scale rock specimens and the scale effect of tests. After that, some empirical methods, which are based on rock mass classifications (described in Chapter 2) and abundant in situ engineering experience, can be used to reduce the deformability and strength characteristics of the intact rock specimens to get those of the rock masses, which can be used in numerical modelling for rock mechanics problems.

The software program RocLab, produced by Rocscience Inc., goes a long way toward obtaining rock masses mechanical properties from the laboratory test results of the intact rock samples. This software has been used in this research project to obtain the input data for numerical modelling. This section presents the important rock strength indices used in this software, what this software can do and how this software works.

3.1.2 Geological Strength Index (GSI)

Bieniawski's RMR had been published in 1974 and has gained popularity within the rock mechanics field. However, by 1995 it had become increasingly obvious that Bieniawski's RMR was difficult to apply to very poor quality rock masses (Hoek and Marinos, 2006). A system based more heavily on fundamental geological observations and less on 'numbers' was needed. This resulted in the development of the Geological Strength Index (GSI).

GSI was proposed and developed by many researchers and geologists: Hoek et al 1995, Hoek 1994, Hoek and Brown 1997, Hoek et al 1998, Marinos and Hoek, 2001. It provides a number which is used to estimate the reduction in rock mass strength, when combined with the intact rock properties, for different geological conditions as identified by fundamental geological field observations. This system is presented in Table 3.1 and Table 3.2. Experience has shown that Table 3.1 is sufficient for field observations since the letter code that identifies each rock mass category can be entered into a field log (Hoek 2000, 2007). Later, these codes can be used to estimate the GSI value from Table 3.2. Generally, controlled blasting and bulk blasting lead to a great difference in the appearance of a rock face. Wherever possible, the undamaged face should be used to estimate the value of GSI since the overall aim is to determine the properties of the undisturbed rock mass (Hoek 2000, 2007).

ROCK MASS CHARACTERISTICS FOR STRENGTH ESTIMATES		SURFACE CONDITIONS				
<p>Based upon the appearance of the rock, choose the category that you think gives the best description of the 'average' undisturbed in situ conditions. Note that exposed rock faces that have been created by blasting may give a misleading impression of the quality of the underlying rock. Some adjustment for blast damage may be necessary and examination of diamond drill core or of faces created by pre-split or smooth blasting may be helpful in making these adjustments. It is also important to recognize that the Hoek-Brown criterion should only be applied to rock masses where the size of individual blocks is small compared with the size of the excavation under consideration.</p>		VERY GOOD Very rough, fresh unweathered surfaces	GOOD Rough, slightly weathered, iron stained surfaces	FAIR Smooth, moderately weathered or altered surfaces	POOR Slickensided, highly weathered surfaces with compact coatings or fillings of angular fragments	VERY POOR Slickensided, highly weathered surfaces with soft clay coatings or fillings
STRUCTURE		DECREASING SURFACE QUALITY ▼				
	BLOCKY - very well interlocked undisturbed rock mass consisting of cubical blocks formed by three orthogonal discontinuity sets	B/VG	B/G	B/F	B/P	B/VP
	VERY BLOCKY - interlocked, partially disturbed rock mass with multifaceted angular blocks formed by four or more discontinuity sets	VB/VG	VB/G	VB/F	VB/P	VB/VP
	BLOCKY/DISTURBED- folded and/or faulted with angular blocks formed by many intersecting discontinuity sets	BD/VG	BD/G	BD/F	BD/P	BD/VP
	DISINTEGRATED - poorly interlocked, heavily broken rock mass with a mixture of angular and rounded rock pieces	D/VG	D/G	D/F	D/P	D/VP
		DECREASING INTERLOCKING OF ROCK PIECES ▼				

In earlier versions of this table the terms BLOCKY/SEAMY and CRUSHED were used, following the terminology used by Terzaghi (1946). However, these terms proved to be misleading and they have been replaced, in this table by BLOCKY/DISTURBED, which more accurately reflects the increased mobility of a rock mass which has undergone some folding and/or faulting, and DISINTEGRATED which encompasses a wider range of particle shapes.

Table 3.1 Characterisation of rock masses on the basis of interlocking and joint alteration (Hoek and Brown, 1997)

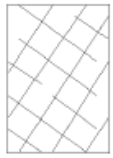
<p>GEOLOGICAL STRENGTH INDEX</p> <p>From the letter codes describing the structure and surface conditions of the rock mass (from Table 4), pick the appropriate box in this chart. Estimate the average value of the Geological Strength Index (GSI) from the contours. Do not attempt to be too precise. Quoting a range of GSI from 36 to 42 is more realistic than stating that GSI = 38.</p>		<p>SURFACE CONDITIONS</p> <p>VERY GOOD Very rough, fresh unweathered surfaces</p> <p>GOOD Rough, slightly weathered, iron stained surfaces</p> <p>FAIR Smooth, moderately weathered or altered surfaces</p> <p>POOR Slacksided, highly weathered surfaces with compact coatings or fillings of angular fragments</p> <p>VERY POOR Slacksided, highly weathered surfaces with soft clay coatings or fillings</p>				
<p>STRUCTURE</p>		<p>DECREASING SURFACE QUALITY ▾</p>				
 <p>BLOCKY - very well interlocked undisturbed rock mass consisting of cubical blocks formed by three orthogonal discontinuity sets</p>	<p>DECREASING INTERLOCKING OF ROCK PIECES ▾</p> <p>80</p> <p>70</p> <p>60</p> <p>50</p> <p>40</p> <p>30</p> <p>20</p> <p>10</p>					
 <p>VERY BLOCKY - interlocked, partially disturbed rock mass with multifaceted angular blocks formed by four or more discontinuity sets</p>						
 <p>BLOCKY/DISTURBED - folded and/or faulted with angular blocks formed by many intersecting discontinuity sets</p>						
 <p>DISINTEGRATED - poorly interlocked, heavily broken rock mass with a mixture of angular and rounded rock pieces</p>						

Table 3.2 Estimate of Geological Strength Index GSI based on geological descriptions (Hoek and Brown, 1997)

For generally competent rock masses (GSI > 25), the 1989 version of Bieniawski's RMR classification (described in Chapter 2, section 2.3) can be

used to estimate GSI (Hoek and Brown, 1997) using the following Equation (3.1),

$$GSI = RMR_{gg'} - 5 \quad (3.1)$$

RMR is the basic RMR value by setting the groundwater rating at 15 (dry) and without adjustment for joint orientation. For very poor quality rock masses ($GSI < 25$), the value of RMR is very difficult to estimate and the correlation between RMR and GSI is no longer reliable. Consequently, RMR classification should not be used for estimating the GSI values for poor quality rock masses.

3.1.3 Hoek-Brown Failure Criterion

It is usually not practical to determine directly the strength properties of the rock mass as described in section 3.1.1. Therefore rock mass failure criteria have been developed that allow estimation of the rock mass strength by reducing that of the intact rock by an amount related to the degree of discontinuity. One of the most popular and widely used rock mass failure criteria is the Hoek-Brown failure criterion (Carter et al 1991), which was first proposed in 1980. It is an empirical relation that characterizes the stress conditions that lead to failure in rock masses. The significant contribution of Hoek-Brown failure criterion was to link the mathematical equation to geological observations. At the beginning, the basic tool for geological input in this failure criterion was Bieniawski's RMR, then turned to a more sophisticated index - GSI.

One of the issues that had been troublesome throughout the development of the Hoek-Brown failure criterion has been the relationship between it (with the non-linear parameters m and s described later in this section)

and the Mohr-Coulomb criterion (with the parameters cohesion c and friction angle ϕ) (Hoek and Marinos, 2006). Since many geotechnical software programs for soil and rock mechanics are written in terms of the Mohr-Coulomb failure criterion, which is used to define the shear strength of soils and intact rocks at different applied normal stress, it is necessary to define the relationship between (m, s) and (c, ϕ) . In this way, the Hoek-Brown failure criterion can be used to determine equivalent Mohr-Coulomb parameters (cohesion c and friction angle ϕ) for each rock mass and stress range to be input into the geotechnical software.

A major revision of the Hoek-Brown criteria was carried out in order to smooth out the curves, necessary for the application of the Hoek-Brown criterion in numerical models, and to update the methods for estimating Mohr-Coulomb parameters (Hoek et al 2002). The final relationships between the Mohr-Coulomb and the Hoek-Brown criteria were derived by comparing hundreds of tunnel and slope stability analyses in which both criteria were used and the best match was found by iteration (Hoek et. al 2002). A set of equations linking the two are presented later in section 3.1.3. The Hoek-Brown criterion (2002) has been found practical in the field and appears to provide the most reliable results for use as input for methods of analysis in current use in rock engineering. A related modification for estimating the deformation modulus of rock masses was made by Hoek and Diederichs (2006).

3.1.4 RocLab Software

RocLab, produced by Rocscience Inc., is a free software program for determining rock mass strength parameters, in which the calculations are based on the latest version of the Generalized Hoek-Brown failure criterion

(Hoek et. al 2002, Hoek and Diederichs 2006). Figure 3.1 shows the RocLab software's user interface.

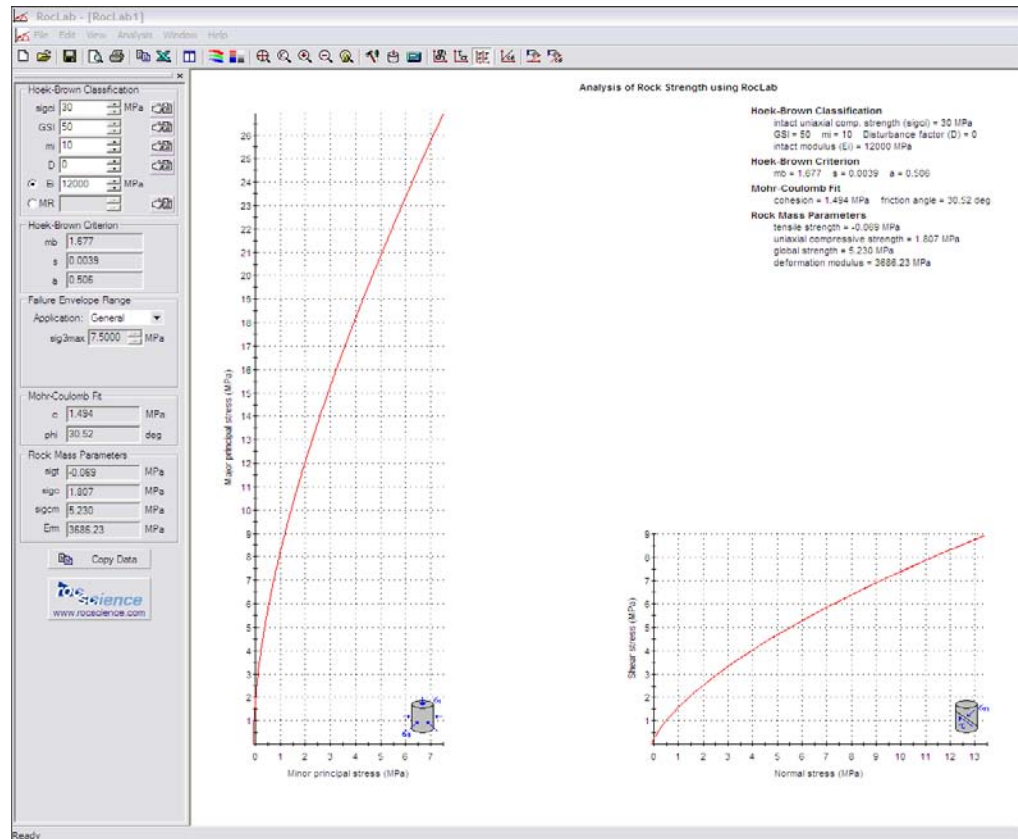


Figure 3.1 RocLab software user interface

The program RocLab provides a simple and intuitive implementation of the Hoek-Brown failure criterion, allowing users to easily obtain reliable estimates of rock mass properties including equivalent Mohr-Coulomb parameters (c , ϕ). This software also visualizes the effects of changing rock mass parameters, on the failure envelopes.

Several parameters are needed for using this software, which are listed and briefly introduced as follows:

- The geological strength index, GSI, as described in section 3.1.2
- The disturbance factor, D

D depends upon the degree of disturbance to which the rock mass has been subjected by blast damage and stress relaxation. It varies from 0 for undisturbed in situ rock masses to 1 for very disturbed rock masses. The guidelines for estimating disturbance factor D are shown in Table 3.3.

- The intact rock parameter (constant), m_i

m_i can also be determined by using triaxial lab tests data on intact rock in the RocLab software.

- Unconfined compressive strength of intact rock, σ_{ci}

σ_{ci} can be also determined by using triaxial lab tests data on intact rock in the RocLab software.

- The intact rock deformation modulus, E_i

- $\sigma'_{3\max}$

The upper limit of confining stress over which the relationship between the Hoek-Brown and the Mohr-Coulomb criteria is considered, has to be determined for each individual case.

Appearance of rock mass	Description of rock mass	Suggested value of D
	Excellent quality controlled blasting or excavation by Tunnel Boring Machine results in minimal disturbance to the confined rock mass surrounding a tunnel.	D = 0
	Mechanical or hand excavation in poor quality rock masses (no blasting) results in minimal disturbance to the surrounding rock mass. Where squeezing problems result in significant floor heave, disturbance can be severe unless a temporary invert, as shown in the photograph, is placed.	D = 0 D = 0.5 No invert
	Very poor quality blasting in a hard rock tunnel results in severe local damage, extending 2 or 3 m, in the surrounding rock mass.	D = 0.8
	Small scale blasting in civil engineering slopes results in modest rock mass damage, particularly if controlled blasting is used as shown on the left hand side of the photograph. However, stress relief results in some disturbance.	D = 0.7 Good blasting D = 1.0 Poor blasting
	Very large open pit mine slopes suffer significant disturbance due to heavy production blasting and also due to stress relief from overburden removal. In some softer rocks excavation can be carried out by ripping and dozing and the degree of damage to the slopes is less.	D = 1.0 Production blasting D = 0.7 Mechanical excavation

Table 3.3 Guidelines for estimating disturbance factor D (Hoek 2007)

The following are some of the tasks that can be accomplished with RocLab.

- **Determine rock mass deformation modulus**

Initially, the rock mass deformation modulus E_{rm} was estimated using

Equation (3.2) (Hoek and Brown 1988)

$$E_{rm} = 10^{((RMR-10)/40)} \quad (3.2)$$

This equation was modified over the years. The GSI was introduced to overcome the deficiencies in Bieniawski's RMR for very poor quality rock masses (Hoek 1994, Hoek et. al 1995). A disturbance factor D to account for stress relaxation and blast damage was also introduced (Hoek et. al 2002). Based on data from a large number of in situ measurements from China and China Taiwan, the equation was again updated (Hoek and Diederichs 2006) to be Equation (3.3), which is used in Roclab to obtain E_{rm} by inputting E_i , GSI and D.

$$E_{rm} = E_i \left(0.02 + \frac{1 - D/2}{1 + e^{((60+15D-GSI)/11)}} \right) \quad (3.3)$$

- **Determine Generalized Hoek-Brown strength parameters**

Initially, RMR and m_i were required for estimating Hoek-Brown strength parameter m_b , and only RMR were required for estimating s (Hoek and Brown 1988). Then the Generalised Hoek-Brown criterion was introduced with the application of GSI replacing RMR (Hoek 1994, Hoek et. al 1995). Hoek et. al (2002) proposed a new set of relationships between GSI, m_b , s and a to give a smoother transition between very poor quality rock masses (GSI < 25) and stronger rocks. A disturbance factor D to account for stress relaxation and blast damage was also introduced. This new set of relationships, Equations (3.4~3.6), are used in the RocLab software:

$$m_b = m_i \exp\left(\frac{GSI - 100}{28 - 14D}\right) \quad (3.4)$$

$$s = \exp\left(\frac{GSI - 100}{9 - 3D}\right) \quad (3.5)$$

$$a = \frac{1}{2} + \frac{1}{6} (e^{-GS/15} - e^{-20/3}) \quad (3.6)$$

- **Determine equivalent Mohr-Coulomb parameters**

There is no direct correlation between the Mohr-Coulomb criterion and the non-linear Hoek-Brown criterion. In the Generalized Hoek-Brown failure criterion (Hoek et. al 2002, Hoek and Diederichs 2006), Equation (3.7) is used to generate a series of triaxial test values, simulating full scale field tests, and a statistical curve fitting process by a linear regression analysis is used to derive an equivalent Mohr envelope.

$$\sigma_1' = \sigma_3' + \sigma_{ci} \left(m_b \frac{\sigma_3'}{\sigma_{ci}} + s \right)^a \quad (3.7)$$

Where σ_1' and σ_3' are the maximum and minimum effective stresses at failure, m_b , s and a are Generalized Hoek-Brown parameters.

In Roclab, the best-fit Mohr-Coulomb strength envelope is determined over a stress range that can be defined based on user application (i.e. tunneling or slope stability), in principal stress space i.e. σ_1 vs. σ_3 and/or normal – shear stress space i.e. σ vs. τ . Equivalent Mohr-Coulomb strength parameters (cohesion c and friction angle ϕ) can be calculated automatically using σ_{ci} , $\sigma_{3\max}'$ and Generalized Hoek-Brown strength parameters m_b , s and a .

The following Equations are used in the RocLab software:

$$\phi' = \sin^{-1} \left[\frac{6am_b(s + m_b\sigma_{3n}')^{a-1}}{2(1+a)(2+a) + 6am_b(s + m_b\sigma_{3n}')^{a-1}} \right] \quad (3.8)$$

$$c' = \frac{\sigma_{ci}[(1+2a)s + (1-a)m_b\sigma'_{3n}](s + m_b\sigma'_{3n})^{a-1}}{(1+a)(2+a)\sqrt{1 + (6am_b(s + m_b\sigma'_{3n})^{a-1}) / ((1+a)(2+a))}} \quad (3.9)$$

$$\text{Where } \sigma'_{3n} = \sigma'_{3\max} / \sigma_{ci}$$

- **Determine the uniaxial compressive strength (UCS) of the rock mass, σ_c**

The UCS of the rock mass σ_c can be obtained by setting $\sigma'_3 = 0$ in Equation (3.7), giving Equation (3.10), which is used in the RocLab software:

$$\sigma_c = \sigma_{ci} \times S^a \quad (3.10)$$

- **Determine the tensile strength of the rock mass, σ_t**

The tensile strength of the rock mass σ_t can be obtained by setting $\sigma'_1 = \sigma'_3 = \sigma_t$ in Equation (3.7), which represents a condition of biaxial tension. Hoek (1983) showed that, for brittle materials, the uniaxial tensile strength is equal to the biaxial tensile strength. This gives Equation (3.11), which is used in the RocLab software:

$$\sigma_t = -s\sigma_{ci} / m_b \quad (3.11)$$

3.2 Rock Materials from Boulby Mine

3.2.1 Laboratory Tests Data Collection

In the early 1970's, much of the research work on Boulby mine shafts sinking and concrete liner installation were undertaken by the University of Newcastle upon Tyne. Two PhD theses (Patchet 1970 and Cook 1974) are

often referred to by this author on the topic of tests to obtain the properties of the rock materials. Project and test reports by consultants engaged by Boulby mine in recent years, such as the RSM (2000) and the NCG (Stace et al 2007 and 2008, Jia et al 2009) have also been helpful to this research project.

The lab testing of the Boulby mine rock materials is restricted by the lack of available material. Most of the specimens were obtained from the cores of the exploratory boreholes sunk from the surface to the Potash seam. Considerable quantities of the Middle Potash, the ore body were required for chemical analysis and ore treatment investigations and this restricted the amount available for the testing programme. The laboratory testing of the borehole cores of the North Yorkshire rocks was carried out by Patchet (1970) and Cook (1974). Their test results, particularly those relating to the strength and deformation properties of the evaporite deposits, are collected together in this thesis with recent tests results (NCG test reports 09/2007 and 06/2008) on Boulby mine rock samples conducted at the NCG, as a database for obtaining the input rock properties for numerical modelling. The detailed strata sequence is shown in Figures 2.8~2.9 and the collected tests data is seen in Appendix I.

Patchet (1970) pointed out in his thesis that all the rock materials from Permian Strata (Figure 2.8) are competent, especially the Anhydrite and Polyhalite, but the Marl, nearly 10m thick just overlying the Potash seam, is the weakest rock material in the geological sequence (Figure 2.8). As a rock material, it has a very low tensile strength and as a stratum it probably has no tensile strength. It can be considered as plastic under most conditions. The Marl's position in the immediate roof is closely associated with the instability of the shaft linings.

The Marl is a weak rock and has a tendency to squeeze. This has been demonstrated by the gripping of the drill rods during boring (Squirrell 1992). This weak rock easily weathers on exposure. It is not normally exposed during mining operations, except during shaft lining restoration work. Therefore it is difficult to obtain and preserve the samples of this rock for laboratory tests, which are the most significant and reliable data source for determining the material properties. In recent tests conducted in the NCG, the Marl was not available. Only two limited sets of test data have been available and utilised for the Marl in this research: Patchet's tests (1970) and tests of the RSM (2000). The results of these two sets of tests are shown in Appendix I. Mohr-Coulomb strength envelopes have been drawn from the triaxial compression test data of these two sets of tests (shown in Figure 3.2).

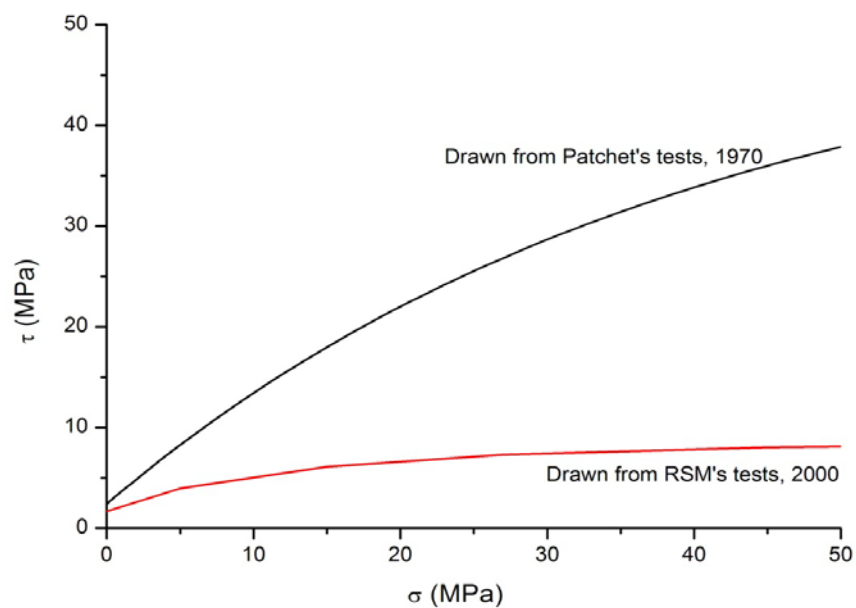


Figure 3.2 Mohr-Coulomb strength envelopes for the Marl obtained from tests data

It can be seen that the two sets of tests data show very different mechanical properties for the Marl. It is thought by the author that the

Marl samples going to the RSM were from the position near the shaft excavation face and were already heavily weathered while the samples in Patchet's tests were obtained from a more protected position and were not weathered as much.

3.2.2 Materials Properties Used in Modelling

Mohr-Coulomb failure criteria have been chosen for all rock materials from the Boulby mine. To account for the influence of scale and the presence of discontinuities in the larger rock mass, input properties (strength and stiffness) of the rock materials used in numerical models were obtained from reducing various tests results shown in the database in Appendix I. As introduced in section 3.1, the RocLab software has been utilized in this research to calculate the input properties for all rock materials in numerical models. Based on the database in Appendix I, Mohr-Coulomb properties of most of the rock materials from Permian Strata (Figure 2.9) were calculated and are listed in Appendix II.

3.3 Laboratory Tests on Concrete Used at Boulby Mine

3.3.1 Introduction

In order to obtain the input data for the concrete material in the numerical models in this research, laboratory tests on high strength concrete (HSC) from the Boulby mine have been carried out at the NCG. Four HSC blocks, one for the first relining, one for the second relining and two for the third relining of the shafts, have been supplied by the Boulby mine. Samples of HSC prepared at the NCG are shown in Figure 3.3.



Figure 3.3 Samples of concrete from Boulby mine (L: 100 mm, D: 50 mm)

It can be seen from Figure 3.3 that the coarse aggregates in the HSC used in the third relining are smooth and round-shaped, and the coarse aggregates in the HSC used in the second relining are smaller than those in the HSC used in the first and third relining. The concrete used in the second relining was most compact in structure and the concrete used in the first relining was the least compact one with sharp-shaped coarse aggregates in it.

The laboratory tests, following the methodology outlined in "Rock Characterisation Testing and Monitoring – ISRM suggested methods" (Pergamon Press 1981), on concrete from the Boulby mine included:

- UCS and Young's modulus tests on 44 samples from 3 concrete types, tests conducted on the RDP 1000 kN press (Figure 3.4). In obtained stress-strain curves for each type concrete, the average gradient at 50% of the elastic region (between the origin and yield point) was calculated as the Young's modulus of this type concrete.
- Tensile tests (Brazilian disc tensile tests) on 15 samples from 3 concrete types, tests conducted on the 200 kN Denison press.

- Single stage triaxial tests on 37 samples from 3 concrete types tested on the RDP 1000 kN press (Figure 3.5).



Figure 3.4 Test set up for UCS and Young's modulus

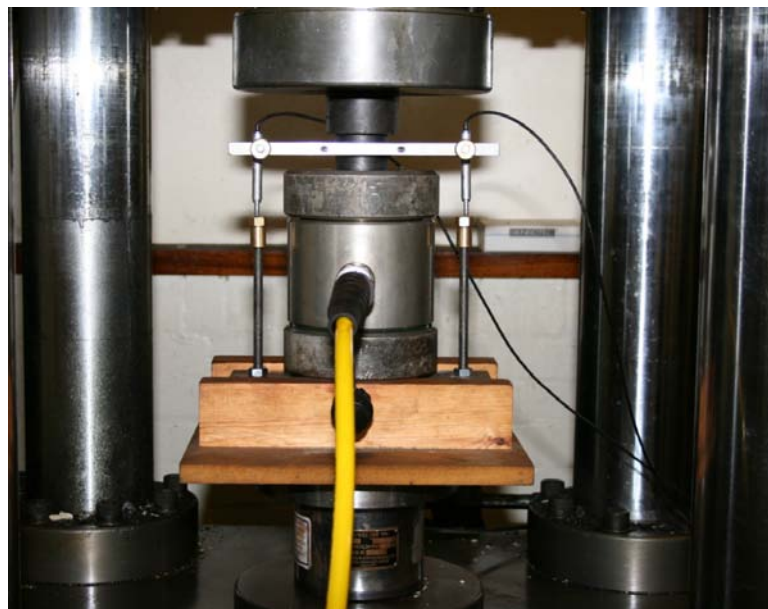


Figure 3.5 Test set up for triaxial compressive tests

3.3.2 Laboratory Tests Results and Analysis

The detailed laboratory tests data on the concrete used in the shaft relinings at Boulby mine are shown in Appendix III. Tables 3.4~3.5 summarize the average UCS tests and tensile tests results of three concrete types used at Boulby mine.

Concrete used in	Sample No.	Density (g/cm ³)	UCS (MPa)	E (GPa)	E/1000UCS (%)
1 st relining	15	2.45	92.14	32.8	35.6
2 nd relining	15	2.49	134.72	36.0	26.7
3 rd relining	14	2.46	118.8	32.7	27.5
					Mean: 29.93

Table 3.4 Average UCS and Young's modulus of HSC used at Boulby mine

Concrete used in	Sample No.	Tensile Strength (MPa)	Tensile/UCS (%)
1 st reline	5	5.47	5.9
2 nd reline	5	7.41	5.5
3 rd reline	5	8.31	7.0
			Mean: 6.13

Table 3.5 Average tensile strength of HSC used at Boulby mine

In this research, the Mohr-Coulomb model, the conventional model used to represent shear failure in soils and rocks, has been chosen for the concrete material in the numerical modelling. Vermeer and deBorst (1984) reported that laboratory test results for sand and concrete matched well with the Mohr-Coulomb criterion. The Mohr-Coulomb material properties

for the concrete obtained from the single state triaxial compressive strength tests are summarized in Table 3.6.

Concrete used in	Sample Diameter (mm)	Sample No.	Cohesion (MPa)	Friction Angle (°)
1 st reline	49	8	23.71	41
	42	5	23.00	45
2 nd reline	49	6	28.64	40
	42	5	32.50	42
3 rd reline	49	7	23.48	44
	42	9	27.07	44
			Mean: 0.23×UCS	

Table 3.6 Mohr-Coulomb properties for HSC used at Boulby mine

It can be seen that there are also conclusions on the approximate relationships of the Young's modulus-UCS, tensile strength-UCS and cohesion-UCS of these concretes in Tables 3.4~3.6. These conclusions were helpful for determining some input properties for numerical modelling in this research, which will be described later in sections 3.3.3, 3.4 and 3.5.

The concrete blocks for the 1st and 2nd relinings were more than 10 years old whereas the concrete blocks for the 3rd relining were recently fresh made. There is years' gained strength for the concrete used in the 1st and 2nd relining. At the same time, it should be noted that the samples tested in UCS tests are cylindrical and tall (Diameter near 50 mm); therefore the strengths obtained from these tests were lower than their expected characteristic strength values which are normally obtained from testing cubic samples (100 mm).

For the single stage triaxial compressive strength tests, under the same confinement, samples with smaller diameter (42 mm) gave stronger strength compared with those with bigger diameter (49 mm). Comparisons between individual test results do not take into account condition of sample flaw, e.g. air hole, aggregates size etc.

3.3.3 Material Properties Used in Modelling

Since laboratory test data of in situ cast concrete used in the original shaft lining at Boulby mine, with the exception of its UCS value (34.5 MPa) was not available, many papers, British Standards and Eurocode were referred to, to find parameters for the Young's modulus, Poisson's ratio and tensile strength of normal strength concrete (NSC). A brief conclusion of these references results is shown in Tables 3.7~3.9. The Mohr-Coulomb properties (cohesion c and friction angle ϕ) of the in situ cast concrete used in the original shaft lining were estimated based on experiences and the approximate relationship between the cohesion and UCS of the concrete (shown in Table 3.6). Based on the above laboratory tests in section 3.3.2 and references in 3.3.3, input properties for all concrete materials used in the numerical modellings for the original shaft lining and relining systems at Boulby mine are summarised in the Table 3.10.

Reference	Young's modulus (GPa)	Note
Structural Eurocode PP1990: 2007	29.8	$E_c = 22 \times (f_{cm}/10)^{0.3}$, GPa ($f_c = 0.8f_{cm}$, 15 ~ 105)
Eurocode: Design of Concrete Structures Part 1	31.25	$E_c = 9.5 \times (f_{ck} + 8)^{1/3}$, GPa ($f_c = 0.8f_{ck}$, 10 ~ 60)
Koksal, H. O. et al 2005	34.5	$E = 1000 f_c$
Arslan, G 2007	27.9	$E = 4750 f_c^{0.5}$
Hughs et al 2005	26.4	$E = 4 \times 10^4 f_c^{0.5} + 1 \times 10^6$ psi ($f_c < 80$ MPa)
BS 8110 Part 2 1985	27	$E_c = 9.1 \times f_c^{0.33}$, MPa (f_c 30 ~ 60)
Average	26	

Note: f_{cm} - Mean value of concrete cylinder compressive strength

f_c - Concrete cube compressive strength

f_{ck} - Characteristic cylinder compressive strength

Table 3.7 Young's modulus of NSC (GPa)

Reference	Poisson's ratio	Note
Dahl 1992	0.15	$\nu = 8 \times 10^{-6}(f_c)^2 + 0.0002f_c + 0.138$ (f_c 40 ~ 100)
Hussein & Marzouk 2000	0.19 ~ 0.28	
Koksal, H. O. et al 2005	0.2	f_c 10 ~ 30
Eurocode: Design of Concrete Structures Part 1	0.2	
Average	0.2	

Note: f_c - Concrete cube compressive strength

ν - Poisson's Ratio

Table 3.8 Poisson's ratio of NSC

Reference	Tensile Strength (MPa)	Note
Structural Eurocode PP1990:2007	2.75	2.6 for C30, 2.9 for C37
Eurocode: Design of Concrete Structures Part 1	2.75	2.6 for C30, 2.9 for C37
Hussein & Marzouk 2000	3.3 (cube, 40)	Test value
Koksal, H. O. et al 2005	3.45	$f_{sp} = 0.1f_c$
Ansar & Li 1998	3.1 (cylinder, 47)	Test value
Zheng et al 2001	2.44	$f_t = 0.42(f_c)^{0.5}$
Average	2.86	

Note: C30 – Concrete with compressive strength of 30 MPa (cubes tested at 28 days).

f_{cm} - Mean value of concrete cylinder compressive strength

f_c - Concrete cube compressive strength

f_t, f_{sp} - Tensile strength of concrete

Table 3.9 Tensile strength of NSC (MPa)

Concrete used in	Young's modulus (GPa)	Poisson's ratio	Cohesion (MPa)	Friction angle (°)	Tensile strength (MPa)
Original lining	26	0.2	7.94	35	2.86
1 st relining	32.8	0.2	23.71	41	5.47
2 nd relining	36	0.2	28.64	40	7.41
3 rd relining	32.7	0.2	23.48	44	8.31

Table 3.10 Input properties for all concrete materials in the numerical modelling

3.4 Interface Problems in the Shaft Lining Modelling

3.4.1 Introduction

For all the shaft relining systems at Boulby mine, HSC blocks were employed, with different materials filled between the concrete blocks each time. Adhesive materials, epoxy resin and cement mortar, were employed between the concrete blocks in the first shaft relining and squeezable plywood packs were used in the second and third shaft relinings.

All these materials compose many "joints" in the concrete relining systems. These joints were actually very thin, 12~18 mm in thickness, compared to the concrete blocks dimensions (around 0.5 m × 0.5 m). However, these joints are important to the mechanical behaviour of the whole concrete lining systems. Because of finite difference mesh generation limitation described later in Chapter 4, solid elements with some thickness cannot be used to represent these materials in the numerical models. To solve this problem, interface elements with appropriate properties have been built into models to be used to represent epoxy resin/cement mortar/plywood packs between concrete blocks in the numerical modelling in this research.

An interface is represented as a normal and shear stiffness (K_n and K_s) between two planes which may contact each other in numerical models. The following material properties are needed for the interface elements used in the Boulby mine shaft lining modelling:

- K_n , Normal stiffness
- K_s , Shear stiffness
- C , Cohesion
- ϕ , Friction angle

- σ_t , Tensile strength

The bonding at interfaces in concrete structures is important for safety and durability (Kunieda et al 2000). Therefore, the performance of the whole restored concrete lining is strongly dependent on the performance of the interfaces. The chances of failure by cracking along the interface are higher because of stress concentrations and rapid change of stress levels along them (Lim et. al 2001). Furthermore, Santosh and Kishen's experimental (2010) results implied that the greater the difference in compressive strength or elastic moduli mismatch between the materials on both sides of the interface, the greater is the vulnerability to cracking and failure for the same loading configuration.

The interfaces used in this numerical modelling project allow slip and separation. For this type of interface, the strength properties (friction angle ϕ , cohesion c and tensile strength σ_t) are important, but the stiffness properties are not (Itasca 2008). A good rule-of-thumb is that K_n and K_s be set to *ten times* the equivalent stiffness of the stiffest neighbouring zone (Itasca 2008). In this research, the results of the early three dimensional numerical models implied that setting different values for K_n with K_s made no difference to the modelling results. Therefore, the same value was assigned to both K_n and K_s for simplification in this research. K_n , K_s and the apparent stiffness (expressed in stress per distance units) of a zone in the normal direction are calculated using the Equations (3.12~3.14):

$$K_n = K_s = 10 \times \max\left[\frac{B + \frac{4}{3} S}{\Delta Z_{\min}}\right] \quad (3.12)$$

$$B = \frac{E}{3(1 - 2\nu)} \quad (3.13)$$

$$S = \frac{E}{2(1 + \nu)} \quad (3.14)$$

Where E , B and S are the Young's modulus, bulk and shear moduli, respectively; ν is the Poisson's ratio; and ΔZ_{\min} is the smallest width of an adjoining zone in the normal direction (Figure 3.6). The "max" notation indicates that the maximum value over all zones adjacent to the interface is to be used (e.g., there may be several materials adjoining the interface).

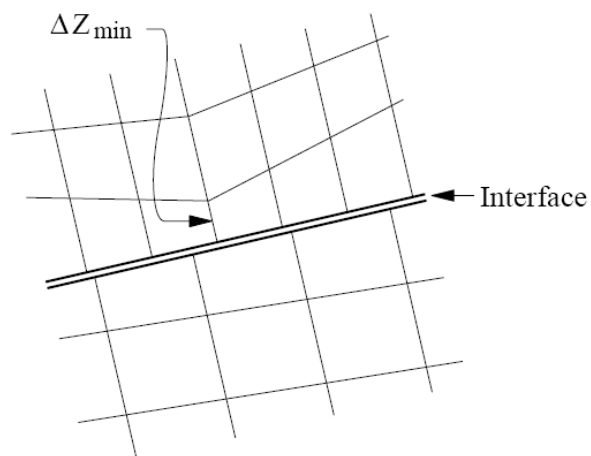


Figure 3.6 Zone dimension used in stiffness calculation (Itasca 2008)

In the following sections, the input stiffness properties for the interface elements used in the numerical models in this research have been calculated using Equations (3.12~3.14), and the strength properties have been estimated from the laboratory tests data and some standards on strength properties of the related materials.

3.4.2 Interfaces between Epoxy Resin and Concrete

Epoxy resin was used as an adhesive between concrete blocks in each single layer in the first relining of the Boulby mine shaft lining. Epoxy resins are the most important class of thermosetting resins for many engineering applications because of their outstanding adhesion to most surfaces, superior mechanical properties (strength and stiffness), low shrinkage and good thermal characteristics (Vabrik et. al 1998, Denq et. al 1999, Kaji et. al 1999, Yang et. al 2007). The use of epoxy resin in civil engineering has been established for over half of a century. For example, use as construction adhesives between pre-cast elements, use as structural mortars and application in concrete repairs works. Being liquid tight and fast curing make them popular as concrete repairing adhesives and joint fillers having a tough and solid network (Spee et. al 2006).

In civil engineering applications, epoxy resins are almost invariably used directly bonded to concrete or other cementitious material. Table 3.11 shows the comparison of the mechanical and other properties of the epoxy resin system with those of cementitious grout (Tabor 1978). It can be seen from Table 3.11 that the epoxy resin system has a lower Young's modulus than the cementitious grout system and this has to be taken into account when choosing input properties for the interfaces between the epoxy resin and concrete in numerical modelling. The data in Table 3.11 also implies that the bond, tensile and shear strengths of correctly formulated epoxy resin based adhesives are considerably higher than those of good quality traditional cementitious mortar jointing techniques. Epoxy resin makes the joined sections as strong as monolithic concrete and allows them to remain waterproof (long-term), even when the joints are less than 1 mm thick (Shaw 1982).

	Grouts, mortars and concretes	
	Epoxy resin	Cementitious
Compressive strength (MPa)	55 - 110	20 - 70
Young's modulus (GPa)	0.5 - 20	20 - 30
Flexural strength (MPa)	25 - 50	2 - 5
Tensile strength (MPa)	9 - 20	1.5 - 3.5
Elongation at break (%)	0 - 15	0
Water absorption, 7 days at 25°C (%)	0 - 1	5 - 15

Table 3.11 Physical properties – a comparison of typical products (Tabor 1978)

According to British Standard BS 7861-1:2007, the polyester resin used to achieve a bond between a rockbolt and the strata in coal mines should have the Young's modulus greater than 11 GPa and the UCS greater than 80 MPa, which is much higher than that of NSC. Based on the reference data above, for the interfaces between the epoxy resin and concrete blocks in the first relining system, the cohesion c and friction angle ϕ of the first relining concrete (bigger samples' results, shown in Table 3.6) was chosen as those of the interfaces; the middle value of the tensile strengths shown in Table 3.11 was chosen as the tensile strength.

For calculating the stiffness properties of the interface in the first relining system, the stiffest neighbouring material for the interface is the HSC concrete with Young's modulus of 32.8 GPa and Poisson's ratio 0.2 (Table 3.10). The minimum zone size adjacent to the interface is designed to be 1.34 m for the first shaft relining model in this research. Therefore, according to the Equations (3.12~3.14), for the interfaces between the

epoxy resin and concrete blocks in the first relining system, the stiffness is 272 GPa/m. The final chosen input properties for the interfaces between the epoxy resin and concrete blocks in the numerical modelling of the first relining in this research are shown in Table 3.12.

	K_n (GPa/m)	K_s (GPa/m)	Cohesion (MPa)	Friction angle (°)	Tensile strength (MPa)
Interfaces	272	272	23.71	41	14.5

Table 3.12 Input properties for the interfaces elements representing the epoxy resin between concrete blocks

3.4.3 Interfaces between Cement Mortar and Concrete

In the first relining of the mine shafts, epoxy resin was used to bond pre-cast concrete blocks together to form rings, then cement mortar was used to bond several concrete-block rings together to form a section. It can be seen as a masonry structure. In order to obtain the mechanical properties of the cement mortar used in the masonry structure, the European Standard for masonry cement BS EN 413-1: 2004 has been referred to. Table 3.13 shows the 28 days compressive strength requirements given as characteristic values for different types of masonry cement.

Type	28 day (standard) strength (MPa)	
MC 5	≥5	≤15
MC 12.5 MC 12.5 X	≥12.5	≤32.5
MC 22.5 X	≥22.5	≤42.5

Table 3.13 Compressive strength requirements given as characteristic values for masonry cement (BS EN 413-1: 2004)

British Cement Association (BCA) points out that its member companies will manufacture masonry cement to class MC 12.5 of BS EN 413-1: 2004. Therefore, it was assumed that MC 12.5 has been used in the first relining of the Boulby mine shafts, with 28 days compressive strength of 12.5 MPa. For the Young's modulus and tensile strength of the masonry cement, the following assumptions based on generalised test data are adopted (Wilson 1980, Reddish 1989), which also approximately agree with the laboratory tests data shown in Tables 3.4 and 3.5:

$$E = 300 \times UCS = 3.75 \text{ GPa} \quad (3.15)$$

$$UTS = \frac{1}{10} \times UCS = 1.25 \text{ MPa} \quad (3.16)$$

Where E is Young's modulus, UCS is uniaxial compressive strength and UTS is tensile strength.

Usually the interface between the cement mortar and concrete is relatively weaker than the material on either side of it. Based on reference data and analysis above, 80% of the cement mortar's tensile strength 1 MPa was chosen as the tensile strength. Table 3.6 shows that in Mohr-Coulomb properties for concrete tested in this research, cohesion is approximately 23% of the UCS . This guideline has been utilised to estimate the cohesion of the interfaces between the cement mortar and concrete blocks in the first relining system. Therefore a slightly lower value, 20% of the masonry cement's UCS , 2.5 MPa, was chosen as the cohesion of the interfaces between the cement mortar and concrete blocks in the first relining system.

The stiffest neighbouring material for the interface is still the HSC concrete. However, for the interfaces between the cement mortar and concrete

blocks in the first relining system, the minimum zone size adjacent to the interface is designed to be 0.6 m in the numerical model in this research. Therefore, according to the Equations (3.12~3.14), for the interfaces between the cement mortar and concrete blocks in the first relining system, the stiffness is 607 GPa/m. The final chosen input properties for the interfaces between the cement mortar and concrete blocks in numerical modelling of the first relining in this research are summarised in Table 3.14.

	K_n (GPa/m)	K_s (GPa/m)	Cohesion (MPa)	Friction angle (°)	Tensile strength (MPa)
Interfaces	607	607	2.5	30	1

Table 3.14 Input properties for the interfaces elements representing the cement mortar between concrete blocks

3.4.4 Interfaces between Plywood Pack and Concrete

The marine grade plywood packs (BS 1088: 1966) were employed between the concrete blocks in the second and third relinings of the Boulby mine shaft lining. The interface elements employed in numerical modelling to represent the plywood packs were without tensile strength since plywood packs were not glued to the concrete blocks in the relining systems. The mechanical properties of the interface between the plywood pack and the concrete blocks were taken from an analysis of compression tests results supplied by Boulby mine and direct shear test (shear box tests) conducted at the NCG.

For the direct shear test (shear box tests) between the plywood pack and concrete block, the auto-shear–direct and residual automatic shear

apparatus (Mod: 27–WF2160, produced by Wykeham Farrance) was utilized. The test equipment consist of a metal shear box in which the sample is placed as shown in diagram Figures 3.7. The box is split horizontally into two halves. Normal force on the sample is applied from the top of the shear box by dead weight. Shear force is applied to the side of the top half of the box to cause failure in the sample.

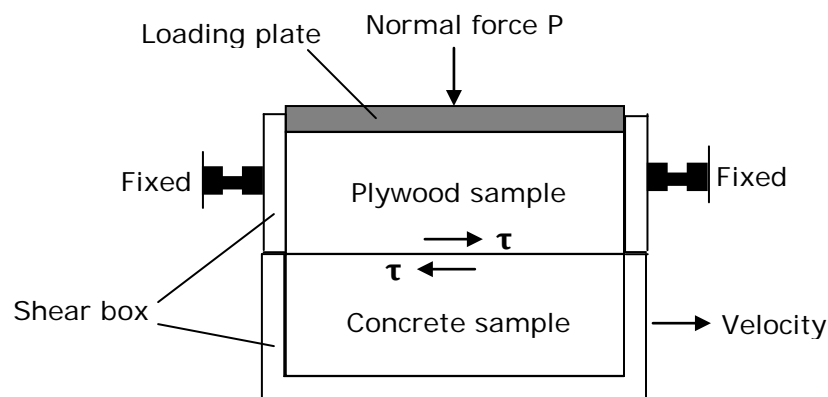


Figure 3.7 Diagram of direct shear test

For the given test, the normal stress and shear stress can be calculated using Equations (3.17~3.18):

$$\sigma = \frac{\text{normal force}}{\text{area of crossection of sample}} = \frac{P}{A} \quad (3.17)$$

$$\tau = \frac{\text{shear force}}{\text{area of crossection of sample}} = \frac{T}{A} \quad (3.18)$$

The test was repeated more than three times with different value for force P (normal force) and difference value for force T (shear force). Mohr-Coulomb properties (cohesion c and friction angle ϕ) then could be obtained from the $\sigma - \tau$ curve.

In this research, the dimension of the marine plywood (BS: 1088) samples was 100 mm×100 mm×18 mm, and the dimension of the concrete blocks was 97 mm×97 mm×20 mm (Figure 3.8), which is NSC (when the direct shear tests were carried out, the HSC blocks used at Boulby mine were not available. So NSC samples were utilised and it was assumed that it would not influence the results much).



Figure 3.8 Marine plywood and concrete samples used in direct shear test

The surface of the plywood sample used in this test was not smooth but with parallel texture shown in Figure 3.8, which would influence the test results. Therefore, two groups of direct shear tests between the concrete sample and the plywood sample have been carried out. In one group test, the shear force direction was parallel to the texture of the plywood surface and in the other group test, the shear force direction was perpendicular to the texture of the plywood surface. For each group tests, the applied shearing rate was 1 mm/min and the applied normal force were 30, 50, 100, 150 kN. The obtained $\sigma - \tau$ curves linearly fitted from the test points are shown in following Figures 3.9 and 3.10.

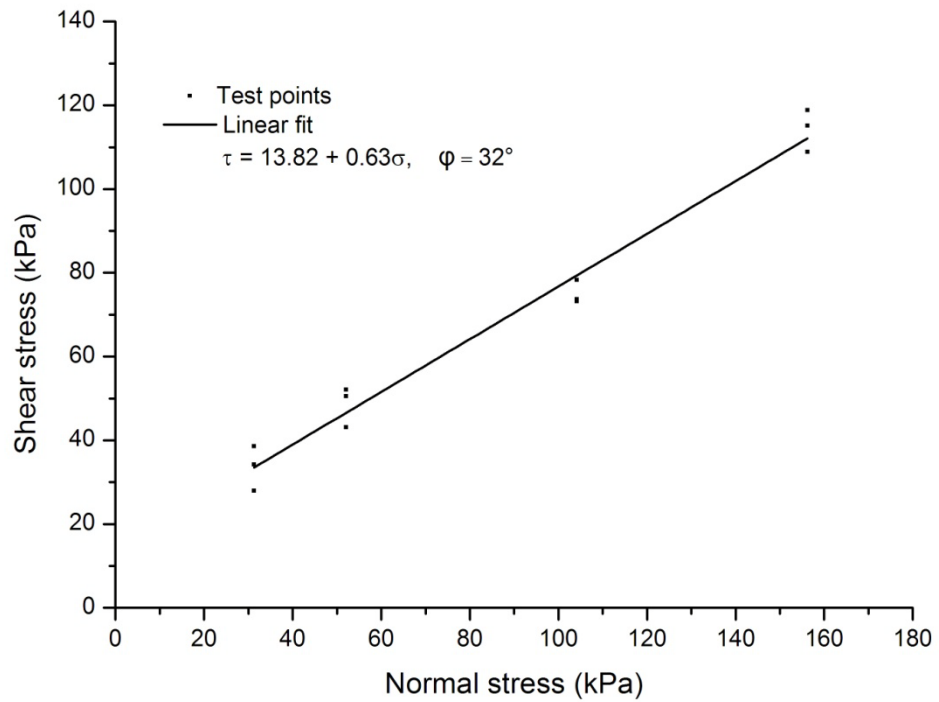


Figure 3.9 $\sigma - \tau$ curves obtained from the direct shear tests: shear force perpendicular to the texture of the plywood surface

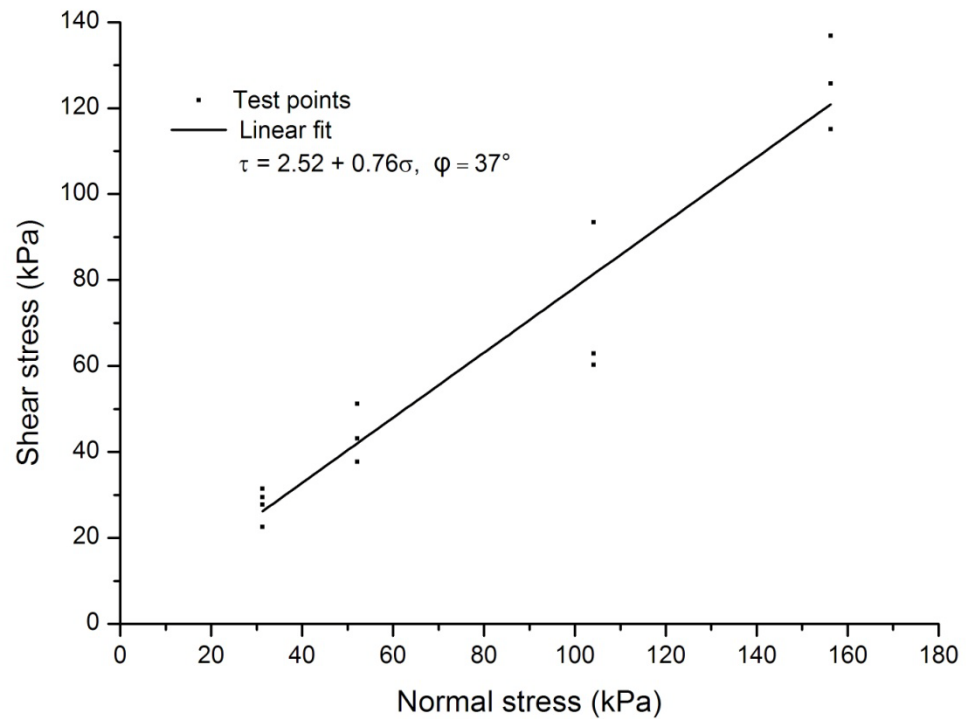


Figure 3.10 $\sigma - \tau$ curves obtained from the direct shear tests: shear force parallel to the texture of the plywood surface

It can be seen from Figures 3.9~3.10 that two groups of Mohr-Coulomb properties (cohesion c and friction angle φ) had been gained, and are shown in Table 3.15. For simplification, the mean values of the two groups' Mohr-Coulomb properties (cohesion c and friction angle φ) were utilised for the interface elements representing the plywood packs between the concrete blocks in the second and third relining modelling in this research.

When the shear force direction is:	Cohesion (kPa)	Friction angle (°)
Perpendicular to the texture of the plywood surface	13.82	32
Parallel to the texture of the plywood surface	2.52	37
Mean value	8.17	35

Table 3.15 Mohr-Coulomb properties obtained from the plywood-concrete direct shear test

Boulby mine (2009) had a series of compression test data on the plywood packs (BS 1088: 1966), in which a compressive stress of 75 MPa was applied to plywood samples. Only one typical group test data has been supplied to this research shown in Table 3.16, in which the original thickness of the sample was 17.1 mm. The complete stress-strain curve is shown in Figure 3.11.

Stress	Strain	Compression rate in thickness
MPa		%
7.9	0.041	4%
23.6	0.409	41%
39.3	0.541	54%
55.0	0.596	60%
70.7	0.632	63%
86.5	0.655	65%
102.2	0.678	68%
117.9	0.696	70%
133.6	0.708	71%

Table 3.16 Compression test data on plywood sample (Boulby mine 2009)

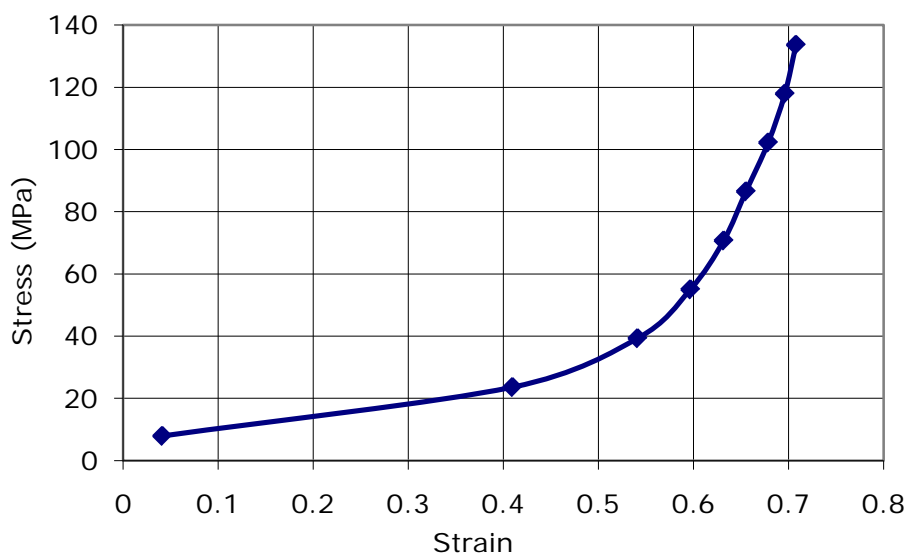


Figure 3.11 Stress-strain curve for the plywood pack used in relining systems (Boulby mine 2009)

It was thought that the residual behaviour of the plywood pack in the compression test was a key factor to the Young's modulus of the plywood pack. Based on the typical group test data supplied by Boulby mine, the

Young's modulus of the plywood packs was calculated from the steeper part of the stress-strain curve in Table 3.16 and Figure 3.11 (strain from 0.596 to 0.708), using the following Equation (3.19):

$$E = \frac{\Delta\sigma}{\Delta\varepsilon} \tag{3.19}$$

Where E is the Young's modulus, $\Delta\sigma$ is the normal stress difference and $\Delta\varepsilon$ is the strain difference.

According to the Equation 3.19, the Young's modulus of the plywood packs is 0.7 GPa. Therefore, in the second and third relining systems, the stiffest neighbouring material for the interface is still the HSC concrete, the stiffness properties of which are shown in Table 3.10. The minimum zone size adjacent to the interface is designed to be 0.6 m for the second and third shaft relinings model in this research. Therefore, according to the Equations (3.12~3.14), for the interfaces between the plywood pack and concrete blocks in the second relining system, the stiffness is 667 GPa/m. For the interfaces between the plywood pack and concrete blocks in the third relining system, the stiffness is 606 GPa/m. All the properties for the interface elements representing the plywood pack between the concrete blocks in second and third relining modelling in this research are summarised in Table 3.17.

Interface in	K_n (GPa/m)	K_s (GPa/m)	Cohesion (kPa)	Friction angle (°)
2 nd relining	667	667	8.17	35
3 rd relining	606	606	8.17	35

Table 3.17 Input properties for the interfaces elements representing the plywood pack between concrete blocks

3.5 Other Parameters used in the Shaft Lining Modelling

3.5.1 Material Properties of Polyurethane and Vermiculite

Polyurethane and vermiculite were utilised as backfill materials in the gap between the concrete liner and the shaft excavation face in the original shaft lining system at Boulby mine. In the numerical modelling in this research, both of these two backfill materials were set to be elastic at all positions to make the numerical calculation faster.

Goodall et al (2002) in University of Cambridge have carried out experiments to measure the stiffness of vermiculite and the results (Table 3.18) show the highly anisotropic nature of vermiculite particles, which exhibit a stiffness nearly 20 times greater in-plane than in the through-thickness direction. Moreover, the stiffnesses in both directions are very low, due to the open exfoliated structure of vermiculite. A low value, 1 MPa was chosen as Young's modulus of the vermiculite in this study.

Material	Young's modulus (MPa)
Vermiculite through thickness	1.0
Vermiculite in-plane	19.9

Table 3.18 The stiffness measured in the compression and nano-indentation tests (Goodall et al. 2002)

With regard to the Poisson's ratio of the polyurethane, it was reported by Campbell (2007) that the polyurethane foam normally has a positive Poisson's ratio when it is stretched. However, when the foam is compressed, it has a negative Poisson's ratio. Gercek (2007) also made a conclusion from previous researchers' study that polymer foam with an inverted or re-entrant cell structure has a negative Poisson's ratio.

However, no value has been found as a reference for the Poissons' ratio of the polyurethane. Therefore, it has been hypothesised that the Poisson's ratio for the polyurethane was zero because of lack of any information. The densities and the Young's modulus of the polyurethane (Table 3.19) were chosen referring to www.shopmaninc.com/foam.html. The vermiculite was thought to have a higher density than the polyurethane and for its Poisson's ratio, it was also assigned zero due to lack of any information. The input material properties for the polyurethane and vermiculite used in this study are summarized in the Table 3.19.

Materials	Density (kg/m ³)	Young's modulus (MPa)	Poisson's ratio
Polyurethane	55	5	0
Vermiculite	110	1	0

Table 3.19 Input properties for polyurethane and vermiculite in the numerical modelling

3.5.2 Material Properties of Cement Grout

A cement grout, Pozament GP2.5 (ordinary Portland cement–pulverized fuel ash) grout with a characteristic strength of 15 N/mm² (based on cubes tested at 28 days) was pumped into the gap between the back of the blocks and the excavation face in the second and third relinings of the Boulby mine shaft lining. It aimed to form a fill of a similar strength to the Marl (Williams & Auld 2002). For simplification, it was assumed in this research that this kind of cement grout had the same material properties as the cement mortar described in the section 3.4.3, which are also similar to those of the Marl. The input properties of the cement grout used in the numerical modelling are shown in Table 3.20.

	Young's modulus (GPa)	Poisson's ratio	Cohesion (MPa)	Friction angle (°)	Tensile strength (MPa)
Cement grout	3.75	0.2	2.88	25	1.25

Table 3.20 Input properties of the cement grout used in the numerical modelling

3.6 Chapter Summary

Chapter 3 concentrates on the methodology of laboratory determination of input geotechnical parameters for all the materials used in the later numerical modellings. Firstly, the RocLab software was introduced, which was used to obtain the input properties for rock materials from Boulby mine used in the numerical modelling. After that, all the related laboratory tests data from previous rock mechanics research at Boulby mine were collected comprising a database, including Patchet's tests (1970), Cook's tests (1974) (both from the University of Newcastle upon Tyne), tests conducted in the RSM (2000) and the NCG (2007~2009). Based on this database, the input properties for the rock materials and concrete used in the numerical modellings were obtained.

Input properties for other support materials used in the numerical modellings were also obtained (by referring to papers, British standards or analysing tests data) and listed in this chapter, such as interfaces between different backfill materials and concrete blocks, backfill materials in the gap between the concrete lining and the excavation face.

The commercial finite difference code FLAC^{2D}/FLAC^{3D} will be briefly introduced in the following Chapter 4.

CHAPTER 4

INTRODUCTION OF FLAC^{2D}/FLAC^{3D}

4.1 Introduction

Fast Lagrangian Analysis of Continua (FLAC^{2D}, Itasca) is a two-dimensional explicit finite difference program and has been specially developed for geotechnical and mining engineering mechanics computation. This program can simulate nonlinear behaviour of structures built of soil, rock or other materials that may undergo plastic collapse and flow when their yield limits in shear or tension are reached. This kind of modelling can be treated very effectively and accurately with Mohr-Coulomb and other elasto-plastic constitutive models, as can nonlinear response associated with large strains and deformations. A variety of functions allow supports such as roof bolts, steel arches and liners to be incorporated into the model.

FLAC^{3D} is developed based on the well-established two-dimensional program and has essentially the same capabilities as FLAC^{2D} at present. Therefore, many of the two-dimensional applications can now be extended into three dimensions with FLAC^{3D}. The main difference between them is that three-dimensional analyses generally need much more random access memory (RAM) and CPU time than a similar two-dimensional model does.

4.2 Fields of Application

FLAC^{2D}/FLAC^{3D} has been used extensively, primarily for analysis and design in mining engineering and underground construction. The explicit, time-marching solution of the full equations of motion (including inertial

terms) permits the analysis of progressive failure and collapse, which are important phenomena in studies related to mine design. Some possible applications of these softwares are noted below.

- Mechanical loading capacity and deformations — in slope stability and foundation design;
- Evolution of progressive failure and collapse — in hard rock mine and tunnel design;
- Factor-of-safety calculation — in stability analyses for earth structures, embankments and slopes;
- Evaluation of the influence of fault structures — in mine design;
- Restraint provided by cable support on geologic materials — in rock bolting, tiebacks and soil nailing;
- Fully and partially saturated fluid flow, and pore-pressure build-up and dissipation for undrained and drained loading — in groundwater flow and consolidation studies of earth-retaining structures;
- Time-dependent creep behaviour of viscous materials — in salt and potash mine design;
- Dynamic loading on slip-prone geologic structures — in earthquake engineering and mine rock-burst studies;
- Dynamic effects of explosive loading and vibrations — in tunnel driving or in mining operations;
- Seismic excitation of structures — in earth dam design;
- Deformation and mechanical instability resulting from thermal-induced loads — in performance assessment of underground repositories of high-level radioactive waste; and
- Analysis of highly deformable materials — in bulk flow of materials in bins and mine caving.

4.3 Fundamental Components of a Problem

FLAC^{2D}/FLAC^{3D} offers a wide range of capabilities to solve complex problems in mechanics, and especially in geomechanics. In order to set up a model to run a simulation, five fundamental components of a problem must be specified:

- A finite difference grid
- Boundary conditions
- Initial stress conditions
- Constitutive model
- Material properties

After these conditions are defined in numerical models, the initial equilibrium state is calculated for the model. An alteration is then made (e.g., excavate material or change boundary conditions), and the resulting response of the model is calculated. The general solution procedure, illustrated in Figure 4.1, is convenient because it represents the sequence of processes that occurs in the physical environment.

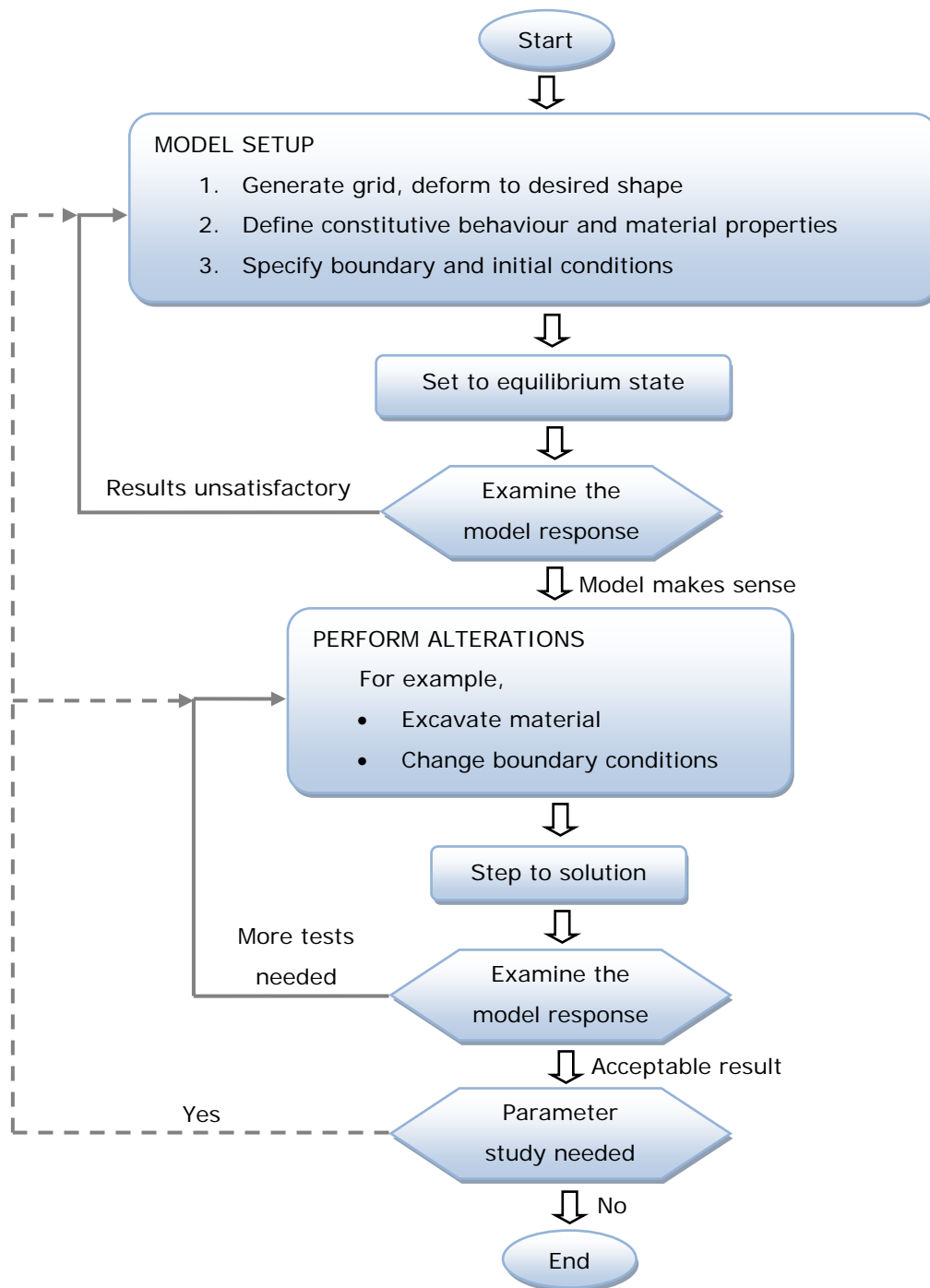


Figure 4.1 General solution procedure (Itasca, 2008)

4.3.1 Finite Difference Grid

The finite difference grid, organised in a row and column fashion, defines the physical geometry of the problem under study. In two-dimensional

models, grids are composed of convex quadrilateral elements. In three-dimensional models, discretization of the volume under study is done into hexahedral zones by default. The user also has the capability to import a tetrahedral mesh into three-dimensional models.

The finite difference grid size and zone numbers must be decided on a balance between the accuracy of results required and the computational time (the solution speed). In general, the finer the meshes are, the more accurate the results should be. However, the increase of the zone numbers may lead to a decrease in computation speed and an increase in computer memory requirements. So relatively fine meshes are defined where the stress or strain gradients are high (e.g., in the vicinity of excavations) and other parts of the model are represented by a coarse grid to obtain the balance, which is illustrated in Figure 4.2.

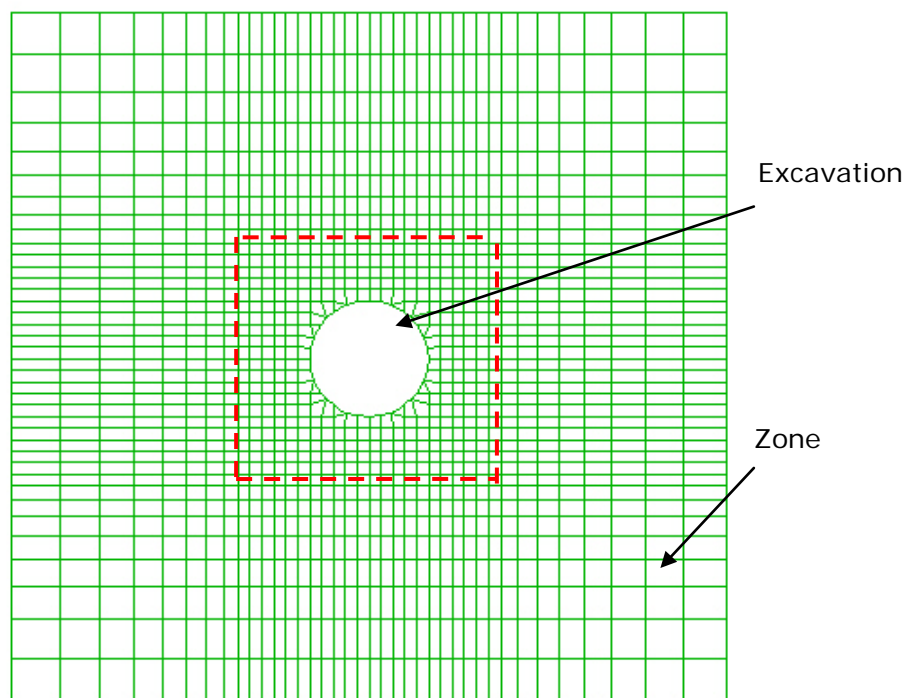


Figure 4.2 Gradually changed mesh: fine mesh in the vicinity of excavation (inside red dashed line), coarse mesh in other parts of the model

For the maximum accuracy, the zone size should increase or decrease gradually (Figure 4.2) with a specific ratio to prevent a sudden change in neighbour zone size (Figure 4.3).

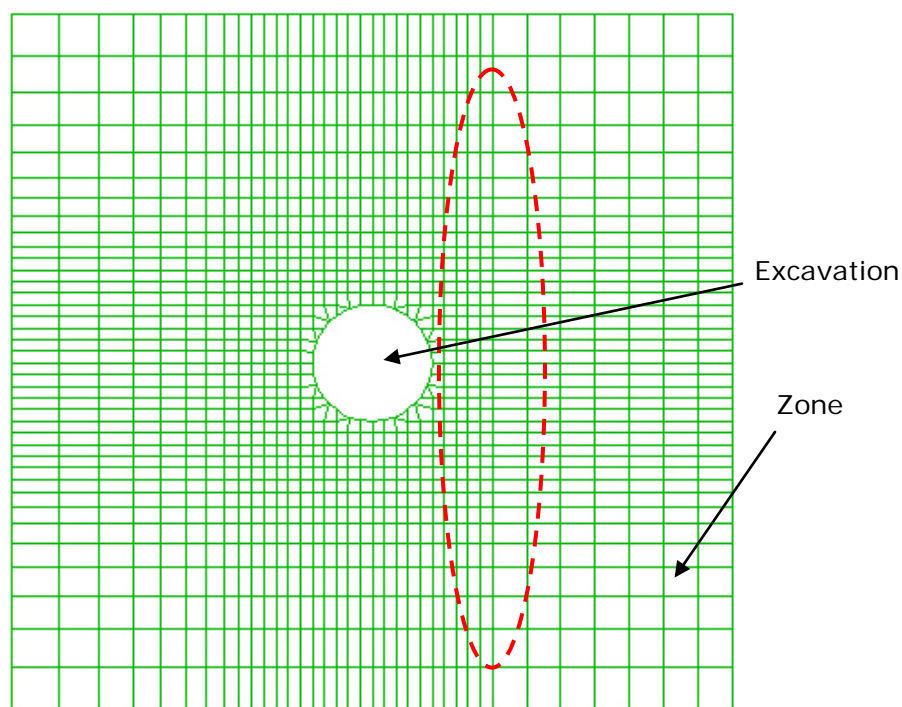


Figure 4.3 Sudden changes in neighbour zone size (inside red dashed line)

The aspect ratio of zone dimensions should also be as near unity as possible; anything above 5:1 is potentially inaccurate. However, high aspect-ratio zones are quite acceptable in regions of low strain gradient, such as remote boundary regions.

If a large and complex problem is under simulation, in which the geometry and loading are symmetrical about one or more planes, a symmetric model is a good choice to decrease the zone numbers and so to speed up the numerical calculation. For example, a problem of stress analysis of a water tunnel (shown in Figure 4.4) is to be solved, which is excavated in rock, subsequently lined, and then pressurized. The layout and geometry

of the tunnel shown in Figure 4.4 are axisymmetric about the center of the tunnel, permitting only half of the problem to be simulated along the line of symmetry.

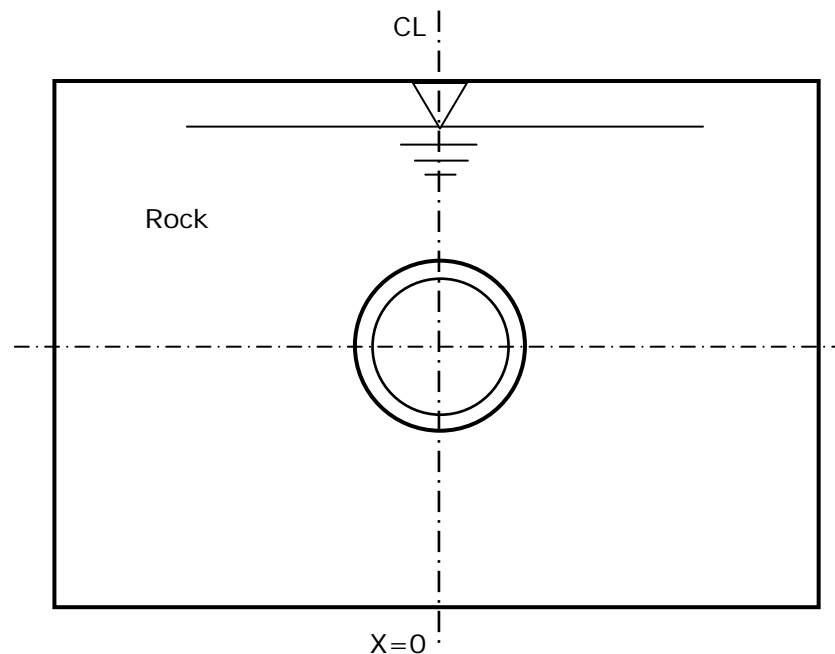


Figure 4.4 Geometry for an example water tunnel

For a specific problem, there are mainly three steps to build up a finite difference grid to fit the physical region under study:

- Firstly, to decide on the geometric extent of the grid, i.e. model boundary described in later section 4.3.2
- Secondly, to specify the number and distribution of zones within the grid based on a balance between the accuracy of results required and the computational time (the solution speed), which has been discussed in the beginning part of section 4.3.1
- Finally, to arrange the position of object under study, such as the excavation and supporting structure

It is helpful to make a rough drawing as a grid draft before building up a finite difference grid in numerical models.

4.3.2 Boundary Conditions

Boundary and initial stress conditions define the in-situ state (i.e., the boundary and stress condition before a change or disturbance in the problem state is introduced) of the geomechanical problem. Boundaries are of two categories: real and artificial. Real boundaries exist in the physical object being modelled, such as the ground surface, the excavation surface, etc. However, artificial boundaries do not exist in reality. Due to constraints on memory and analysis time, it may not be possible to cover the whole body with zones when modelling very large bodies (e.g., tunnels and very deep shafts). Then, artificial boundaries are placed sufficiently far away from the problem domain of interest (area of high stress and strains) so that the behaviour in that area is not affected greatly.

To obtain the balance between modelling results as accurate as possible and run time considerations, one must be very careful to define the position of the artificial boundary. In general, for the analysis of a single underground excavation, boundaries should be located roughly ten excavation diameters from the excavation periphery. This distance, however, can vary depending on the purpose of the analysis. If failure is of primary concern, then the model boundaries may be closer; if displacements are important, then the distance to the boundaries may need to be increased (Itasca, 2008).

Mechanical boundaries are of two main types in a numerical model: prescribed-displacement or prescribed-stress. A free surface is a special case of the prescribed-stress boundary. Stress boundaries can be determined by applying forces or stresses to the boundary. In order to

apply a given displacement to a boundary, the boundary's velocity is prescribed first and then the desired displacement will occur in the boundary after a given number of time steps. A fixed boundary causes both stress and displacement to be underestimated, while a stress boundary does the opposite. The two types of boundary condition "bracket" the true solution. There is a third type, the "infinite elastic boundary" (IEB), which covers artificial boundaries.

Boundary conditions (shown in Figure 4.5) allow the model to be loaded on different specified boundaries, whilst allowing others to remain fixed, thereby facilitating stress regeneration within the model. Initially, this model was loaded under gravity conditions representing overburden load applied vertically. Internal stresses must also be applied, both horizontal and vertical. However, a limited number of reliable in situ stress measurements were carried out prior to the commencement of mining, therefore only post-mining stress configurations are known.

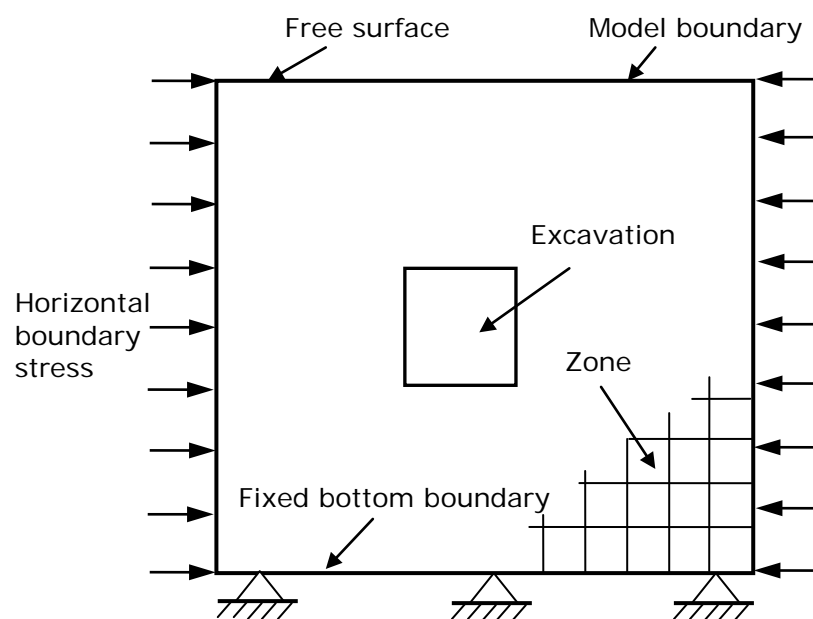


Figure 4.5 Example of boundary conditions

4.3.3 Initial Stress Conditions

There are in-situ virgin stresses in the ground in all civil or mining engineering projects before any excavation or construction is started. These in-situ stresses will be redistributed after excavation or construction especially in the domain surrounding the excavation and construction. The virgin stresses can greatly influence the subsequent behaviour of the model. So it is important to reproduce this in-situ state in numerical model grids by setting initial stress conditions. Ideally, information about the initial stress state comes from field measurements but, when these are not available, the model can be run for a range of possible conditions. Although the range is potentially infinite, there are a number of constraining factors (e.g., the system must be in equilibrium, and the chosen yield criteria must not be violated anywhere).

4.3.4 Constitutive Models

The constitutive model in numerical models dictates the type of response the model will display upon disturbance (e.g., deformation response due to excavation). There are twelve basic constitutive models provided in FLAC^{2D} Version 6.0 and FLAC^{3D} Version 3.1, respectively, arranged into null, elastic and plastic model groups.

The null material model in numerical models represents material that is removed or excavated. The stresses within a null zone are set to zero and no body forces (e.g., gravity) act on these zones. The null model is useful to model the excavation and backfilling of the excavation. Models in the elastic group are utilized to represent materials which are characterized by reversible deformation upon unloading and the stress-strain laws are linear and path-independent. No failure happens to the elastic material

since the strength is infinite in the elastic model. The plastic models are used to describe almost all materials with a property that includes some degree of permanent, path-dependent deformation (failure) and the consequence of the nonlinearity of the stress-strain relations.

Table 4.1 presents a summary of all the models with examples of representative materials and possible applications of the models. It should be noted that orthotropic elastic model is only supplied in three-dimensional models and the Cap-Yield (Cysoil) model only exists in two-dimensional models. The Mohr-Coulomb model in the plastic model group is applicable for most general engineering studies and utilized widely. Also, Mohr-Coulomb parameters for cohesion and friction angle are usually more-readily-available than other properties for geo-engineering materials. Except for these basic models, several optional features are available as separate modules that can be included in numerical models at an additional cost per module, such as models for dynamic analysis, thermal analysis, modelling creep-material behaviour, and two-phase flow analysis. With the powerful built-in programming language, FISH, the user can also define new variables, functions and their own constitutive models.

Group	Model	Representative Material	Example Application
Null	Null	Void	Holes, excavations, regions in which material will be added at later stage
Elastic group	Isotropic Elastic	Homogeneous, isotropic continuum; linear stress-strain behavior	Manufactured materials (e.g., steel) loaded below strength limit; factor-of-safety calculation
	Orthotropic Elastic	Materials with three mutually perpendicular planes of elastic symmetry	Columnar basalt loaded below strength limit
	Transversely Isotropic Elastic	Thinly laminated material exhibiting elastic anisotropy (e.g., slate)	Laminated materials loaded below strength limit
Plastic group	Drucker-Prager Plasticity	Limited application; soft clays with low friction	Common model for comparison to implicit finite-element programs
	Mohr-Coulomb Plasticity	Loose and cemented granular materials; soils, rock, concrete	General soil or rock mechanics (e.g., slope stability and underground excavation)
	Strain-Hardening / Softening Mohr-Coulomb Plasticity	Granular materials that exhibit nonlinear material hardening or softening	Studies in post-failure (e.g., progressive collapse, yielding pillar, caving)
	Ubiquitous-Joint Plasticity	Thinly laminated material exhibiting strength anisotropy (e.g., slate)	Excavation in closely bedded strata
	Bilinear Strain-Hardening/Softening Ubiquitous-Joint Plasticity	Laminated materials that exhibit nonlinear material hardening or softening	Studies in post-failure of laminated materials
	Double-Yield Plasticity	Lightly cemented granular material in which pressure causes permanent volume decrease	Hydraulically placed backfill
	Modified Cam-Clay Plasticity	Materials for which deformability and shear strength are a function of volume change	Geotechnical construction on clay
	Hoek-Brown Plasticity	Isotropic rock materials	Geotechnical construction in rock
	Cap-Yield (Cysoil) Plasticity	Soils that exhibit decreasing stiffness as plastic strains develop	Geotechnical construction in soft soils

Table 4.1 FLAC^{2D}/FLAC^{3D} constitutive models (Itasca, 2008)

4.3.5 Material Properties

The material properties required in numerical models are generally categorized in two groups: elastic deformability properties and strength properties. Additionally, there are special considerations such as the definition of post-failure properties, the extrapolation of laboratory-measured properties to the field scale and so on.

The selection of properties is often the most difficult part in the generation of a model because of the high uncertainty in the property database. The field data will never be known completely, especially in geomechanics. However, with the appropriate selection of properties based upon the available limited database, an important insight into the physical problem can still be gained. Material properties are conventionally derived from laboratory testing programs. As for the intact rock, the Young's modulus can be determined in the laboratory tests and the deformation modulus required for a Mohr-Coulomb model can be derived:

$$B = \frac{E}{3(1 - 2\nu)} \quad (4.1)$$

$$S = \frac{E}{2(1 + \nu)} \quad (4.2)$$

Where E , Young's modulus; ν , Poisson's ratio; B and S , bulk and shear modulus.

Determining the cohesion c and friction angle ϕ of the rock material requires a series of triaxial tests of which the results for various confining stresses are plotted as Mohr's circles. With Mohr's circles plotted, a failure envelope can be drawn and the cohesion c and friction angle ϕ can be determined from this envelope (Figure 4.6). The rocks around an underground tunnel are generally under compressive stress and thus generally fail in shear.

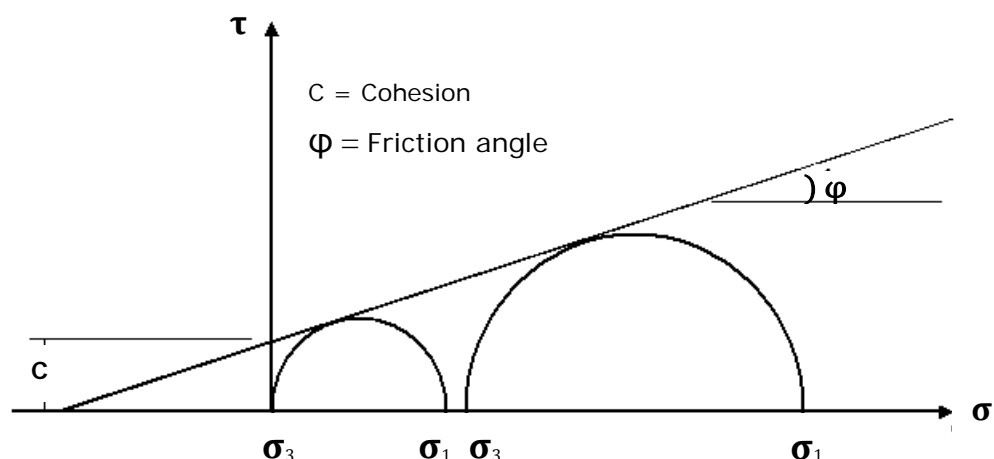


Figure 4.6 Determination of material properties for Mohr-Coulomb model

4.4 Chapter Summary

The commercial finite difference codes FLAC^{2D}/FLAC^{3D} were briefly introduced in this chapter, including their fields of application and fundamental components of numerical modelling. The numerical modelling of shafts' lining systems will be described and discussed in detail in the following Chapters 5~6.

The reader is reminded that the running time in the numerical Mohr-Coulomb model in this research is a series of time-steps, totally different from the shaft linings' total work time, which is around 10 years, or more. The deformation and stress results shown in this thesis were the final state of the numerical models when mechanical equilibrium was reached and do not represent fully the ongoing situation experienced over the lining life. They are however, useful when drawing comparisons between the performances of the four different lining types. Any further additional loading or creep properties put into the model would lead to additional deformations and stresses, which represent continuous deforming conditions in the shaft concrete lining systems during their working life.

CHAPTER 5

TWO-DIMENSIONAL NUMERICAL MODELLING OF SHAFT LINING SYSTEMS

5.1 Introduction

The FLAC^{2D} numerical code has been used to set up two-dimensional models for the stability analysis of the shaft linings' through the Marl stratum at Boulby mine. A plane-strain 2D analysis has been performed in this research because of small deformation along the shafts vertical axis compared with their lengths, which can be neglected. The investigation presented in this chapter focuses on the following aspects:

- Parametric studies on the effect of rock properties of the Marl, and the effect of the extent of weathered Marl on the stress and deformation conditions of the shaft linings,
- A parametric study on the effect of the ground stress field (hydrostatic or not) on the stress and deformation conditions of the shaft linings,
- The effect of possible "point" loading on the shaft linings on the stress and deformation conditions of the shaft linings,
- Modelling for the stress and deformation conditions of the original shaft lining and relinings.

In this research, the most detailed information available for the original shaft lining and relining systems was obtained from several CAD drawings of the man shaft. Additionally, it has already been stated in Chapters 1~2 (sections 1.2 and 2.6) that the shaft relinings through the Marl zone have always been started with the man shaft and the rock shaft relining has

adopted a similar design as that for the man shaft although internal dimensions have differed slightly between shafts. All numerical models in Chapters 5~6 in this research have been based on the man shaft at Boulby mine.

As already briefly introduced in Chapter 4, a variety of functions in FLAC^{2D}/FLAC^{3D} codes allow supports such as rock bolts, steel arches and liners (called structural elements) to be incorporated into the numerical models. Therefore, the liner elements in FLAC^{2D}/FLAC^{3D} codes can be used to model the shaft linings in this research. However, these structural elements are in the format of 'line' (2D) or 'plane' (3D) without thicknesses shown in Figure 5.1. The liner elements in the format of 'line' (2D) or 'plane' (3D) make it impossible in this research to analyze the detailed stress conditions (e.g. stress contours) within the shaft concrete linings, which have a significant physical thickness (0.75~1.2 m).

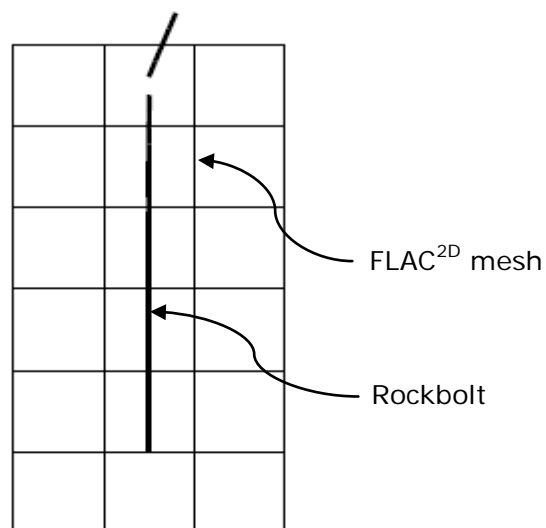


Figure 5.1 Deformed shape of 25 mm diameter rockbolt following rupture at end of shear test (Itasca, 2008)

Additionally, for the shaft HSC relinings with various joint fillings (epoxy resin, cement mortar and plywood packs), it is impracticable to model these important structural 'joints' interacted with the line/plane liner elements in numerical models. The solid two/three dimensional elements have been utilised to model the shaft linings in all numerical models in this research to solve these problems.

5.2 Parametric Study

The Marl zone is the weakest near-seam zone in the rock sequence and the shaft lining repair work always occurred within this over-9m-thick weak zone. Therefore, the first modelling task focuses on simulating the shaft linings' stress and displacement conditions through this zone. The effects of the properties of the Marl and the ground stress field (hydrostatic or not) on the stress and deformation conditions of the shaft linings have been studied in the models, using the original shaft lining as an example.

Additionally, the concept of a plastic zone of the weathered Marl has been introduced into this research. The effect of the extent of weathered Marl on the stress and deformation conditions of the original shaft lining has also been studied in the models.

5.2.1 Geometry of the Model and Mesh Definition

Due to the numerical modelling constraints on computer memory and analysis time, it is not possible to cover the whole structure with zones when modelling very large structures (e.g., deep shafts). In that case, artificial boundaries are placed around the model domain, which are sufficiently far away from the problem domain of interest (the area of high

stresses and strains), so that the behaviour in that area is not greatly affected. The guidelines for defining the position of the artificial boundary in the numerical models have been discussed in Chapter 4.

Figure 5.2 shows the conceptual layout of the model domain for a circular shaft of 7.9 m in diameter supported by a 0.75 m thick concrete lining, with a 0.45 m thick compressible material between the concrete lining and the excavation face (dimensions can be found in Table 2.5 in Chapter 2).

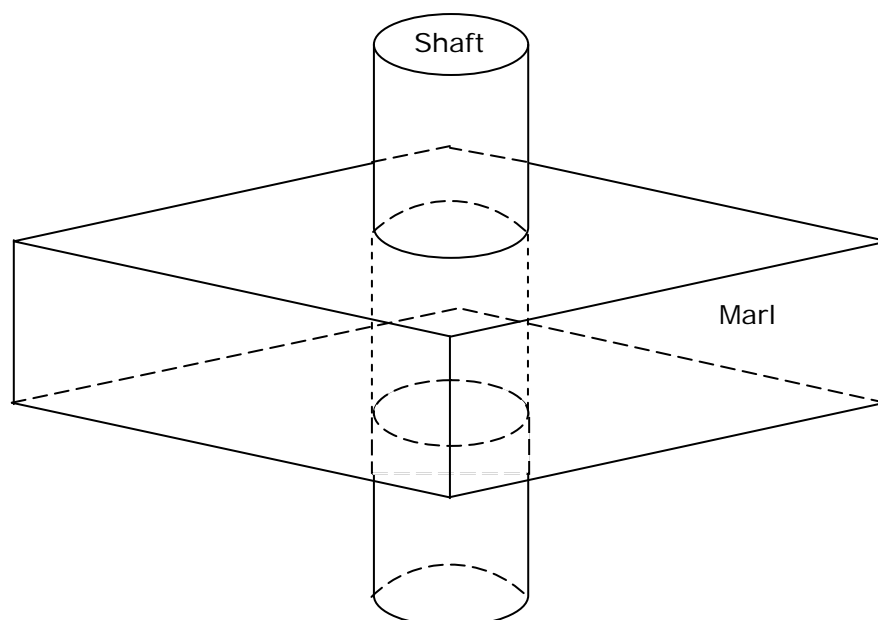


Figure 5.2 A horizontal slice in Marl in two-dimensional model (not to scale)

The geometry of the problem area and the finite difference grid used in models are shown in Figure 5.3. Laterally, the model was approximately ten times the shaft excavation radius. Because this is a symmetrical problem, only a quarter shaft has been modelled to save the programme running time and memory.

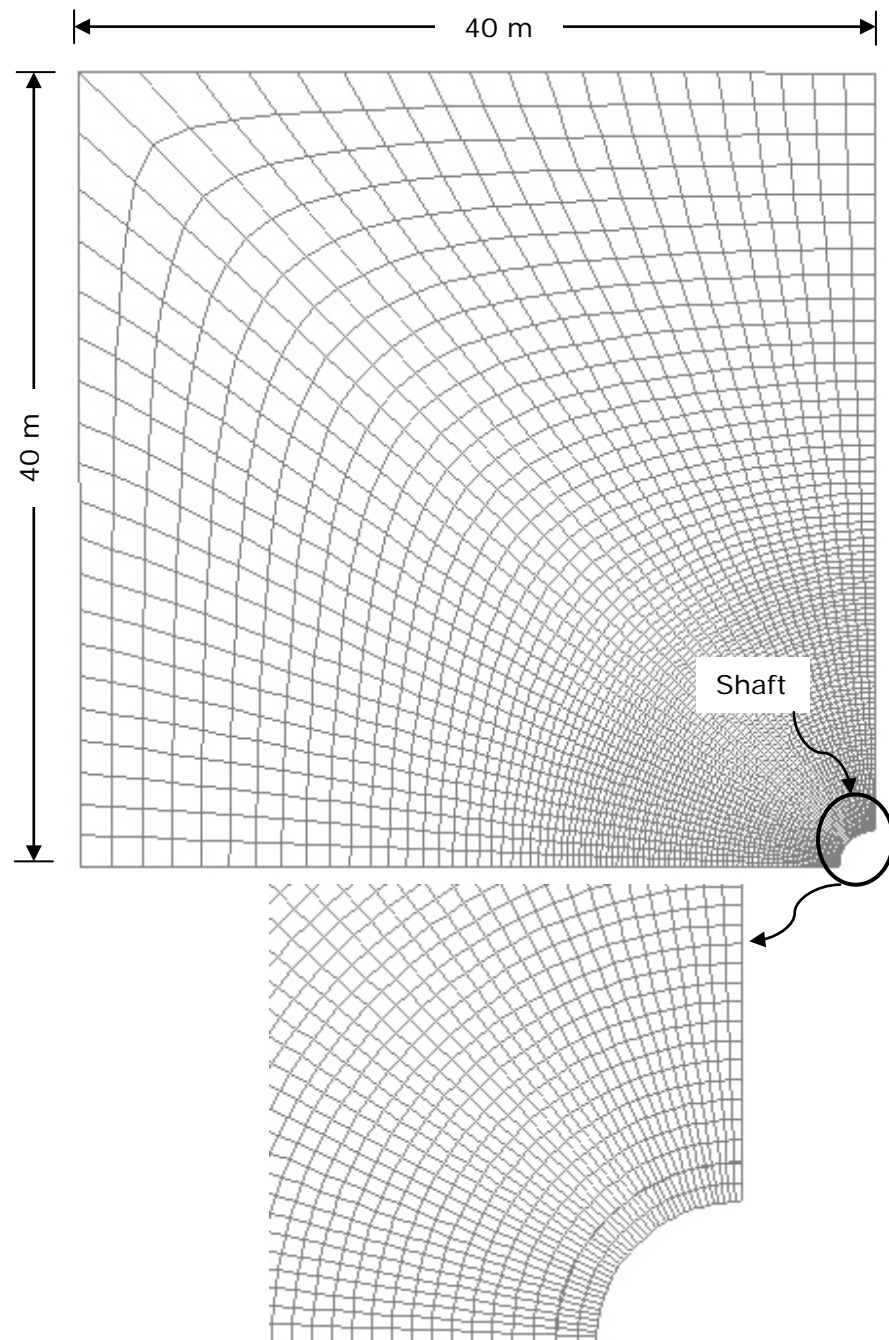


Figure 5.3 Finite difference grid used in the two-dimensional models

5.2.2 Boundary and Initial Stress Conditions

The boundary and initial in situ stress conditions have a significant influence on the behaviour of a geotechnical engineering model. It is very important to accurately reproduce these conditions before any

construction or excavation process is started. In order to estimate the initial stress state existing near the shaft, the vertical and horizontal stresses must be input into the models.

In Chapter 2 of this thesis, the in situ state of ground stress and the available results of stress measurements made around the world have been reviewed and discussed in detail. Based on those measured results, Brown and Hoek (1978) obtained the Equation (2.7) giving the average relationship for the vertical component of stress in relation to depth.

Stress measurement results also show that $\sigma_{h\ av}$ (the average horizontal stress and σ_z (the vertical stress) tend to equalise (i.e. hydrostatic stress conditions) when the depth increases towards and beyond 1000 m. This rule is widely used in weak rocks (e.g. coal measures and evaporites) and it has been found to give a good approximation of the in situ stress field in these materials (Hoek and Brown, 1980). This rule is also used in this modelling project. The initial background stress was reconstructed based on hydrostatical in situ stresses in the whole model domain, calculated from the following Equation (5.1):

$$\sigma_x = \sigma_y = \sigma_z = 0.027 \times h \quad MPa \quad (5.1)$$

Where h is the stratum depth.

Based on Figures 2.9 and 2.11 in Chapter 2, $h = 1090 \text{ m}$ has been chosen for the Marl stratum and Figure 5.4 shows the boundary and hydrostatic (horizontally) initial stress conditions used in most of the two-dimensional models.

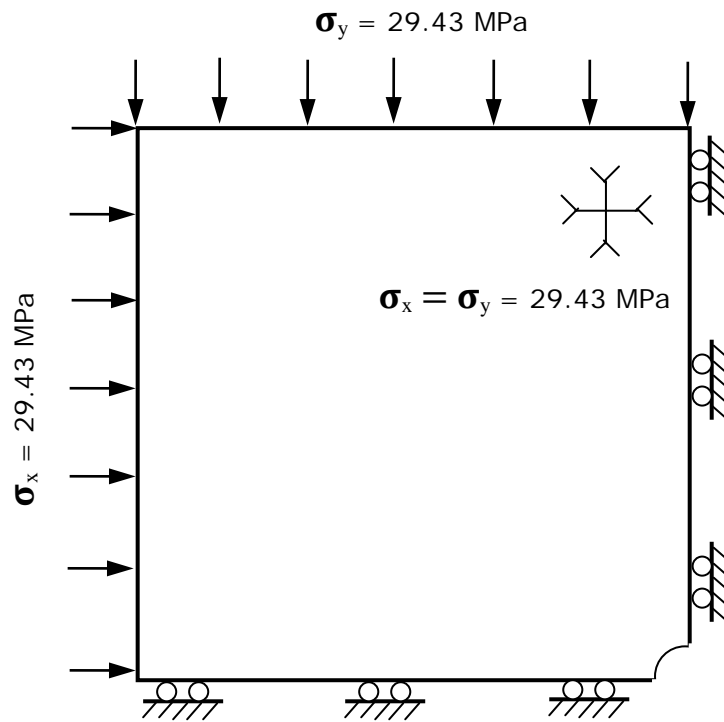


Figure 5.4 Boundary and initial stress conditions of the two-dimensional numerical model

Except for the parametric study on the influence of the ground stress field on the stability of the original shaft lining, all other models for parametric studies and the possible “point” loading on shaft lining have been done under a hydrostatic stress field in the models. When the effect of the ground stress field (hydrostatic or not) on the stress and deformation conditions of the original shaft lining was studied, the initial background stress state was reconstructed in the numerical models based on the following Equation (5.2):

$$\sigma_x = \lambda \sigma_y = \lambda \sigma_z = \lambda \times 29.43 \quad (5.2)$$

Where λ is the background stress ratio σ_x / σ_y , with a range from 0.5 to 1.0 in this research which is shown in Table 5.1.

σ_x (MPa)	σ_y (MPa)	λ
14.72	29.43	0.5
17.66	29.43	0.6
20.60	29.43	0.7
23.54	29.43	0.8
26.49	29.43	0.9
29.43	29.43	1.0

Table 5.1 Background stress ratio λ used in the models

5.2.3 Material Properties

Various materials are involved in the models in this research, such as the surrounding rock types, concretes used as shaft linings, cement grout backfilled in the gap between the linings and excavation face and so on. As described in Chapter 3 (section 3.3), Mohr-Coulomb failure criteria has been chosen for all rock, concrete and cement grout materials in this research. The methodology for obtaining the input material properties and the final version of them used in the numerical models has been presented and discussed in Chapter 3 in this thesis. In this section, only the final input material properties used in the models are briefly introduced.

5.2.3.1 Marl

Patchet's test results (1970) after reduction using the RocLab software (introduced in Chapter 3) were chosen as the base material properties of the Marl in the parametric studies. The GSI used in the RocLab software was estimated to be a lower value (30) for the Marl according to previously reported in situ experience. The Young's modulus, cohesion c

and friction angle ϕ of the Marl have been decreased (Table 5.2) to investigate their effects on stress and deformation conditions of the shaft linings (using the original lining as an example).

Materials	Young's modulus (GPa)	Poisson's ratio	Cohesion (MPa)	Friction angle ($^{\circ}$)	Tension (MPa)
Marl	<u>0.41</u>	<u>0.35</u>	<u>0.97</u>	<u>18</u>	<u>0.01</u>
	0.35		0.75	17	
	0.30		0.50	16	
	0.25		0.25	15	
	0.20		0.10	14	

Note: The properties underlined are Patchet's (1970) test results after reduction using $GSI=30$, and are the base properties.

Table 5.2 Input properties for the Marl in parametric studies on the effect of its properties on the stability of the linings

It has been mentioned by Patchet (1970) that the Marl can be considered as plastic under most conditions and as a stratum, it probably has no tensile strength (Chapter 2, section 2.5). Therefore, no parametric study on the tensile strength of the Marl will be carried out although some low values have been assigned to the Marl in this part of the research.

When the effect of the ground stress field (hydrostatic or not) on the stress and deformation conditions of the original shaft lining was studied, Patchet's (1970) tests results after the reduction shown in Table 5.2 were used as the properties of the Marl and kept unchanged.

In Chapter 2 it was stated that the Marl is a weak rock and more easily weathers on exposure when compared with other surrounding rock types at Boubly mine. It has been assumed by the author in this research that,

in the real engineering situation, a plastic zone of weathered Marl was modified away from the shaft excavation face because of its exposure in the shaft excavation process and its subsequent relinings. This plastic zone of weathered Marl is schematically shown in the Figure 5.5. Figure 5.6 shows how this concept has been simulated in the models.

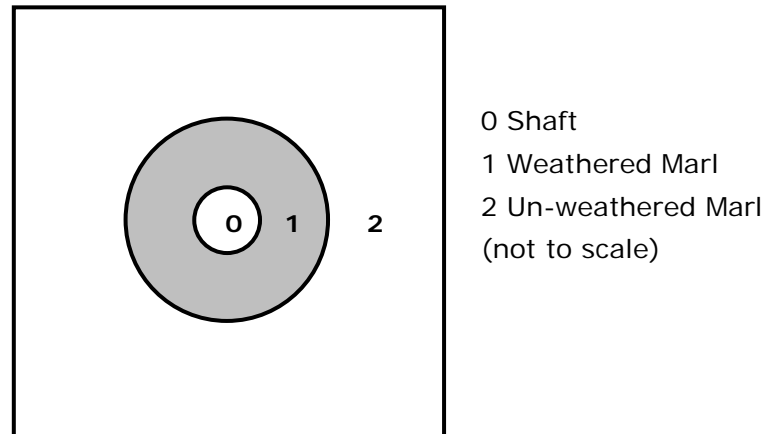


Figure 5.5 Conceptual plastic zone around the shaft

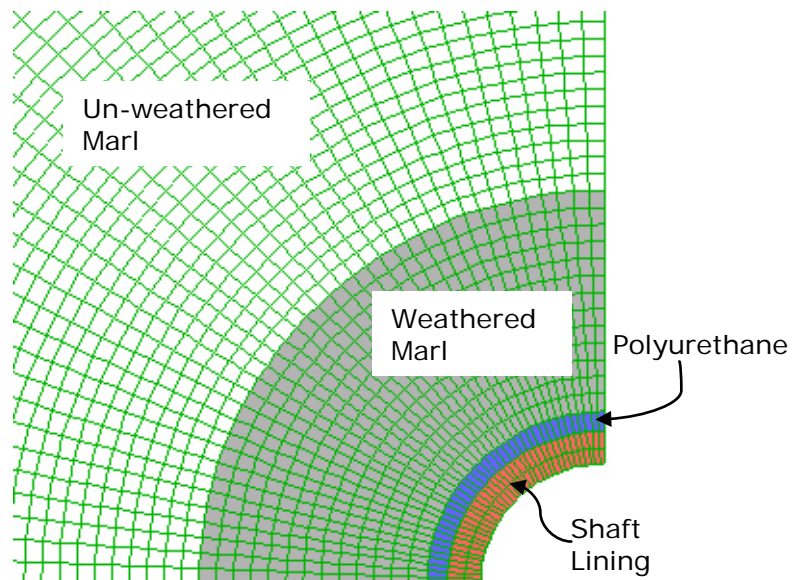


Figure 5.6 Weathered Marl simulated in the two-dimensional models

The extent of weathered Marl into the shaft wall refers to the thickness of weathered zone that is the distance between the outer boundaries of

weathered zone and the polyurethane layer. Distances of 1, 2, 3, 4, 6 m have been adopted in this part of the research, which were approximately 0.25, 0.5, 0.75, 1 and 1.5 times the shaft initial excavation radius (nearly 4 m), respectively.

When the effect of the extent of weathered Marl on the stress and deformation conditions of the original shaft lining were studied, the RSM tests (2000) results after reduction using the RocLab software were chosen as the material properties of the weathered Marl. Table 5.3 shows the input properties for the weathered and un-weathered Marl in the models for the parametric study on the effect of the extent of weathered Marl on the stress and deformation conditions of the original shaft lining. Figure 5.7 shows the Mohr-Coulomb strength envelopes for the laboratory test data and input properties used in this part of parametric study for the un-weathered and weathered Marl.

Materials	Young's modulus (GPa)	Poisson's ratio	Cohesion (MPa)	Friction angle (°)	Tension (MPa)
Un-weathered Marl	0.41	0.35	0.97	18	0.01
Weathered Marl	0.17	0.18	0.24	5	0.03

Table 5.3 Input properties for the weathered and un-weathered Marl in parametric studies on the effect of the extent of weathered Marl on the stability of the original shaft lining

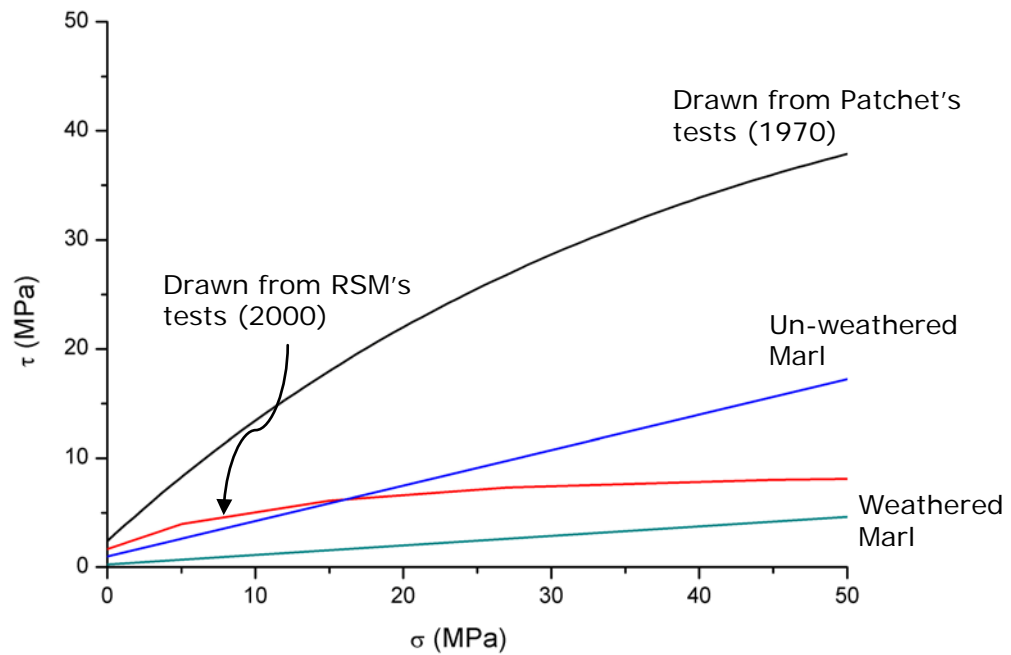


Figure 5.7 Mohr-Coulomb strength envelopes for the Marl

5.2.3.2 *In Situ Cast Concrete and Polyurethane*

Since laboratory test data of the in situ cast concrete used in the original shaft lining at Boulby mine, with the exception of its UCS value (34.5 MPa) was not available, the input properties for this concrete used in the models have been estimated based on experiences and references as described in section 3.3.3 in Chapter 3. The final input properties for the in situ cast concrete can be found in Table 3.10. The input properties for the polyurethane, which has been set as pure elastic in the models for the original shaft lining system, can be found in Table 3.19.

5.2.4 Stress Relaxation and Modelling Sequence

After the grid was generated and the input material properties were assigned for rock materials, in situ stresses were applied to the model boundary and domain. Then the measuring points (for both displacements and stresses) were set up and the program run to establish the

equilibrium conditions to initialize stresses. The simulations were designed such that they represented the actual sequence of events leading to the shaft excavation at Boulby mine.

After the initial equilibrium was established, the next steps were the shaft excavation and the installation of the support. In the practical situation, the shaft lining is not installed immediately after shaft excavation. An important issue in these stages is the amount of stress relief and redistribution and consequent ground movement due to the shaft excavation that occurs prior to support placement. This is known as the 'head-end effect' in tunnel design. The major implication of the head-end effect is that a support installed at a distance behind the face will not be subjected to the full loading and deformation as a result of the full overburden pressure (Whittaker and Frith 1990). So if no change in loads acting on the support is assumed to occur, the pressure acting on the support will be over-predicted. If complete stress relaxation at the shaft periphery is assumed to occur, zero loads will develop in the support at the installation step, provided that the relaxation state is at equilibrium.

In fact, even if the support is installed at the face, a degree of stress relief and movement will have already taken place in the immediate ground in front of the face, see Figure 5.8 (Muir Wood 1979). It is necessary to take account of stress relaxation in shaft excavation and support installing stages of the model, for economic reasons and to make the numerical simulation as close to the real engineering situation as possible. It will result in a support more correctly matched to the expected ground behaviour rather than one over-designed if the full overburden pressure is considered.

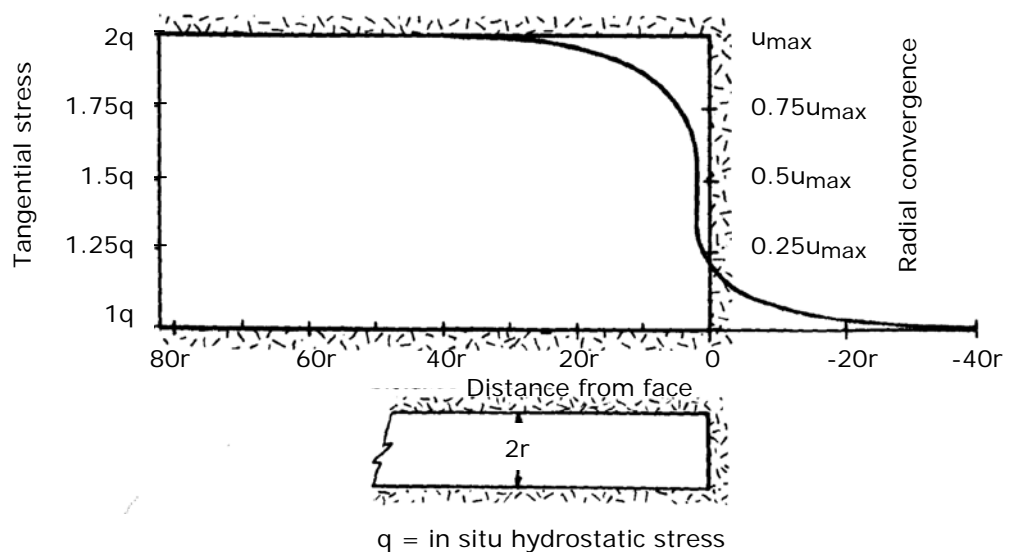


Figure 5.8 Radial convergence and tangential stress in vicinity of tunnel face (Muir Wood 1979)

However, it is difficult to choose the amount of stress relief at the point of support installation and the result of over-estimating this effect may lead to false conclusions concerning the stability of the support in question. One way to model the relaxation is to decrease the Young's modulus of the shaft core, equilibrate, remove the core and install the support. The models are then cycled to equilibrium, with stresses and displacements being monitored throughout the cycling process. In this research, according to modelling experience, the Young's modulus of the shaft core was decreased by 50% to model the stress relaxation.

The flow chart (Figure 5.9) shows the detailed operations for the shaft excavation and support installation in the models for the mine shaft project, which have been designed to take the practical construction situation into account in the numerical modelling.

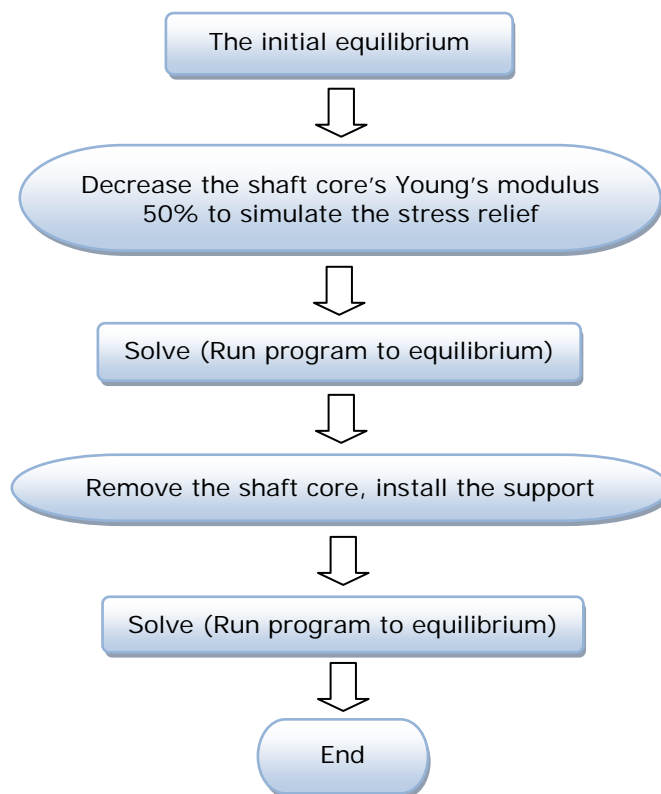


Figure 5.9 Modelling sequence flow chart in the two-dimensional models

5.3 Modelling Results of the Parametric Studies

As described in section 5.1, parametric studies in the models for the mine shaft linings focus on the effects of rock properties of the un-weathered Marl, the extent of weathered Marl and the ground stress field (hydrostatic or not) on the stress and deformation conditions of the shaft linings, using the original lining as an example. The modelling results from all the parametric studies are presented in this section, respectively.

It should be noted that in the following figures, the shaft lining closures refer to the radial inwards displacement of the inner surface of the concrete lining in the numerical models. It was chosen as the deformation index in studying the effect of the properties of the un-weathered Marl on the stability of the shaft lining, since the space left in the shaft is

important to the mining work. The max. σ_1 is the maximum major principal stress in the concrete lining in the numerical models.

To compare different rock properties' effects on the stability of the original shaft lining in this research, the shaft lining closure and maximum major principal stress σ_1 in the lining have been plotted against percentage of the basic properties, which are the Patchet's (1970) tests results after reduction (shown in Table 5.2).

5.3.1 The Effect of the Properties of the Marl

Figures 5.10~5.11 show the modelling results of the parametric study on the effect of properties of the un-weathered Marl on the stress and deformation conditions of the original shaft lining. It can be seen from Figures 5.10~5.11 that the shaft lining closure and the maximum major principal stress σ_1 increased with a decrease in property value (strength cohesion C and friction angle F, and stiffness E).

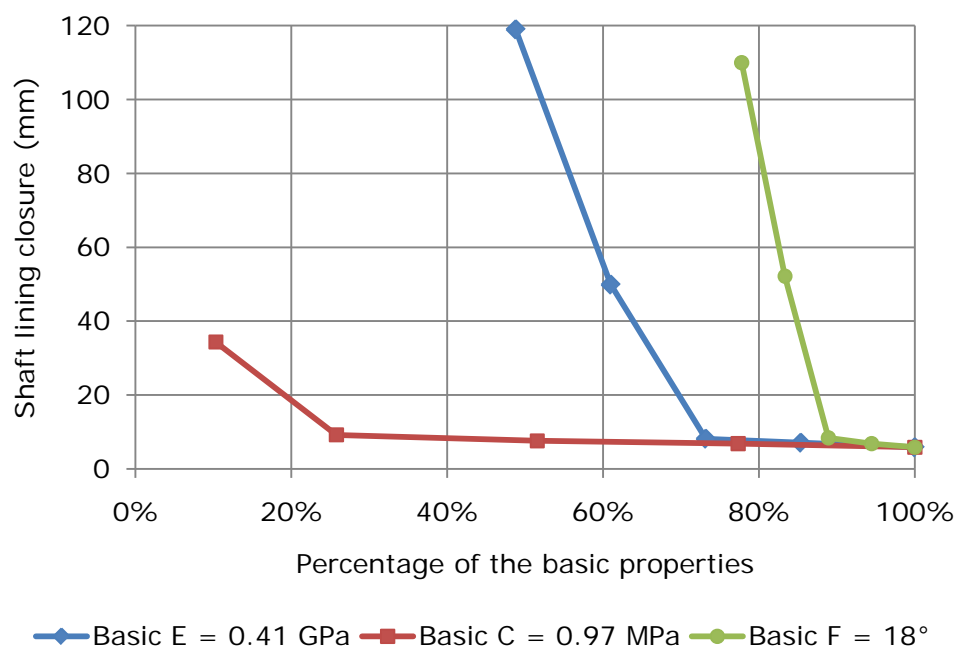


Figure 5.10 Shaft lining closure vs. the properties of the Marl

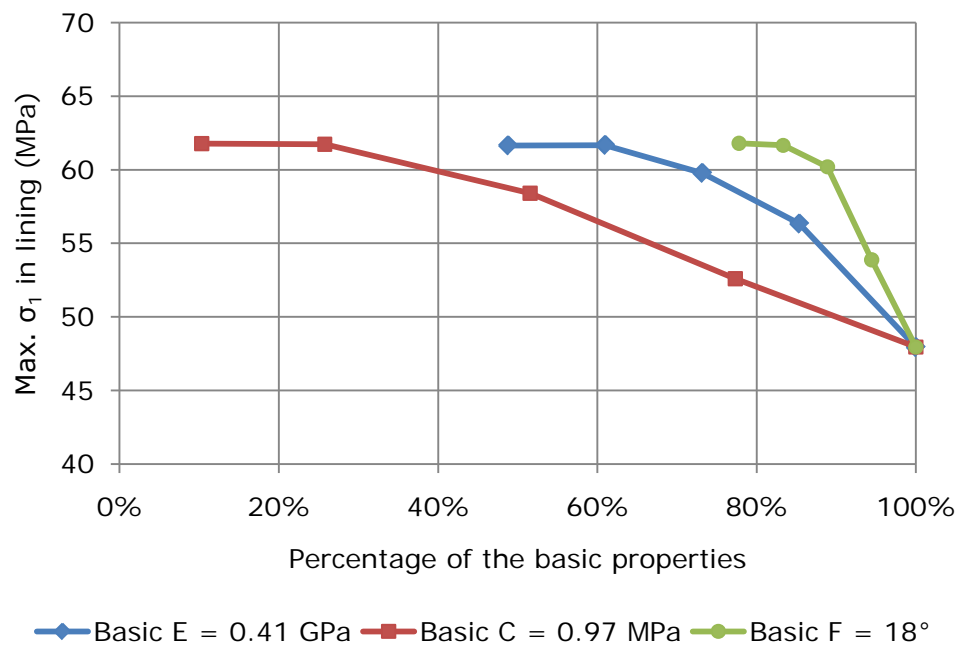


Figure 5.11 Max. σ_1 in shaft lining vs. the properties of the Marl

When the friction angle and the Young's modulus of the Marl decreased to be lower than 16° and 0.3 GPa, respectively, the original shaft lining closure increased dramatically (Figure 5.10, from approximately 0.006 m to nearly 0.12 m) in numerical models. However, the maximum major principal stress curve (Figure 5.11) in the original shaft lining gradually increased at the early stage (from approximately 48 MPa to 60 MPa) but tended to be steady around 62 MPa at the later stage when the properties of the Marl decreased in numerical models. Corresponding to each maximum major principal stress σ_1 in the original shaft lining, the minor principal stress σ_3 was approximately 8 MPa in all models in this part of the parametric study. This implies that corresponding to the end stage of the maximum major principal stress curve (Figure 5.11), the principal stress difference (deviator stress ($\sigma_1 - \sigma_3$)) in the shaft lining became increasingly greater, threatening the stability of the shaft lining.

A decrease in the value of each single property in the Marl means a more severe ground stress from the surrounding Marl acting on the shaft lining, leading to greater deformation and stress conditions in it. It can be seen from the modelling results shown and described above that, in this research case, the stability of the original shaft lining was most sensitive to the friction angle of the surrounding Marl, and least sensitive to the cohesion of the Marl. That is to say, for shear strength properties of the Marl, the cohesion has less effect on the stability of the shaft lining than the friction angle. It is thought by the author that it is because in the numerical models in this research, soft Marl with fairly low cohesion (lower than 1 MPa in Table 5.2) in an environment of high ground stress field (nearly 30 MPa in Table 5.1). The following Equations (5.3~5.5) are used to demonstrate this condition in this research.

$$\tau = c + \sigma \tan \varphi \quad (5.3)$$

$$\Delta \tau_c = \Delta c \quad (5.4)$$

$$\Delta \tau_\varphi = \sigma \tan \varphi_1 - \sigma \tan \varphi_2 \quad (5.5)$$

Where, τ is shear stress, σ is normal stress, c is cohesion, Δc is cohesion difference, φ is friction angle, $\Delta \varphi$ is friction angle difference, $\Delta \tau_c$ is shear stress difference caused by Δc , $\Delta \tau_\varphi$ is shear stress difference caused by $\Delta \varphi = \varphi_1 - \varphi_2$.

According to Tables 5.1~5.2, let $\sigma = 29.43 \text{ MPa}$, $\varphi_1 = 18^\circ$, $\varphi_2 = 17^\circ$ and $\Delta c = 0.97 - 0.75 = 0.22 \text{ MPa}$, then $\Delta \tau_c = 0.22 \text{ MPa}$ and $\Delta \tau_\varphi = 0.56 \text{ MPa}$. It can be seen obviously that $\Delta \tau_\varphi > \Delta \tau_c$.

5.3.2 The Effect of the Extent of the Weathered Marl

Figures 5.12~5.13 show the modelling results of the parametric study on the effect of the extent of the weathered Marl on the stress and deformation conditions of the original shaft lining. As shown in Figures 5.12~5.13, the shaft lining closure increased gradually at the early stage and dramatically at the later stage with the increasing extent of the weathered Marl in the numerical models.

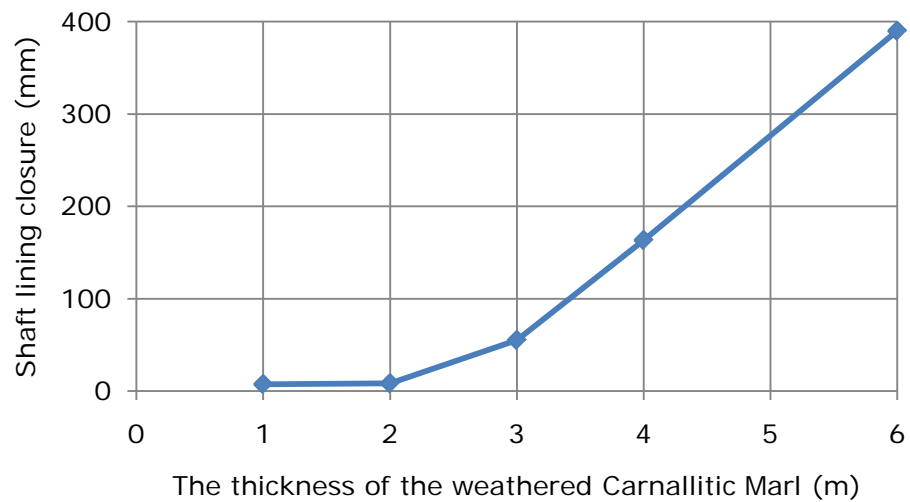


Figure 5.12 Shaft lining closure vs. the thickness of the weathered Marl

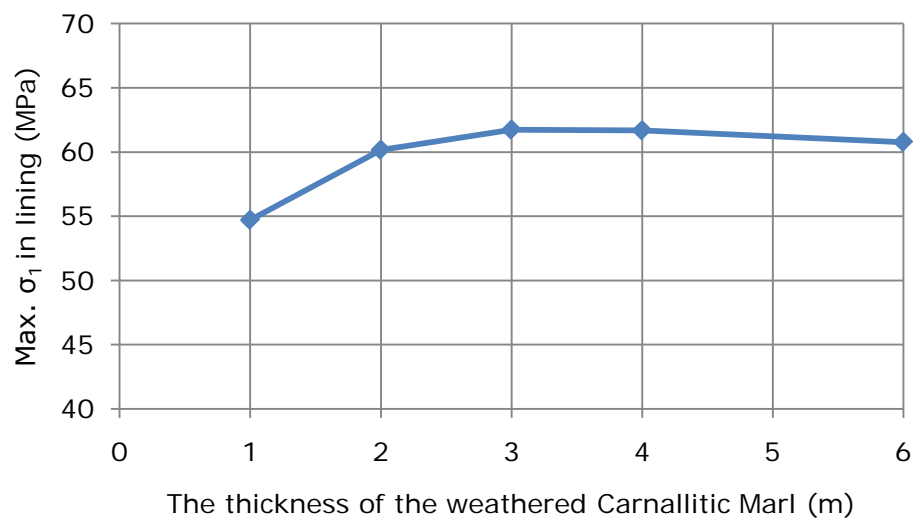


Figure 5.13 Max. σ_1 in shaft lining vs. the thickness of the weathered Marl

When there was 6 m (1.5 times the shaft excavation radius) thick weathered Marl surrounding the shaft in the model, up to 0.39 m closure occurred in the original shaft lining, which was 14% of the original shaft lining inner radius. This magnitude closure would be a serious problem for shaft operations and severely compromise the shaft lining stability.

The maximum major principal stress curve in the original lining (Figure 5.13) gradually increased then tended to be steady when the extent of the weathered Marl increased in the numerical models. However, when the weathered Marl was 6 m thick, the ground stress field was so severe that the original lining could not provide support and became plastic in most area. Therefore, the maximum major principal stress σ_1 in it started decreasing. This confirms that 6 m thick weathered Marl caused a serious problem for the original lining stability in the two-dimensional models.

The modelling results imply that the increasing extent of the weathered Marl leads to an increasingly severe ground stress field working on the original shaft lining and all relinings, resulting in higher deformation and stress conditions in them. As seen from Figures 5.12~5.13, it is suggested by the author that in this research case, 4 m (approximately equal to the shaft excavation radius) is a critical value for the extent of the weathered Marl. When the weathered Marl extent is greater than 4 m, the original lining confronts a severe ground stress field, threatening its stability.

5.3.3 The Effect of the Ground Stress Field

The modelling results of the parametric study on the effect of ground stress field (hydrostatic or not) on the stress and deformation conditions of the original shaft lining are shown in Figures 5.14~5.15. The modelling results in Figures 5.14~5.15 show that the shaft lining closure and the

maximum major principal stress σ_1 increased with the background stress ratio decreasing. However, when the background stress ratio λ decreased to 0.5, extremely large closure (nearly 0.25 m, 9% of the original lining inner radius) occurred in the original shaft lining and the maximum major principal stress σ_1 decreased dramatically. These were because the original lining became plastic under severe ground stress field and lost some of its supporting capacity.

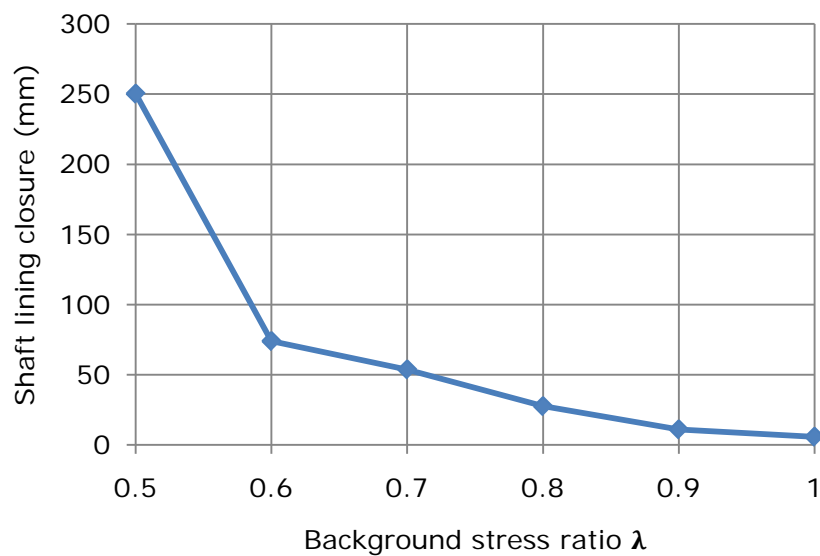


Figure 5.14 Shaft lining closure vs. background stress ratio λ

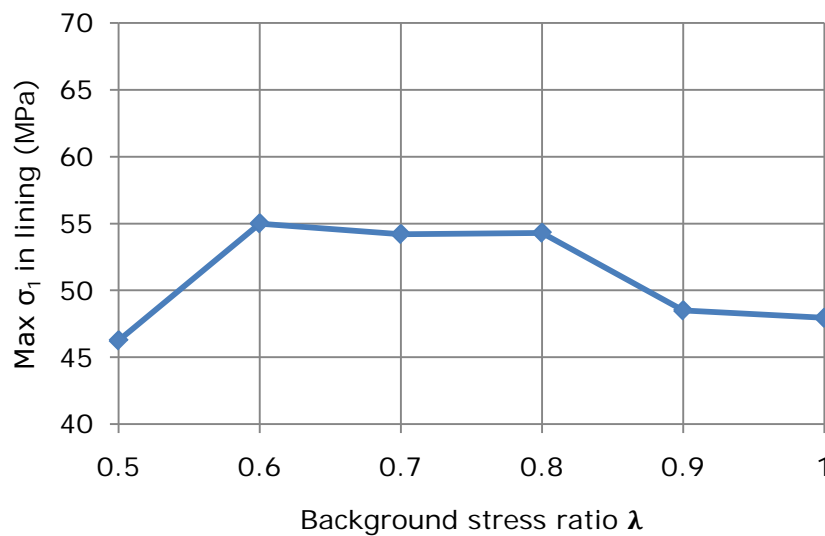


Figure 5.15 Max. σ_1 in lining vs. background stress ratio λ

When the background stress ratio λ was 0.6 and 0.5, tensile stress occurred in the original shaft lining and caused tension failure (shown in Figure 5.16). These imply that the severe non-hydrostatic stress field with background stress ratios, λ equal to 0.5 and 0.6 caused serious problems for the shaft lining stability in the two-dimensional models.

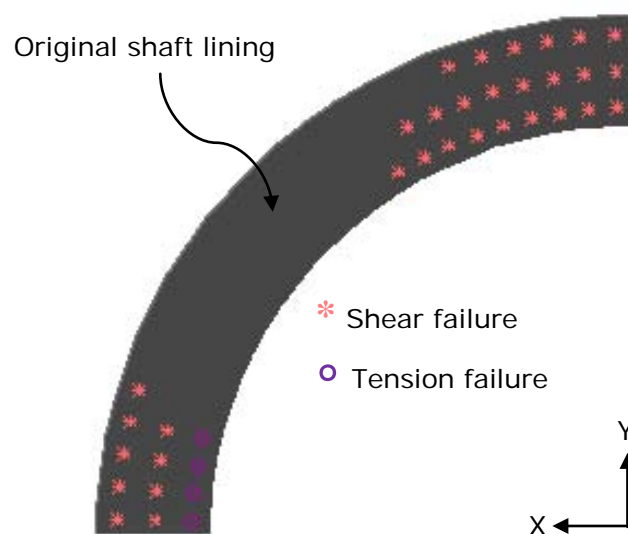


Figure 5.16 Failure state of the original shaft lining under background stress ratio $\lambda = 0.5$

The modelling results described and discussed above imply that non-hydrostatic stress field would result in uneven loading on the circular shaft linings and threaten their stabilities. However, when the background stress ratio λ was close to 1 implying a hydrostatic stress field, the original shaft lining was less compromised.

5.4 The Possible “Point” Loading on the Original Lining

In practical engineering, the cross-section of the shaft excavation cannot be a perfect circle. However, the concrete lining was designed to be a perfect circle. That means the backfill materials in the gap between the

surrounding rock and concrete lining was not of an even thickness. In the original concrete lining system, the backfill material was very soft polyurethane through the Marl stratum, which can be easily and highly compressed.

The polyurethane could not accommodate the high pressure from the surrounding Marl. This situation may well have caused uneven loading on the original concrete lining. Usually, the circular concrete structure can exhibit good stability under even loading, but it has a much lower ability to resist uneven loading, which has been confirmed by the numerical modelling results shown in section 5.3. A simple extreme case of the possible uneven loading (called "point" loading) on the original concrete lining system was simulated and discussed in this section.

5.4.1 Model Configurations

The artificial boundary and the hydrostatic ground stress field shown in Figure 5.4 described in section 5.2 were also employed in this model. For the simulation of the possible "point" loading on the original lining, a full circular shaft model has been utilized. Therefore, the model domain for this model was 80 m × 80 m. At the same time, the concept of the weathered Marl zone introduced in section 5.2 has been used in this possible "point" loading model. According to the modelling results in section 5.3, 4 m was chosen as the extent of the weathered Marl, which was approximately equal to the shaft excavation radius. Figure 5.17 shows the "point" loading's position, 1m in length along the periphery of the original shaft lining, and the different material groups in this model.

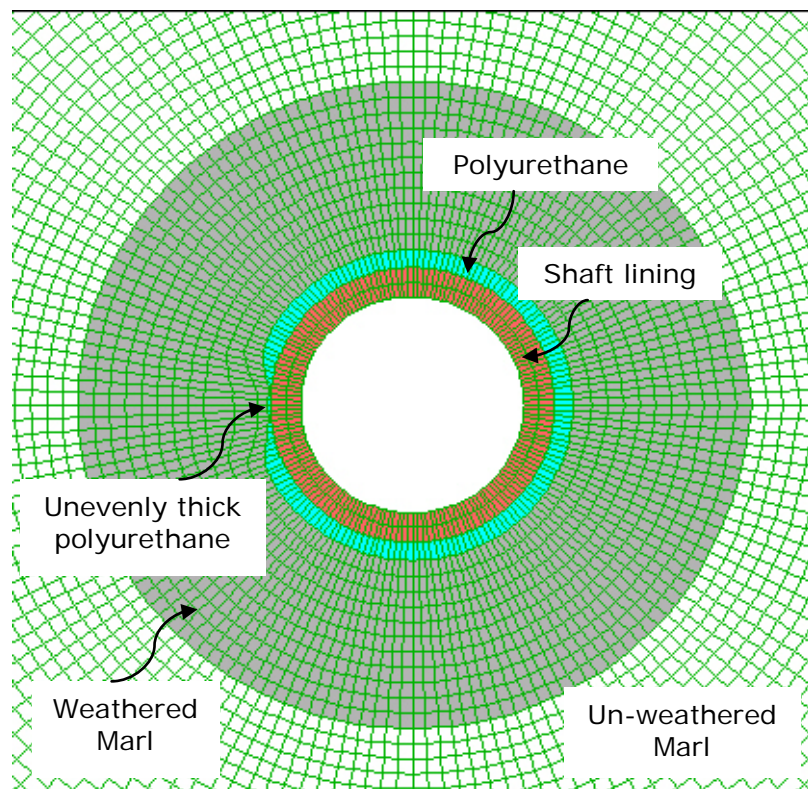


Figure 5.17 Mesh for possible “point” loading model (not full window)

The input material properties for the weathered and un-weathered Marl can be found in Table 5.3. As described in section 5.2, the input properties for the in situ cast concrete and the polyurethane can be found in Tables 3.10 and 3.19.

5.4.2 Modelling Results and Discussion

Figure 5.18 shows the failure state of the original shaft lining under possible “point” loading caused by unevenly thick distribution of the polyurethane along its periphery. It can be seen that a massive tension failure and shear failure occurred near the “point” loading position in the concrete lining. In this numerical model, the maximum radial inwards displacement (closure) of the original lining at the “point” loading area was approximately 0.2 m, much bigger than those of other parts of the

concrete lining (0.03 m). Additionally, the original shaft lining moved slightly in a horizontal direction because of the “point” loading, schematically shown in Figure 5.18. This result was consistent with the lining condition indicated by in-situ measurements described in Cook’s thesis (1974) shown in Figure 5.19. However, Cook’s figure (1974) showed no shape change of the shaft lining. It is thought by the author that Cook just emphasized the lateral movement of the lining but ignored its shape change.

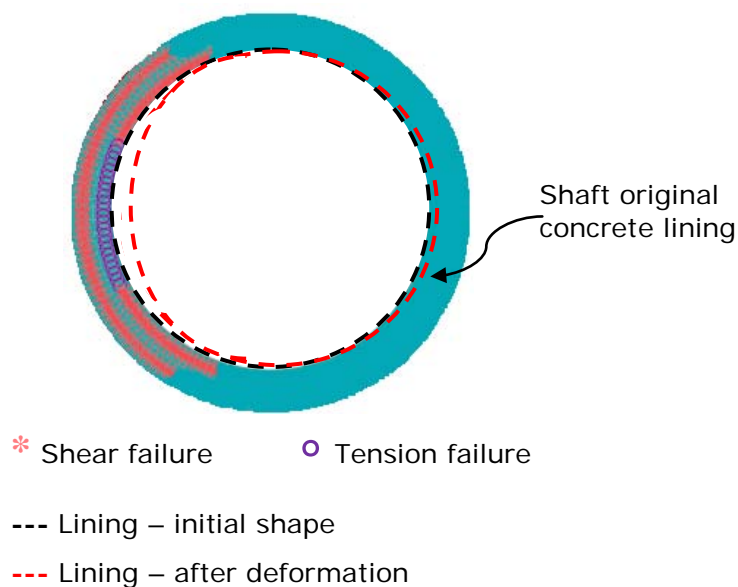


Figure 5.18 Failure state and schematic shape change of the original shaft lining under possible “point” loading

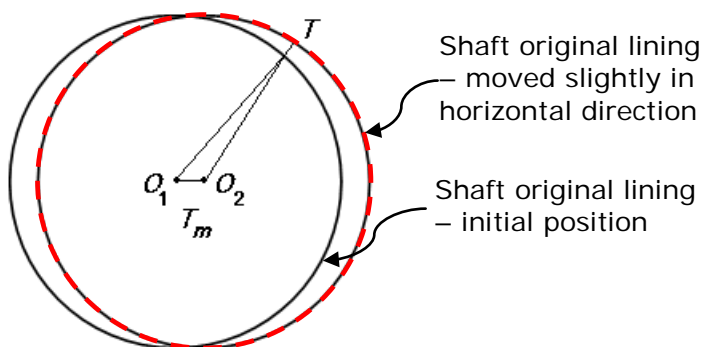


Figure 5.19 Lateral movement of the original lining (Cook, 1974)

Based on these modelling results, it was deduced that a possible reason for the original shaft lining's failure may be due to uneven loading on the concrete lining caused by uneven thicknesses of the backfill material. Uneven loading could lead to high tensile stress and shear stress in the concrete which causes a severe threat to the stability of the circular concrete structure. However, the cement grout, a rigid backfill material when compared with polyurethane, was employed in the shaft relinings and would accommodate the high pressure before they affected the concrete linings. The buffering cement grout layer transferred high ground pressure to the concrete blocks gradually and facilitated the avoidance of possible uneven loading on the concrete linings, which would have threatened the stability of the shaft lining system.

5.5 Modelling for the Original Lining and Relinings

The stress and deformation conditions of the shaft's concrete linings at Boulby mine have been numerically simulated, from the cast concrete lining that were originally installed when the shafts were sunk to their first, second and third entire relinings through the Marl stratum. The assumptions made during the modelling and the modelling results have been presented and discussed in this section.

5.5.1 Model Configurations

One limitation affecting the finite difference mesh in all the numerical models is that the mesh cannot be changed once the programme starts running. However, the original shaft lining and relinings through the Marl zone at Boulby mine did not have the same dimensions. In fact, the circular shaft relinings through the Marl zone gradually increased in radius as shown in Table 5.4.

In:	Lining's Inner Radius (m)	Lining's Outer Radius (m)	Shaft's Excavation Radius (m)
Original lining	2.74	3.49	3.94
1 st relining	2.88	3.95	4.35
2 nd relining	2.93	4.1	4.5
3 rd relining	3.09	4.3	4.7

Table 5.4 Dimensions of shaft linings through the Marl zone at Boulby

To solve this problem in the models, all the shaft's relinings through the Marl zone have been simulated in their own true dimensions, which means that three new finite difference meshes were required, one for each relining system, and each different from the one for the original shaft lining.

The artificial boundary and the hydrostatic ground stress field shown in Figure 5.4 described in section 5.2 were employed in all the quarter models for the original shaft lining and relinings. As with the model configuration set for the model of "point" loading on the original lining, there was a 4 m thick weathered Marl surrounding the original shaft concrete lining, from the shaft excavation face to the un-weathered Marl. Additionally, it has been assumed by the author that during the shaft relining process and working time, the weathered Marl zone extended outwards slightly. Table 5.5 shows the detailed dimensions used for the weathered Marl in different relining stages in the models. The input material properties for the in situ cast concrete, the polyurethane, the weathered and un-weathered Marl can be found in Tables 3.10, 3.19 and 5.3.

Materials	Radial thickness in models (m)			
	Original lining	1 st relining	2 nd relining	3 rd relining
Excavation radius	3.94	4.35	4.5	4.7
Weathered Marl	4	4.5	5	5.5
Un-weathered Marl	The remainder of the model			

Table 5.5 Dimensions of the weathered Marl zone in the two-dimensional models

5.5.2 Interfaces between Concrete Blocks

For all the shaft relining systems at Boulby mine, HSC blocks were employed, with different materials filled between the concrete blocks each time. Adhesive materials, epoxy resin and cement mortar, were employed between the concrete blocks in the first relining and squeezable plywood packs were used in the second and third relinings. These joints were actually very thin but are important to the mechanical behaviour of the whole concrete lining systems.

Because of mesh generation limitations, solid elements with some thickness cannot be used to represent these materials in the numerical models. To solve this problem, interface elements with appropriate properties have been built into the models to be used to represent the joints between concrete blocks in the numerical modelling in this research. Figure 5.20 illustrates the detailed finite difference mesh in the zone close to the lining in the shaft lining systems. The input properties for the interface elements representing these joints can be found in Tables 3.12 and 3.17.

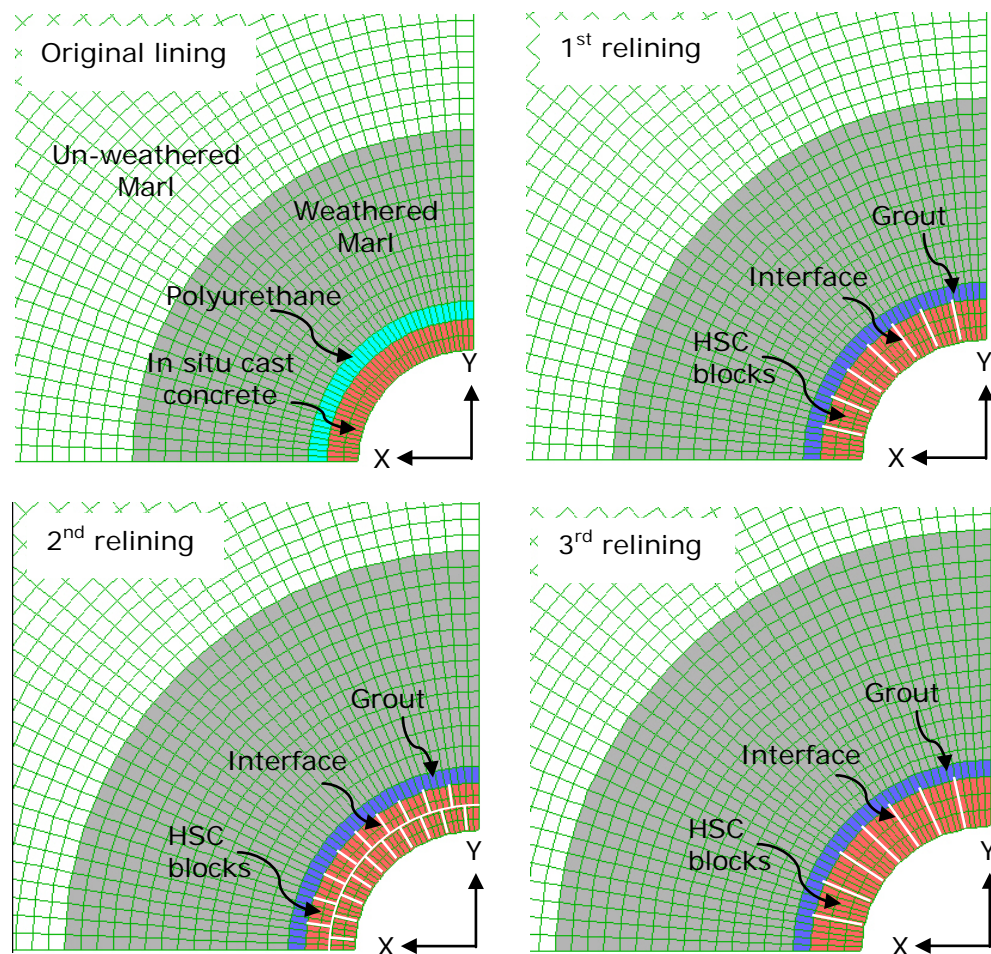


Figure 5.20 Detailed finite difference mesh of the shaft linings

5.5.3 Modelling Results and Discussion

The numerical modelling results for the mine shaft's original lining and relinings are presented and discussed in this section, including the radial closures of each concrete lining system and principal stress conditions in the shaft linings.

5.5.3.1 Concrete linings' radial closure

The radial closures of the shaft lining systems taken from the numerical models are shown in Figure 5.21. Figure 5.22 shows the ratios of concrete lining's closure with the lining's inner radius of each lining system.

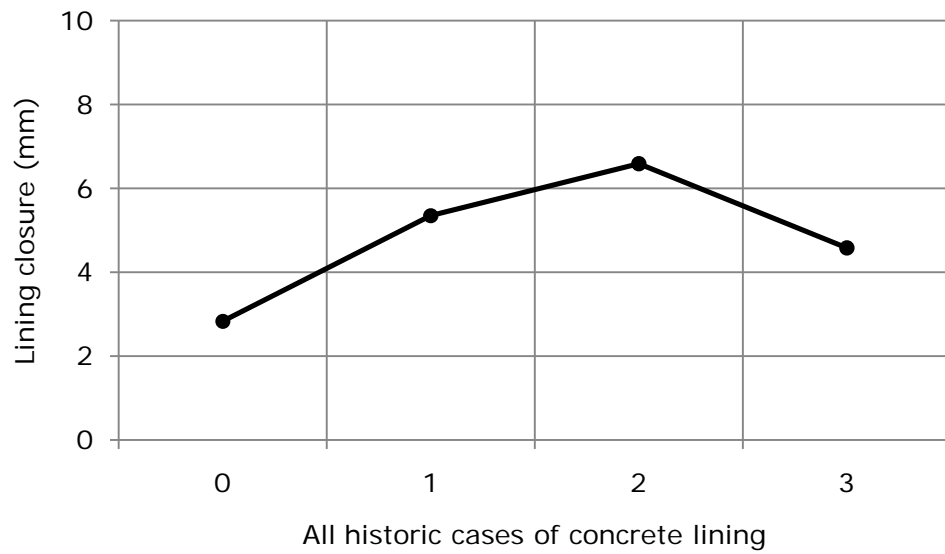


Figure 5.21 Shaft linings' closure from the two-dimensional models

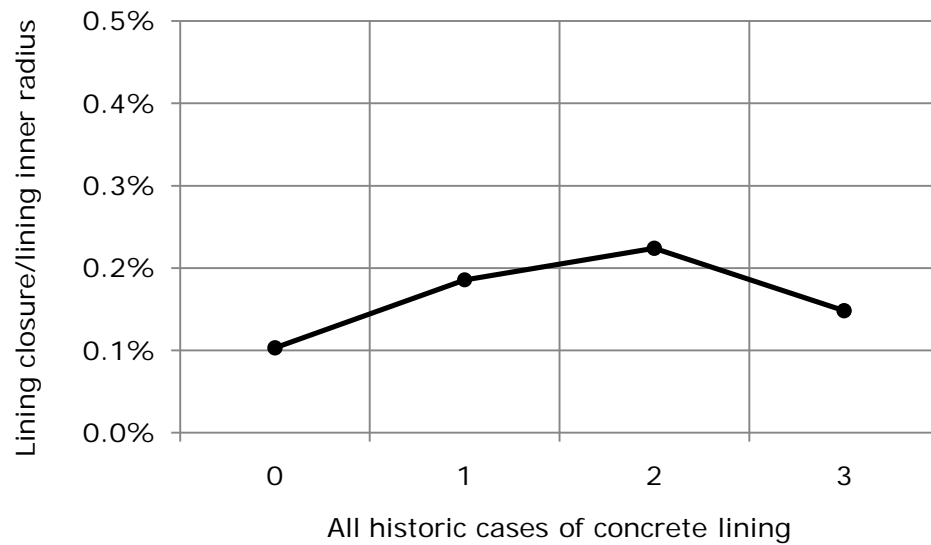


Figure 5.22 Ratio of lining's closure with inner radius of each lining

It can be seen that the biggest lining's closure occurred in the second relining – a double ring of concrete blocks (Figure 5.21). The ratio of shaft lining's closure with its inner radius also reached its peak in the second relining (Figure 5.22). For the newly designed third thicker relining, modelling results show that its closure and the ratio of its closure with its inner radius were lower than those of the first and second relinings.

As described in section 5.3, the shaft linings' closure should be as small as possible to keep the space inside the shaft large enough to allow unaffected shaft conveyance operations. In achieving this, the numerical modelling results imply that the single ring concrete blocks lining (the first and third relinings) was more effective, leaving more space in the shafts. It was thought by the author that more plywood packs between concrete blocks involved in second relining (double ring concrete blocks lining) made the relining more flexible in deformability compared with the first and third relinings. The models also show that the newly designed third relining should perform better than the previous relinings in terms of lining closure.

It can be noticed that the closures of the shaft relinings were bigger than that of the original lining. This was because of the filled materials between the HSC blocks in the relining, especially the squeezable plywood packs, which were designed to allow some radial displacements of the concrete blocks to improve the flexibility of the whole lining systems (Williams and Auld, 2002).

5.5.3.2 *Principal stress conditions in concrete linings*

Figure 5.23 shows the principal stress tensors in the numerical model for the first relining. It can be seen that the major principal stress (σ_1) was a tangential hoop stress, normal to the radial direction and its maximum value always occurred at the inner surface of linings as expected. The minor principal stress (σ_3), in the radial direction, usually was very low compared with the major principal stress (σ_1), even less than 1% of the major principal stress (σ_1) at some positions in the second relining.

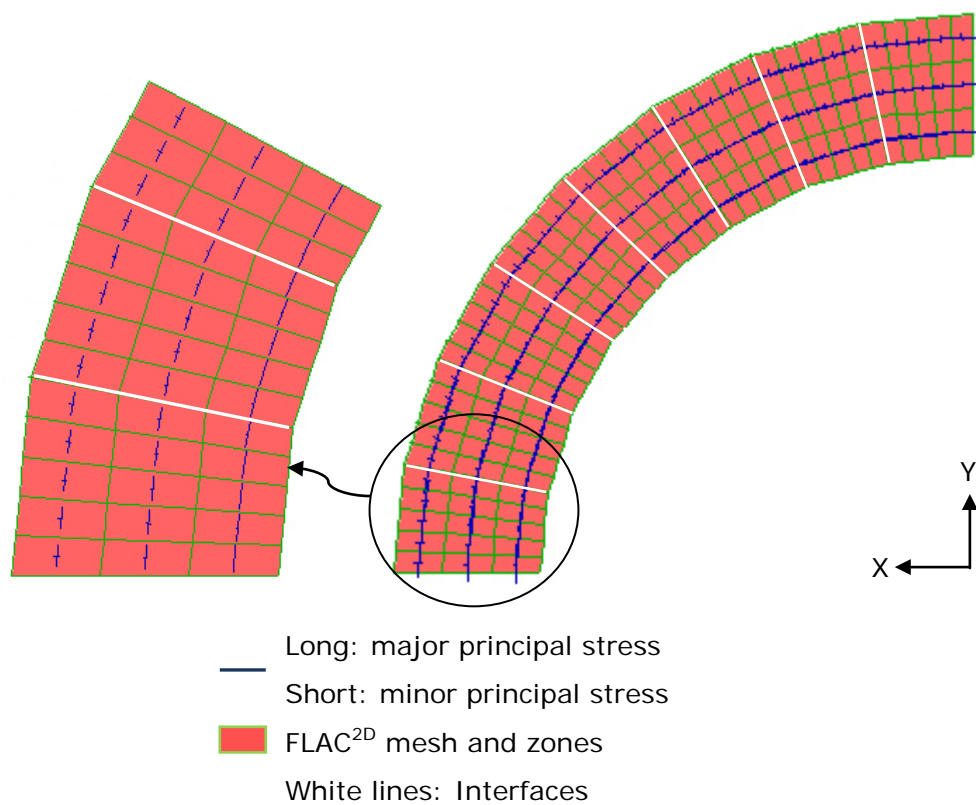


Figure 5.23 Principal stress tensors in the first relining

The difference between the principal stresses led to a very high deviator stress ($\sigma_1 - \sigma_3$) in the concrete lining in the numerical models. The maximum value of the deviator stress ($\sigma_1 - \sigma_3$) also always occurred at the inner surface of linings. High deviator stress ($\sigma_1 - \sigma_3$) would threaten the stability of the concrete lining system, since higher deviator stress ($\sigma_1 - \sigma_3$) will bring the Mohr circle closer to the strength envelope in the Mohr-Coulomb failure criteria (shown in Figure 5.24).

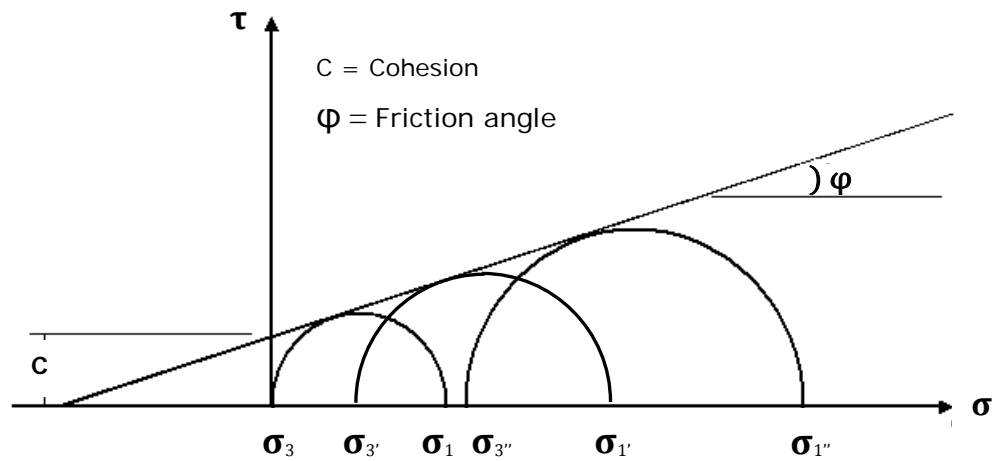


Figure 5.24 Mohr circles and strength envelop in the Mohr-Coulomb failure criteria

Figures 5.25~5.26 show the maximum major principal stress σ_1 and the maximum deviator stress ($\sigma_1 - \sigma_3$) in the shaft linings in the numerical models and the ratio of the maximum deviator stress ($\sigma_1 - \sigma_3$) with the corresponding characteristic strength of the HSC in each relining system at the mine.

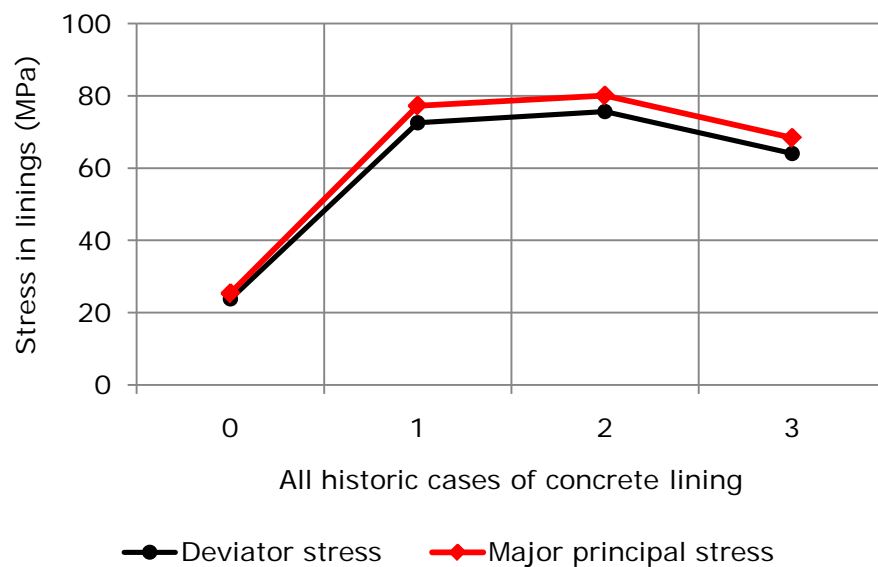


Figure 5.25 Max. major principal stress σ_1 and max. deviator stress ($\sigma_1 - \sigma_3$) in shaft linings

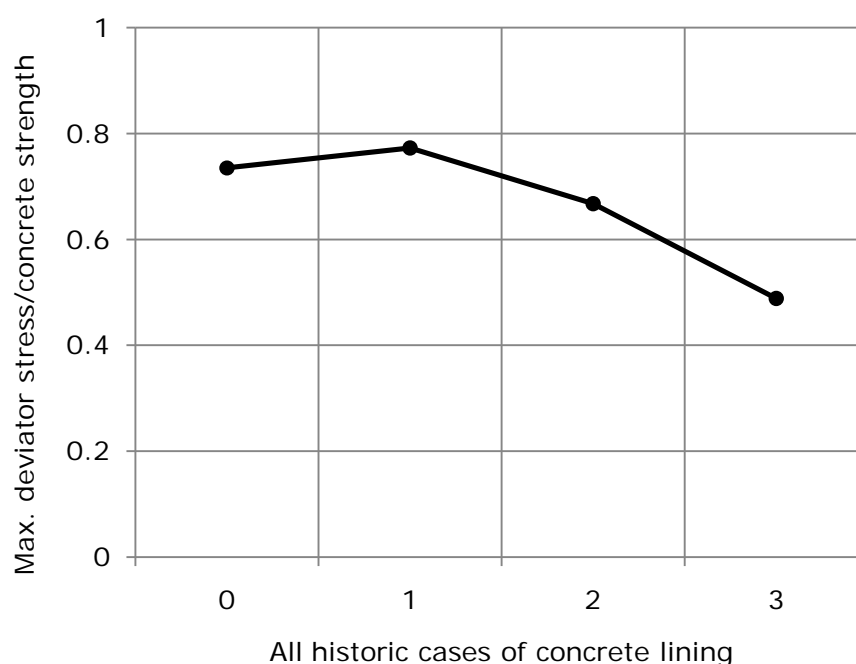


Figure 5.26 The ratio of the max. deviator stress ($\sigma_1 - \sigma_3$) in shaft linings with the corresponding HSC strength

As seen from the Figure 5.25, under high ground stress compression, the maximum major principal stress σ_1 and the maximum deviator stress ($\sigma_1 - \sigma_3$) in different linings increased with the increasing concrete strength, reaching the peak in the second relining and decreasing in the newly designed third relining. This result again implies that the single ring concrete blocks lining (the first and third relinings) was more effective than the double rings.

Figure 5.26 shows that the maximum deviator stresses ($\sigma_1 - \sigma_3$) in the shaft's original lining and the first relining were very close to the strength of the concrete (approximately 80%). However, the ratio of the maximum deviator stresses ($\sigma_1 - \sigma_3$) with the HSC characteristic strength decreased in the second and third thicker relining in the modelling, to only approximately 46% in the third relining. These modelling results illustrate

again that the newly designed third relining should perform better than the previous relinings in terms of the lower value of maximum deviator stress ($\sigma_1 - \sigma_3$) in the concrete lining. Figure 5.27 shows the major principal stress σ_1 contour of the first relining at the mine in the numerical model.

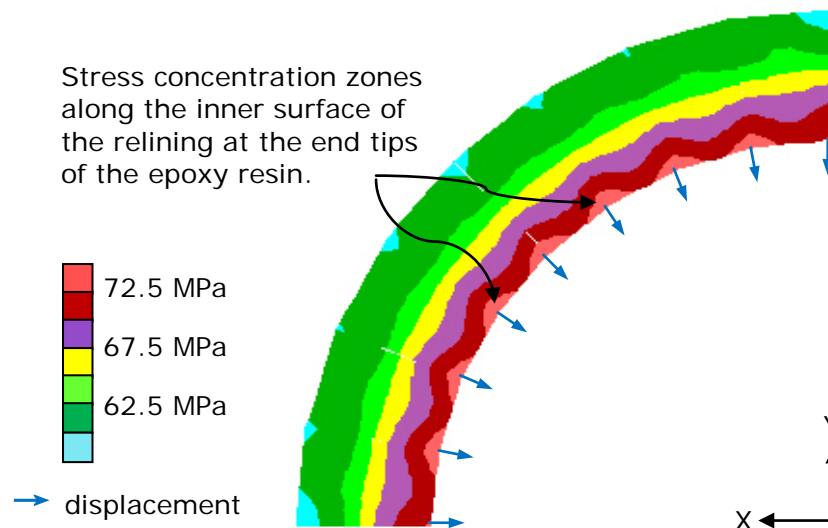


Figure 5.27 Major principal stress contour and direction of displacement in the first relining

It can be seen that there were stress concentration zones along the inner surface of the concrete lining at the end tips of the interfaces (epoxy resin in the first relining). A similar phenomenon happened in the models of the second and third relining. It demonstrated that interface materials between HSC blocks in shaft relinings improved the flexibility of the shaft lining systems successfully but caused stress concentrations at the inner surface of the concrete linings thus decreasing the strength of the whole lining system.

5.6 Conclusions

This chapter presented the results of parametric studies on the effects of rock properties of the Marl, the extent of weathered Marl and the ground stress field (hydrostatic or not) on the stress and deformation conditions of the shaft linings through the Marl zone. The possible “point” loading on the original shaft lining due to unevenly thick polyurethane was then simulated.

Based on the modelling results of the parametric studies, a series of numerical models have been carried out to simulate the stress and deformation conditions in the various historic stages of the lining systems employed in the Boulby mine shafts since the time that they were sunk. According to the modelling results presented above, some conclusions are drawn as follows:

- 1) In this research case, the parametric studies in the models imply that the stability of the original shaft lining was most sensitive to the friction angle of the surrounding Marl, and least sensitive to the cohesion of the Marl, because of soft Marl with fairly low cohesion (lower than 1 MPa) in an high ground stress field (nearly 30 MPa).
- 2) The concept of the plastic zone of the weathered Marl adjacent to the shaft has been introduced. Assumptions about the properties of the Marl have been largely based upon the results of tests conducted at the NCG and the RSM. The extent of the weathered Marl has been increased with each successive relining in numerical models indicating likely change to the Marl rock mass with time.
- 3) The increasing extent of the weathered Marl resulted in bigger deformation and stress conditions in the shaft's linings. It is suggested

by the author that 4 m (approximately equal to the shaft excavation radius) is a critical value for the extent of the weathered Marl in this research case. This critical value has been used in the later models.

- 4) The non-hydrostatic stress field would result in uneven loading on the circular shaft linings and threaten their stabilities.
- 5) A possible reason for the original shaft lining's failure may be due to uneven (point) loading on it, due to uneven thicknesses of backfill material. The cement grout backfilled in the relinings transferred high ground pressure to the concrete blocks gradually and facilitated the avoidance of potential uneven loading on the concrete linings.
- 6) In the models the maximum major principal stress (a hoop stress) and the maximum deviator stress always occurred at the inner surface of shaft linings as expected. A high deviator stress would threaten the stability of the concrete lining system.
- 7) The single ring concrete blocks are a more effective lining than the double rings, because more plywood packs involved in double rings concrete blocks lining made the relining more deformable.
- 8) For the newly designed third thicker relining, the ratio of lining's closure with its inner radius was lower than those of the previous relinings. The ratio of the maximum deviator stress with the HSC characteristic strength was only approximately 46% in the third relining. These modelling results illustrate that the newly designed third relining will perform better than the previous ones.
- 9) Stress concentration zones were evident along the inner surface of the shaft relining at the end tips of the interfaces. This demonstrated that interface materials between HSC blocks in shaft relinings improved the flexibility of the lining systems successfully but these weak "joints" decreased the strength of the whole lining systems.

Based on the two-dimensional modelling results presented in this chapter and conclusions listed in 1~9 above, it is thought that the Marl with weak mechanical properties should not be the only reason for the failure of the shaft linings through this stratum since the modelling results show that even in the second relining, the lining's closure was less than 0.3% of the lining's inner radius. To find other reasons for the failure of the shaft linings and the effect of surrounding strata on the shaft lining's stability in three-dimension, three-dimensional numerical models of the shaft linings at Boulby mine have been conducted, which are presented in detail in the following Chapter 6.

CHAPTER 6

THREE-DIMENSIONAL NUMERICAL MODELLING OF SHAFT LINING SYSTEMS

6.1 Introduction

The FLAC^{3D} numerical code has been used to set up three dimensional models for the mine shaft relining's stability analysis, considering the effect of the shaft inset and the roadway leading to it, on the stress distribution and subsequent displacement of the shaft lining wall above the inset at Boulby mine. The shaft inset is schematically shown in Figure 6.1.

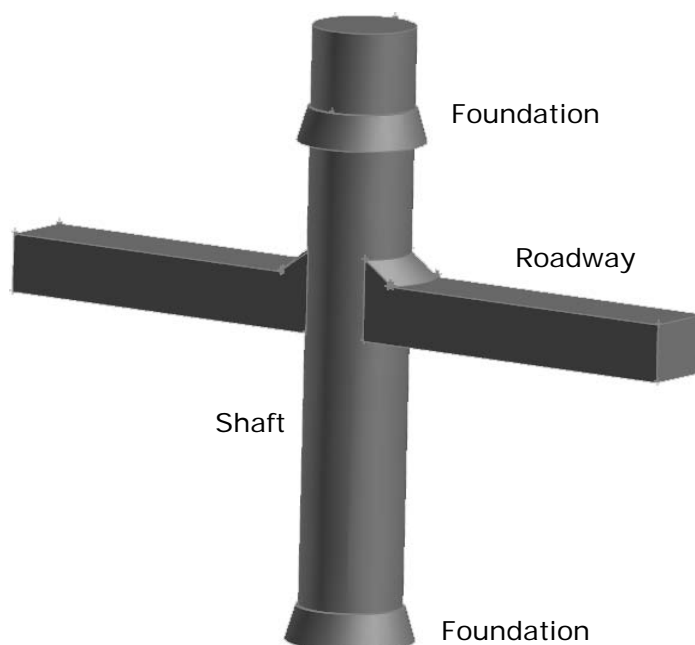


Figure 6.1 Schematic inset of the shaft and the roadway

As described in Chapter 5, all numerical models in this chapter have been based on the man shaft, and the solid three-dimensional elements have been utilised to model the shaft linings. Due to the limitation of the finite

difference mesh in numerical models and the difference between the dimensions of the mine original shaft lining and relinings through the Marl zone, two modelling methods have been developed in three-dimensional models in this research to simulate each stage in the shaft linings. The detailed modelling methodology, model configurations and modelling results are presented and discussed in this chapter.

6.2 Modelling Methodology - A Continuous Model for the Original Lining and All Relining Systems

As stated and shown in Chapter 5 (section 5.5, Table 5.4), the original shaft lining and relinings through the Marl zone at Boulby mine did not have the same dimensions. However, the finite difference mesh in numerical models cannot be changed once the programme starts running. Additionally, joint fillings (epoxy resins, cement mortar and plywood packs) between the concrete blocks make the relining systems and the numerical modelling of them more complicated and time-consuming. To solve these problems, two modelling methods have been utilised in the three-dimensional models to simulate each stage in the shaft construction and lining at the mine. The aims and particular procedures of these two methods are described and discussed as follows.

The first method used was to simulate the shaft's original lining and all subsequent relinings through the Marl zone continuously in one finite difference mesh. By this method, the effect of the historic changes in the stress field on each shaft lining's stability could be investigated from the shaft's initial construction, original lining installation, the construction of the inset and the roadway leading from the shaft, and subsequent relining phases. However, only one set mesh was involved in this method, in which

all the relinings through the Marl zone have the same dimensions as the original shaft lining, which were originally smaller than their own particular dimensions. At the same time, joints between concrete blocks were not directly included in the numerical modelling in this method to save numerical calculation time. However these existed in all relinings at Boulby mine: epoxy resin and cement mortar in the first shaft's relining, plywood packs in the second and third shaft's relinings.

Due to these differences between the real situation and numerical modelling of the relinings through the Marl zone, values of the actual material properties for the high strength concrete (HSC) used in the relinings, which had been obtained through the laboratory tests conducted at the NCG (shown in Appendix III) cannot be utilised in the numerical modelling directly. A set of equivalent material properties for the HSC relining system is required to be used in the numerical modelling in the first proposed method. The problem is then how to calculate accurately the equivalent properties for the HSC relining system?

Simple three-dimensional models were employed modelling the lining alone to obtain the equivalent properties for the shaft's relining systems through the Marl zone. The shaft's first relining system was taken as an example to demonstrate the process of obtaining the equivalent properties for the relining systems.

Firstly, a mesh was set up representing three layers of concrete block rings in the first relining system through the Marl zone, using the actual dimensions of the first relining system shown in Table 5.4. Interfaces elements have been introduced into this mesh to represent the joints between concrete blocks filled with epoxy resin and cement mortar. This mesh is shown in Figure 6.2. Only a quarter of a circular shaft's lining was

modelled since it is a symmetrical problem. The blue zones in the mesh (Figure 6.2), representing concrete blocks, were assigned with the actual material properties (cohesion C , friction angle ϕ and tensile strength σ_t) for the HSC blocks used in the shaft's first relining. The red planes in Figure 6.2 indicate the interface elements and were assigned interface properties which have been described in Chapter 3 (section 3.4).

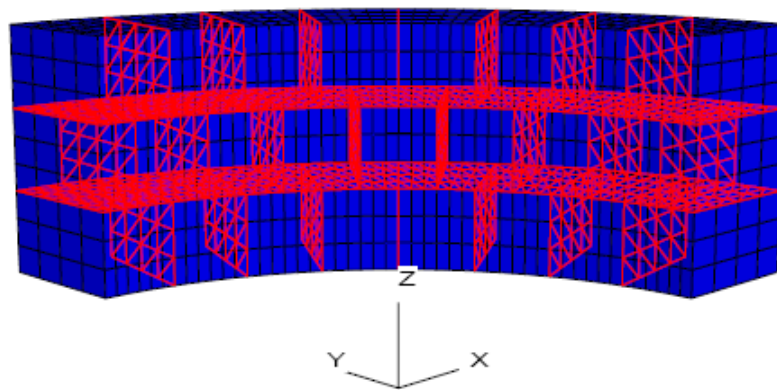


Figure 6.2 Mesh in the dimensions of the first relining system

The top plane and the inner surface of the model in Figure 6.2 were free. The bottom plane in Figure 6.2 was fixed in the Z direction. A series of radial compressive stresses were applied onto the outer surface of the model in Figure 6.2. The boundary planes in Y-Z and X-Z planes in Figure 6.2 were fixed in X and Y directions, respectively. Horizontal displacements of several points on the inner surface of the model were monitored during the modelling calculations. Vertical displacements were very small compared with horizontal displacements and neglected in this exercise. Each concrete lining's inner radius decreasing ratio ($\Delta r/r$) plotted against radial loading curve was obtained after a series of models of increasing load were completed. This is called the TARGET curve (shown as black line) in Figure 6.3.

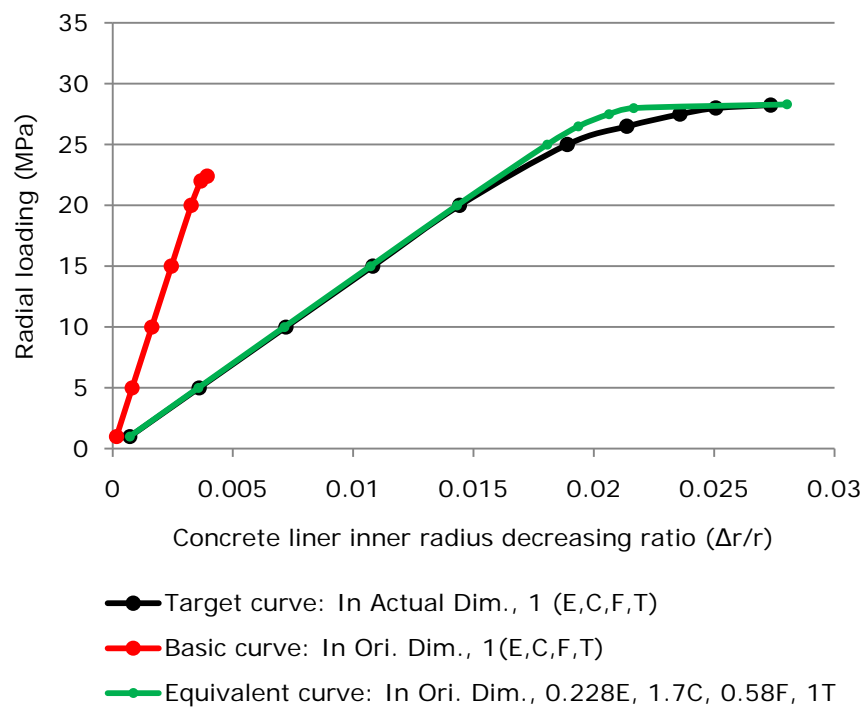


Figure 6.3 Curves obtained in the process of calculating equivalent properties for the shaft's first HSC relining system

Secondly, another mesh was built up representing three layers of concrete block rings in the shaft's first relining system through the Marl zone, but using the dimensions of the original lining system shown in Table 5.4, without interface elements to represent the joints between concrete blocks. This mesh is shown in Figure 6.4. The actual material properties (cohesion c , friction angle ϕ and tensile strength σ_t) for the HSC used in shaft's first relining were assigned to the whole model. The boundary conditions and displacements monitoring were set to be the same as the previous model. Another concrete lining's inner radius decreasing ratio - radial loading curve was obtained after a series of models were completed. This was called the BASIC curve (shown as the red line) in Figure 6.3.

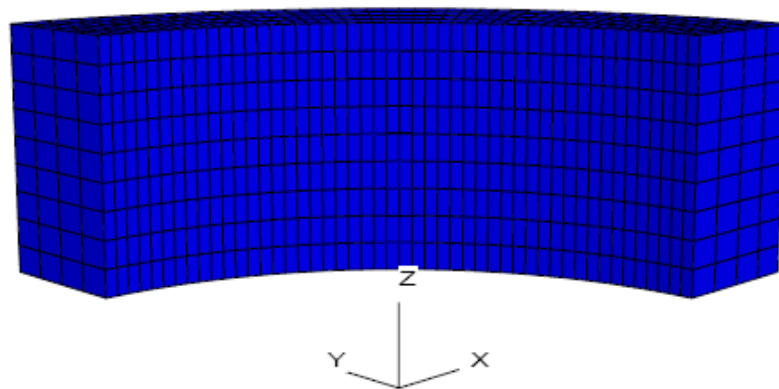


Figure 6.4 Mesh in the dimensions of the shaft's original lining

What was needed next was to adjust input material properties for the HSC used in the shaft's first relining in the model shown in Figure 6.4, to obtain an EQUIVALENT curve as close to the target curve as possible shown in Figure 6.3. This was achieved through an iterative trial and error process. Only the Mohr-Coulomb properties (cohesion c and friction angle ϕ) have been changed in this procedure since the numerical test examples show that the tensile strength σ_t has little effect on the curve. The input material properties determined corresponding to the equivalent curve in Figure 6.3 are called equivalent material properties for the HSC used in the shaft's first relining for the first modelling method. This process was then repeated for the other relinings. All the equivalent properties for the HSC used in the relining systems at Boulby mine are shown in Table 6.1.

	Young's modulus (GPa)	Cohesion (MPa)	Friction angle (°)	Tensile strength (MPa)
1 st relining concrete	7.48 (0.228)	40.31 (1.7)	27 (0.58)	5.47 (1)
2 nd relining concrete	16.56 (0.46)	48.69 (1.7)	25 (0.55)	7.41 (1)
3 rd relining concrete	17.0 (0.52)	27.94 (1.19)	48 (1.17)	8.31 (1)

Note: the values in brackets are the ratios of equivalent properties to the corresponding actual properties. For friction angles, they are the ratios of equivalent tangents to the corresponding actual tangents.

Table 6.1 Equivalent input properties for the HSC used in shaft's relining systems at Boulby mine

6.3 Modelling Methodology - Independent Models for the Original Lining and All Relining Systems

The second modelling method simulated all the shaft's relinings through the Marl zone in their own true dimensions, which means that three new finite difference meshes were required, one for each relining system, and each different from the one for the shaft's original lining. Figures 6.5~6.6 show the vertically consistent and non-consistent finite difference meshes used to model the mine shaft's original lining and the first relining (the terms 'consistent' and 'non-consistent' are related to the inner surface of the shaft linings).

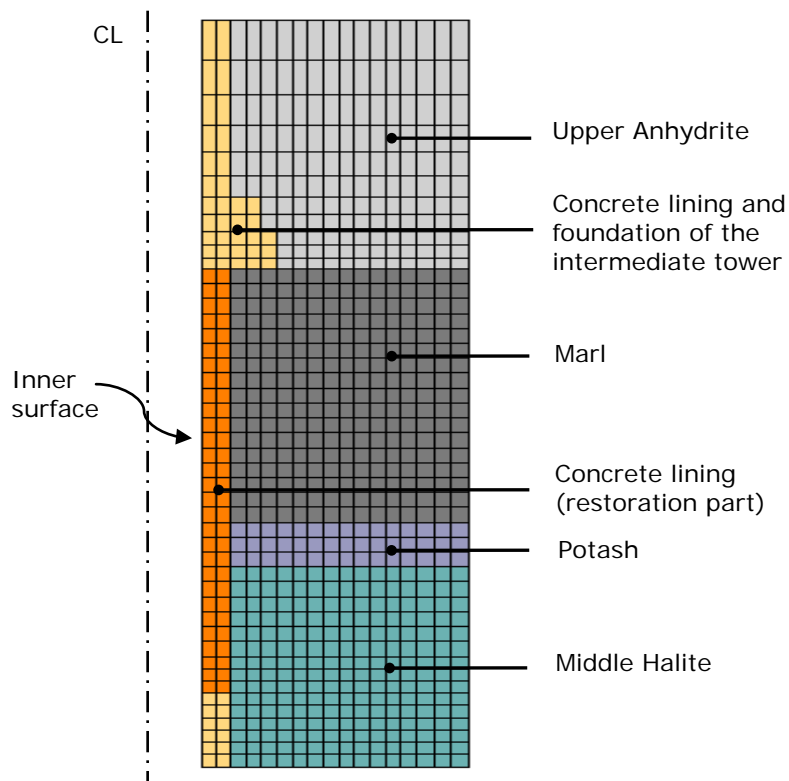


Figure 6.5 Consistent mesh for the original lining (part of vertical section)

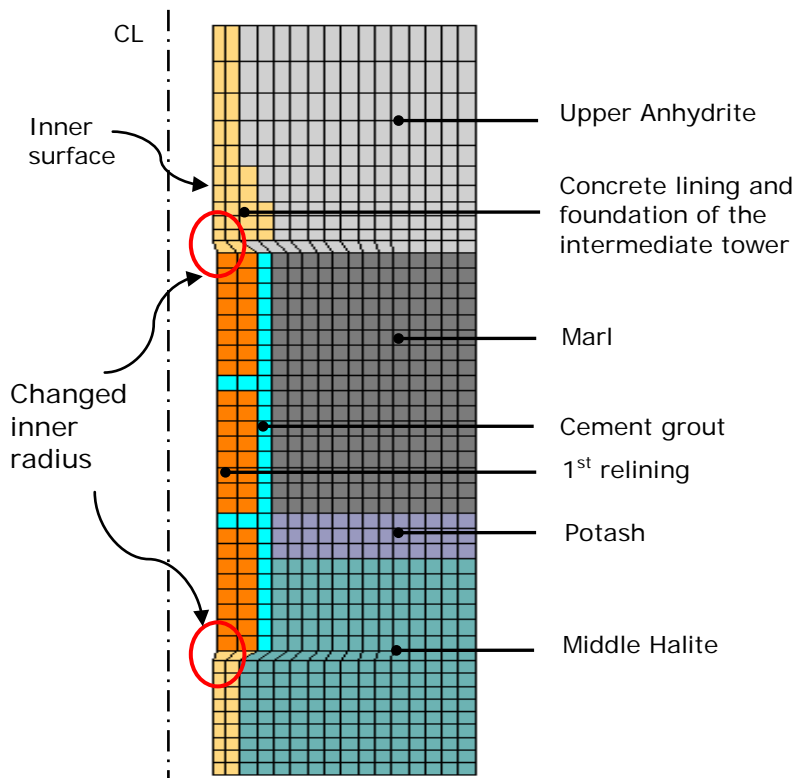


Figure 6.6 Non-consistent mesh for the 1st relining (part of vertical section)

By this method, the actual material properties for the HSC used in relinings through the Marl zone were utilised directly in the numerical modelling. Joints (epoxy resin, cement mortar and plywood packs) between concrete blocks have also been included in the models in this method, and are represented by interface elements (shown in Figure 6.7).

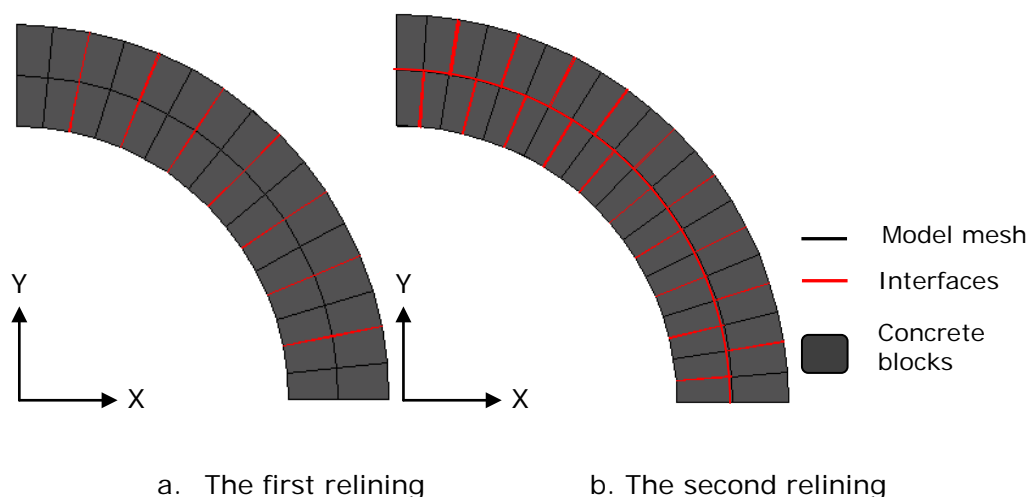


Figure 6.7 Interfaces in the relining systems in the numerical models

Although this method models the geometry accurately it is not possible to carry over stresses induced by previous relining, with the stress having to be reset back to its original hydrostatic value for each model. The other disadvantage of this method is that it is fairly time-consuming due to the large number of interface elements involved in each shaft relining model representing joints between concrete blocks. Lots of interfaces make the numerical calculation very slow. In the three-dimensional model for the first, second and third relining systems at the mine, there were 205, 146, 152 interface elements, respectively (326 interface elements will be required in the second relining system if they were set up according to the practical situation. To reduce the number of the interface elements, 16 layers of concrete rings have been replaced in the model by 7 “big rings”).

It takes approximately 24 hours to finish the whole model calculation if using the continuous model for the original lining and all relining systems, with equivalent properties for the relining systems. However, nearly 70 hours are taken to finish calculation using the independent models for the original lining and all relining systems with all practical dimensions and interface elements.

6.4 Modelling Methodology - Excavation and Relining Sequences

To avoid a catastrophic collapse failure in the model (especially in soft stratum like the Marl) and to make the numerical simulation as close to the real engineering situation as possible, the excavations of the shaft/roadway and the relinings through the Marl zone in all numerical models were carried out in multiple-steps. Shaft excavation (from the top down direction) sequences in different strata used in the modelling are shown in Table 6.2. The roadway excavation, made after the whole shaft had been fully excavated, included four steps, around 9 m forward each step. Therefore, there are in total 17 excavation steps in all numerical models before all relining work.

In which strata	Strata thickness in model (m)	1 st step (m)	2 nd step (m)	3 rd step (m)	4 th step (m)	5 th step (m)
Upper Anhydrite	10	3	3	4 (3 m foundation inclusive)		
Marl	10	2	2	2	2	2
Potash	2	2				
Middle Halite	46	11	10	10	15 (6.8 m foundation inclusive)	

Table 6.2 Shaft excavation sequences used in the numerical models

The following flow chart (Figure 6.8) shows the detailed operations in excavation modelling for the Boulby mine shaft project, which have been designed to take the practical construction situation into account in the numerical modelling. In the practical situation, the shaft lining is not installed immediately after shaft excavation. During this time period before the lining installation, stress relief usually occurs in the surrounding rock near the excavation face (described in Chapter 5, section 5.2). This stress relief in the surrounding rock was simulated by running the program to equilibrium ("Solve" part in Figure 6.8) after a one step excavation but before installing the lining in this step excavation in numerical models.

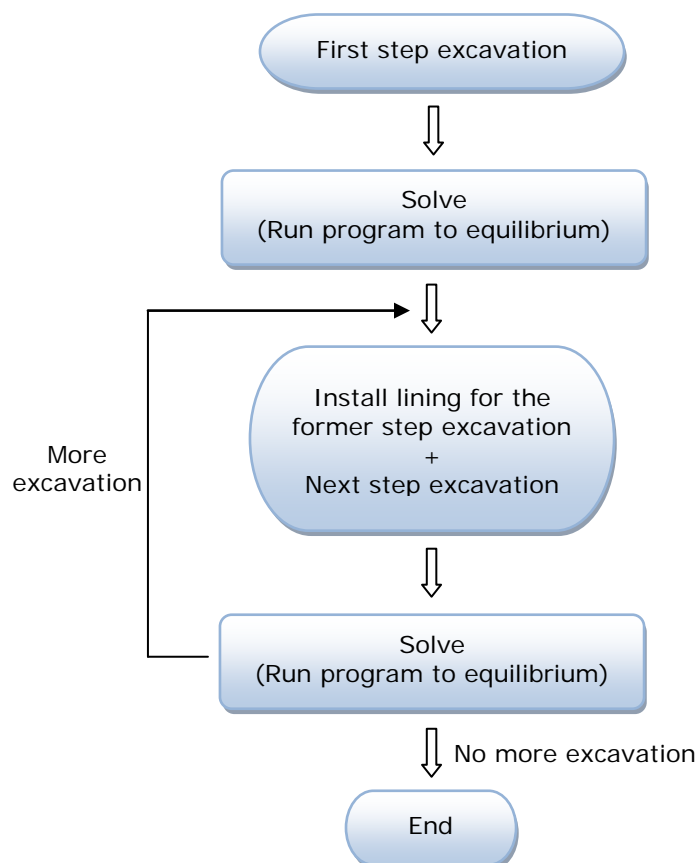


Figure 6.8 Excavation steps flow chart in numerical models

In all three-dimensional models, the shaft's relining was simulated after the excavations of the shaft and roadway, also in multiple-steps, but from

the bottom up direction. In fact, shafts at Boulby mine have been relined through the Marl zone in different lengths each time. According to the figures quoted by Williams and Auld (2002), approximately 15.8 m of the original shaft lining through the Marl and Potash strata was replaced in the first relining; in the second relining, approximately 11.4 m of the first relining was replaced. It is reported by the mine that in the third relining, approximately 10.8 m of the second relining will be replaced. Figure 6.9 shows schematically the Boulby mine shaft's relining sequences through the Marl zone used in all three-dimensional models.

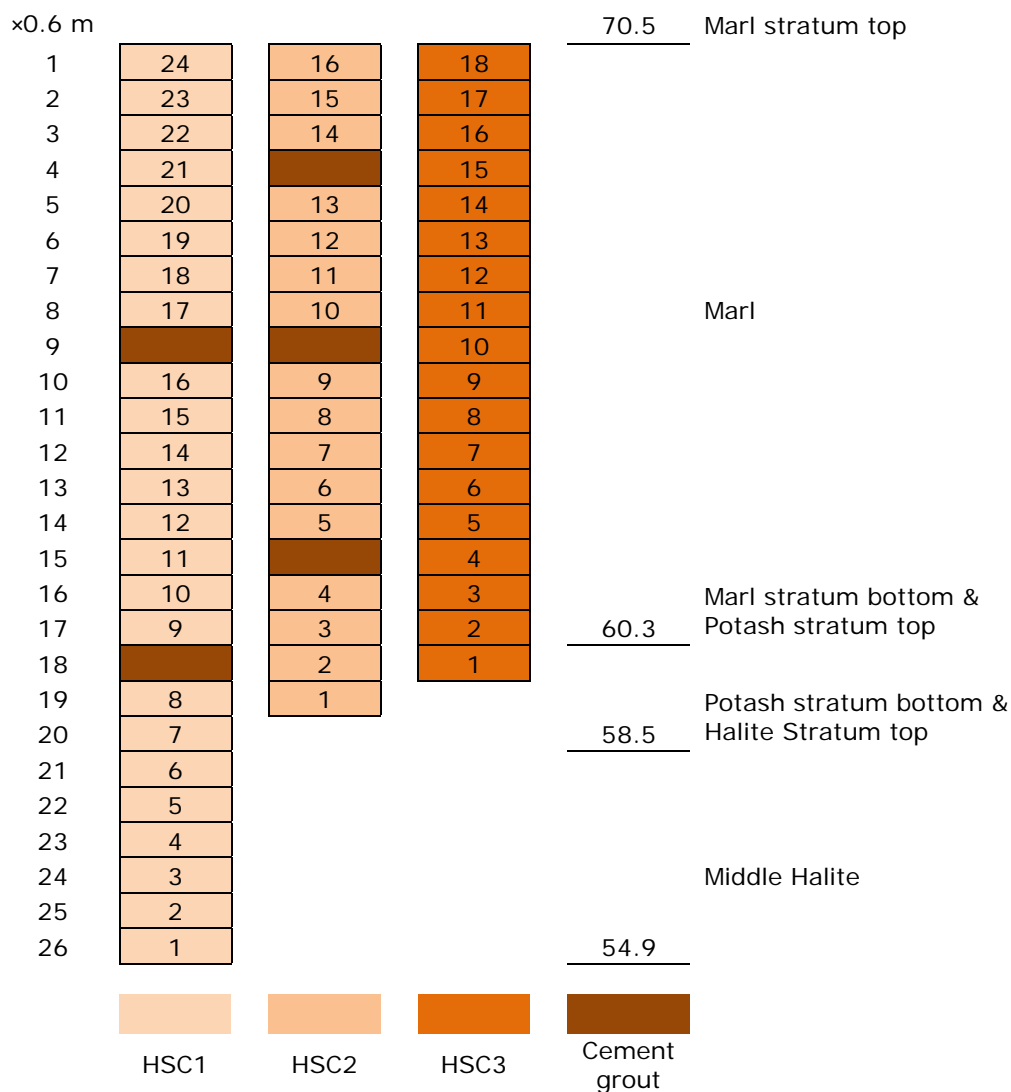


Figure 6.9 Schematic shaft relining sequences in the continuous model

The horizontal gaps between shaft lining sections in the first and second relining systems, have been backfilled with cement grout in the models instead of being left open during numerical modelling, to avoid massive inwards displacements of the host rock at these levels. This cement grout possessed the same properties as that backfilled into the gap between the relining and shaft's excavation face. These horizontal cement grout layers divided the first and second relining systems into 3 and 4 sections, respectively. These practical engineering sections have been treated as relining steps in all models, from the bottom up direction which is the practical construction direction. For the third relining, 18 layers of concrete rings have been evenly separated into 3 steps, 6 layers each step.

In each independent model for the shaft relinings, firstly, the original NSC lining was installed through the whole shaft during the shaft excavation from the top down (though the dimensions of the lining through the Marl and Potash strata are actually bigger than those of the original NSC lining and interface elements have to be kept in the model because of the limitation of the finite difference mesh generation). Then the roadway excavation was carried out, followed by the corresponding shaft HSC relining from the bottom up.

6.5 Model Configurations

6.5.1 Model Domain and Mesh Design

As described in Chapter 5 (section 5.2), due to the numerical modelling constraints on computer memory and analysis time, it is not possible to cover the whole length of the mine shaft in the numerical models. Artificial boundaries have been placed around the model domain. Therefore, not all strata beneath the ground surface were included in the models.

The artificial top and bottom boundaries of the whole model domain in this research were set to be 1075 m and 1155 m beneath the ground surface, respectively. This domain contains the Upper Anhydrite stratum (above the Marl), the Marl stratum, the Potash, the Middle Halite and the Middle Anhydrite strata (beneath the Marl), shown in Figure 6.10. The roadway was driven in the Middle Halite and its roof was located 8 m below the Potash floor. The dimensions for the whole domain are shown in Figure 6.11. Laterally, the model was about ten times the shaft excavation radius. Because this is a symmetrical problem, only a quarter shaft with inset and one side roadway has been modelled to save the programme running time and memory.

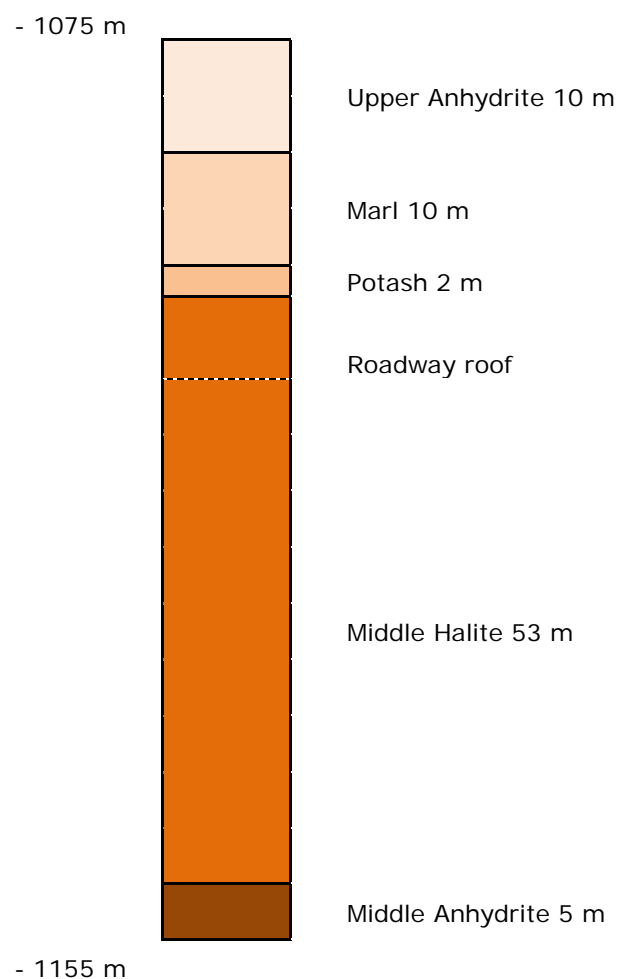


Figure 6.10 Geological stratigraphy in the study

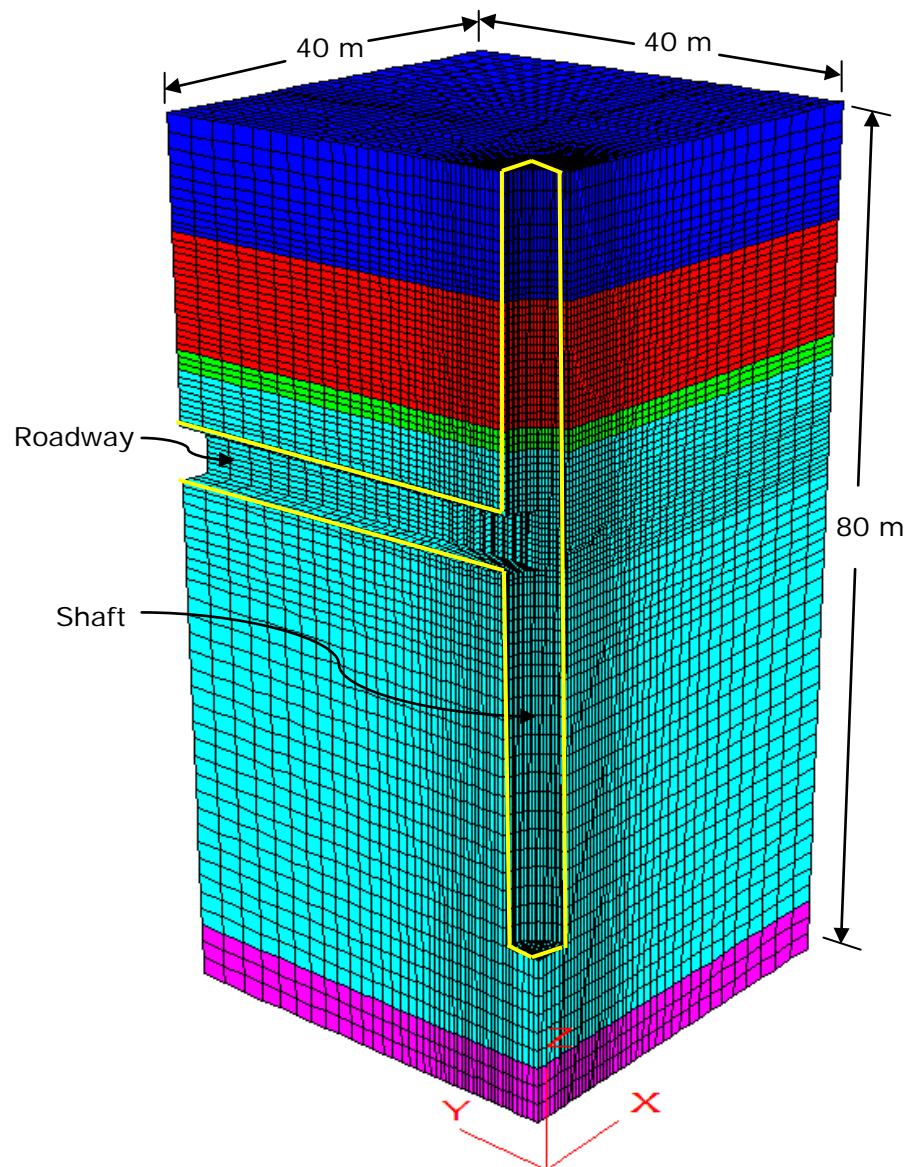


Figure 6.11 Numerical model domain and mesh in the study

6.5.2 Dimensions Used in the Models

In order to obtain dimensions used in the numerical models, two CAD drawings from Cleveland Potash Ltd. have been referred to:

- *Manshaft: Vertical Sections Through N/S Axis July 1976 (-2677' ~ -3754'),*

- *Manshaft: Miscellaneous Sections (JULY 1976)*

These CAD drawings show that the thickness of the shaft's original concrete lining at Boulby mine varied through the whole shaft, and was approximately 0.61~0.75 m thick and at the top end of this range in the Marl and Potash strata. Polyurethane was backfilled in the gap between surrounding rock and original shaft lining through the Marl and Potash strata. Meanwhile, vermiculite powder was used as backfill material in the gap between surrounding rock and concrete lining in the Upper Anhydrite and Middle Halite strata. These gaps were about 0.45 m in thickness. In later shaft relinings, polyurethane was replaced by the cement grout, and the gap between surrounding rock and shaft relinings through the Marl and Potash strata was around 0.4 m in thickness.

For simplification of the three-dimensional models in this research, the shaft's original lining was kept at a uniform thickness, 0.75 m, and 0.4 m was used for the gaps between the concrete linings and the surrounding rock through the whole model domain. The detailed dimensions for the original shaft lining and relinings are shown in Table 5.4.

The CAD drawings from Cleveland Potash Ltd. also show that the roadway was driven approximately 6 m wide and 4.6 m high. In this study, 6 m wide by 4.5 m high has been used for the dimension of the roadway in the Middle Halite, with roadway height adjusted a little according to the finite difference mesh density in the numerical models. It was assumed that the roof of the roadway in the Middle Halite was 8 m beneath the Potash floor.

6.5.3 Support for the Roadway

To support the roadway, it is known by the author that steel sets have been applied at Boulby mine and it has been assumed that steel sets with

heavy section were utilised. A table of maximum support pressures (Hoek and Brown, 1980) for various steel set systems was referred to. Based on this table and the available information of the steel sets used at the mine, the maximum support pressure of these steel sets is 2.53 MPa when the tunnel radius is 5 m wide and steel set spacing is 1 m. This was chosen for supporting the roadway's roof and sidewalls in the numerical models.

At the area near the roadway inset with the shaft, stronger support was needed because of the anticipated severe stress conditions caused by the massive excavation. Therefore, for the first 5 m (away from the shaft inner surface) roadway, 3.5 MPa as a support pressure has been used for the roof and a pressure of 2.53 MPa has been applied to the floor. During simulating the shaft relinings in the three-dimensional models, massive upwards displacements in the whole roadway floor occurred due to high ground stress in the underlying rock strata. To solve this problem, a 0.5 m thick concrete slab, the same material as the original concrete lining in the Marl, has been employed for the roadway's floor in numerical models.

6.5.4 Detailed Engineering Design Modelling

To obtain as accurate numerical modelling results as possible, an attempt has been made to set up the three-dimensional models for the Boulby mine's shaft project according to the practical situation. It is known that the complete mine shaft comprises three parts: the top tower, the intermediate tower and the lower tower. Each tower has a foundation at its base. The foundations of the intermediate tower in the Upper Anhydrite stratum and the whole man shaft in the Middle Halite stratum have been included in the models. Additionally, the wing walls at the shaft inset level have also been considered in setting up the models. The dimensions and the finite difference mesh for these structures are presented in this section.

6.5.4.1 Foundations in the Man Shaft

The dimensions of the reinforced foundation of the intermediate tower can be found in Figure 6.12. According to the CAD drawing *Manshaft: Vertical Sections Through N/S Axis July 1976*, the man shaft at Boulby mine is seated on a concrete foundation about 1144 m deep beneath the ground surface, i.e. the foundation of the lower tower of the man shaft. The dimensions of this foundation can be found in Figure 6.13.

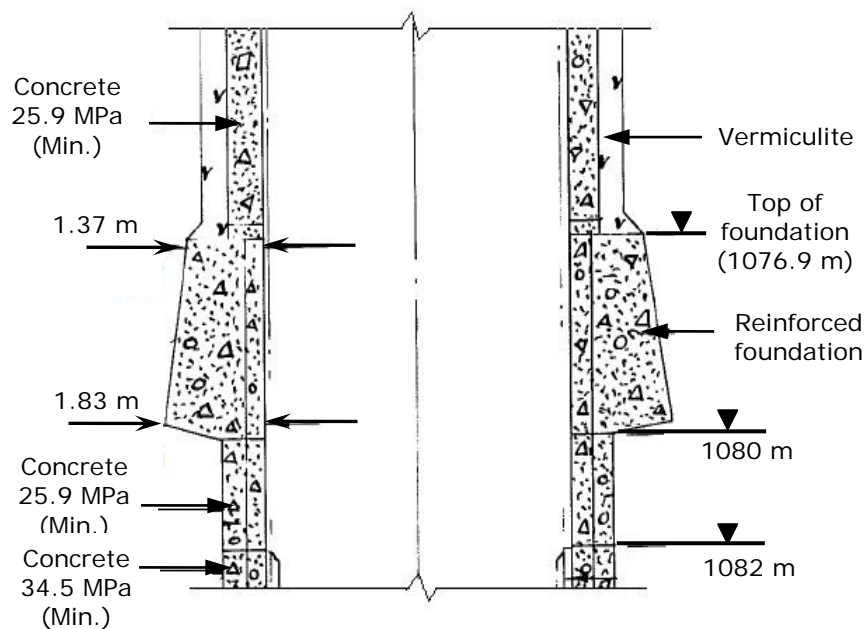


Figure 6.12 Foundation of the intermediate tower - vertical section
(*Manshaft: Vertical Sections through N/S Axis July 1976*)

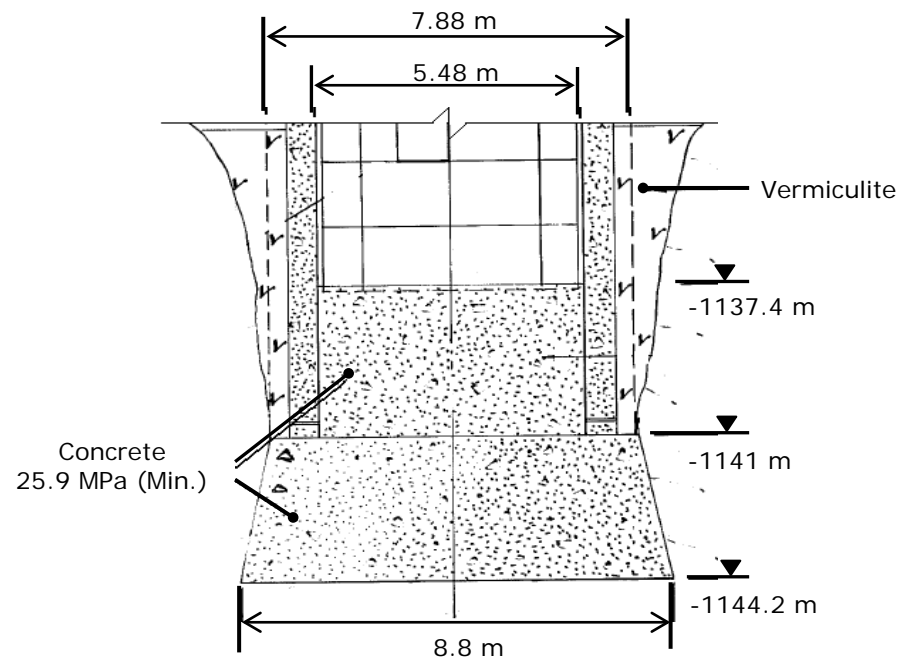


Figure 6.13 Foundation of the Manshaft - vertical section (*Manshaft: Vertical Sections through N/S Axis July 1976*)

Because of the limitations of the rectangular meshes utilized in the three-dimensional models, these two foundations' shapes have been approximately modelled using a 'step-shape' in this study. Figure 6.14 shows the whole model mesh in the X-Z plane (vertical section of the shaft) used for this study.

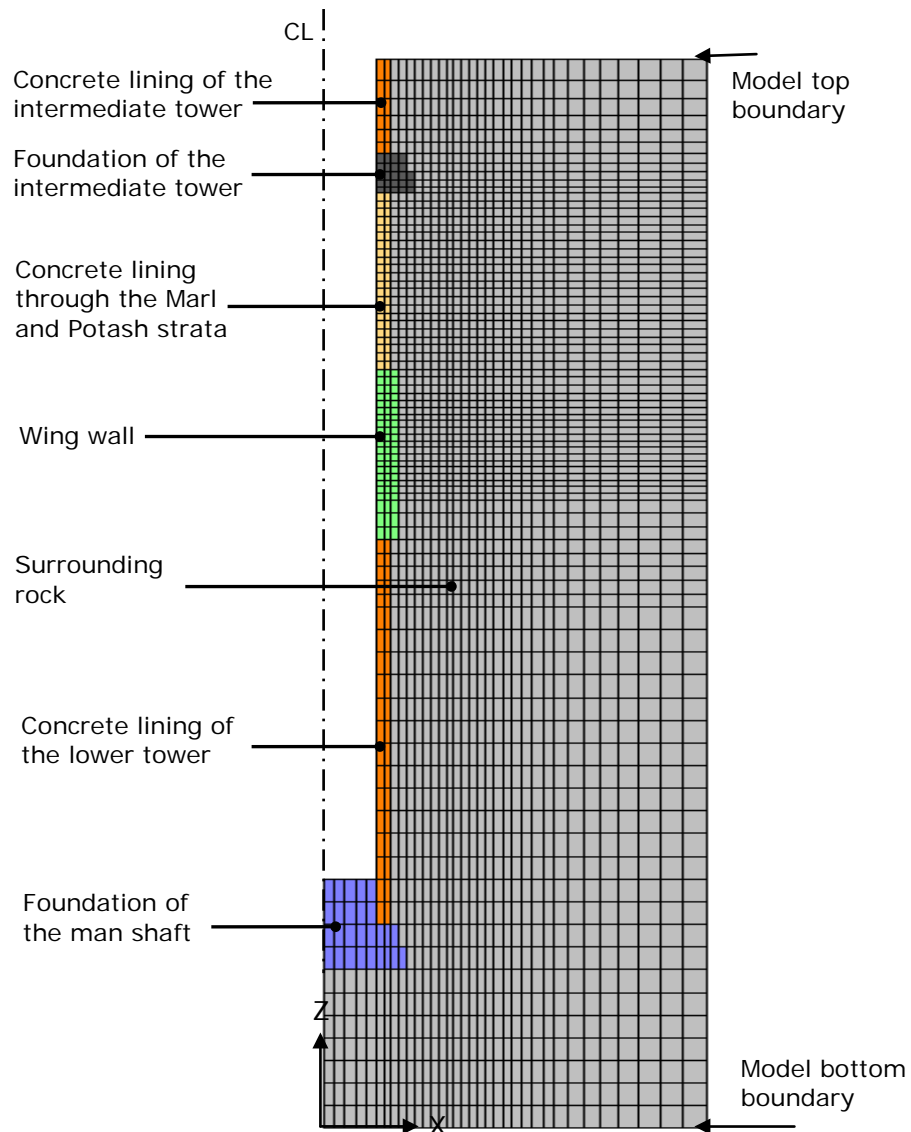


Figure 6.14 Vertical section of the whole model mesh for this study
(through X-Z plane)

6.5.4.2 Wing Wall at Shaft Inset Level

Wing walls were built at the shaft inset level, shown in Figure 6.15, to resist high stresses caused by the massive excavation in this area. Figure 6.15 shows that the wing walls are a little thicker than the original shaft lining (0.75 m) and wider than the outer diameter of the lining (6.98 m). The CAD drawings mentioned in section 6.5 show that the wing walls are 0.91 m thick and 12.2 m high.

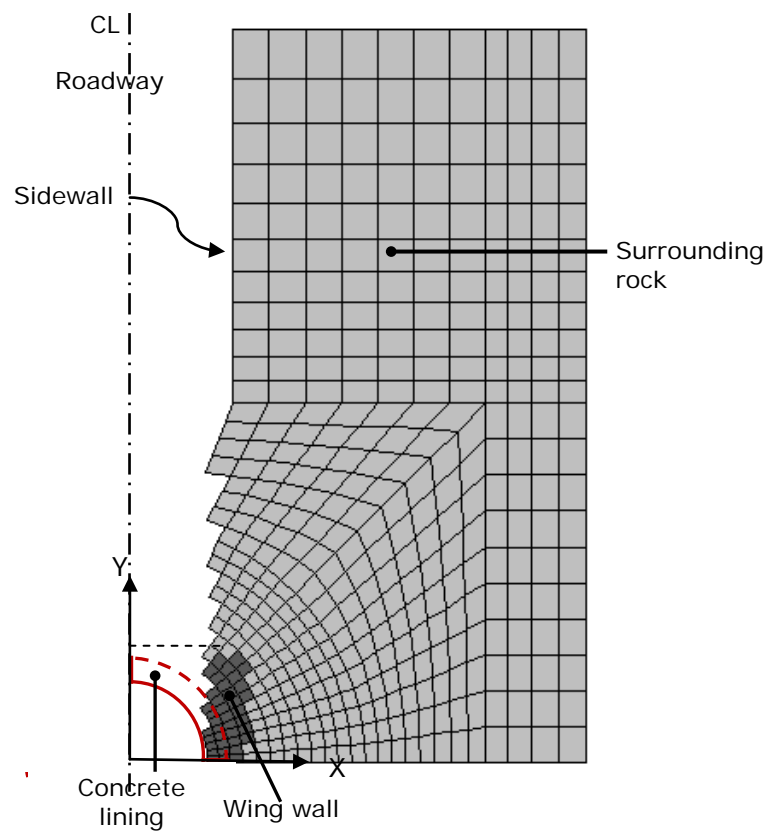


Figure 6.16 Plan view of wing walls modelled in this study (through the X-Y plane)

6.6 Boundary and Initial Stress Conditions

Boundary and initial stress conditions in numerical models define the in situ state (i.e., the boundary and stress condition before a change or disturbance in the problem state is introduced) of the geomechanical problem. The boundary and initial stress conditions utilised in the three-dimensional models are presented in this section, and shown in Figure 6.17.

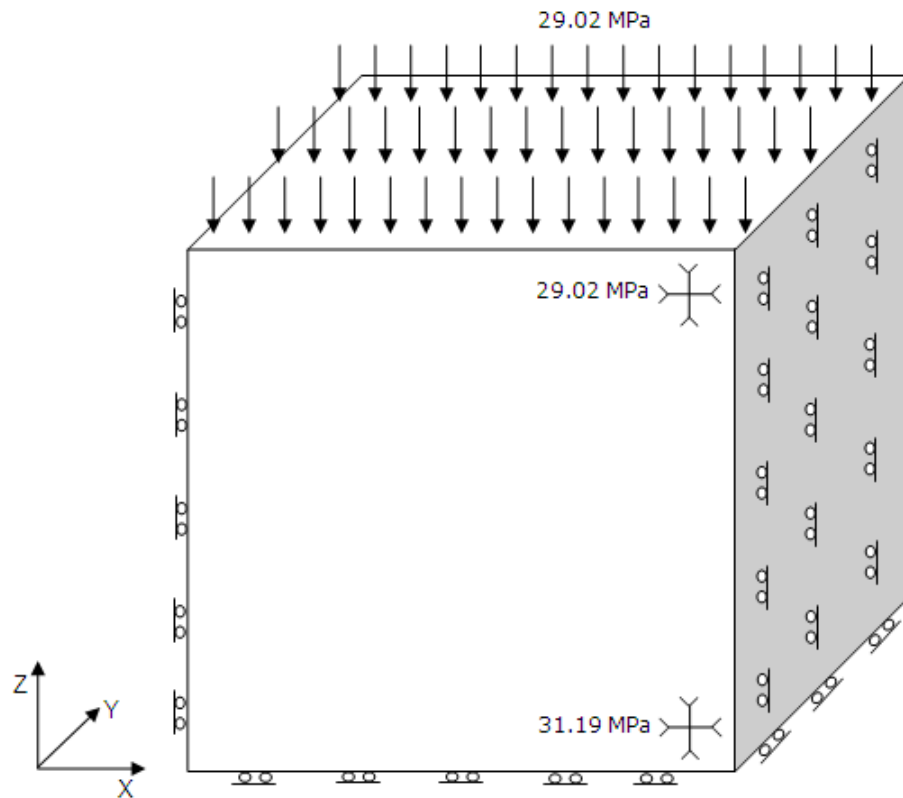


Figure 6.17 Boundary conditions in the three-dimensional models in this study

As described in Chapter 5 (section 5.2), the hydrostatic initial stresses were reconstructed in the numerical models according to Equation (5.1). Based on the description in section 6.5, $h = 1075\text{ m}$ for the top boundary, and $h = 1155\text{ m}$ for the bottom boundary were used in the models. The front boundary plane (X-Z plane in Figure 6.17) and back boundary plane were fixed in the horizontal direction (Y direction). A vertical ground stress 29.02 MPa, calculated using Equation (2.7), was applied on the top boundary plane. Gradient ground stresses changing with depth were applied to all the elements inside the whole model domain, i.e.

$\sigma_x = \sigma_y = \sigma_z = 0.027 \times 1075 = 29.02\text{ MPa}$ for the elements at the top of the model domain, and

$\sigma_x = \sigma_y = \sigma_z = 0.027 \times 1155 = 31.19 \text{ MPa}$ for the elements at the bottom of the model domain.

6.7 Material Properties

Various materials are involved in this research (the surrounding rock types, concretes, cement grout etc.) which have been described in Chapter 5 (section 5.2). The detailed methodology for obtaining the input material properties and the final version of them used in the numerical models has been presented and discussed in Chapter 3. In this section, only the final input material properties used in the models are briefly introduced.

6.7.1 Surrounding Rock

As described in Chapter 3 (sections 3.1~3.2), to account for the influence of scale and the presence of discontinuities in the rock mass, strength and stiffness properties of the rock materials used in the numerical models were obtained by reducing various test results shown in the database in Appendix I using the RocLab software. GSI and triaxial compressive tests data were employed in the RocLab software.

6.7.1.1 Upper Anhydrite, Middle Potash, Middle Halite and Middle Anhydrite

For the Upper Anhydrite, Middle Potash, Middle Halite and Middle Anhydrite, the RMR (Rock Mass Rating) of 89 is assumed, which indicates the relatively consistent and stable condition of the in situ rock mass (Hoek et al., 1995; Swift and Reddish, 2005). Then the GSI for these four rock types was calculated by Equation (3.1) described in Chapter 3 (section 3.1): $GSI = RMR_{89} - 5 = 89 - 5 = 84$. The final reduced rock

material's Mohr-Coulomb properties with GSI of 84 used in the modelling can be found in Appendix II.

6.7.1.2 Marl

The concept of the plastic zone of weathered Marl, which has been introduced in Chapter 5 (section 5.2), has also been employed in the three-dimensional models, with further development. It has been further assumed by the author that the plastic zone of weathered Marl was modified in grade away from the shaft excavation face because of its exposure in the shaft excavation process and its subsequent relinings. To take account of this condition and variations in the properties of the Marl as the distance from the shaft lining increases, another concept of a graded weathered Marl has been introduced into the three-dimensional models in this research, schematically shown in Figure 6.18. Figure 6.19 shows how this concept was simulated in numerical models.

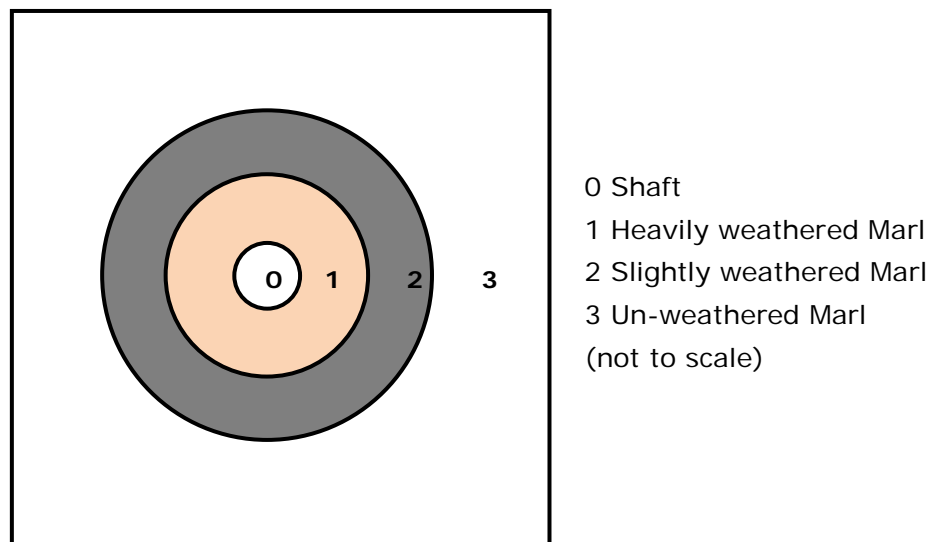


Figure 6.18 Conceptual graded plastic zone around the shaft

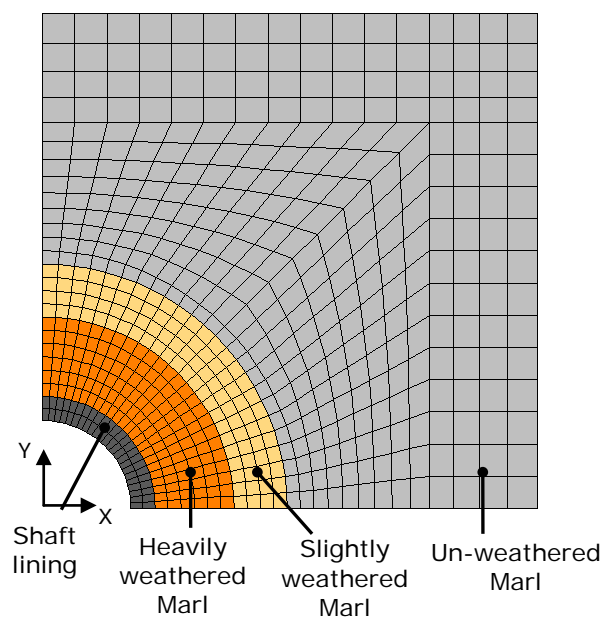


Figure 6.19 Plan view of graded weathered Marl simulated in the three-dimensional models

The model configurations for the extent of the weathered Marl used in two-dimensional models for the original shaft lining and relinings, which have been described in Chapter 5 (section 5.5), were also employed in the three-dimensional models with further development. In the three-dimensional models, the developing weathered Marl zone with the shaft relining process and working time have been separated into two graded parts: heavily weathered Marl and slightly weathered Marl. Table 6.3 shows the detailed dimensions used for the graded weathered Marl in different shaft lining stages.

Materials	Radial thickness in models (m)			
	Original lining	1 st relining	2 nd relining	3 rd relining
Excavation radius	3.94	4.35	4.5	4.7
Heavily weathered Marl	2.5	3	3.5	4
Slightly weathered Marl	1.5	1.5	1.5	1.5
Un-weathered Marl	The remainder of the model			

Table 6.3 Dimensions used for the weathered Marl zone in the three-dimensional models

For the material properties, similarly as described in Chapter 5, the RSM (2000) test results and Patchet's test (1970) results after reduction were chosen for the heavily weathered and un-weathered Marl, respectively. For the Marl, the GSI was estimated to be a lower value (30) according to previous reported in situ experience. The mean values of the above two groups' values were chosen for the slightly weathered Marl. Table 6.4 shows the input properties for the Marl in the three-dimensional models.

Materials	Elastic modulus (GPa)	Poisson's ratio	Cohesion (MPa)	Friction Angle (°)	Tensile strength (MPa)	GSI estimated
Heavily weathered Marl	0.17	0.18	0.24	5	0.03	30
Slightly weathered Marl	0.29	0.27	0.61	12	0.02	N/A
Un-weathered Marl	0.41	0.35	0.97	18	0.01	30

Table 6.4 Input properties for the Marl used in three-dimensional models

Figure 6.20 shows the Mohr-Coulomb strength envelopes for the laboratory test data and input properties for the highly weathered, slightly weathered and un-weathered Marl used in the three-dimensional models.

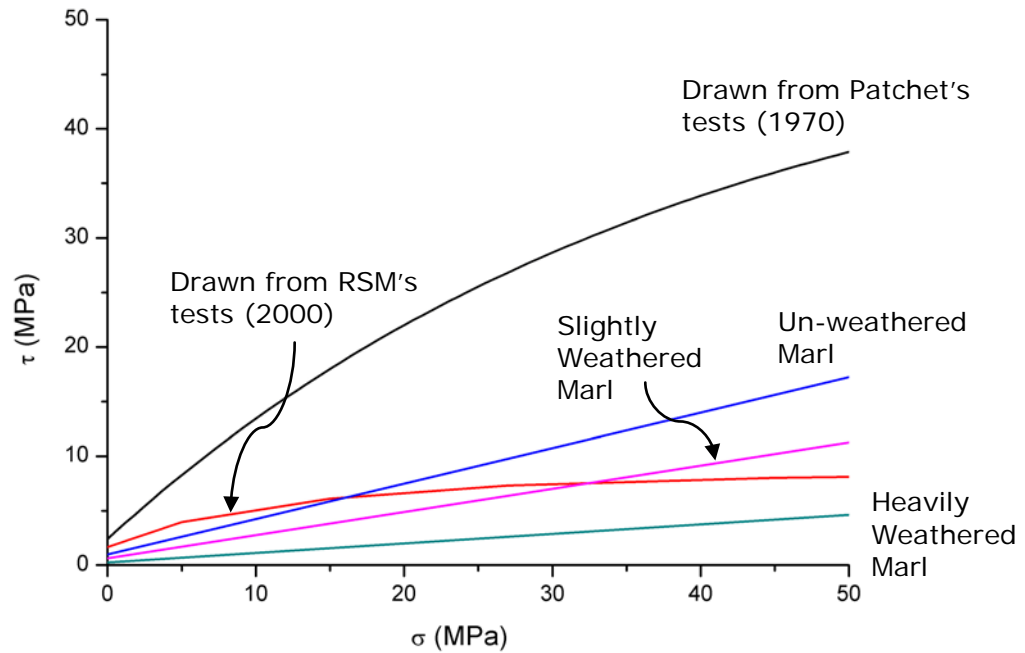


Figure 6.20 Mohr-Coulomb strength envelopes for the Marl in the three-dimensional models

6.7.2 Concrete and Cement Grout

Based on all the available laboratory test results and references in Chapter 3 (section 3.3), input properties for all concrete materials used in the numerical models for the original shaft lining and relining systems at Boulby mine can be found in Table 3.10. The input properties for cement grout used in models for the relining systems can be found in Table 3.20.

6.7.3 Interfaces

It has been described in Chapter 5 (section 5.5) that different materials had been filled between the high strength concrete blocks in each relining at the mine: epoxy resin and cement mortar in the first relining and squeezable plywood packs in the second and third relinings. Because of limitations of finite difference mesh generation, the interface elements with appropriate properties have been built into the numerical models in

this research to represent these very thin joints between concrete blocks, which were important to the mechanical behaviour of the whole concrete lining systems. The input properties for the interface elements representing these joints only used in the independent models for the shaft relining systems can be found in Tables 3.12, 3.14 and 3.17.

6.7.4 Polyurethane and Vermiculite

Polyurethane and vermiculite were the backfill materials in the gap between the shaft linings and surrounding rocks at Boulby mine (introduced in Chapter 2, section 2.6). At the very beginning of the three-dimensional modelling research, the polyurethane and vermiculite had been characterised as pure elastic materials in the model for the original shaft lining system, as they were in the two-dimensional models in Chapter 5 (section 5.2). Very low stiffness properties compared with the surrounding rock were assigned to these backfill materials, which are shown in Table 6.5.

Surrounding rock stiffness E_{rock} (GPa)		Backfill materials and stiffness E_{backfill} (GPa)		$E_{\text{rock}} / E_{\text{backfill}}$
Upper Anhydrite	17.55	Vermiculite	1e-3	17550
Heavily weathered Marl	0.17	Polyurethane	5e-3	34
Potash	6.65	Polyurethane	5e-3	1330
Middle Halite	3.87	Vermiculite	1e-3	3870

Table 6.5 Stiffness comparison between rocks and backfill materials

These soft backfill materials caused some difficult simulation problems in the early three-dimensional models for the original lining system, such as

unacceptable deformation and stress conditions. For example, it is known that the soft backfill materials were severely compressed in the original shaft lining system at Boulby mine. However, the modelling results show that massive deformation (0.6~6.6 m, even bigger than the excavation radius) occurred in the original shaft concrete lining while deformations of the soft backfill materials and surrounding rock were very small (0.01~0.1 m) in comparison. Acceptable behaviour of the backfill materials in the early three-dimensional models was only in the Marl stratum, where the polyurethane was severely compressed by the surrounding rock, from the original 0.45 m to approximately 0.1 m, and smaller closure (approximately 0.11 m) occurred in the original shaft concrete lining.

Table 6.5 shows that the surrounding Marl's stiffness was 34 times that of the polyurethane which was acceptable in the three-dimensional models, meanwhile the surrounding rock's stiffness was 17,550 times, 1,330 times and 3,870 times that of the soft backfill materials which show huge differences. It was thought that the soft backfill materials between the much stiffer materials (concrete and surrounding rocks) made the behaviour of stiffer concrete lining unrealistically out of control in the three-dimensional models, especially when the stiffness difference between the soft backfill materials and surrounding rocks was very high. To avoid these problems, these soft backfill materials have been ignored in the three-dimensional models presented in this Chapter since they were severely compressed and did not supply any support.

6.8 Modelling Results

A significant number of modelling results have been obtained including deformation and stress conditions of the surrounding rock and shaft linings, since the whole shaft and the roadway were excavated in multiple-steps in

the models. It is not thought necessary to present all modelling results in this thesis. Therefore, for both the continuous and independent models for the shaft's original lining and relinings, the modelling results of the following stages' are shown and discussed in this section:

- After the shaft excavation but before the roadway excavation (original lining)
- After completion of the roadway excavation (original lining)
- After completion of the first shaft relining
- After completion of the second shaft relining
- After completion of the third shaft relining

The areas that this research focuses on are the part of shaft concrete linings through the Marl and Potash strata, and the inset of the shaft with the roadway. Therefore, emphasis in this section has been placed on presenting and discussing the modelling results of deformation and stress of the shaft linings above the roadway roof through the Potash and Marl strata, and the inset of the shaft with the roadway.

6.8.1 Results of the Continuous Model

6.8.1.1 Deformation of the Concrete Lining (Inner Surface)

Several points at different height levels were chosen to measure the displacements of the inner surface of the concrete linings (points A' and B') and the rock excavation face (points A and B) in Figure 6.21. Measurements were taken after each key stage.

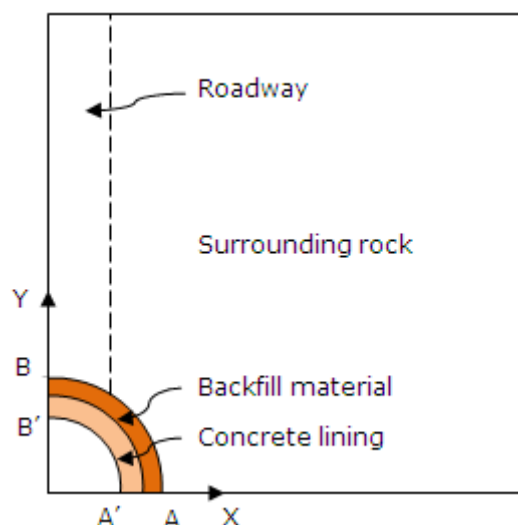


Figure 6.21 Displacement measure points in the three-dimensional models
(not to scale)

It should be noted that the displacements after the roadway excavation presented in this section were accumulated during the shaft and roadway excavations. However, the displacements after each relining were just the displacements generated during each relining being carried out. The displacements here refer to both those of the inner surface of the shaft linings and of the rock excavation face.

Figure 6.22 shows the horizontal displacements (inwards closure) of the inner surface of the original shaft lining through the Potash and Marl strata after the five different stages in the continuous model. Figures 6.23~6.24 show the horizontal displacement contour of the original shaft lining through the Potash and Marl strata before and after the roadway excavation.

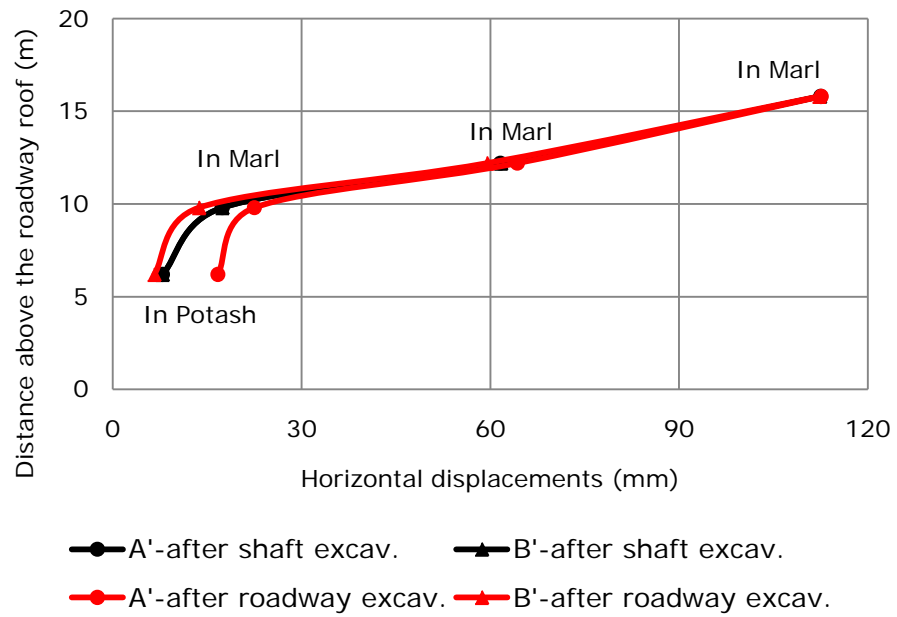


Figure 6.22 Horizontal displacements of the original lining's inner surface

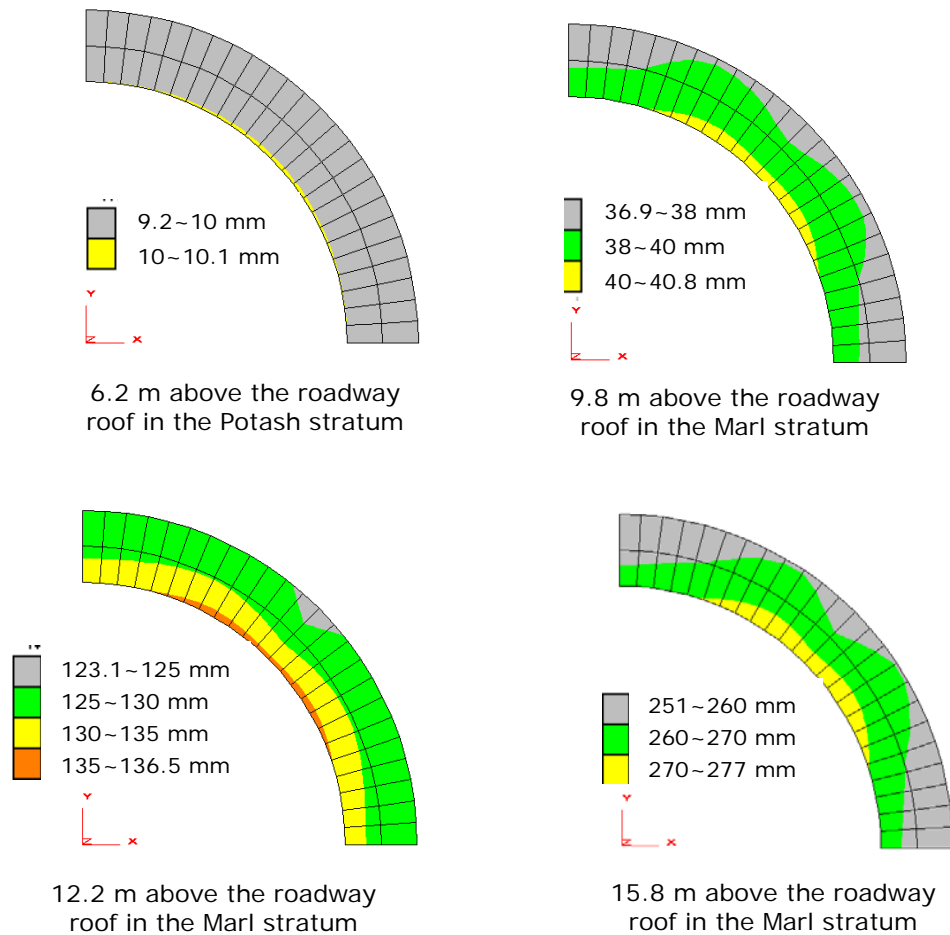


Figure 6.23 Horizontal displacement contour of the original shaft lining before the roadway excavation (Roadway direction: Y)

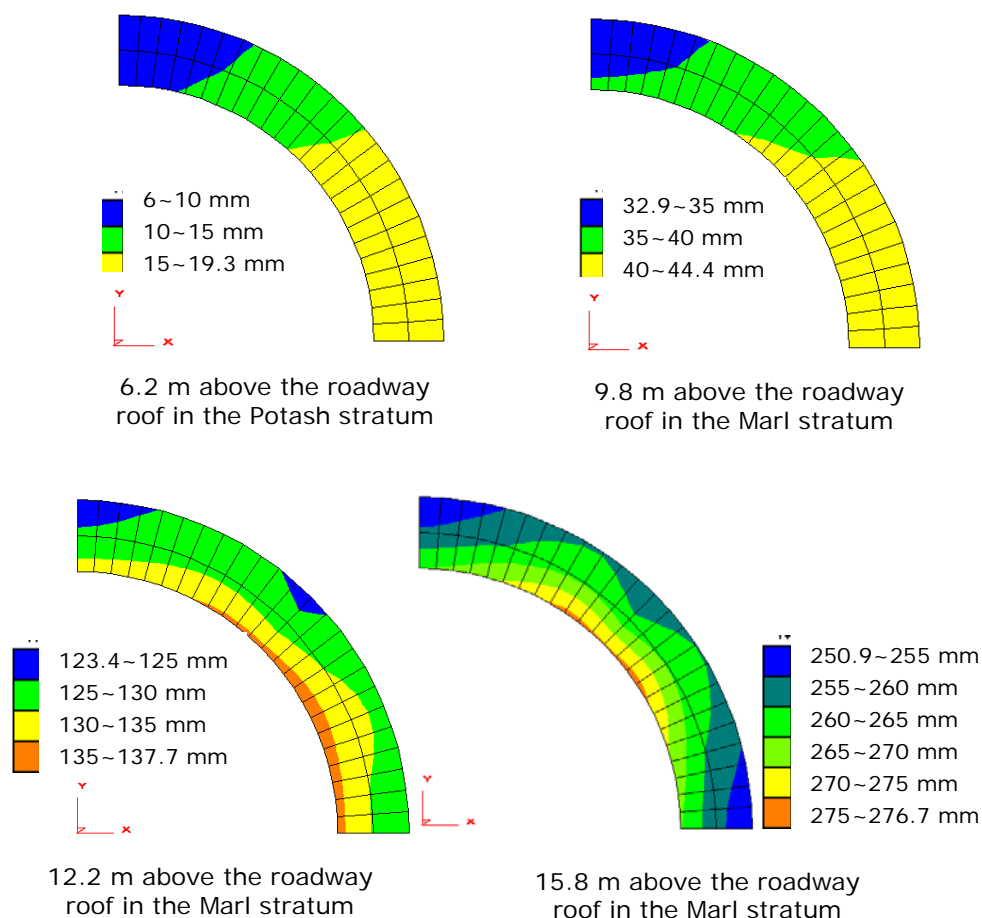
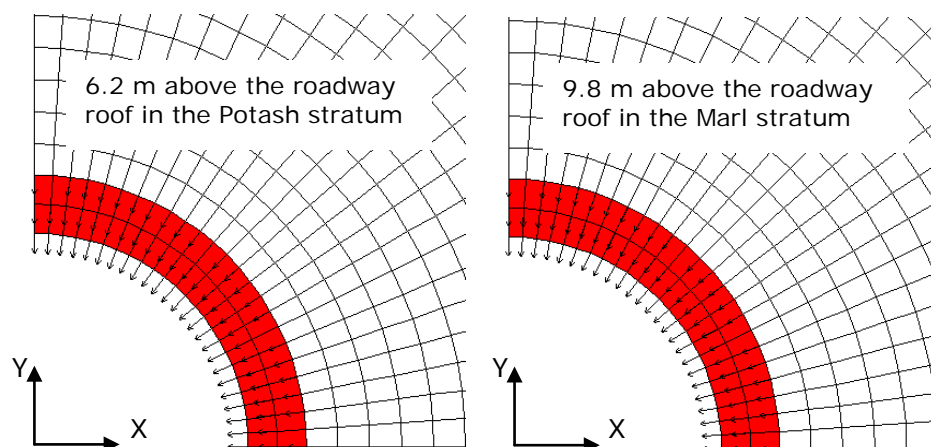


Figure 6.24 Horizontal displacement contour of the original shaft lining after the roadway excavation (Roadway direction: Y)

It can be seen from Figure 6.22 that in this continuous model, before and after the roadway excavation, the horizontal displacements of the original shaft lining was larger in the Marl stratum than in the Potash stratum (also shown in Figures 6.23~6.24). This implied that the original shaft lining through the Marl stratum suffered more severe stress conditions during the excavations of the shaft and roadway. Figure 6.22 shows that the horizontal displacements of the points A' and B' in the original shaft lining were similar (the repeated black lines) before the roadway excavation. It can be seen in Figure 6.23 that the horizontal displacement contours of the original shaft lining were evenly distributed. This implied even horizontal deformation of the original shaft lining before the roadway

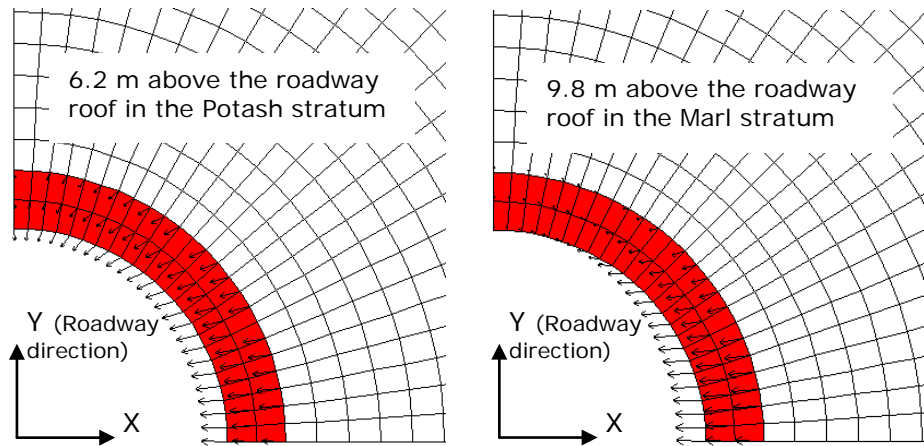
excavation. This is also shown in Figure 6.25 – displacement vectors of the concrete lining.



Colours: Red - original concrete lining, white - surrounding rock

Figure 6.25 Horizontal displacement vectors of the original shaft lining before the roadway excavation

After the roadway excavation, different horizontal displacements occurred at points A' and B' in the inner surface of the original shaft lining (red lines in Figure 6.22), especially at the positions close to the roadway. The displacement of point A' increased and that of point B' decreased after the roadway excavation (Figure 6.22). The biggest displacement difference between the points A' and B' was in the Potash stratum, around 10 mm and 13% of the thickness of the original lining. It can be seen in Figure 6.24 that the horizontal displacement contours of the original lining were unevenly distributed. The original shaft lining through the Marl and Potash strata changed from a circular shape to an ellipse during the roadway excavation, with the major axis parallel to the roadway direction, the minor axis perpendicular to the roadway direction. This implied that the nearby roadway excavation caused uneven horizontal deformation of the original lining through the Marl and Potash strata, shown in displacement vectors of the concrete lining (Figure 6.26).



Colours: Red - original concrete lining, white - surrounding rock

Figure 6.26 Horizontal displacement vectors of the original shaft lining after the roadway excavation

This uneven horizontal deformation of the lining through the Potash and Marl strata also occurred in all relinings, even if the biggest displacements difference between the points A' and B' was fairly small (Figure 6.27, 2~5 mm) compared with the thicknesses of the relinings (about 1~1.2 m).

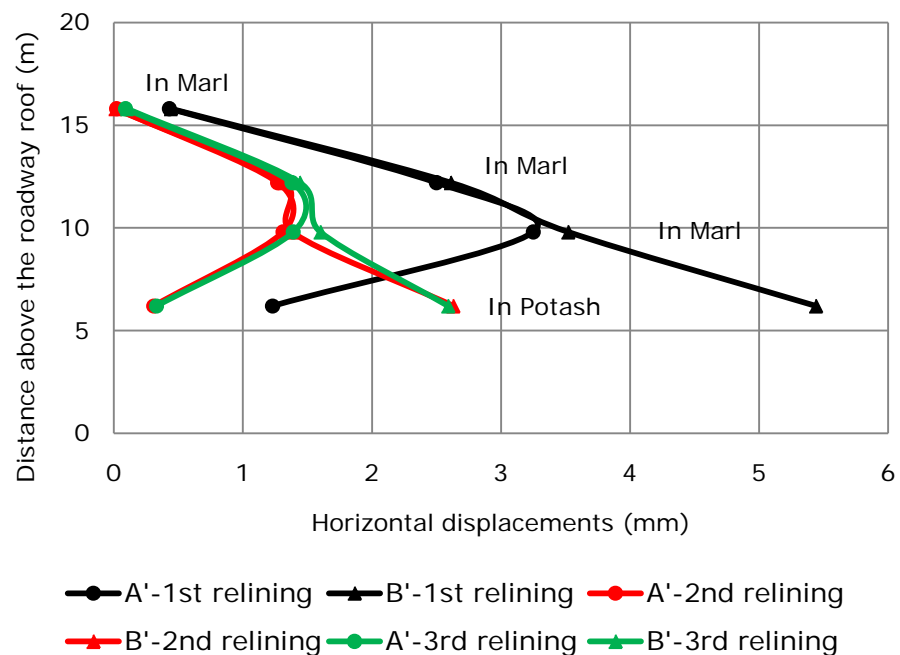


Figure 6.27 Horizontal displacements of the shaft relinings' inner surface

Figures 6.28~6.29 confirm the uneven horizontal deformation of the shaft relinings through the Marl and Potash strata. The horizontal displacements of the inner surface of all the shaft HSC relinings through the Marl and Potash strata were far smaller than those in the shaft's original NSC lining. This implied that HSC relinings through the Marl and Potash strata performed far better than the shaft's original NSC lining, which was expected. The horizontal displacement of the inner surface of the shaft's first relining through the Marl and Potash strata was bigger than those of the second and third relinings (Figure 6.27~6.30). This implied that the later two HSC shaft relinings supplied stronger support than the first relining. Although the shaft HSC relinings through the Marl and Potash strata were also ellipses in plan, their major axes were perpendicular to the roadway direction (Figures 6.27~6.29, displacement of point B' was bigger than that of point A'), totally contrary to that of the original lining.

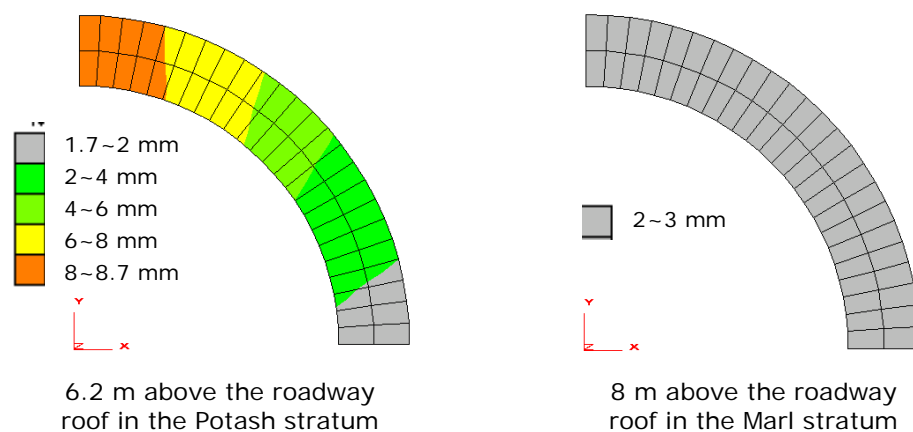


Figure 6.28 Horizontal displacement contour of the first relining

(Roadway direction: Y)

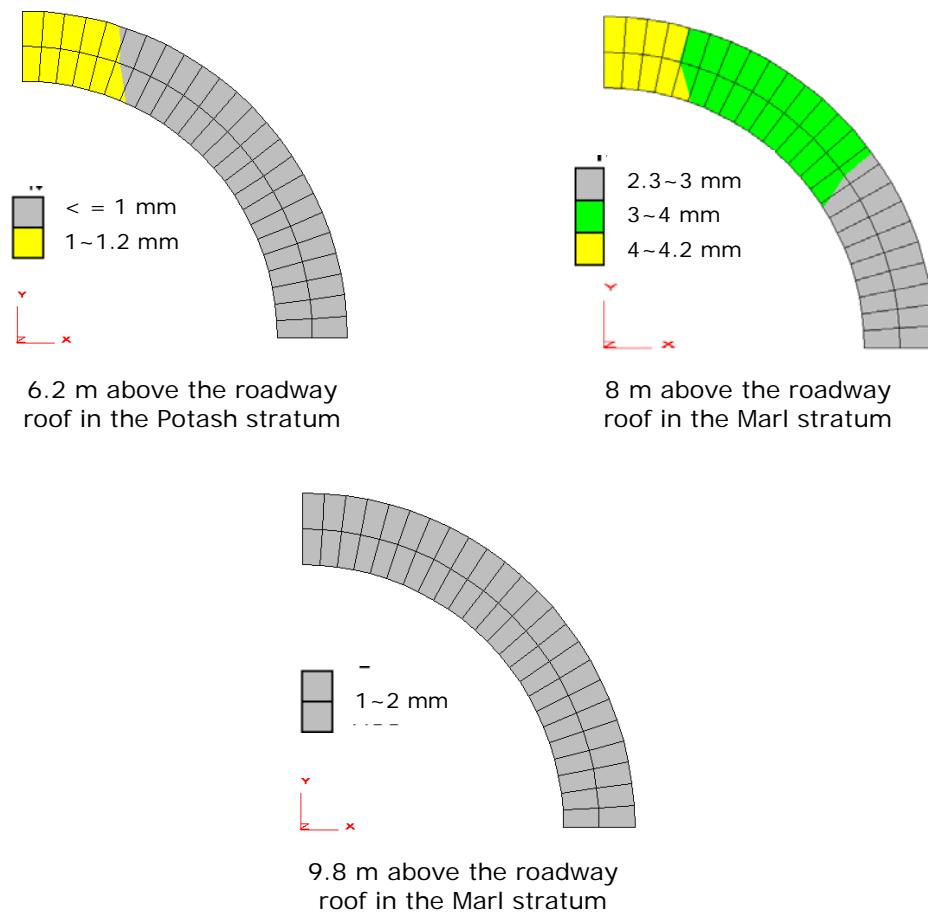


Figure 6.29 Horizontal displacement contour of the second relining
(Roadway direction: Y)

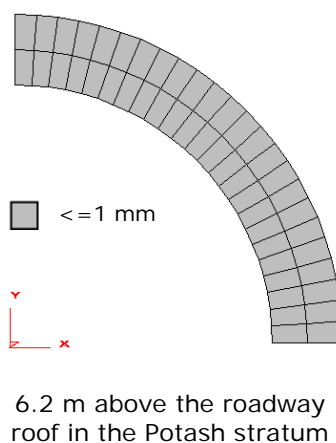


Figure 6.30 Horizontal displacement contour of the third relining
(Roadway direction: Y)

It can be noticed from Figures 6.22~6.24 and Figures 6.27~6.30 that before the shaft relinings through the Marl and Potash strata, maximum horizontal displacement occurred in the inner surface of the original shaft lining through the upper part of the Marl stratum. However, contrary to this, during the shaft relining stages, the minimum horizontal closure occurred in the inner surface of the shaft HSC relinings through the upper part of the Marl stratum. This was because of different modelling directions during the shaft excavation and relinings through the Marl and Potash strata. It was from the top down during the shaft excavation, as the original shaft lining through the upper part of the Marl stratum was installed at the first step. However, it was from the bottom up during the relinings, as the shaft HSC relinings through the upper part of the Marl stratum were installed at the last step.

The horizontal displacements of the rock excavation face were 5~35 mm bigger than those of the inner surface of the shaft linings through the Marl and Potash strata after five different stages in the continuous model. This was expected during the modelling since the linings were compressed under severe ground stress, especially in the original shaft lining system through the Marl stratum (approximately 35 mm horizontal displacements difference between the rock excavation face and the inner surface of the original lining).

Due to the vertical stress acting on the model and lining weight during the shaft and roadway excavations, the whole shaft linings and surrounding rock moved downwards approximately 70 mm. The whole Marl stratum had been compressed during the shaft excavation. The roadway excavation resulted in more downwards movements in the roadway roof area (up to 85 mm) and some upwards movements (approximately 48

mm) in the roadway floor area due to the vertical stress relief caused by the roadway excavation.

The horizontal displacement of the rock excavation face and the vertical displacements at measured points show similar trends with Figure 6.22 and Figure 6.27, respectively. Before the roadway excavation, even deformation (horizontal and vertical) occurred in the circular original shaft lining; after the roadway excavation and relinings, uneven deformation (horizontal and vertical) occurred in the circular original lining and relinings through the shaft inset adjacent strata, especially the roadway immediate roof and floor horizon in this model.

6.8.1.2 *Stress Conditions*

Figures 6.31~6.35 show the vertical stress (σ_z) contours of the whole model after different stages in the continuous model. It should be remembered that the negative values mean compressive stress and positive values mean tensile stress in these figures. It can be seen from Figures 6.31~6.35 that in this continuous model:

- The shaft excavation resulted in a vertical stress relief zone in the surrounding rock in the Marl and Potash strata, which became bigger during the shaft relinings being carried out.
- The roadway excavation led to: a) the vertical stress concentration in the roadway roof corner and floor corner, and b) vertical stress relief in the roadway immediate roof and floor within the Middle Halite stratum and in the original shaft lining (Figure 6.32).
- During relinings, significant tensile stress developed in the relinings in the Marl and Potash strata (Figure 6.33) and wing wall (Figures 6.34~6.35). At the same time, the vertical stress concentration in the

roadway roof corner and floor corner also became more severe with the relining being carried out.

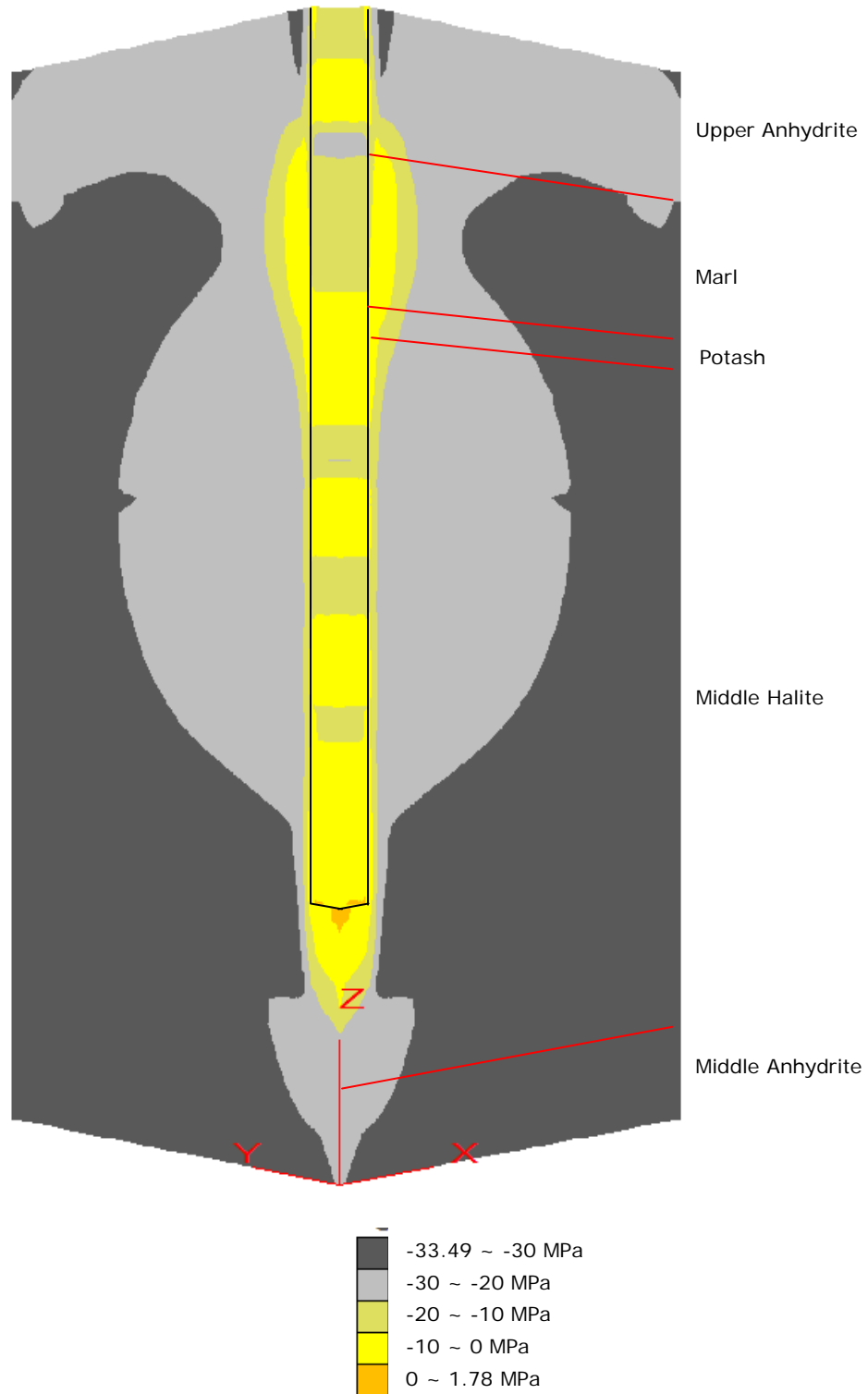


Figure 6.31 Vertical stress σ_z in the original lining after the shaft excavation

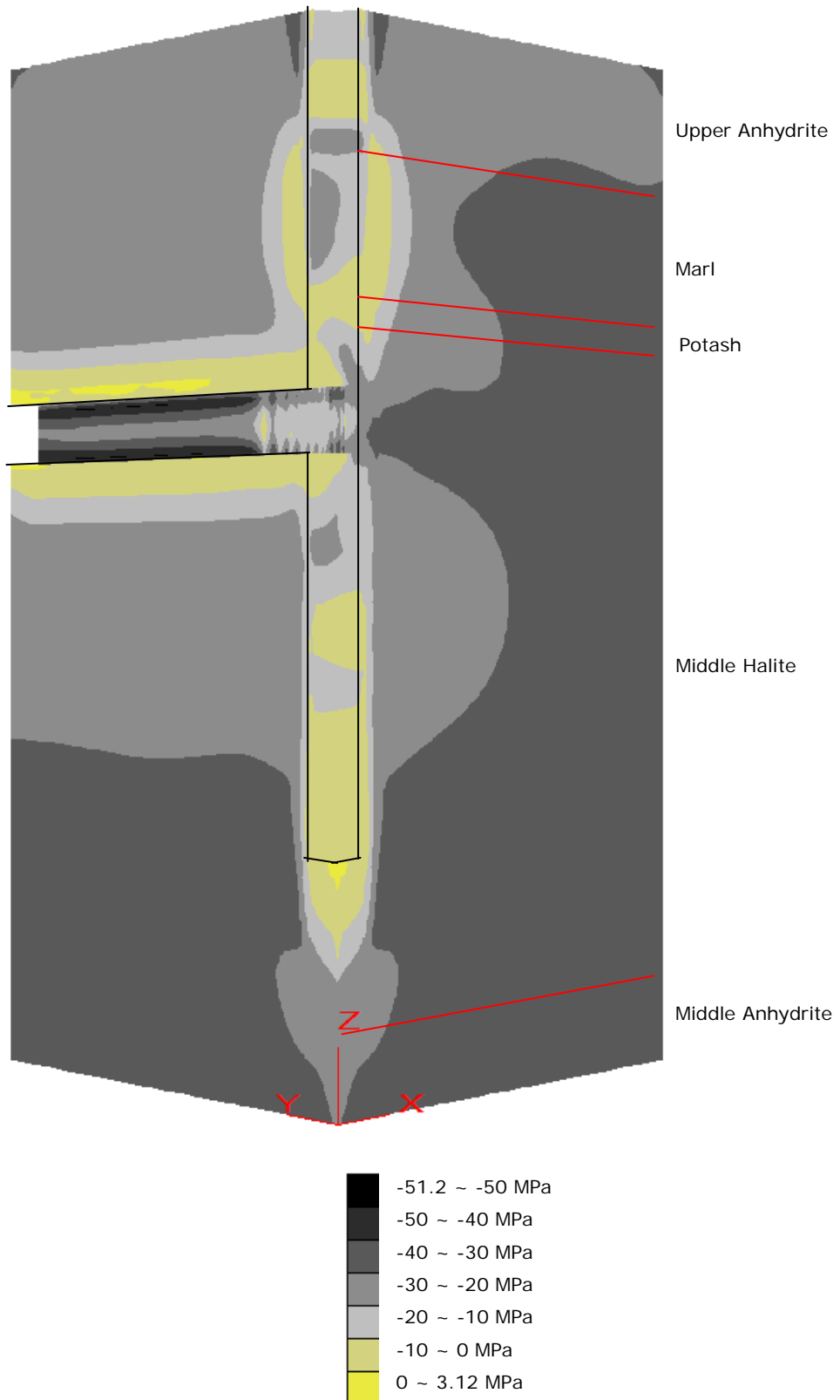


Figure 6.32 Vertical stress σ_z in the original lining after the roadway excavation

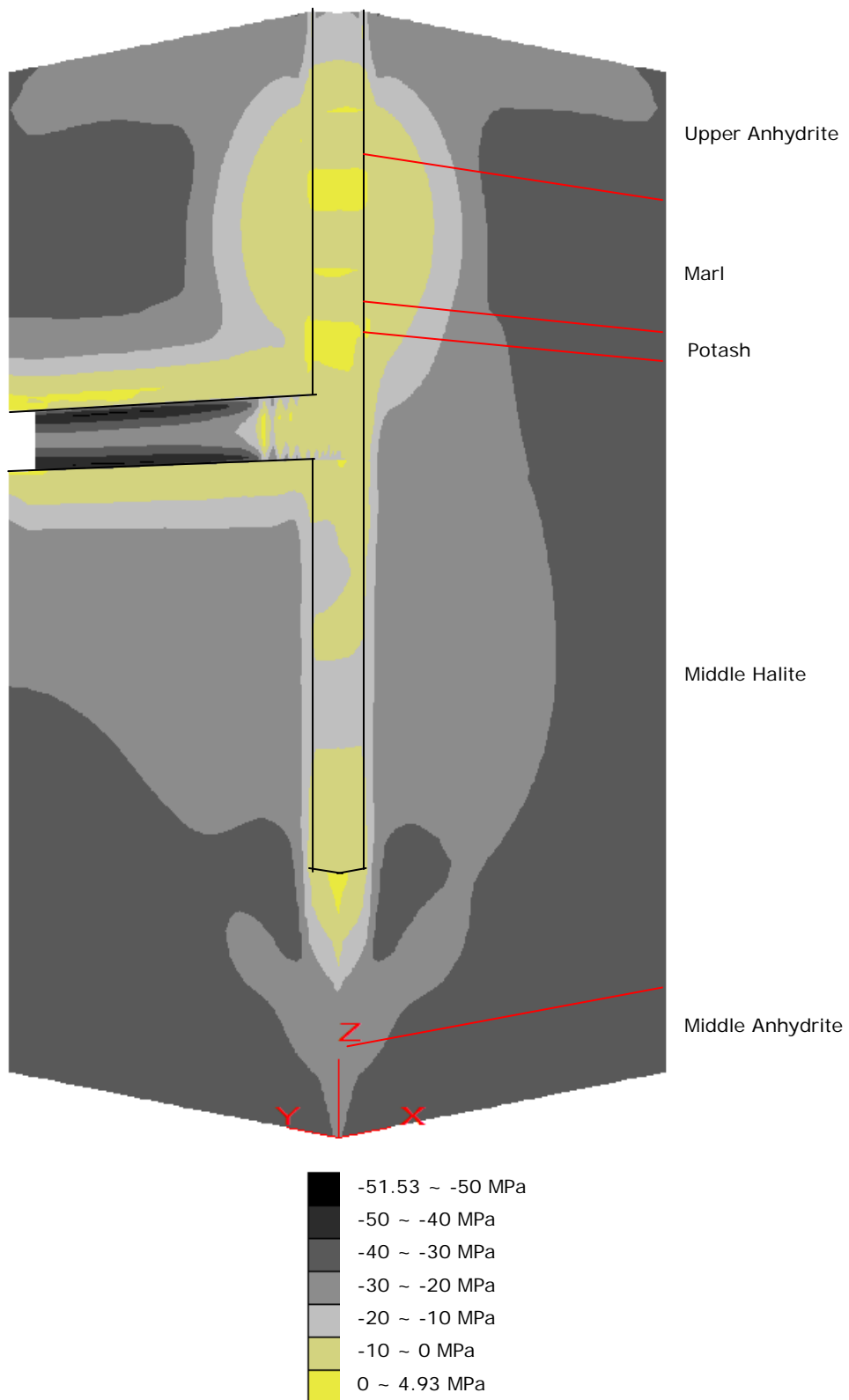


Figure 6.33 Vertical stress σ_z in the first relining

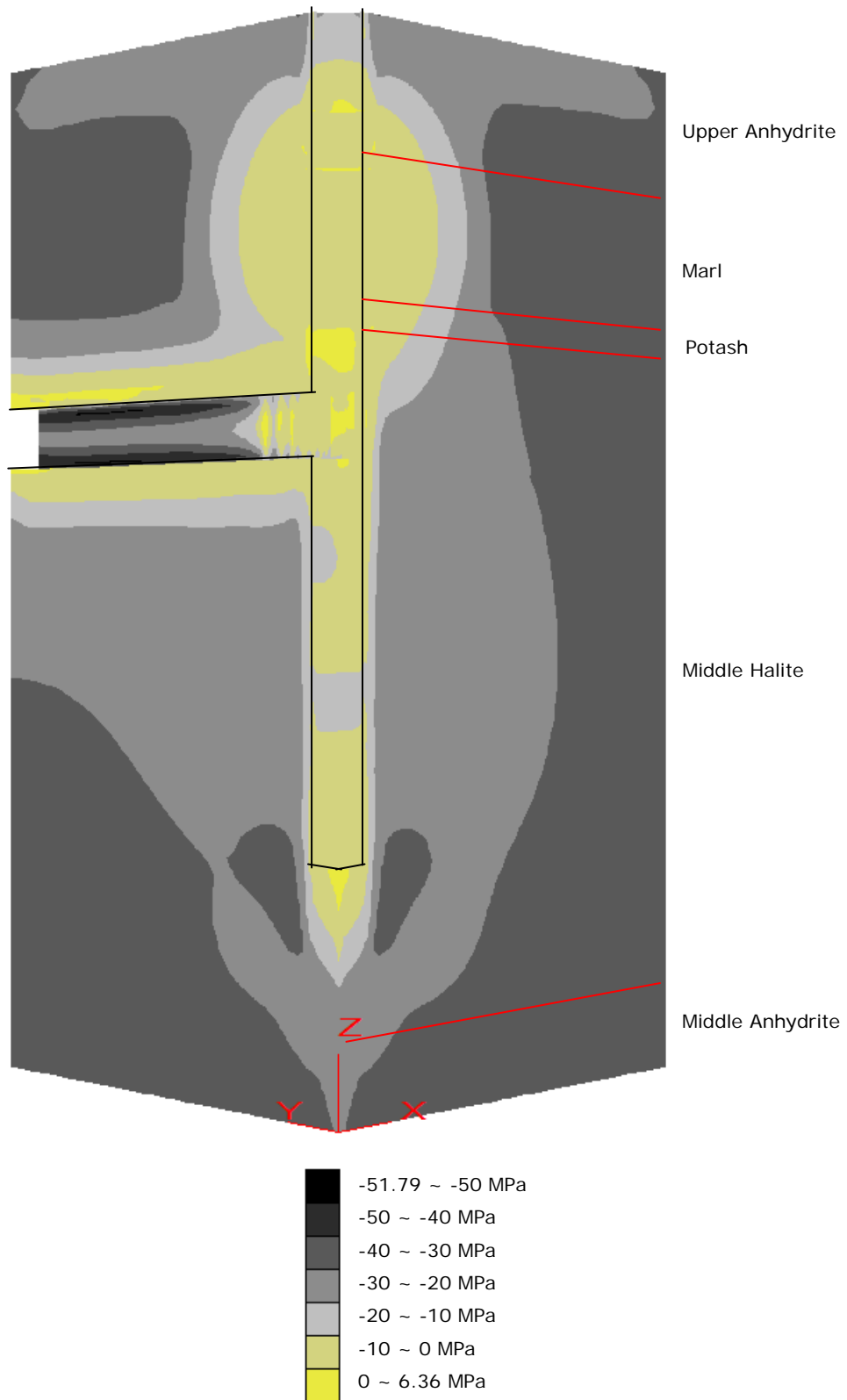


Figure 6.34 Vertical stress σ_z in the second relining

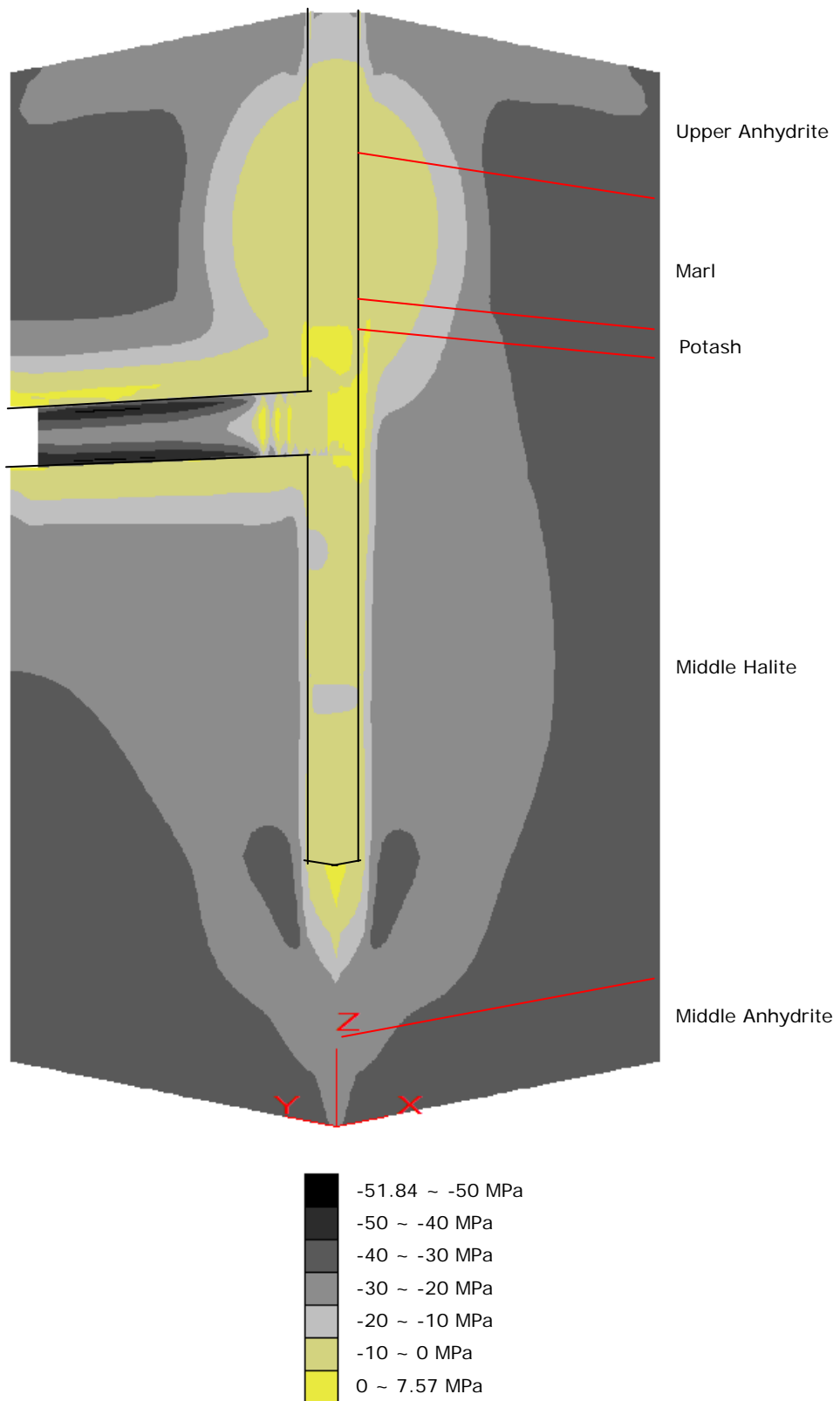


Figure 6.35 Vertical stress σ_z in the third relining

Again, points A' and B' shown in Figure 6.21 were used to measure the principal stresses conditions of the concrete linings in the strata near to the shaft inset. Tables 6.6~6.7 show the principal stresses measurement results from this continuous model.

Measure points position above the roadway roof		Before the roadway excavation (MPa)		After the roadway excavation (MPa)		After 1 st relining (MPa)		After 2 nd relining (MPa)		After 3 rd relining (MPa)	
In strata	(m)	A'	B'	A'	B'	A'	B'	A'	B'	A'	B'
Marl	15.8	-2.6	-2.6	-2.4	-2.7	0.2	0.2	0.1	0.1	-0.1	-0.1
Marl	12.2	-2.1	-2.1	-1.8	-2.3	-0.3	-0.3	-0.4	-0.4	-0.5	-0.5
Marl	9.8	-2.2	-2.2	-1.7	-2.5	-0.4	-0.3	-0.4	-0.4	-0.7	-0.7
Potash	6.2	-2.5	-2.5	-1.4	-2.8	-0.2	0.5	-0.4	-0.03	-0.5	-0.2

Table 6.6 Major principal stress σ_1 of the shaft linings' inner surface

Measure points position above the roadway roof		Before the roadway excavation (MPa)		After the roadway excavation (MPa)		After 1 st relining (MPa)		After 2 nd relining (MPa)		After 3 rd relining (MPa)	
In strata	(m)	A'	B'	A'	B'	A'	B'	A'	B'	A'	B'
Marl	15.8	-	-	-	-	-1.3	-1.3	-0.2	-0.1	-0.8	-0.8
Marl	12.2	-	-	-	-	-7.3	-7.1	-6.6	-6.5	-8.6	-8.6
Marl	9.8	-	-	-	-	-9.1	-8.9	-7.8	-7.7	-	-
Potash	6.2	-	-	-	-	-8.5	-5.1	-6.7	-4.5	-7.4	-3.6

Table 6.7 Minor principal stress σ_3 of the shaft linings' inner surface

It should be noted that in this continuous model, equivalent properties (shown in Table 6.1) were utilised for the HSC in all shaft relinings. The equivalent Young's modulus of the HSC used in the model was only 0.23~0.52 that of the HSC obtained from the laboratory tests. This resulted in equivalent principal stresses in the shaft relinings (columns in

light gray in Tables 6.6~6.7), which were fairly low compared with those in the original shaft lining (columns in light blue and green). Although they were not the practical principal stresses developed in the shaft relinings in the model, they show the developing principal stress trends during the shaft relining being carried out in the model.

It can be seen clearly from Tables 6.6~6.7 (columns in light blue) that the principal stresses in the original shaft lining at points A' and B' in this model were approximately equal to each other at the same vertical level through the Marl and Potash strata before the roadway excavation, i.e.

$$\sigma_n @ A' \cong \sigma_n @ B', n=1, 3$$

This modelling result implied that the original shaft lining was under an even loading condition before the roadway excavation in this model. This is also shown in Figure 6.36.

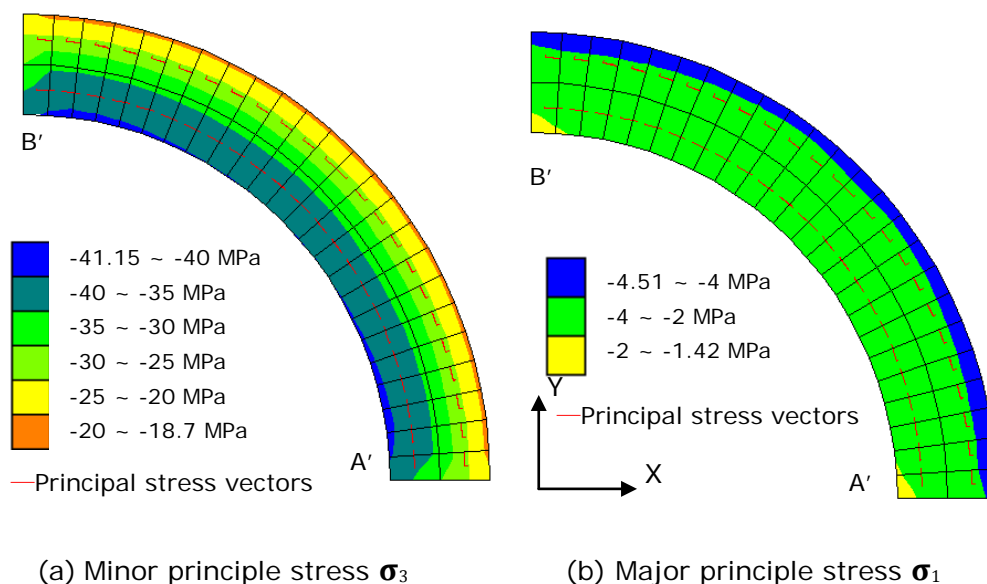


Figure 6.36 Principal stress contours for the original lining: 9.8 m above the roadway roof in the Marl stratum, before the roadway excavation

Figure 6.36 shows that there was a large difference between the major principal stress σ_1 and the minor principal stress σ_3 in the concrete lining in this model, and the inner surface of the concrete lining suffered higher compression stress compared with the outer surface of the lining. The directions of the principal stresses in the concrete lining are also shown in Figure 6.36: the minor principal stress σ_3 was a hoop stress (long red lines), the major principal stress σ_1 was in the radial direction (short red lines, perpendicular with the long red lines).

However, the roadway excavation changed the even loading condition of the original shaft lining and relinings, which can be seen from Tables 6.6~6.7 (columns in light green and gray). Stress measurement results in Tables 6.6~6.7 show that the roadway excavation caused a reduction of the minor principal stress σ_3 at point A' and an increasing of the minor principal stress σ_3 at point B' in the original shaft lining, which was a severe one through the bottom of the Marl and the Potash strata. The minor principal stress σ_3 difference between points A' and B' was especially large in the original shaft lining through the bottom of the Marl, the Potash strata and the roadway immediate roof and floor. The σ_3 at point B' was up to 182% the σ_3 at point A' at the position of 6.2 m above the roadway roof in the Potash stratum. The σ_3 at point B' was approximately 126% the σ_3 at point A' at the position of 9.8 m above the roadway roof in the Marl stratum.

In the shaft relinings, the differences between the minor principal stresses (σ_3 , columns in light gray in Table 6.7) at points A' and B' through both the Marl and Potash strata were also significant, e.g. in the first relining,

the σ_3 at point B' was up to 167% the σ_3 at point A' at the position of 6.2 m above the roadway roof in the Potash stratum. The σ_3 at point B' was approximately 102% the σ_3 at point A' at the position of 9.8 m above the roadway roof in the Marl stratum. After the roadway excavation, the principal stresses in the original lining and relinings at points A' and B' in this model do not equalise to each other anymore at the same vertical level through the Marl and Potash strata. i.e.

$$\sigma_n @ A' \neq \sigma_n @ B', n=1, 3$$

This uneven distribution of the principal stresses in the shaft linings implied that the original shaft lining and relinings were under an uneven loading condition due to the shaft inset with the roadway in this model which is also shown in Figure 6.37.

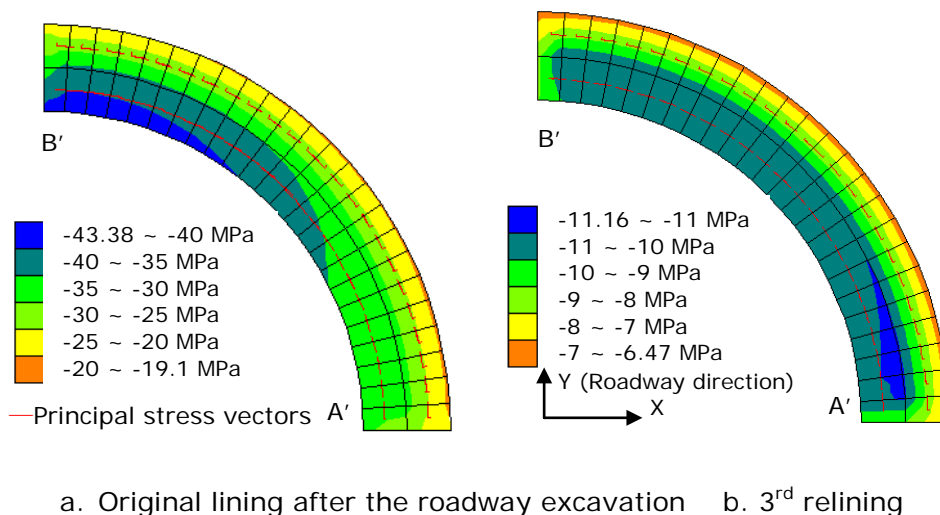


Figure 6.37 Minor principal stresses σ_3 contour of the shaft linings: 9.8 m above the roadway roof in the Marl stratum

It can be noticed from Figure 6.37 that the uneven stress condition (the position of the maximum absolute value of the σ_3) in the shaft HSC relining is different from that in the original shaft NSC lining through the

Marl and Potash strata. This difference is similar to the direction difference of the ellipses' major axis between the original lining and relinings, which has been described in section 6.8.1.1. These modelling results need validation with the in situ observation.

6.8.1.3 Discussion

In this continuous model, the deformation (horizontal and vertical) and stress conditions in the original shaft lining were evenly distributed before the roadway excavation. However, these conditions disappeared after the roadway excavation in the numerical model. The uneven deformation (horizontal and vertical) and uneven distribution of the principal stresses (especially the minor principal stress σ_3) of the original lining through the Marl and Potash strata caused by the roadway excavation was quite significant: approximately 15 m above the roadway roof and 15 m below the roadway floor in this continuous model, including the Marl, the Potash and the Middle Halite strata (the roadway immediate roof and floor).

However, for the shaft HSC relinings, the extent of the uneven deformation and uneven distribution of the principal stresses caused by the existence of the nearby roadway was not as much as that of the original shaft lining. The existence of the roadway has more effect on the deformation and stress conditions of the shaft relinings through the Potash and the bottom of the Marl strata (less than 10 m above the roadway roof). That is to say, the uneven deformation and uneven stress distribution conditions in the shaft relinings through the Marl and Potash strata were not as severe as those in the original shaft NSC lining. This was expected, as the HSC relinings should perform better than the NSC lining at Boulby mine. Figure 6.30 shows that even in the Potash stratum, the shaft HSC

lining suffered little uneven horizontal deformation, which implied that the third shaft relining would perform better than the previous shaft relinings.

These uneven deformations (schematically shown in Figure 6.38) and uneven stress conditions in the shaft linings in the continuous model were caused by uneven loading on the annular concrete linings from the surrounding rock. This uneven loading (vertical and horizontal) can bring high shear and tensile stress threatening the stability of the circular concrete structures, as shown in Figure 2.16 in Chapter 2, and massive shear failure in the shaft's second relining system.

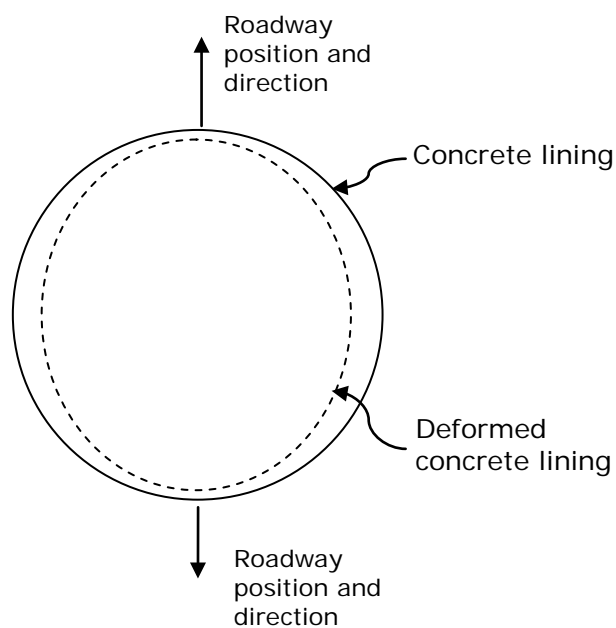


Figure 6.38 Schematic horizontal closure of the shaft lining through the Marl and Potash strata in the model

The uneven loading originated from the rock surrounding the shaft. That is to say, the stresses and failure conditions of the rock surrounding the shaft controlled the shaft linings' stability. The roadway caused severe uneven stresses and failure conditions of the surrounding rock (shown in

Figure 6.39), leading to uneven loading on the shaft concrete linings through the nearby strata in this model, especially the weak Marl and the Potash. Therefore, the shaft concrete linings through the Marl and Potash strata suffered the most severe displacement in this model.

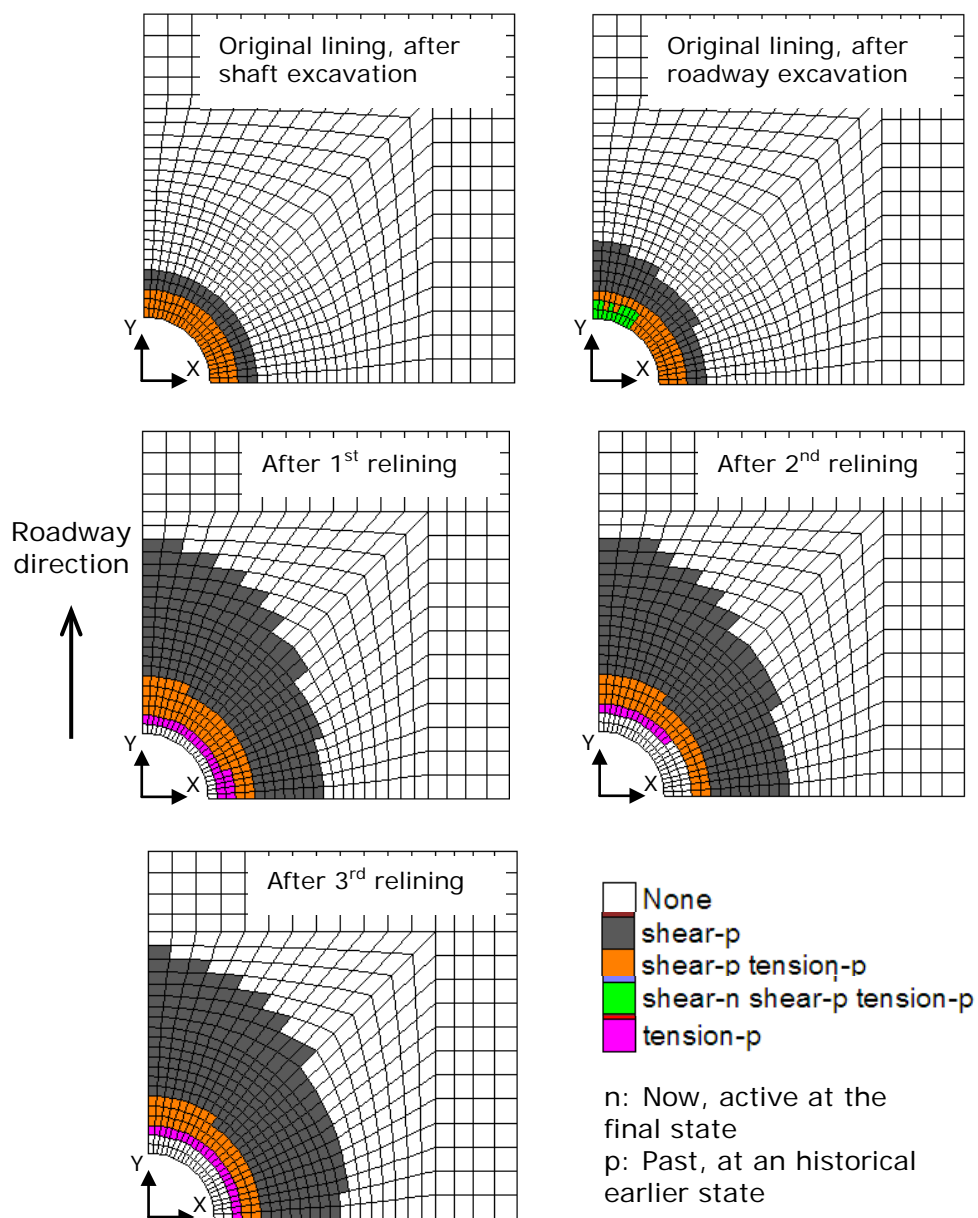


Figure 6.39 Plastic states of the shaft linings at 7 m above the roadway roof in the Potash stratum (the inside two rings are the shaft linings)

6.8.2 Results of the Independent Models

6.8.2.1 Deformation of the Concrete Lining (Inner Surface)

In these independent models, fairly low displacements occurred in the shaft relinings (less than 0.5 mm, take the model of the first relining as an example shown in Figure 6.40), which were extremely low when compared with the thicknesses of the shaft linings (0.75~1.2 m) and displacements of the shaft NSC/HSC linings in the continuous model (in Figures 6.22, 6.27). This was very difficult to understand since the shaft lining systems were under very high ground stress field (around 30 MPa) and severe underground in situ conditions (very soft surrounding rock mass - Marl).

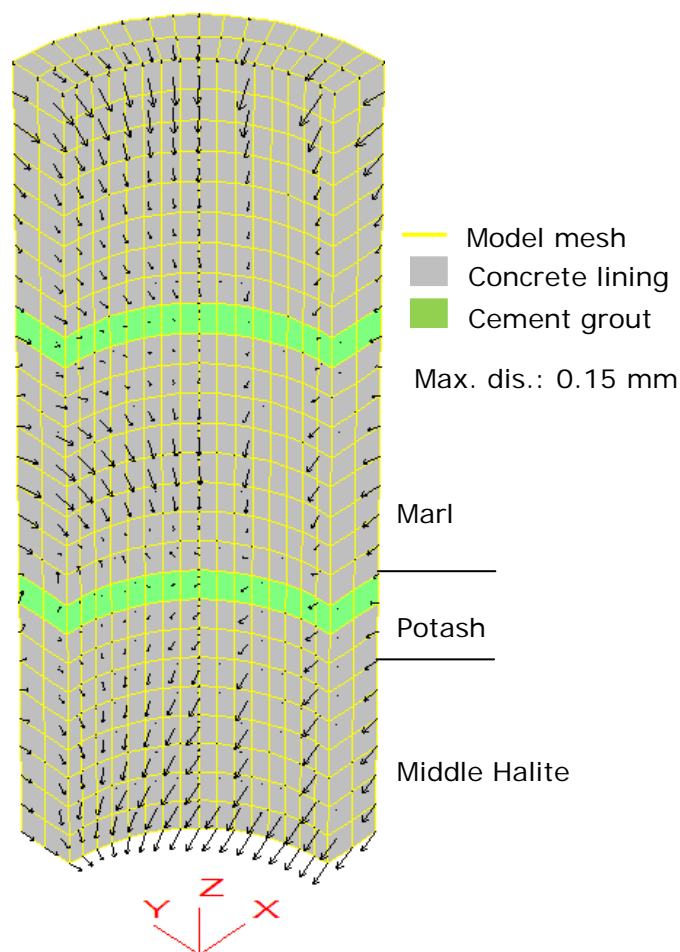


Figure 6.40 Displacement vectors of the first relining in independent model
(Roadway direction: Y)

6.8.2.2 Deformation and Stress Conditions of the Interfaces

The obtained shear displacements of the interfaces between concrete blocks were even lower (less than 0.01 mm) in the shaft HSC relinings through the Marl and Potash strata. Shear and normal stresses in the interfaces in the independent models for the first and third relinings were very low (-0.01 MPa~0.01 MPa) compared with the stress in the surrounding rock (around 30 MPa). However, the shear and normal stresses in the interfaces in the independent model for the second relining shown in Figures 6.41~6.42 cannot be ignored.

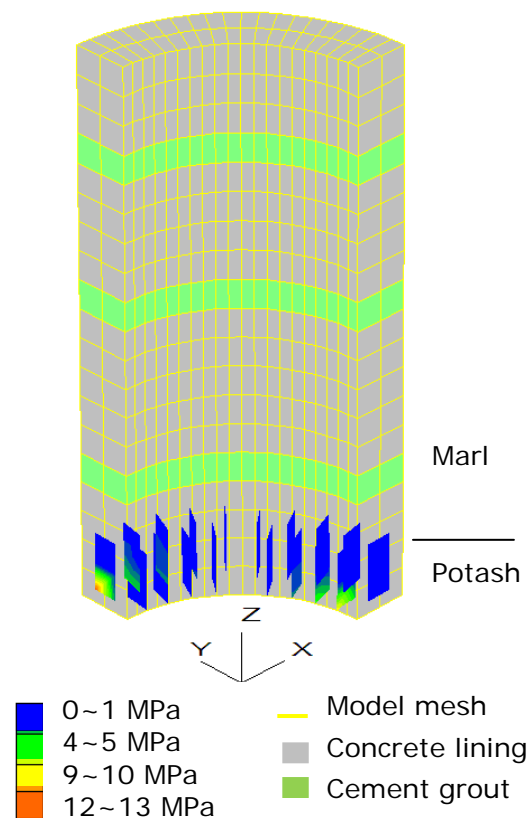


Figure 6.41 Interface normal stress in the second relining in independent model (Roadway direction: Y)

(For clarity, only interfaces at the bottom part of relining are shown, since stress in other interfaces are very low, between 0~1 MPa)

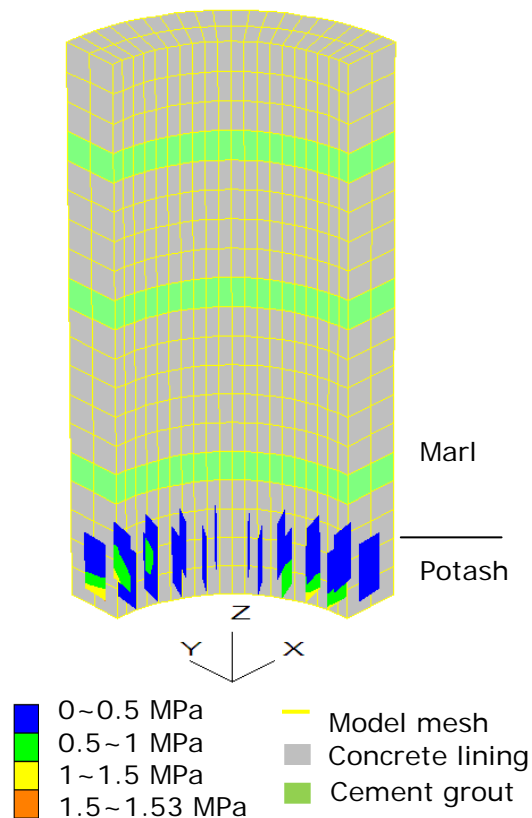


Figure 6.42 Interface shear stress in the second relining in independent model (Roadway direction: Y)

(For clarity, only interfaces at the bottom part of relining are shown, since stress in other interfaces are very low, between 0~0.5 MPa)

At the bottom part of the HSC lining in the Potash stratum, the shear and normal stresses in the interfaces were up to 13 MPa and 1.5 MPa, respectively. High shear and normal stresses that developed in the interfaces in the second relining were thought to threaten the stability of the whole relining system.

Figures 6.43~6.45 show the interfaces' shear failure conditions in the inner surface of the shaft HSC linings in each independent model. It can be seen that massive interface shear failure occurred in the second and third relinings through the Marl and Potash strata during the numerical

calculation in the three-dimensional models. Less historical shear failure occurred in the first relining due to epoxy resin's higher adhesive strength with the concrete blocks compared with the plywood packs (Tables 3.12 and 3.17). However, at the final equilibrium state, some interface shear failure stayed active only in the second relining. These modelling results implied again that the single ring of concrete blocks as shaft lining (the first and third relinings) was more effective than the double rings of concrete blocks (the second relining).

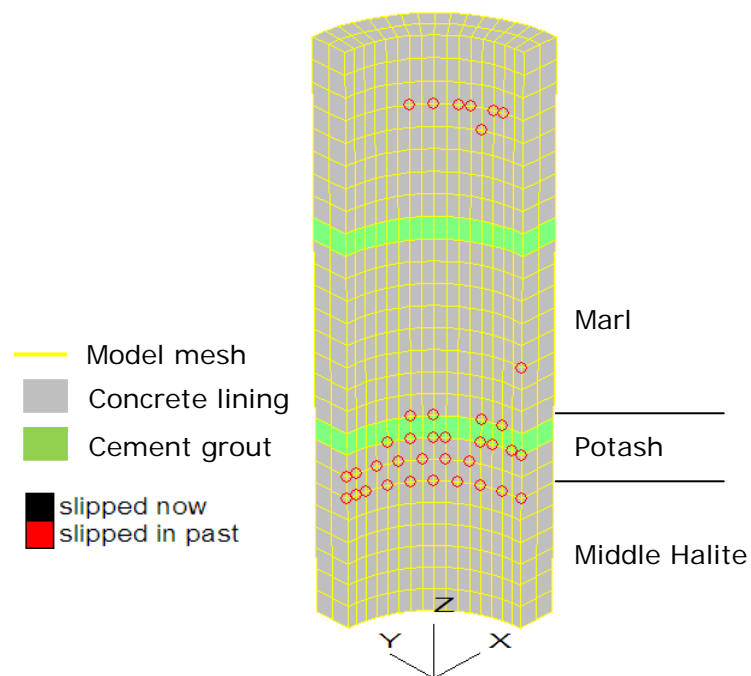
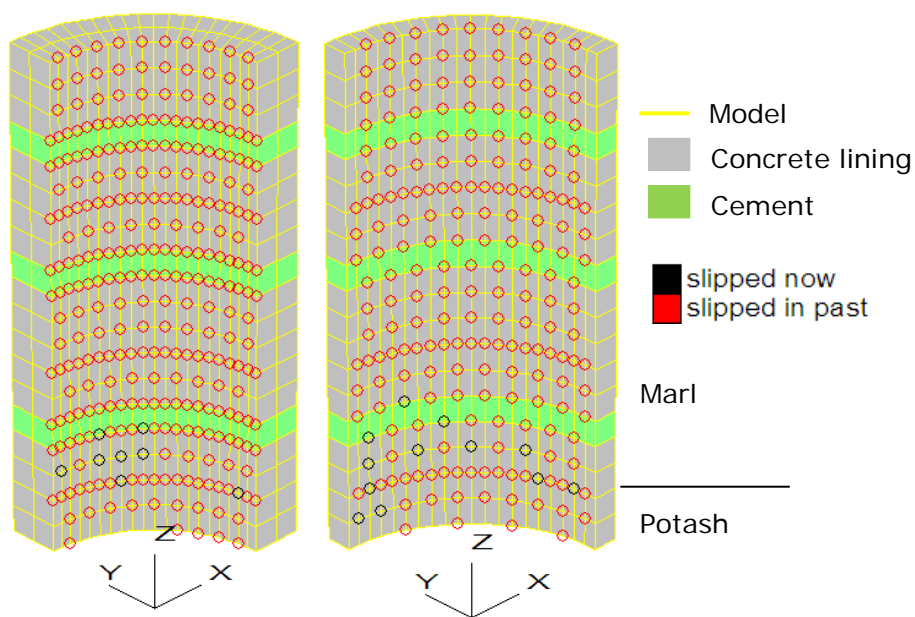


Figure 6.43 Interface shear failure in the first relining in independent model (Roadway direction: Y)



Shaft lining inner surface Surface between double rings

Figure 6.44 Interface shear failure in the second relining in independent model (Roadway direction: Y)

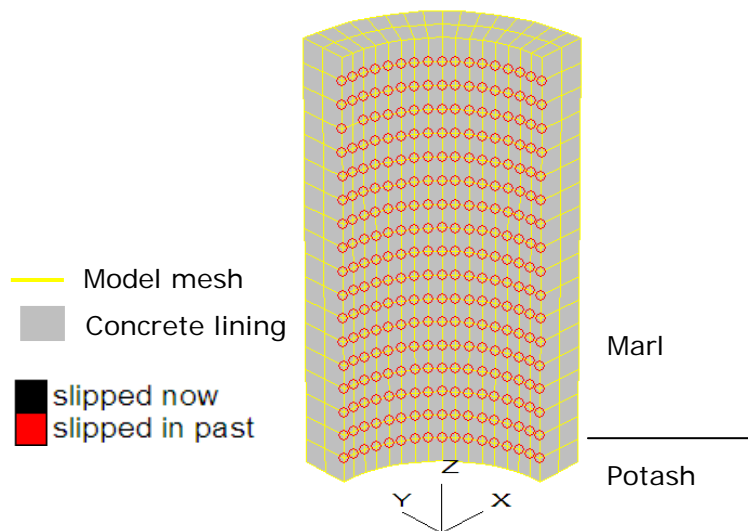


Figure 6.45 Interface shear failure in the third relining in independent model (Roadway direction: Y)

6.8.2.3 *Stress Condition of the Concrete Lining*

Figures 6.46~6.48 show the vertical stress σ_z contours of the whole model domain after relining in each independent model. It can be seen that the independent models for shaft relinings show very consistent modelling results with the continuous model for shaft relinings (Figures 6.33~6.35), which have been described in the early part of the section 6.8.1.2 and are not repeated in this section. However, for the stress relief zone in the Marl and Potash strata caused by the shaft excavation and subsequent original lining and relinings, its extent in the independent models for shaft relinings was bigger than that in the continuous model. This can be found by a comparison of the stress zones (-20~-10 MPa) between Figures 6.33&6.46, 6.34&6.47, 6.35&6.48.

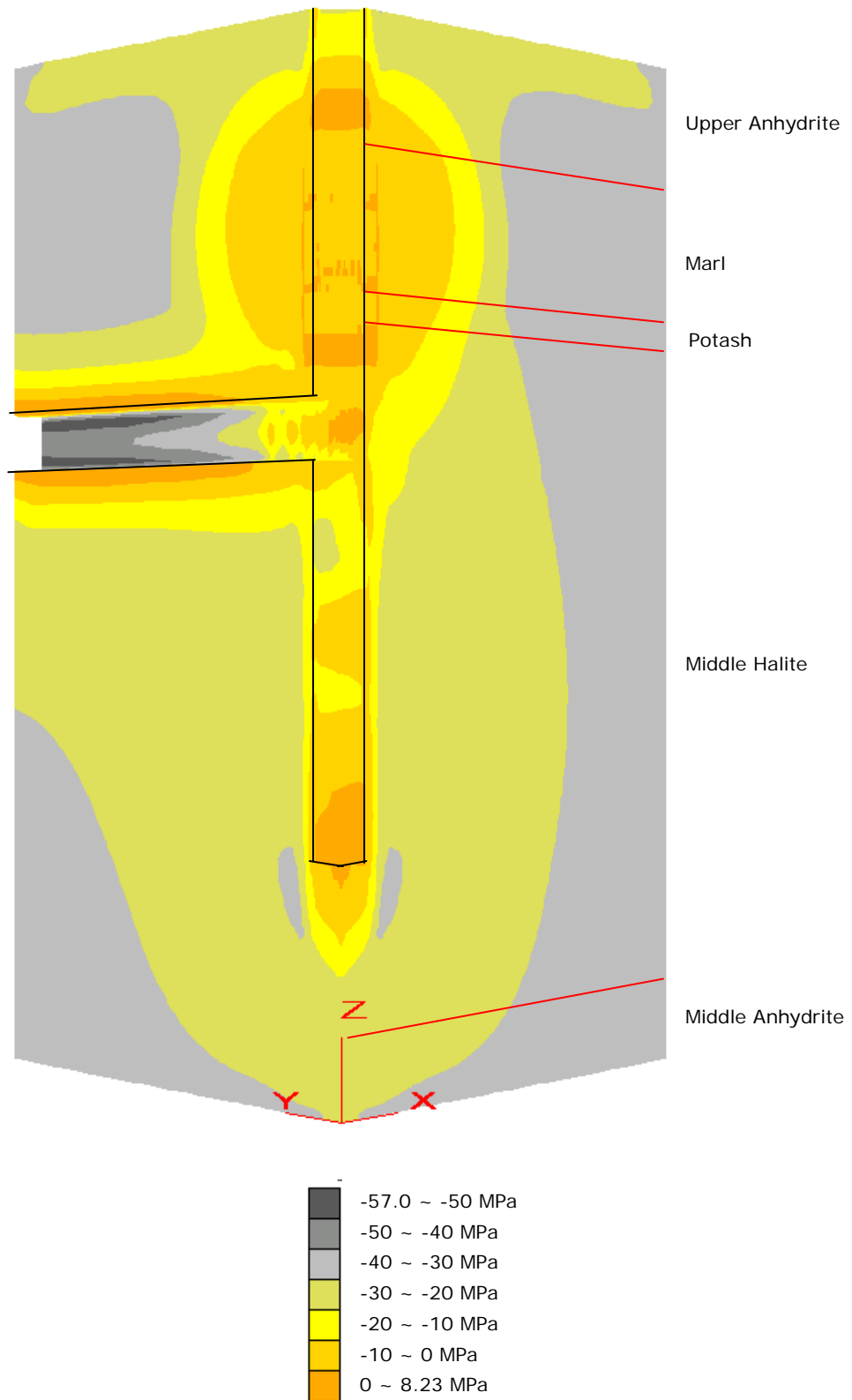


Figure 6.46 Vertical stress σ_z in the first relining in independent model

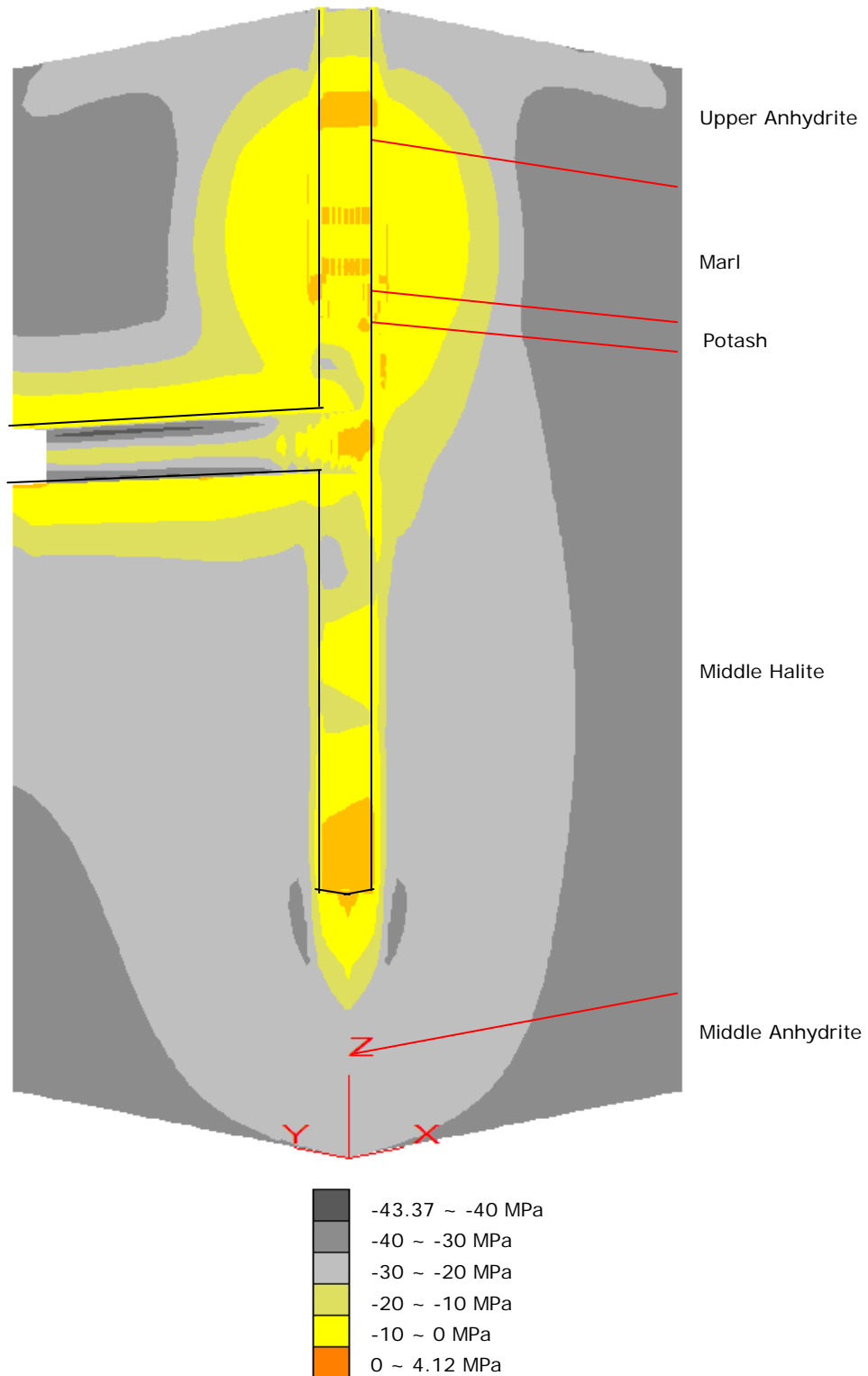


Figure 6.47 Vertical stress σ_z in the second relining in independent model

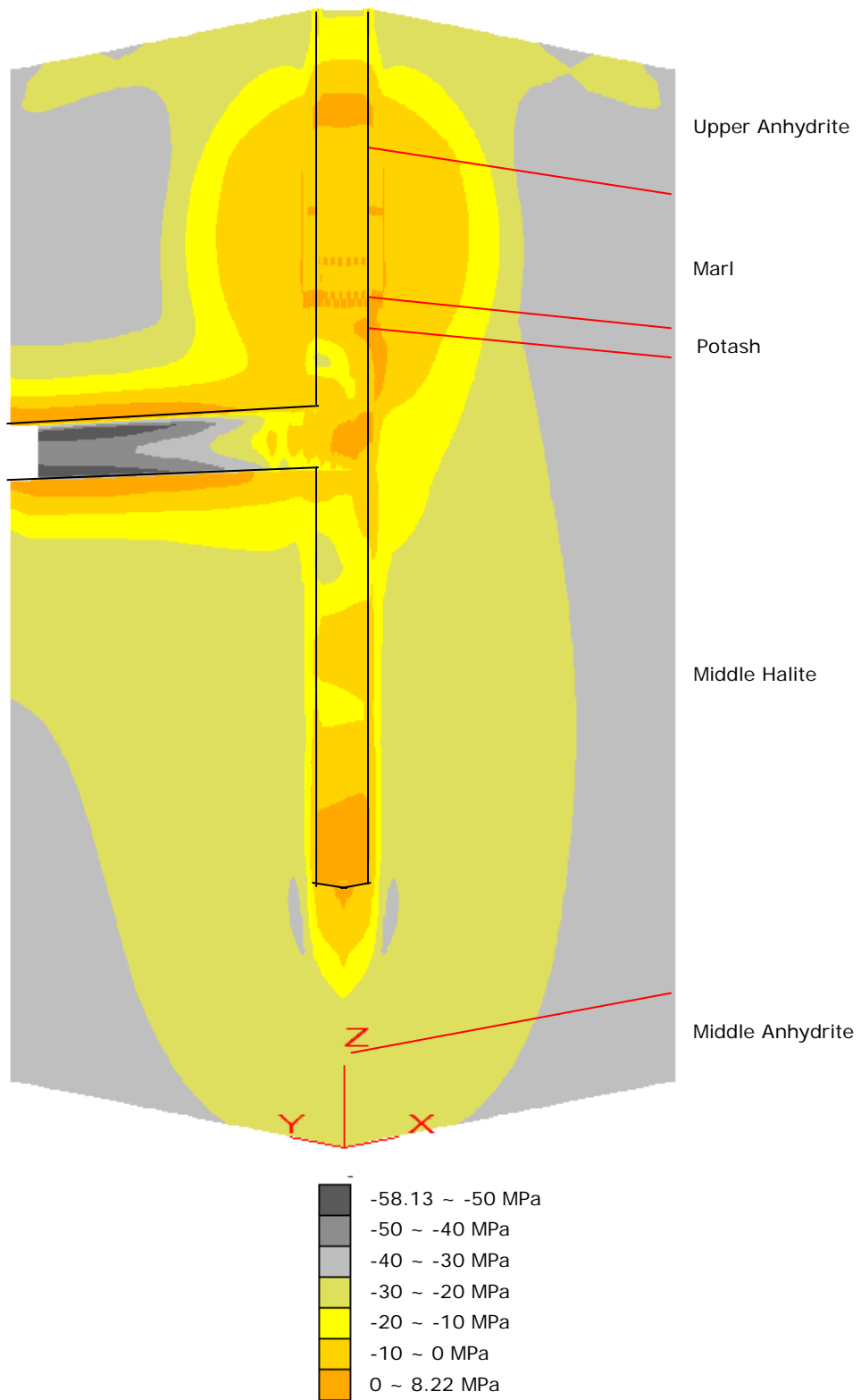


Figure 6.48 Vertical stress σ_z in the third relining in independent model

Because of interface elements involved in all relining models, complicated stress conditions occurred in all relinings through the Marl and Potash strata. The modelling results from the independent model for the first relining are taken as an example to illustrate the complicated stress condition. Again, points A' and B' in Figure 6.21 were used to measure the principal stresses in the concrete linings in the strata near to the shaft inset. Tables 6.8~6.9 show the principal stress measurement results from the model.

Measure points position above the roadway roof		Before the roadway excavation (MPa)		After the roadway excavation (MPa)		After relining (kPa)	
In strata	(m)	A'	B'	A'	B'	A'	B'
Marl	15.8	0.15	0.15	0.24	0.18	0.22	0.26
Marl	12.2	0.07	0.62	0.14	0.66	0.13	0.11
Marl	9.8	0.04	0.24	0.04	0.24	0.82	0.53
Potash	6.2	0.13	0.15	0.04	0.16	0.1	0.03

Table 6.8 Major principal stress σ_1 of the 1st relining's inner surface

Measure points position above the roadway roof		Before the roadway excavation (MPa)		After the roadway excavation (MPa)		After relining (kPa)	
In strata	(m)	A'	B'	A'	B'	A'	B'
Marl	15.8	-0.89	-0.86	-0.87	-0.85	-2.9	-2.96
Marl	12.2	-0.39	-0.2	-0.37	-0.25	-3.88	-4.21
Marl	9.8	-0.32	-0.12	-0.3	-0.12	-2.11	-2.08
Potash	6.2	-0.17	-0.1	-0.19	-0.08	-5.15	-5.93

Table 6.9 Minor principal stress σ_3 of the 1st relining's inner surface

It was expected that the shaft NSC lining suffered even loading before the roadway excavation in the independent model, since the stress field used in the models was hydrostatic (described in section 6.6) and the interface

elements distributed in any plane symmetrically (Figure 6.7). That is to say, points A' and B' in the shaft NSC lining were expected to suffer similar stress conditions before the roadway excavation in each independent model. However, it is clearly shown in Tables 6.8~6.9 (columns in light blue) that there were large differences between the principal stresses in the NSC lining at points A' and B' in the model (in most areas) at the same vertical level through the Marl and Potash strata before the roadway excavation.

In the continuous model, the principal stresses at point A' decreased and those at point B' increased in the original shaft lining (columns in light green Tables 6.6~6.7) after the roadway excavation. However, in the independent model, the major principal stresses (columns in light green in Table 6.8) at both points A' and B' in the original shaft lining increased in most areas after the roadway excavation. The minor principal stresses (columns in light green in Table 6.9) did not change a lot.

In the continuous model, the minor principal stresses at point A' were bigger than those at point B' in the first HSC relining through the Marl and Potash strata (Table 6.7), implying uneven loading on the shaft linings. However, in the independent model, there was no clear rule between the minor principal stresses at points A' and B' in the first HSC relining through the Marl and Potash strata (Table 6.9).

Additionally, major principal stresses in Table 6.8 were tensile stress, totally different from those in the continuous model (most were compressive stress in Table 6.6). Most of the minor principal stresses shown in Table 6.9 were very low when compared with the applied stress (around 30 MPa) and the compressive strength of the HSC (100~140 MPa) used in the three-dimensional models, although the practical material

properties for the HSC obtained from the laboratory tests have been used in each independent model.

Clearly, the deformation and stresses conditions of the shaft linings in the independent model were very different from those in the continuous model (section 6.8.1). The modelling results described above are thought to result from the massive number of interface elements (146~205 described in section 6.3) employed in the independent models. These interface elements are helpful in making three-dimensional models as close to the real engineering situation as possible. However, the obtained modelling results on stresses and deformations of the shaft relinings were difficult to understand, due to the complexity of the structures representing the relining systems and the difficulty in defining appropriate properties for the interface elements in the models.

6.9 Conclusions

Many conclusions can be drawn from this study in terms of stress and deformation conditions of the shaft linings and surrounding rock near the shaft inset largely because of the volume of data that was generated in modelling exercises of this type. In the targeted strata, the Marl was the weakest rock material. Therefore, the shaft linings through the Marl stratum suffered the most severe stress and deformation conditions while the shaft was being excavated before the roadway excavation. The roadway excavation in the models led to increased deformation (horizontal and vertical) of the shaft lining through the nearby strata, especially at the bottom of the Marl and the strata forming the roadway immediate roof and floor. Vertical stress relief in the roadway immediate roof and floor within the Middle Halite stratum was also generated by the roadway excavation.

1) In the continuous model

- The deformation/stresses in the original shaft lining were evenly distributed before the roadway excavation. However, these conditions changed to be uneven due to the roadway excavation.
- The uneven deformation/stress conditions in the original shaft lining and relinings through the Marl and Potash strata imply that, the roadway excavation caused uneven loading on the shaft concrete linings through the nearby strata, especially the weak Marl and the Potash. This uneven loading caused a build up of high shear stress threatening the stability of the circular concrete lining.
- The uneven deformation/stress conditions in the HSC relinings (horizontal displacement difference about 2~4 mm) were not as severe and extensive as those in the original shaft NSC lining (horizontal displacement difference about 12 mm). This implied that HSC relinings through the Marl and Potash strata performed far better than the original shaft NSC lining, which was expected.
- The uneven deformation/stress conditions of the original shaft lining after the roadway excavation was quite significant: approximately 15 m above the roadway roof and 15 m below the roadway floor in the continuous model, including the Marl, the Potash and the Middle Halite strata (the roadway immediate roof and floor).
- The horizontal displacement of the inner surface of the shaft's first relining (around 5.4 mm) through the Marl and Potash strata was bigger than those of the second and third relinings (around 2.8 mm). This implied that the later two relinings supplied stronger support than the first one. Even in the Potash stratum, the third relining suffered little uneven horizontal displacement, implying that the third relining would perform better than the previous ones.

- During relining exercises,
 - a) Significant tensile stress developed in the relinings through the Marl and Potash strata and wing wall,
 - b) The vertical stress relief zone in the surrounding rock in the Marl stratum became bigger.
 - Although the shaft HSC relinings through the Marl and Potash strata were deformed into ellipses in plan view, their major axes were perpendicular to the roadway direction, totally contrary to that of the original lining, which needs validation with in situ observations.
- 2) In the independent models
- Very low displacements occurred in the shaft relinings (<0.5 mm) when compared with those in the continuous model. The shear displacements of the interfaces were even lower (<0.01 mm) in the shaft HSC relinings through the Marl and Potash strata.
 - High shear and normal stresses (13 MPa/1.5 MPa) developed in the interfaces in the second relining, which threatened the stability of the whole relining. At the final equilibrium state, some interface shear failure stayed active only in the second relining. These implied that a single ring of concrete blocks as lining (the first and third relinings) was more effective than the double rings of concrete blocks (the second relining).
 - The extent of the stress relief zone in the Marl and Potash strata caused by the shaft excavation and subsequent original lining and relinings, in the independent models for shaft relinings was bigger than that in the continuous model. This implied that the historic stress field was over simulated in extent in the independent models.
 - The shaft NSC lining was expected to be subjected to even loading before the roadway excavation in the model. However, modelling
-

results show that the principal stresses in the NSC lining were uneven through the Marl and Potash strata before the roadway excavation, due to the effect of the complicated interface elements built in the model, representing the various materials between HSC blocks.

- The principal stresses in the shaft relining (-5.93~0.03 kPa) were far lower than the applied stress and the compressive strength of the HSC used in the three-dimensional models.

The interface elements are helpful to make the models as close to the real engineering situation as possible. However, the modelling results on stress and deformation of the shaft relinings were difficult to understand, due to the complexity of the structures representing the shaft relining systems and difficulty in defining appropriate properties for the interface elements in the numerical models. This is the main obstacle in developing the numerical models as close to the real engineering situation as possible for Boulby mine shaft relinings stability analysis.

Therefore, the continuous model described in section 6.2 that gives the analysable modelling results is recommended by the author. By this method, the effect of the historic changes in the stress field on each shaft lining's stability can be investigated from initial construction, original lining installation, inset and roadway construction leading from the shaft and subsequent relining phases. Absence of the interface elements in the models made the simulation quicker and gave computer memory-savings. Although the dimensions of the shaft relinings through the Marl and Potash strata in the continuous model were actually smaller than their own particular dimensions, using equivalent properties for the shaft relining systems in the continuous model was an effective way to solve this problem. However, an appropriate method needs developing to convert

the equivalent stress (discussed in sections 6.8.1.2) to the practical stress developed in the shaft relinings in the model. This will be helpful to compare the model stress results with the in situ measurements and predict the stress conditions which will occur in the third relining.

The two-dimensional modelling results implied that the Marl with weak mechanical properties should not be the only reason for the failure of the shaft linings through this stratum. The three-dimensional modelling results implied that the roadway just approximately 10 m below the Marl stratum was also a key factor in the stability of the shaft linings through the Marl stratum. When the shaft or the roadway is excavated underground in a virgin rock mass field, the virgin stress field will be redistributed. The shaft excavation at Boulby mine resulted in a stress redistribution in the underground rock mass. After that, the roadway was driven, which led to a further stress redistribution around the shaft perimeter above and below the roadway. If the rock had been stronger, it could have carried the induced stress within its elastic limits with little or no deformation.

However, the Marl is very weak, which can be considered as plastic under most conditions (section 2.5 in Chapter 2). It cannot carry the stress redistribution around the shaft caused by the roadway excavation, which was an uneven loading acting on the shaft linings. The squeeze from the rock surrounding the shaft, where it was perpendicular to the roadway direction, led to the uneven horizontal inwards deformation. This uneven loading (vertical and horizontal) brought high shear and tensile stresses threatening the stability of the circular concrete structures, as observed in the shaft second relining system. This is the key problem for the stability of the shaft lining through the Marl stratum above the roadway at the mine.

CHAPTER 7

CONCLUSIONS AND RECOMMENDATIONS

7.1 Conclusions

The objective of this research was to develop a practical numerical modelling approach using Finite Difference Method (FDM) for a particular rock mechanics problem, combining theoretical, experimental and numerical modelling works. The shaft lining's stability at Boulby mine has been investigated as a practical engineering example using commercial FDM codes - FLAC^{2D}/FLAC^{3D} in this thesis.

There are two shafts at Boulby mine, approximately 1150 m in depth. A soft rock Carnallitic Marl (about 9 m thick, Marl for short) occurs close to the bottom of the shafts. Both shafts concrete linings through this stratum have suffered considerable pressure, which caused gradual failure of both shaft's linings through this zone and failure of the relatively weak unsupported wing walls at the bottom of the shafts at the inset level. So far, both shaft linings have been restored twice since the shafts were sunk during 1968~1974 and a further repair (third relining) is now required and being planned.

The most important advantage to using a practical engineering example was that the in situ observations, the rock engineers' experience, and the available in situ measurements at the mine have been significantly helpful in validating the numerical models. However, many factors at the mine site have made this numerical models research a big challenge, including complicated lining structures, complex lining failure conditions and the scarcity of laboratory test data for the weakest rock material – the Marl.

A comprehensive literature review has been carried out, concentrating on the virgin in situ ground stress state, rock mass classification systems, previous rock mechanics research and the history of the shafts at the mine. Based on this literature review and new laboratory tests conducted at the NCG, the database of material (e.g. rocks, concrete, plywood packs) properties related to this research had been built up. The methodology of obtaining appropriate input material properties for rock masses in numerical modelling from laboratory tests data has then been studied.

Numerical modelling was then conducted following these preparatory works, including all the historical cases of the shaft concrete relining systems. Parametric studies on the effects of rock properties of the Marl, the extent of weathered Marl, the ground stress field (hydrostatic or not) and the possible "point" loading on the original lining on the stress and deformation conditions of the shaft linings have been studied in the two-dimensional models. Due to the limitation of the finite difference mesh and the difference between the dimensions of the mine original shaft lining and relinings through the Marl zone, two modelling methods have been developed in the three-dimensional models in this research to simulate each stage in the shaft linings: the continuous model for all shaft linings and independent models for each shaft lining system.

According to the two-dimensional numerical modelling results presented in Chapter 5, some conclusions have been drawn as follows:

- 1) The increasing extent of the weathered Marl resulted in higher deformation and stress conditions in the shaft's linings.
- 2) The non-hydrostatic stress field would result in uneven loading on the circular shaft linings and threaten their stabilities. A possible reason for the original lining's failure may be due to uneven (point) loading

on it caused by uneven thicknesses of backfill material. The rigid cement grout backfilled in the relinings facilitated the avoidance of potential uneven loading on the relinings.

- 3) The maximum major principal stress and the maximum deviator stress always occurred at the inner surface of the shaft linings in the models as expected, and this would threaten the concrete linings' stability.
- 4) The single ring concrete blocks are a more effective lining than the double rings in terms of lining closure, because more plywood packs involved in double rings concrete blocks lining made the relining more deformable.
- 5) For the newly designed third thicker relining, the ratio of lining's closure with its inner radius was lower than those of the previous relinings. The ratio of the maximum deviator stress with the HSC characteristic strength was only approximately 46% in the third relining. These modelling results illustrate that the newly designed third relining will perform better than the previous ones.
- 6) Stress concentration zones were evident along the inner surface of the shaft relining at the end tips of the interfaces. This demonstrated that interface materials between HSC blocks in shaft relinings improved the flexibility of the lining systems successfully but decreased the strength of the whole lining systems as the weak "joints".

According to the three-dimensional numerical modelling results presented in Chapter 6, the following conclusions can be drawn:

- 1) In the targeted strata, the Marl was the weakest rock material. Therefore, the shaft concrete linings through the Marl stratum suffered the most severe failure condition while the shaft was being excavated before the roadway excavation.

- 2) The roadway excavation led to increased deformation of the shaft concrete lining through the nearby strata, especially at the bottom of the Marl and in the strata forming the roadway immediate roof and floor.
- 3) The original shaft lining was under even loading before the roadway excavation in the continuous model. However, the roadway excavation caused uneven loading on the original shaft lining and relinings through the nearby strata, especially the weak Marl and the Potash. This uneven loading caused a build up of high shear stress threatening the stability of the circular concrete lining.
- 4) The uneven deformation/stress conditions of the original shaft lining after the roadway excavation were quite significant in the continuous model. These conditions expended approximately 15 m above the roadway roof and 15 m below the roadway floor, including the Marl, the Potash and the Middle Halite strata (the roadway immediate roof and floor).
- 5) The uneven deformation/stress conditions in the HSC relinings (horizontal displacement difference about 2~4 mm) were not as severe and extensive as those in the original shaft NSC lining (horizontal displacement difference about 12 mm) in the continuous model. This implied that HSC relinings through the Marl and Potash strata performed far better than the shaft's original NSC lining, which was expected.
- 6) The horizontal displacements of the inner surface of the shaft's first relining (around 5.4 mm) through the Marl and Potash strata were bigger than those of the second and third relinings (around 2.8 mm) in the continuous model. This implied that the later two relinings supplied stronger support than the first one. Even in the Potash

stratum, the modelled third relining suffered little uneven horizontal displacement, implying that the third relining would perform better than the previous ones.

- 7) Although the shaft HSC relinings through the Marl and Potash strata were deformed into ellipses in plan view in the continuous model, their major axes were perpendicular to the roadway direction, totally contrary to that of the original lining. This modelling result requires validation with in situ observations.
- 8) In the independent model, high shear and normal stresses (13 MPa/1.5 MPa) developed in the interfaces in the second relining threatening the stability of the whole relining system. At the final equilibrium state, some interface shear failure stayed active only in the second relining. These again implied that a single ring of concrete blocks as shaft lining (the first and third relinings) was more effective than the double rings of concrete blocks (the second relining).
- 9) The extent of the stress relief zone in the Marl and Potash strata caused by the shaft excavation and subsequent original lining and relinings, in the independent models was bigger than that in the continuous model. This implied that the historic stress field was over simulated in extent in the independent models.

The interface elements are helpful in making the three-dimensional models as close to the real engineering situation as possible. However, the modelling results on stresses and deformations of the shaft relinings obtained were difficult to understand, such as very low principal stresses (-5.93~0.03 kPa) in the shaft relining, very low displacements occurring in the shaft relining (<0.5 mm) and uneven loading condition of the shaft NSC lining before the roadway excavation, even though this was expected to be subjected to even loading. These were due to the complexity of the

structures representing the shaft relining systems and difficulty in defining appropriate properties for the interface elements in the independent models. This is the main obstacle in developing the three-dimensional models as close to the real engineering situation as possible for Boulby mine shaft relinings stability analysis.

Therefore, the continuous model that gives the analysable modelling results is recommended by the author. By this method, the effect of the historic changes in the stress field on each shaft lining's stability can be investigated from initial construction, original lining installation, inset and roadway construction leading from the shaft and subsequent relining phases. Absence of the interface elements in the numerical models made the simulation quicker and computer memory-saving. Although the dimensions of the shafts' relinings through the Marl and Potash strata in the continuous model were actually smaller than their own actual dimensions, using equivalent properties for the shaft relining systems in the continuous model was an effective way to solve this problem. However, an appropriate method needs developing to convert the equivalent stress to the practical stress developed in the shaft relinings in the model. This will be helpful to compare the modelling stress results with the in situ measurements and predict the stress conditions which will occur in the third relining.

Based on the two-dimensional modelling results, it is thought that the weak rock Marl should not be the only reason for the shaft linings' failure through this stratum. The three-dimensional modelling results implied that the roadway just approximately 10 m beneath the Marl stratum was also a key factor for the stability of the shaft linings through this stratum. The Marl is so weak that it can be considered as plastic under most conditions.

It cannot carry the stress redistribution around the shaft caused by the roadway excavation, which was an uneven loading acting on the circular shaft linings. This uneven loading brought high shear and tensile stress threatening the stability of the circular concrete structures. This would always be the key problem for the stability of the shaft linings through the Marl stratum above the roadway at the mine.

7.2 Recommendations

The reader is reminded that the running time in the Mohr-Coulomb model is a series of time-steps, totally different from the real time. The stress and deformation results shown in this thesis were the final state of the numerical models when mechanical equilibrium was reached and did not represent fully the ongoing situation experienced over the lining life. They are however, useful when drawing comparisons between the performances of the four different lining types. Any further additional loading or time-dependant (creep) properties put into the model would lead to additional closure and stresses, which represent continuous deforming conditions in the shaft concrete lining systems during their working life.

In fact, the creep behaviour of rocks is an important parameter which should be considered when determining the strength of the rock mass surrounding a void. As a recommendation for the further modelling work, it is worth attempting to simulate the longer term deformation and stress conditions of the shaft lining systems by introducing creep properties of the related materials into the model. To achieve this objective, the Creep model built in FLAC^{2D}/FLAC^{3D} codes can be utilized, in which the program running time can be set to be the shaft linings' total work time, which is around 10 years, or more.

A series of uniaxial creep tests for the Middle Halite and Potash, and triaxial creep tests for the Marl from Boulby mine were carried out at the University of Newcastle upon Tyne in 1970. Salamon and Quinteiro (1991) proposed creep laws for these three rock types based on these tests data. Some uniaxial creep tests for other rock materials from the mine were conducted at the NCG in 2009. All these laboratory test data are important database for the creep models.

Additionally, engineering experience judgment had been used to estimate parameter values (GSI in Chapter 3) thus increasing the uncertainty of the final version of input material properties used in numerical models in this research. Deeper research work combined with in situ investigation can be done to decrease this uncertainty level to make the numerical models as close to the real engineering situation as possible.

References

Ansar, F. and Li, Q.B. (1998). High-strength Concrete Subjected to Triaxial Compression, *American Concrete Institute Materials Journal*, November-December, 1998, 95(6): p747~755

Arslan, G. (2007). Sensitivity Study of the Drucker-Prager Modeling Parameters in the Prediction of the Nonlinear Response of Reinforced Concrete Structures, *Materials and Design*, 2007, 28: p2596~2603

Barton, N., Lein, R. and Lunde, J. (1974). Analysis of Rock Mass Quality and Support Practice in Tunnelling and a Guide for Estimating Support Requirements. *Norges Geotekniste Institute Report Internal Report*.

Beus, M.J. and Board, M.P. (1984). Field Measurement of Rock Displacement and Support Pressure at 5,955- Ft Level During Sinking of Deep Circular Shaft in North Idaho. *Bureau of Mines Report of Investigations, RI 8909, 1984, United States Department of the Interior*.

Beus, M.J. and Chan, S.S.M. (1985). Field Measurement and Finite-Element Modelling of Circular and Rectangular Shaft Shapes in the Coeur d'Alene Mining District, Idaho. *Bureau of Mines Report of Investigations, RI 8972, 1985, United States Department of the Interior*.

Bieniawski, Z.T. (1973). Engineering Classification of Jointed Rock Masses. *Transition of South African Institute of Civil Engineers*, 1973, 15: p335~344

Bieniawski, Z.T. (1974). Estimating the Strength of Rock Materials. *Journal of South African Institute of Mining and Metallurgy*. 1974, 8: p312~320

Bieniawski, Z.T. (1974). Geomechanics Classification of Rock Masses and Its Application in Tunnelling. *Advances in Rock Mechanics 2, part A: p27~32. Washington, D.C.: National Academy of Sciences*

Bieniawski, Z.T. (1976). Rock Mass Classification in Rock Engineering. *Exploration for Rock Engineering, proceeding of the symposium (editor: Z.T. Bieniawski) 1, 97-106. Cape Town: Balkema*.

Bieniawski, Z.T. (1989). Engineering Rock Mass Classification: a Complete Manual for Engineers and Geologist in Mining, Civil and Petroleum Engineering. 1989, John Wiley and Sons.

Bothma, A. (2001). The Rehabilitation of Impala No.1A Ventilation Shaft. *Journal of the South African Institute of Mining and Metallurgy*, 2001, 101(4): p177~182

Boulby Mine. (1976). Manshaft: Miscellaneous Sections (July 1976)

Boulby Mine. (1976). Manshaft: Vertical Sections Through N/S Axis July 1976 (-2677' ~ -3754')

Brace, W.F. (1964). Brittle Fracture of Rocks. In: *State of Stress in Earth's Crust* (ed. By W.R. Judd). New York: Elsevier 1964.

Brown, E.T. and Hoek, E. (1978). Trends in Relationship between Measured In-situ Stresses and Depth, *International Journal of Rock Mechanics and Mining Sciences*, 1978, 15(4): p211~215

Bruneaua, G., Tylerb, D.B., Hadjigeorgioua, J., Potvin, Y. (2003) Influence of Faulting on a Mine Shaft — A Case Study: Part I—Background and Instrumentation. *International Journal of Rock Mechanics and Mining Sciences*, 2003, 40: p95~111

Bruneaua, G., Tylerb, D.B., Hadjigeorgioua, J., Potvin, Y. (2003) Influence of Faulting on a Mine Shaft — A Case Study: Part II —Numerical Modelling. *International Journal of Rock Mechanics and Mining Sciences*, 2003, 40: p113~125

BS 1088: 1966 British Standard for Marine Plywood

BS 8110: 1985 Structural Use of Concrete Part 2: Code of Practice for Special Circumstances

BS EN 413-1: 2004, Masonry cement – Part 1: Composition, Specifications and Conformity Criteria

BS 7861-1:2007, Strata Reinforcement Support System Components Used in Coal Mines – Part 1: Specification for Rockbolting

Buzdar, S.A.R.K. (1968). A Laboratory Investigation into the Mechanical Properties of some Sedimentary Rocks with Special Reference to Potash. PhD thesis, 1968, the University of Newcastle-upon-Tyne

Campbell, D. (2007). Exploring the Nanoworld with LEGO® Bricks. Board of Trustees of Bradley University.

(www.mrsec.wisc.edu/Edetc/LEGO/PDFfiles/nanobook.PDF)

Carter, B.J., Duncan E.J. and Lajtai E.Z. (1991). Fitting Strength Criteria to Intact Rock. *Geotechnical and Geological Engineering*, 1991, 9: p73~81

Chilton F. and Maxwell A.S. (1989). Boulby Shaft Restoration. *The Mining Engineer*, February 1989, p371~376

Cleasby, J.V., Pearse, G.E. and Grieves, M. (1975) Shaft-sinking at Boulby Mine, Cleveland Potash, Ltd. *Transaction of the Institution of Mining and Metallurgy (Section A: Mining Industry)*, 1975, 84: pA7~A28, A113~119, A147~148

Cook, R.F. (1974). Rock Mechanics Investigation Associated with Shaft Excavations in a Deep Evaporite Deposit. PhD thesis, 1974, the University of Newcastle-upon-Tyne

Cook, R.F. (1983). Long Term Closure of a Shaft Excavation through Evaporite Deposites. *Potash Technology (Mining: Rock Mechanics)*, 1983: p275~281

Dahl, K.K.B. (1992). A Failure Criterion for Normal and High Strength Concrete. Project 5, Rep. 5.6, American Concrete Institute, Detroit.

Deere, D.U. (1964). Technical Description of Rock Cores for Engineering Purpose. *Rock Mechanics and Engineering Geology*. 1964, 1(1): p17~22

Denq, B. L., Hu, Y. S., Chen, L. W., Chiu, W. Y., Wu, T. R. (1999). The Curing Reaction and Physical Properties of DGEBA/DETA Epoxy Resin Blended with Propylester Phosphazene. *Journal of Applied Polymer Science*, 1999, 74(1): p229~237

Erasmus, W.P., Swanepoel, C.D., Munro, D., Hague, I., Northcroft, I., Parrish, A. and Bassett, A. (2001). Shotcrete Lining of South Deep Shafts. *Journal of the South African Institute of Mining and Metallurgy*, 2001, 101(4): p169~176

Eurocode: Design of Concrete Structures Part 1 DD ENV 1992-1-1:1992

Extracts from the Structural Eurocodes for students of structural design
PP1990:2007

Farmer, I.W. (1983). *Engineering Behaviour of Rocks* (2nd edition). Chapman & Hall. London

Franklin, J.A. (1975). Safety and Economy of Tunneling. In: *Proceedings of the 10th Canadian Rock Mechanical Symposium*, Kingstone, p27~53

Gercek, H. (2007). Poisson's Ratio Values for Rocks. *International Journal of Rock Mechanics and Mining Sciences*, 44: p1~13

Golder Associates. (1997) Report, No. 972-2434, Golder Associates Dec. 1997

Goodall, R., Williams, C., Fernie, J.A., Clyne T.W. (2002). Thermal Expansion and Stiffness Characteristics of a Highly Porous, Fire-resistant Composite Material.

(<http://www.docstoc.com/docs/20997782/Thermal-Expansion-and-Stiffness-Characteristics-of-a-Highly-Porous>)

Goodman, R.E. (1980). *Introduction to Rock Mechanics*. John Wiley and Sons, 1980, U.S.A.

Grimstad, E. and Barton, N. (1993). Updating the Q-System for NMT. *Proceeding of international symposium: On Sprayed Concrete - Modern Use of Wet Mix Sprayed Concrete for Underground Support*, Fagernes, (editors: Kompen, Opsahl and Berg). Oslo: Norwegian Concrete Association.

Hebblewhite, B.K. (1977). *Underground Potash Mine Design Based on Rock Mechanics Principles and Measurements*. PhD thesis, 1977, the University of Newcastle-upon-Tyne

-
- Heim, A. (1912). Zur Frage der Gebirgs- und Gesteinsfestigkeit. Schweiz. Bauztg, v50.
- Herget, G. (1973). Variation of Rock Stress with Depth at a Canadian Iron Mine, *International Journal of Rock Mechanics and Mining Sciences*, 1973, 10: p37~51
- Herget, G. (1988). *Stresses in Rock*. A. A. Balkema, 1988, Rotterdam, Brookfield.
- Hoek, E. (1983). Strength of Jointed Rock Masses. 23rd. Rankine Lecture. *Géotechnique*, 1983, 33(3): p187~223
- Hoek, E. (1994). Strength of Rock and Rock Masses, *ISRM News Journal*, 1994, 2(2): p4~16
- Hoek, E. (2000, 2007). *Practical Rock Engineering*.
(<http://www.rocscience.com/hoek/PracticalRockEngineering.asp>)
- Hoek, E. and Brown, E.T. (1980). *Underground Excavations in Rock*. The Institution of Mining and Metallurgy, 1980, London
- Hoek, E. and Brown, E.T. (1988). The Hoek-Brown Failure Criterion - a 1988 update. In *Rock Engineering for Underground Excavations*, in: *Proceeding of 15th Canadian Rock Mechanics Symposium* (ed. J.C. Curran), p31~38. Toronto: Department of Civil Engineering, University of Toronto
- Hoek, E. and Brown, E.T. (1997). Practical Estimates of Rock Mass Strength. *International Journal of Rock Mechanics & Mining Science & Geomechanics, Abstracts*, 1997, 34(8): p1165~1186
- Hoek, E., Carranza-Torres, C.T., and Corkum, B. (2002). Hoek-Brown Failure Criterion – 2002 edition. *Proceedings of North American Rock Mechanics Society meeting in Toronto, July 2002*, 1: p267~273
- Hoek, E and Diederichs, M.S. (2006). Empirical Estimation of Rock Mass Modulus. *International Journal of Rock Mechanics and Mining Sciences*, 2006, 43: p203~215
- Hoek, E., Kaiser, P.K. and Bawden. W.F. (1995). *Support of Underground Excavations in Hardrock*. A. A. Balkema, 1995, Rotterdam, Brookfield.
-

-
- Hoek, E., Marinos, P. and Benissi, M. (1998). Applicability of the Geological Strength Index (GSI) Classification for Very Weak and Sheared Rock Masses: the Case of the Athens Schist Formation. *Bulletin of Engineering of Geology and the Environment*, 1998, 57(2): p151~160
- Hojem, J.M.P. and Cook, N.G.W. (1968). The Design and Construction of a Triaxial and Polyaxial Cell for Testing Rock Specimens. *The South African Institution of Mechanical Engineering*. 1968, 18: p57~61
- Hughs, E. A., Liang, Z.Y., Idriss, R. L. and Newton, C. M. (2005). In-place Modulus of Elasticity for High-performance Concrete Bridge, *American Concrete Institute Materials Journal*, November-December, 2005, 102 (6): p454~458
- Hussein, A. and Marzouk, H. (2000). Behavior of High-Strength Concrete Under Biaxial Stresses, *American Concrete Institute Materials Journal*, January-February 2000, 97 (1): p27~36
- ISRM. *Rock Characterisation Testing and Monitoring – ISRM suggested methods*. Editor Brown, E.T. Pergamon Press 1981.
- Itasca. (2008) *FLAC^{2D} V6.0/FLAC^{3D} V3.1: Fast Lagrangian Analysis of Continua*, User Manuals, Itasca Consulting Group, Inc., Minneapolis.
- Jia, Y.D., Stace, R.L., Reddish, J.D. and Dale, M. (2010). *Boulby Mine Concrete Test Report 0210/01*, Nottingham Centre for Geomechanics.
- Kaji, M., Nakahara, K. and Endo, T. (1999). Synthesis of a Bifunctional Epoxy Monomer Containing Biphenyl Moiety and Properties of Its Cured Polymer with Phenol Novolac. *Journal of Applied Polymer Science*, 1999, 74(3): p690~698
- Kirsch, G. (1898). *Die Theorie der Elastizität und die Bedürfnisse der Festigkeitslehre*. Veit. Ver. Deut. Ing., 1898, 42(28): p797~807
- Koksal, H. O., Karakoc, C. and Yildirim, H. (2005). Compression Behavior and Failure Mechanics of Concrete Masonry Prisms, *Journal of Materials in Civil Engineering*, February, 2005, 17(1): p107~115
-

Kozel, A.M. (2001). Conditions of Support, State, Types and Causes of Deformations in the Vertical Shafts. In: Geomechanical Problems of Shaft Design and Support (in Russian), Book 1, Nedra, Saint Petersburg.

Kunieda, M., Kurihara, N., Uchida, Y., Rokugo, K. (2000). Application of Tension Softening Diagrams to Evaluation of Bond Properties at Concrete Interfaces. *Engineering Fracture Mechanics*, 2000, 65: p299~315

Laubscher, D.H. and Taylor, H.W. (1976). The Importance of Geomechanics Classification of Jointed Rock Masses in Mining Operations. In *Exploration for Rock Engineering*, (editor: Z.T. Bieniawski) 1, p119~128. Cape Town: Balkema.

Laubscher, D.H. (1977). Geomechanics Classification of Jointed Rock Masses – Mining Applications. *Transactions of the Institution of Mining and Metallurgy*, 1977, 86: pA1~A8

Laubscher, D.H. (1984). Design Aspects and Effectiveness of Support Systems in Different Mining Conditions. *Transactions of the Institution of Mining and Metallurgy*, 1984, 93: pA70~A82

Laubscher, D.M. and Page, C.H. (1990). The Design of Rock Support in High Stress or Weak Rock Environments. *Proceedings of 92nd Canada Institution of Mining and Metallurgy Annual General Meeting*, Ottawa, Paper # 91

Lauffer, H. (1958). Gebirgsklassifizierung für den Stollenbau. *Geol. Bauwesen*, 1958, 24(1): p46~51

Lim, Y.M., Kim, M.K., Shin, S.K., Li, V.C. (2001). Numerical Simulation for Quasi-brittle Interface Fracture in Cementitious Bi-material System, In: *Proceedings of Fourth International Conference on Fracture Mechanics of Concrete Structures*. Cachan, France, Balkema, 2001: p73~80

Marinos, P., and Hoek, E. (2001). Estimating the Geotechnical Properties of Heterogeneous Rock Masses Such As Flysch. *Bulletin of Engineering of Geology and the Environment (IAEG)*, 2001, 60: p85~92

Marinos, P., and Hoek, E. (2006). A Brief History of the Development of the Hoek-Brown Failure Criterion.

Muir Wood, A.M. (1979). Ground Behaviour and Support for Mining and Tunnelling. 14th Sir Julius Wernher Memorial Lecture, Tunnelling 1979, IMM London, pA23~A24

Nikolaichuk, N.A. (1978). Study of Rock Salt Deformation and Fracture to Get Initial Data for Shaft Supporting Design (with Reference to Yakutia Diamond-bearing Deposits). In Cand. Tech. Sci. Thesis (in Russian), VNIMI, Leningrad.

Olovyanny, A.G. and Kozel, A.M. (2005). Numerical Modelling of Deformation in a Shaft in the Interstratified Salt Rocks. Fiz. –Tekh. Probl. Razrab. Polezn. Iskop., 2005, No. 3.

Ortlepp, W.D. (1974). Failure of the Concrete Lining in an Inclined Shaft at Great Depth. International Society for Rock Mechanics, 3rd Congress, Sept. 1974. Denver, Co, USA.

Patchet, S.J. (1970). Rock Mechanics Studies Associated with the Development of a Deep Potash Mine. PhD thesis, the University of Newcastle-upon-Tyne

Potts, E.L.J., Hebblewhite, B.K. and Miller, H.D.S. (1976) Initial Report on Installation and Overcoring of Strain Cells in the Potash and Marl Strata at Boulby Mine. Report No. 47-0476. University of Newcastle upon Tyne, Department of Mining Engineering

Priest, S.D. and Hudson, J.A. (1976). Discontinuity Spacings in Rock. International Journal of Rock Mechanics and Mining Science, 1976, 13: p135~148

Rabcewicz L. (1964). The New Austrian Tunnelling Method, Part one, Water Power, November 1964, p453~457; Part two, Water Power, December 1964, p511~515

Rabcewicz L. (1965). The New Austrian Tunnelling Method, Part Three, Water Power, January 1965, p19~24

Reddish, D.J. (1989). The Modelling of Rock Mass Behaviour Over Large Excavations Using Non-Linear Finite Element Techniques. Mining Department Magazine, XLI: p93~105

Royal School of Mines, Imperial College. (2000). Laboratory Test Report (Cleveland Potash), July 2000, Lab Reference #812

Santosh, G.S. and Kishen, J.M.C. (2010). Fracture Behavior of Concrete–concrete Interface Using Acoustic Emission Technique, Engineering Fracture Mechanics, 2010, 707: p908~924

Salamon, M.D.G. and Quinteiro C.R. (1991). A Summary Report to Cleveland Potash Limited on Stress Analysis Project. Report T-4122, Department of Mining Engineering, Colorado School of Mines, 1991.

Shaw, J.D.N. (1982). A Review of Resins Used in Construction, Types of Resin, Applications and Case Histories. International Journal of Adhesion and Adhesives. 1982, 2(2): p77~83

Spee, T., Duivenbooden, C. V. and Terwoert, J. (2006). Epoxy Resins in the Construction Industry. Annals of the New York Academy of Sciences, September 2006, 1076 (0): p429~438

Squirrell P. (1992). Yield Pillars in a Deep Potash Mine. Effects of Geomechanics on Mine Design. A. A. Balkema, 1992, Rotterdam, Brookfield, ISBN 90 5410 0400, p139~145

Stace, R.L., Reddish, J.D. and Dale, M. (2007, 2008). Boulby Mine Rock Materials Test Report 0907/01 and 0608/01, Nottingham Centre for Geomechanics.

Swift, G.M. and Reddish, D.J. (2005). Underground Excavation in Rock Salt. Geotechnical and Geological Engineering, 2005, 23: p17~42

Tabor, L.J. (1978). Effective Use of Epoxy and Polyester Resins in Civil Engineering Structures. The Construction Industry Research and Information Association (CIRIA) Report 69, 1978

Talobre, J. (1957). La Mécanique des Roches. Dunod, Paris.

Terzaghi, K. (1946). Rock Defects and Loads on Tunnel Supports, in *Rock Tunneling with Steel Supports*, (editors: R. V. Proctor and T. L. White) 1, p17-99. Youngstown, OH: Commercial Shearing and Stamping Company.

Terzaghi, K. and Richart, F.E. (1952). Stresses in Rock about Cavities. *Geotechnique*, 1952, 3: p57~90

Vabrik, R., Czajlik, I., Tuřry, G., Rusznaćk, I., Ille, A., AndraćSvićg. (1998). A Study of Epoxy Resin–Acrylated Polyurethane Semi-Interpenetrating Polymer Networks. *Journal of Applied Polymer Science*, 1998, 68(1): p111~119

Vandewalle, M. (1998). The Use of Steel Fibre Reinforced Shotcrete for the Support of Mine Openings. *Journal of the South African Institute of Mining and Metallurgy*, 1998, 98(3): p113~120

Vermeer, P.A. and R. deBorst. (1984). Non-Associated Plasticity for Soils, Concrete and Rock. *Heron*, 1984, 29(3): p3~64

Whittaker, B.N. and Frith, R.C. (1990). *Tunnelling: Design, Stability and Construction*. The Institution of Mining and Metallurgy, 1990, London

Whittles, D.N. (1999). *The Application of Rock Mass Classification Principles to Coal Mine Design*. PhD thesis, University of Nottingham

Whittles, D.N., Reddish, D.J. and Lowndes, I.S. (2007). The Development of a Coal Measure Classification (CMC) and its Use for Prediction of Geomechanical Parameters. *International Journal of Rock Mechanics and Mining Sciences*, 2007, 44: p496~513

Wickham, G.E., Tiedemann, H.R. and Skinner, E.H. (1972). Support Determination Based on Geologic Predictions. In *Proceedings of North American Rapid excavation Tunnelling conference*, Chicago, (editors: K.S. Lane and L.A. Garfield), p43-64. New York: Society of Mining Engineers, the American Institute of Mining, Metallurgical, and Petroleum Engineers.

Williams A. and Auld F.A. (2002). Boulby Mine Shaft Lining Design- Second Restoration. *Transition of the Institution of Mining and Metallurgy (Section A: Mining technology)*, 111, January–April 2002, pA13~A27

Williams, A., Richards, C.B., Aarup, B. and Auld, F.A. (2001). Compact Reinforced Composite (CRC) High Strength (120 N/mm^2) Precast Concrete Block Deep Shaft Flexible Linings. In *Underground Construction 2001*, London: Brintex for Institution of Mining and Metallurgy, British Tunnelling Society, Federation of Piling Specialists and Pipe Jacking Association, p487~497

Williamson, D.A. (1984). Unified Rock Classification System. *Bulletin, Association of Engineering Geologists*, 21(3): p345~354

Wilson, A.H. (1980). *The Stability of Underground Workings in the Soft Rocks of the Coal Measures*. PhD thesis, 1980, University of Nottingham

Yang, G., Fu, S.Y. and Yang, J.P. (2007). Preparation and Mechanical Properties of Modified Epoxy Resins with Flexible Diamines. *Polymer*, 2007, 48: p302~310

Zheng, W., Kwan, A.K.H. and Lee, P.K.K. (2001). Direct Tension Test of Concrete, *American Concrete Institute Materials Journal*, January-February, 2001, 98(1): p63~71

APPENDIX I: Summary of Boulby Mine Rock Materials Laboratory Tests Data**Summary of Boulby Mine Rock Materials**

At shaft depth (m)		Time Periods			Stratum	Tested @ NCG	Reviewed	Data Sheet	
From	To								
0	37				Drift				
37	82	Jurassic	Lias Shales		Middle Lias (Lower Lias i)		√	√	
82	375				Lower Lias ii		√	√	
375	392	Triassic			Rhaetic		√	√	
392	640		Mercia Mudstones		Keuper Marl		√	√	
640	976		Sherwood Sandstone		Bunter Sandstone		√	√	
976	1040	Permian	Permian Evaporites	Upper Evaporites	Upper Permian Marl i		√	√	
					Upper Permian Marl ii				
1040	1070				Upper Halite		√	√	
1070	1085				Upper Anhydrite		√	√	
1085	1100			Middle Evaporites		Carnallite / Carnallitic Marl		√	√
1100	1105					Halite Parting		√	√
						Middle Potash		√	√
1105	1145					Middle Halite		√	√
1145						Middle Anhydrite		√	√
						Dolomite		√	√
						Lower Anhydrite		√	√
				Lower Evaporites		Lower Halite		√	√
						Polyhalite Roof Beds		√	√
						Polyhalite (Low Grade Polyhalite)		√	√
						Polyhalite Floor Beds (Anhydrite)		√	√

Middle Lias (Lower Lias I)

Description: silty sandstone with frequent partings, medium grey to black in color, often highly laminated, fossiliferous with some pyrite.

Density	UCS				Triaxial Compressive Strength			Tensile Strength			Static Elastic Modulus	Poisson's Ratio	Note
	g/cm ³	Number of samples	D/H ratio	Mean MPa	Range MPa	Number of samples	σ_3 MPa	σ_1 MPa	Number of samples	Mean MPa			
		0.5	51.97			3.45	77.96	5	3.50	2.18-5.47	8.41	0.37	
						6.90	79.78						
						10.34	91.87						
2.6			77.61						3.88		16.83	0.2	Conclusion for Lias

From: Rock Mechanics Studies Associated With The Development Of A Deep Potash Mine, S.J.Patchet's thesis, 1970

Lower Lias (Lower Lias II)

Description: silty sandstone with frequent partings, medium grey to black in color, often highly laminated, fossiliferous with some pyrite.

Density	UCS				Triaxial Compressive Strength			Tensile Strength			Static Elastic Modulus	Poisson's Ratio	Note
	g/cm ³	Number of samples	D/H ratio	Mean MPa	Range MPa	Number of samples	σ_3 MPa	σ_1 MPa	Number of samples	Mean MPa			
		0.5	103.26			3.45	59.04*	5	4.28	2.76-7.08	25.86	0.03	

From: Rock Mechanics Studies Associated With The Development Of A Deep Potash Mine, S.J.Patchet's thesis, 1970

* Broken between wrapping and testing

Rhaetic

Description: shales & sandstones, often highly color in cream, grey & red.

Density g/cm ³	UCS				Triaxial Compressive Strength			Tensile Strength			Static Elastic Modulus	Poisson's Ratio	Note
	Number of samples	D/H ratio	Mean MPa	Range MPa	Number of samples	σ_3 MPa	σ_1 MPa	Number of samples	Mean MPa	Range MPa	GPa		
		0.5	51.63			3.45	54.71	6	4.25	1.03-15.36	12.97	0.05	
						6.90	101.66						
						10.34	76.37						
2.5			51.63						4.25		12.97	0.05	Conclusion

From: Rock Mechanics Studies Associated With The Development Of A Deep Potash Mine, S.J.Patchet's thesis, 1970

Keuper Marl

Description: marls & mudstones with occasionally gypsums, dark grey to reddish, occasional layers of gypsum & anhydrite, some lamination with little cohesion.

Density g/cm ³	UCS				Triaxial Compressive Strength			Tensile Strength			Static Elastic Modulus	Poisson's Ratio	Note
	Number of samples	D/H ratio	Mean MPa	Range MPa	Number of samples	σ_3 MPa	σ_1 MPa	Number of samples	Mean MPa	Range MPa	GPa		
2.7		0.5	113.06			6.90	159.34	3	2.78	2.18-3.64	34.07	0.08	
2.7			113.06			6.90	159.34		2.78		34.07	0.08	Conclusion

From: Rock Mechanics Studies Associated With The Development Of A Deep Potash Mine, S.J.Patchet's thesis, 1970

Bunter Sandstone

Description: sandstone with frequent mudstone partings, cream to reddish brown, occasionally friable, often finely bedded, contains brines at high pressure.

Density g/cm ³	UCS				Triaxial Compressive Strength			Tensile Strength			Static Elastic Modulus	Poisson's Ratio	Note
	Number of samples	D/H ratio	Mean MPa	Range MPa	Number of samples	σ_3 MPa	σ_1 MPa	Number of samples	Mean MPa	Range MPa	GPa		
		0.5		49-72*				14	5.19	4.26-6.49	21	0.07	
						0.00	>58.97						Saturated in brine
						6.90	190.00						
						13.79	156.90						
						20.69	185.86						
						27.59	225.52						
						0.00	>58.97						Air dried
						6.90	139.31						
						13.79	167.59						
						20.69	205.17						
						27.59-25.86	226.55						
						34.48-20.69	215.86						
2.5				59.9					5.19		20.83	0.07	Conclusion

From: Rock Mechanics Studies Associated With The Development Of A Deep Potash Mine, S.J.Patchet's thesis, 1970

* From: Rock Mechanics Investigation Associated With Shaft Excavations In A Deep Evaporite Deposit, R.F.Cook's thesis, 1974

Upper Permian Marl (I & II)

Description: marl & mudstone, reddish-brown in color, compact but occasionally laminated.

Density g/cm ³	UCS				Triaxial Compressive Strength			Tensile Strength			Static Elastic Modulus	Poisson's Ratio	Note
	Number of samples	D/H ratio	Mean MPa	Range MPa	Number of samples	σ_3 MPa	σ_1 MPa	Number of samples	Mean MPa	Range MPa	GPa		
		0.5	77*			0	75.68	8	5.50	3.52-7.46	18.28	0.09	Upper Permian Marl I
						3.45	155.92	9	8.23	5.39-9.83	22.28	0.05	Upper Permian Marl II
						6.90	160.02						
						10.34	181.68						
						13.79	165.49						
						17.24	186.46						
2.3			85.79						6.86		20.28	0.07	Conclusion

From: Rock Mechanics Studies Associated With The Development Of A Deep Potash Mine, S.J.Patchet's thesis, 1970

* From: Rock Mechanics Investigation Associated With Shaft Excavations In A Deep Evaporite Deposit, R.F.Cook's thesis, 1974

Upper Halite

Description: halite, coarse grained but several fine grained zones occur, colourless to light pink or orange in color.

Density g/cm ³	UCS				Triaxial Compressive Strength			Tensile Strength			Static Elastic Modulus GPa	Poisson's Ratio	Note
	Number of samples	D/H ratio	Mean MPa	Range MPa	Number of samples	σ_3 MPa	σ_1 MPa	Number of samples	Mean MPa	Range MPa			
		0.5	31.01			0.00	31.01	11	1.59	1.08-1.99	1.86	0.24	
						3.45	67.24						
						6.90	87.53						
						10.34	104.86						
						13.79	113.97						
						17.24	123.54						
2.2			31.01						1.59		1.86	0.24	Conclusion

From: Rock Mechanics Studies Associated With The Development Of A Deep Potash Mine, S.J.Patchet's thesis, 1970

	1	0.5	29.35*	28-31				2	2.05^				
	4	0.5	31.5^					1	1.39*				
	1	0.66	32.5*					1	1.25*				
	1	0.66	39.2^										
	1	0.66	23.5*										
	3	1	32.5^										
	1	1	39^										
	1	1	41.45*										

From: Rock Mechanics Investigation Associated With Shaft Excavations In A Deep Evaporite Deposit, R.F.Cook's thesis, 1974

* direction of bedding to axis of specimen (major failure plane in tensile): parallel

^ direction of bedding to axis of specimen (major failure plane in tensile): perpendicular

Upper Anhydrite - 1

Description: anhydrite, coarse to fine grained, white to gray in color, often with halite and sylvite occasionally in the form of veins or stringers.

Density g/cm ³	UCS				Triaxial Compressive Strength			Tensile Strength			Static Elastic Modulus	Poisson's Ratio	Note
	Number of samples	D/H ratio	Mean MPa	Range MPa	Number of samples	σ_3 MPa	σ_1 MPa	Number of samples	Mean MPa	Range MPa	GPa		
	9	0.5	43.99	24.9-97.41		0.00	85.41	31	6.08	2.75-12.8*	16.62	0.18	E & v at Borehole S6
	5	0.5	60.34	41.55-106.3		3.45	122.97				21.66	0.25	E & v at Borehole S11
	1	1	108.73	--		5.17	122.97						
	7	1	101.08	79.41-119.7		6.90	88.41						
	9	0.5	43.99			10.34	132.07						UCS samples from Borehole S6
	1	0.7	98.15			13.79	140.00						
	1	1	108.73			17.24	95.72						
	1	1.3	129.76			31.03	196.00						
	1	1.6	110.21			44.83	210.34						
	1	2	129.14										
	2	2.6	163.77										
	2	4	199.43										
2.8			49.83						6.08		19.1	0.22	Conclusion

From: Rock Mechanics Studies Associated With The Development Of A Deep Potash Mine, S.J.Patchet's thesis, 1970

* The maximum of tensile strength is at the base of upper anhydrite

Upper Anhydrite - 2

Density g/cm ³	UCS			Triaxial Compressive Strength			Static Elastic Modulus GPa	Poisson's Ratio	Dynamic elastic moduli GPa	Cohesion MPa	Friction Angle Degree	Ultrasonic pulse velocities		Note	
	Number of samples	D/H ratio	Mean MPa	Number of samples	σ_3 MPa	σ_1 MPa						V_p (m/s)	V_s (m/s)		
2.93				1	36	231.2		0.357*D	50.52*			5346*	2520*	Single stage triaxial compression	
2.94				1	1	98.04		0.348*^D	59.22*^	25.43	35.19	5665*^	2738*^	Multi-stage triaxial compression	
			5		117.2		0.349*D	54.85*					5467*		2631*
			10		139	35.4*^	0.466*^								
			20		173.9	42.1^	0.477^								
			40		245.1										

From: Royal School of Mines, Imperial College Laboratory Test Report (Cleveland Potash), July 2000, Lab Reference #812 (Anhydrite)

* Confining pressure 0MPa

^ Confining pressure 1MPa

*^ Confining pressure 36MPa

D Dynamic Poisson's ratio

Carnallite

Density g/cm ³	UCS			Triaxial Compressive Strength		Tensile Strength		Static Elastic Modulus GPa	Poisson's Ratio	Dynamic Elastic Modulus GPa	Cohesion MPa	Friction Angle Degree	Note	
	Number of samples	D/H ratio	Mean MPa	Number of samples	σ_3 MPa	σ_1 MPa	Number of samples							Mean MPa
1.67				3	1	12.68	6	4.09	0.321*D	26.51*	6.12	16.37	Multi-stage triaxial, Cohesion, □ sample C1	
2.25			5		26.2	3.59		0.286*^D	36.76*^					
2.22			10		38.88	4.1		0.309*D	26*					
1.75	1	0.5	6.53		20	56.8		4.91	2.08^	0.257^				
					40	82.83		5.15	15.8*^	0.313*^				
					36	85.9		3.66	3.9^	0.171^				
					1	19.71					7.14	19.84		Multi-stage triaxial, Cohesion, □□ sample C3
					5	32.46								
					10	43.03								
					20	59.43								
				40	101.14									

From: Royal School of Mines, Imperial College Laboratory Test Report (Cleveland Potash), July 2000, Lab Reference #812

* Confining pressure 0MPa

^ Confining pressure 1MPa

*^ Confining pressure 36MPa

D Dynamic Poisson's ratio

Marl (Carnallitic Marl) - 1

Density g/cm ³	UCS				Triaxial Compressive Strength			Tensile Strength			Static Elastic Modulus GPa	Poisson's Ratio	void ratio	Note
	Number of samples	D/H ratio	Mean MPa	Range MPa	Number of samples	σ_3 MPa	σ_1 MPa	Number of samples	Mean MPa	Range MPa				
2.29			10.00										0.05	

From: Engineering Behaviour of Rocks, Ian Farmer, 1983

Description: marl, compact but with little cohesion, red brown in colour but occasionally greyish green, halite and sylvite are common often as veins and stringers.

	5	0.5	14.2	13.5-15.0	7	0	20.37	13	1.24	0.49-1.97	5.1	0.16		
	3	0.5	15.4	6.05-26.9		3.45	26.34				5.03	0.4		
	3	1	11	6.71-20.3		6.21	37.10							
	5	1	15.8	10.7-30.3		8.62	55.10							
						17.24	96.14							
						34.48	91.38							
						51.72	136.21							
2.30			14.67						1.24		5.03	0.35		Conclusion

From: Rock Mechanics Studies Associated With The Development Of A Deep Potash Mine, S.J.Patchet's thesis, 1970

Marl (Carnallitic Marl) - 2

Density g/cm ³	UCS			Triaxial Compressive Strength		Tensile Strength		Static Elastic Modulus GPa	Poisson's Ratio	Dynamic Elastic Modulus GPa	Cohesion MPa	Friction Angle Degree	Ultrasonic pulse velocities		Note	
	Number of samples	D/H ratio	Mean MPa	Number of samples	σ_3 MPa	σ_1 MPa	Number of samples						Mean MPa	V _p (m/s)		V _s (m/s)
2.3	1	0.5	10.03	1	1	8.25	6	2.35		0.19*D	6.13*	3.73	5.74	1711*	1061*	Multi-stage triaxial compression
					5	14.1		2.8		0.34*D	7.42*			2249*	1096*	
					10	21.7		1.47	2.1^	0.18^						
					20	33.9		1.29								
					40	56.2		1.64								
								1.81								

From: Royal School of Mines, Imperial College Laboratory Test Report (Cleveland Potash), July 2000, Lab Reference #812

* Confining pressure OMPa

^ Confining pressure 1MPa

D Dynamic Poisson's ratio

Halite Parting

Description: halite, contacts indistinct greyish to light reddish-brown, considerable marl and other impurities.

Density g/cm ³	UCS				Triaxial Compressive Strength			Tensile Strength			Static Elastic Modulus	Poisson's Ratio	Note
	Number of samples	D/H ratio	Mean MPa	Range MPa	Number of samples	σ_3 MPa	σ_1 MPa	Number of samples	Mean MPa	Range MPa	GPa		
	6	0.5	30.59	11.92-47.72		0	23	23	2.42	1.41-3.39	10.48	0.1	
	3	0.5	28.88	21.97-41.66		10.34	55.34				7.31		
	2	1	32.66			10.34	78.28						
	1	1	45.59			10.34	82.90						
2.1			30						2.42		8.9	0.1	Conclusion

From: Rock Mechanics Studies Associated With The Development Of A Deep Potash Mine, S.J.Patchet's thesis, 1970

Middle Potash

Description: sylvinite, light grey to dark red in color, anhydrite and other impurities are present fairly uniformly throughout the bed.

Density g/cm ³	UCS				Triaxial Compressive Strength			Tensile Strength			Static Elastic Modulus	Poisson's Ratio	Note
	Number of samples	D/H ratio	Mean MPa	Range MPa	Number of samples	σ_3 MPa	σ_1 MPa	Number of samples	Mean MPa	Range MPa	GPa		
	7	0.5	30.23	25.3-39.2		0.00	30.14	70	1.79	1.06-3.27	9.86	0.15	
	14	0.5	28.95	25.3-30.8		3.45	56.00				5.03	0.32	
	3	1	44.73	32.1-53.1		4.83	62.83						
	12	1	33.70	31.4-35.9		6.90	74.48						
						17.24	109.59						
						34.48	143.10						
						51.72	121.79 [^]						
2.1			29.05						1.79		7.24	0.27	Conclusion

From: Rock Mechanics Studies Associated With The Development Of A Deep Potash Mine, S.J.Patchet's thesis, 1970

[^] not typical failure

Middle Halite

Description: halite, coarse grained, upper zone argillaceous, clear to grey in colour.

Density g/cm ³	UCS				Triaxial Compressive Strength			Tensile Strength			Static Elastic Modulus	Poisson's Ratio	Note
	Number of samples	D/H ratio	Mean MPa	Range MPa	Number of samples	σ_3 MPa	σ_1 MPa	Number of samples	Mean MPa	Range MPa	GPa		
	7	0.5	29.39	22.12-39.21		0.00	26.88	55	1.63	0.93-3.70	3.9-4.6	0.21-0.24	
	6	0.5	23.71	19.42-31.34		3.45	48.00						
	7	2	48.65	46.3-52.77		4.83	64.41						
	4	2	56.74	52.23-59.23		6.90	78.48						
						10.34	86.21						
						20.69	143.79						
						34.48	241.38						
						44.83	192.41						
						55.17	198.62						
						65.52	207.93						
2.20			26.80						1.63		4.21	0.23	Conclusion

From: Rock Mechanics Studies Associated With The Development Of A Deep Potash Mine, S.J.Patchet's thesis, 1970

Middle Anhydrite

Density g/cm ³	UCS				Triaxial Compressive Strength			Tensile Strength			Static Elastic Modulus	Poisson's Ratio	Note
	Number of samples	D/H ratio	Mean MPa	Range MPa	Number of samples	σ_3 MPa	σ_1 MPa	Number of samples	Mean MPa	Range MPa	GPa		
2.84	5	0.47	92		4*	1.97	90.30	5	10.22		33.6	0.18	Single stage triaxial compression
2.94			76			5.96	142.00		5.56		52.8	0.55	
2.91			93			7.95	134.80		8.2		57.9	0.52	
2.81			72			9.94	137.60		7.37		43.79	0.76	
2.75			64			1.97	97.80		6.27		26.9	0.41	
2.94					1*	3.97	109.30					Multi-stage triaxial compression	
2.90				5.96		121.40							
2.90				7.95		133.10							
2.89				9.95		157.70							
2.95					1*	1.97	101.80					Multi-stage triaxial compression	
2.94				3.97		112.20							
				5.96		121.90							
				7.95		131.00							
				9.95		148.40							

From: Nottingham Center for Geomechanics test report 09/2007 (Job Number: 0907/01)

* From: Nottingham Center for Geomechanics test report 06/2008 (Job Number: 0608/01)

Dolomite

Density g/cm ³	UCS				Triaxial Compressive Strength			Tensile Strength			Static Elastic Modulus	Poisson's Ratio	Note
	Number of samples	D/H ratio	Mean MPa	Range MPa	Number of samples	σ_3 MPa	σ_1 MPa	Number of samples	Mean MPa	Range MPa	GPa		
2.70	5	0.47	148					5	11.17		27.10	0.42	
2.77			194						17.01		52.91	0.41	
2.78			311						19.21		55.26	0.32	
2.74			178						12.29		44.53	0.71	
2.76			173						15.60		23.13	0.28	

From: Nottingham Center for Geomechanics test report 09/2007 (Job Number: 0907/01)

2.77	5	0.47	249.2		5	1.97	172.2	5	18.07		56.591		Single stage triaxial compression
2.79			260.5			3.97	214.2		14.24		57.806		
2.75			171.2			5.96	302		7.52		44.015		
2.72			149.9			7.95	189.2		17.07		36.418		
2.6			89.6			9.94	204.6		9.08		18.015		
2.76					1	1.97	240.1					Multi-stage triaxial compression	
2.69				3.96		250.6							
2.76				5.96		262.1							
2.7				7.95		271.5							
2.63				9.94		305.4							
2.77					1	1.98	85.7					Multi-stage triaxial compression	
2.63				3.96		92							
				5.95		98.9							
				7.95		105.8							
				9.94		131.3							

From: Nottingham Center for Geomechanics test report 06/2008 (Job Number: 0608/01)

Lower Anhydrite

Density g/cm ³	UCS				Triaxial Compressive Strength			Tensile Strength			Static Elastic Modulus GPa	Poisson's Ratio	Note
	Number of samples	D/H ratio	Mean MPa	Range MPa	Number of samples	σ_3 MPa	σ_1 MPa	Number of samples	Mean MPa	Range MPa			
2.70	5	0.47	67					5	12.36		21.1	0.37	
2.82			83						5.54		43.3	0.43	
2.93			114						11.85		54.4	0.31	
2.94			115						11.22		45.3	0.38	
2.92			87						10.76		40.58	0.45	

From: Nottingham Center for Geomechanics test report 09/2007 (Job Number: 0907/01)

2.86	5	0.47	69.1		5	1.97	99.4	5	4		24.28		Single stage triaxial compression
2.24			30.7			3.97	79.3		3.04		2.14		
2.55			58			5.96	148.8		6.46		12.13		
2.89			120.9			7.95	157.7		10.23		47.76		
2.94			126.6			9.94	159.6		10.14		54.69		
2.84					1	1.95	29					Multi-stage triaxial compression	
2.61				3.97		33.6							
2.93				5.96		38.5							
2.94				7.95		43.3							
2.93					1	9.95	85.1					Multi-stage triaxial compression	
2.55				1.98		123.9							
2.93				3.97		124.7							
				5.96		136.5							
					1	7.95	146.1						
				9.95		163.3							

From: Nottingham Center for Geomechanics test report 06/2008 (Job Number: 0608/01)

Lower Halite

Density g/cm ³	UCS				Triaxial Compressive Strength			Tensile Strength			Static Elastic Modulus	Poisson's Ratio	Note
	Number of samples	D/H ratio	Mean MPa	Range MPa	Number of samples	σ_3 MPa	σ_1 MPa	Number of samples	Mean MPa	Range MPa	GPa		
2.15	5	0.50	29		5*	1.98	37.6	3	6.93		0.97	0.63	Single stage triaxial* compression
2.13		0.48	56			3.97	52.3		5.93	1.01	0.55		
2.12		0.49	26			5.96	52.2		6.49	0.96	0.64		
2.12		0.53	26			7.95	60.7		1.42	0.57			
2.14		0.50	31			9.95	62.3		1.16	0.39			
2.15					1*	1.95	21						Multi-stage triaxial* compression
2.16						3.97	24.5						
2.17						5.96	27.3						
2.16						7.95	30						
2.15						9.95	62.8						
2.16					1*	1.97	23.2						Multi-stage triaxial* compression
2.21						3.97	26.2						
						5.96	29						
						7.95	31.9						
						9.95	68.3						

From: Nottingham Center for Geomechanics test report 09/2007 (Job Number: 0907/01)

* From: Nottingham Center for Geomechanics test report 06/2008 (Job Number: 0608/01)

Polyhalite Roof Beds

Density g/cm ³	UCS				Triaxial Compressive Strength			Tensile Strength			Static Elastic Modulus	Poisson's Ratio	Note
	Number of samples	D/H ratio	Mean MPa	Range MPa	Number of samples	σ_3 MPa	σ_1 MPa	Number of samples	Mean MPa	Range MPa	GPa		
2.47	5	0.47	45.4		5	1.98	55	5	4.62		12.17		Single stage triaxial compression
2.66			83.7			3.97	68.8		7.11	33.71			
2.54			53.6			5.96	114.2		6.28	18.08			
2.16			38.7			7.96	95.8		2.86	3.02			
2.16			37.3			9.95	117.7		2.78	2.09			
2.24					1	1.96	15.8						Multi-stage triaxial compression
2.55				3.97		19.3							
2.7				5.96		22.8							
2.63				7.96		25.4							
2.62				9.95		37.1							
2.16					1	1.98	111.3						Multi-stage triaxial compression
2.72				3.97		121.6							
				5.96		132.4							
				7.95		142.3							
				9.95		175.1							

From: Nottingham Center for Geomechanics test report 06/2008 (Job Number: 0608/01)

Polyhalite (Low Grade Polyhalite) - 1

Density g/cm ³	UCS				Triaxial Compressive Strength			Tensile Strength			Static Elastic Modulus	Poisson's Ratio	Note
	Number of samples	D/H ratio	Mean MPa	Range MPa	Number of samples	σ_3 MPa	σ_1 MPa	Number of samples	Mean MPa	Range MPa	GPa		
2.78	5	0.47	150		5	1.97	110.2	5	6.55		54.91		Single stage triaxial compression
2.78			106.8			3.97	195		11.05		56.11		
2.82			136.7			5.96	147.4		6.06		56.97		
2.82			129.6			7.96	215.4		6.67		51.82		
2.83			155.6			9.95	259.8		8.17		55.02		
2.65					1	1.97	98.2					Multi-stage triaxial compression	
2.74				3.97		108.6							
2.71				5.96		119.7							
2.78				7.95		129.1							
2.76				9.95		158.6							
2.7					1	1.97	138.2					Multi-stage triaxial compression	
2.77				3.97		153.2							
				5.97		167.7							
				7.96		179.2							
				9.95		209							

From: Nottingham Center for Geomechanics test report 06/2008 (Job Number: 0608/01)

Polyhalite (Low Grade Polyhalite) - 2

Density g/cm ³	UCS			Triaxial Compressive Strength		Tensile Strength		Static Elastic Modulus GPa	Poisson's Ratio	Dynamic elastic moduli GPa	Cohesion MPa	Friction Angle Degree	Ultrasonic pulse velocities		Note
	Number of samples	D/H ratio	Mean MPa	Number of samples	σ_3 MPa	σ_1 MPa	Number of samples						Mean MPa	V _P (m/s)	
2.78	1	0.5	110.2	1	36	345.78	4	7.07	0.315*D	55.1*	39.26	44.12	5289*	2750*	Single stage triaxial compression
				1	1	175.88		13.36	0.265* [^] D	66.67* [^]			5451* [^]	3084* [^]	Multi-stage triaxial compression
			5		217.85	14.12		0.267*D	64*	5347*			3016*		
			10		251.57	11.16		0.273*	65.19*	5467*			3057*		
			20		309.74			59.5* [^]	0.4* [^]						
			40		396.88			62.6 [^]	0.361 [^]						

From: Royal School of Mines, Imperial College Laboratory Test Report (Cleveland Potash), July 2000, Lab Reference #812

* Confining pressure OMPa

[^] Confining pressure 1MPa

*[^] Confining pressure 36MPa

D Dynamic poisson's ratio

Polyhalite Floor Beds (Anhydrite)

Density g/cm ³	UCS				Triaxial Compressive Strength			Tensile Strength			Static Elastic Modulus	Poisson's Ratio	Note
	Number of samples	D/H ratio	Mean MPa	Range MPa	Number of samples	σ_3 MPa	σ_1 MPa	Number of samples	Mean MPa	Range MPa	GPa		
2.93	5	0.47	109.1		5	1.97	126.80	5	7.47		56.34		Single stage triaxial compression
2.93			109.6			3.97	120.10		7.96	55.58			
2.94			113.1			5.96	150.30		9.11	61.99			
2.92			111.2			7.96	154.90		9.08	55.37			
2.93			107.3			9.95	161.90		8.60	57.23			
2.94					1	1.97	113.00						Multi-stage triaxial compression
2.94						3.97	122.50						
2.95						5.96	132.90						
2.94						7.95	142.50						
2.93						9.95	159.40						
2.94					1	1.97	104.10						Multi-stage triaxial compression
2.94						3.97	115.60						
						5.96	126.30						
						7.96	137.30						
						9.96	158.00						

From: Nottingham Center for Geomechanics test report 06/2008 (Job Number: 0608/01)

APPENDIX II:

**Mohr-Coulomb/Hoek-Brown Properties of Rock Materials at
 Boulby Mine (Obtained from Roclab Software)**

For the Following Rock Materials:

Time Periods		Stratum	Tested @ NCG	Reviewed
Permian Evaporites	Upper Evaporites	Upper Halite		√
		Upper Anhydrite		√
	Middle Evaporites	Carnallitic Marl		√
		Middle Potash		√
		Middle Halite		√
		Middle Anhydrite	√	√
		Dolomite	√	
	Lower Evaporites	Lower Anhydrite	√	
		Lower Halite	√	
		Polyhalite (Low Grade Polyhalite)	√	√
		Polyhalite Floor Beds (Anhydrite)	√	

Upper Halite

Ref: Rock Mechanics Studies Associated With The Development Of A Deep Potash Mine,
 S.J.Patchet's thesis, 1970

	Para.	Test	GSI				
			100	84	70	60	50
Rock Mass	Density (g/cm ³)	2.2	2.2	2.2	2.2	2.2	2.2
	Poisson's Ratio	0.24	0.24	0.24	0.24	0.24	0.24
	<i>D</i>		0	0	0	0	0
	<i>m_i</i> (RL)		20.654	20.654	20.654	20.654	20.654
	E (GPa)	1.86	1.85	1.71	1.36	0.97	0.57
	Tensile strength (MPa)	1.59	1.59	0.48	0.17	0.08	0.04
M-C	Cohesion (MPa)		6.28	3.91	2.99	2.56	2.21
	Friction Angle (Degree)		49	45	42	39	36
H-B	<i>m_b</i>		20.654	11.664	7.074	4.950	3.463
	<i>s</i>		1.0000	0.1690	0.0357	0.0117	0.0039
	<i>a</i>		0.500	0.500	0.501	0.503	0.506
	S3cv (MPa)		13	13	13	13	13
	<i>σ_{ci}</i> (RL, MPa)		32.93	32.93	32.93	32.93	32.93
UCS (Test, MPa)		31.01	31.01	31.01	31.01	31.01	31.01
<i>σ_c</i> (RL, MPa)			32.93	13.53	6.19	3.52	1.98

m_i and *σ_{ci}* are calculated automatically by RocLab using test results data.
m_{ib}, *σ_{ci}*, GSI and *D* are used to calculate other parameters by RocLab.

Upper Anhydrite

Ref: Rock Mechanics Studies Associated With The Development Of A Deep Potash Mine,
 S.J.Patchet's thesis, 1970

	Para.	Test	<i>GSI</i>				
			<i>100</i>	<i>84</i>	<i>70</i>	<i>60</i>	<i>50</i>
Rock Mass	Density (g/cm ³)	2.8	2.8	2.8	2.8	2.8	2.8
	Poisson's Ratio	0.22	0.22	0.22	0.22	0.22	0.22
	<i>D</i>		<i>0</i>	<i>0</i>	<i>0</i>	<i>0</i>	<i>0</i>
	<i>m_i (RL)</i>		<i>10.608</i>	<i>10.608</i>	<i>10.608</i>	<i>10.608</i>	<i>10.608</i>
	E (GPa)	19.1	18.99	17.55	14.00	9.93	5.87
	Tensile strength (MPa)	6.08	6.70	2.01	0.70	0.33	0.15
M-C	Cohesion (MPa)		13.58	6.55	4.29	3.46	2.88
	Friction Angle (Degree)		45	43	39	37	34
H-B	<i>m_b</i>		10.608	5.991	3.633	2.542	1.779
	<i>s</i>		1.0000	0.1690	0.0357	0.0117	0.0039
	<i>a</i>		0.500	0.500	0.501	0.503	0.506
	S3cv (MPa)		13	13	13	13	13
	<i>σ_{ci} (RL, MPa)</i>		<i>71.09</i>	<i>71.09</i>	<i>71.09</i>	<i>71.09</i>	<i>71.09</i>
UCS (Test, MPa)		49.83	49.83	49.83	49.83	49.83	49.83
<i>σ_c</i> (RL, MPa)			71.09	29.20	13.37	7.61	4.28

Carnallitic Marl - 1

Ref: Rock Mechanics Studies Associated With The Development Of A Deep Potash Mine,
 S.J.Patchet's thesis, 1970

	Para.	Test	<i>GSI</i>				
			<i>100</i>	<i>84</i>	<i>70</i>	<i>50</i>	<i>30</i>
Rock Mass	Density (g/cm ³)	2.3	2.3	2.3	2.3	2.3	2.3
	Poisson's Ratio	0.35	0.35	0.35	0.35	0.35	0.35
	<i>D</i>		<i>0</i>	<i>0</i>	<i>0</i>	<i>0</i>	<i>0</i>
	<i>m_i (RL)</i>		<i>10.593</i>	<i>10.593</i>	<i>10.593</i>	<i>10.593</i>	<i>10.593</i>
	E (GPa)	5.03	5.00	4.62	3.69	1.55	0.41
	Tensile strength (MPa)	1.24	1.33	0.40	0.14	0.03	0.01
M-C	Cohesion (MPa)		3.88	2.49	1.91	1.38	0.97
	Friction Angle (Degree)		36	32	28	23	18
H-B	<i>m_b</i>		10.593	5.982	3.628	1.776	0.870
	<i>s</i>		1.0000	0.1690	0.0357	0.0039	0.0004
	<i>a</i>		0.500	0.500	0.501	0.506	0.522
	S3cv (MPa)		13	13	13	13	13
	<i>σ_{ci} (RL, MPa)</i>		<i>14.08</i>	<i>14.08</i>	<i>14.08</i>	<i>14.08</i>	<i>14.08</i>
UCS (Test, MPa)		14.67	14.67	14.67	14.67	14.67	14.67
<i>σ_c (RL, MPa)</i>			14.08	5.78	2.65	0.85	0.24

Carnallitic Marl - 2

Ref: Royal School of Mines, Imperial College Laboratory Test Report (Cleveland Potash), July 2000, Lab Reference #812

	Para.	Test	<i>GSI</i>				
			100	84	70	50	30
Rock Mass	Density (g/cm ³)	2.3	2.3	2.3	2.3	2.3	2.3
	Poisson's Ratio	0.18	0.18	0.18	0.18	0.18	0.18
	<i>D</i>		0	0	0	0	0
	<i>m_i</i> (RL)		1.028	1.028	1.028	1.028	1.028
	E (GPa)	2.1	2.09	1.93	1.54	0.65	0.17
	Tensile strength (MPa)	1.89	6.39	1.91	0.67	0.15	0.03
M-C	Cohesion (MPa)	3.73	2.48	1.10	0.65	0.39	0.24
	Friction Angle (Degree)	5.74	12	11	9	7	5
H-B	<i>m_b</i>		1.028	0.581	0.352	0.172	0.084
	<i>s</i>		1.0000	0.1690	0.0357	0.0039	0.0004
	<i>a</i>		0.500	0.500	0.501	0.506	0.522
	S3cv (MPa)		13	13	13	13	13
	σ_{ci} (RL, MPa)		6.57	6.57	6.57	6.57	6.57
UCS (Test, MPa)		10.03	10.03	10.03	10.03	10.03	10.03
σ_c (RL, MPa)			6.57	2.70	1.24	0.40	0.11

Middle Potash

Ref: Rock Mechanics Studies Associated With The Development Of A Deep Potash Mine,
 S.J.Patchet's thesis, 1970

	Para.	Test	<i>GSI</i>				
			<i>100</i>	<i>84</i>	<i>70</i>	<i>60</i>	<i>50</i>
Rock Mass	Density (g/cm ³)	2.1	2.1	2.1	2.1	2.1	2.1
	Poisson's Ratio	0.27	0.27	0.27	0.27	0.27	0.27
	<i>D</i>		<i>0</i>	<i>0</i>	<i>0</i>	<i>0</i>	<i>0</i>
	<i>m_i (RL)</i>		<i>14.954</i>	<i>14.954</i>	<i>14.954</i>	<i>14.954</i>	<i>14.954</i>
	E (GPa)	7.24	7.20	6.65	5.31	3.76	2.22
	Tensile strength (MPa)	1.79	1.82	0.54	0.19	0.09	0.04
M-C	Cohesion (MPa)		5.74	3.49	2.62	2.23	1.91
	Friction Angle (Degree)		44	41	37	34	31
H-B	<i>m_b</i>		<i>14.954</i>	<i>8.445</i>	<i>5.122</i>	<i>3.584</i>	<i>2.507</i>
	<i>s</i>		<i>1.0000</i>	<i>0.1690</i>	<i>0.0357</i>	<i>0.0117</i>	<i>0.0039</i>
	<i>a</i>		<i>0.500</i>	<i>0.500</i>	<i>0.501</i>	<i>0.503</i>	<i>0.506</i>
	S3cv (MPa)		<i>13</i>	<i>13</i>	<i>13</i>	<i>13</i>	<i>13</i>
	<i>σ_{ci} (RL, MPa)</i>		<i>27.15</i>	<i>27.15</i>	<i>27.15</i>	<i>27.15</i>	<i>27.15</i>
UCS (Test, MPa)		29.05	29.05	29.05	29.05	29.05	29.05
<i>σ_c (RL, MPa)</i>			<i>27.15</i>	<i>11.15</i>	<i>5.10</i>	<i>2.91</i>	<i>1.64</i>

Middle Halite

Ref: Rock Mechanics Studies Associated With The Development Of A Deep Potash Mine,
 S.J.Patchet's thesis, 1970

	Para.	Test	GSI				
			100	84	70	60	50
Rock Mass	Density (g/cm ³)	2.2	2.2	2.2	2.2	2.2	2.2
	Poisson's Ratio	0.23	0.23	0.23	0.23	0.23	0.23
	<i>D</i>		0	0	0	0	0
	<i>m_i (RL)</i>		15.711	15.711	15.711	15.711	15.711
	E (GPa)	4.21	4.19	3.87	3.09	2.19	1.29
	Tensile strength (MPa)	1.63	1.67	0.50	0.17	0.08	0.04
M-C	Cohesion (MPa)		5.75	3.61	2.75	2.35	2.02
	Friction Angle (Degree)		44	40	36	33	31
H-B	<i>m_b</i>		15.711	8.872	5.381	3.765	2.634
	<i>s</i>		1.0000	0.1690	0.0357	0.0117	0.0039
	<i>a</i>		0.500	0.500	0.501	0.503	0.506
	S3cv (MPa)		13	13	13	13	13
	<i>σ_{ci} (RL, MPa)</i>		26.19	26.19	26.19	26.19	26.19
UCS (Test, MPa)		26.8	26.8	26.8	26.8	26.8	
<i>σ_c (RL, MPa)</i>			26.19	10.76	4.92	2.80	1.58

Middle Anhydrite

Ref: Nottingham Center for Geomechanics test reports 09/2007 (Job Number: 0907/01)
 and 06/2008 (Job Number: 0608/01)

	Para.	Test	<i>GSI</i>				
			<i>100</i>	<i>84</i>	<i>70</i>	<i>60</i>	<i>50</i>
Rock Mass	Density (g/cm ³)	2.89	2.89	2.89	2.89	2.89	2.89
	Poisson's Ratio	0.3	0.3	0.3	0.3	0.3	0.3
	<i>D</i>		<i>0</i>	<i>0</i>	<i>0</i>	<i>0</i>	<i>0</i>
	<i>m_i (RL)</i>		<i>11.564</i>	<i>11.564</i>	<i>11.564</i>	<i>11.564</i>	<i>11.564</i>
	E (GPa)	43	42.76	39.50	31.51	22.36	13.21
	Tensile strength (MPa)	7.52	7.57	2.27	0.79	0.37	0.17
M-C	Cohesion (MPa)		15.63	7.16	4.50	3.56	2.94
	Friction Angle (Degree)		48	46	43	40	37
H-B	<i>m_b</i>		<i>11.564</i>	<i>6.530</i>	<i>3.961</i>	<i>2.771</i>	<i>1.939</i>
	<i>s</i>		<i>1.0000</i>	<i>0.1690</i>	<i>0.0357</i>	<i>0.0117</i>	<i>0.0039</i>
	<i>a</i>		<i>0.500</i>	<i>0.500</i>	<i>0.501</i>	<i>0.503</i>	<i>0.506</i>
	S3cv (MPa)		<i>13</i>	<i>13</i>	<i>13</i>	<i>13</i>	<i>13</i>
	<i>σ_{ci} (RL, MPa)</i>		<i>87.54</i>	<i>87.54</i>	<i>87.54</i>	<i>87.54</i>	<i>87.54</i>
UCS (Test, MPa)		79.4	79.4	79.4	79.4	79.4	79.4
<i>σ_c</i> (RL, MPa)			87.54	35.96	16.46	9.37	5.27

Dolomite

Ref: Nottingham Center for Geomechanics test reports 09/2007 (Job Number: 0907/01)
 and 06/2008 (Job Number: 0608/01)

	Para.	Test	GSI				
			100	84	70	60	50
Rock Mass	Density (g/cm ³)	2.73	2.73	2.73	2.73	2.73	2.73
	Poisson's Ratio	0.36	0.36	0.36	0.36	0.36	0.36
	<i>D</i>		0	0	0	0	0
	<i>m_i</i> (RL)		11.953	11.953	11.953	11.953	11.953
	E (GPa)	44.2	43.95	40.60	32.39	22.98	13.58
	Tensile strength (MPa)	14.9	15.01	4.49	1.56	0.74	0.35
M-C	Cohesion (MPa)		30.46	12.83	7.41	5.63	4.54
	Friction Angle (Degree)		50	49	47	44	42
H-B	<i>m_b</i>		11.953	6.750	4.094	2.865	2.004
	<i>s</i>		1.0000	0.1690	0.0357	0.0117	0.0039
	<i>a</i>		0.500	0.500	0.501	0.503	0.506
	S3cv (MPa)		13	13	13	13	13
	σ_{ci} (RL, MPa)		179.47	179.47	179.47	179.47	179.47
UCS (Test, MPa)		190.48	190.48	190.48	190.48	190.48	190.48
σ_c (RL, MPa)			179.47	73.73	33.74	19.20	10.81

Lower Anhydrite

Ref: Nottingham Center for Geomechanics test reports 09/2007 (Job Number: 0907/01)
 and 06/2008 (Job Number: 0608/01)

	Para.	Test	GSI				
			100	84	70	60	50
Rock Mass	Density (g/cm ³)	2.77	2.77	2.77	2.77	2.77	2.77
	Poisson's Ratio	0.39	0.39	0.39	0.39	0.39	0.39
	D		0	0	0	0	0
	m_i (RL)		11.112	11.112	11.112	11.112	11.112
	E (GPa)	38.2	37.98	35.09	27.99	19.86	11.73
	Tensile strength (MPa)	8.56	8.62	2.58	0.90	0.42	0.20
M-C	Cohesion (MPa)		17.68	8.34	5.37	4.30	3.57
	Friction Angle (Degree)		46	44	41	38	36
H-B	m_b		11.112	6.275	3.806	2.663	1.863
	s		1.0000	0.1690	0.0357	0.0117	0.0039
	a		0.500	0.500	0.501	0.503	0.506
	S3cv (MPa)		13	13	13	13	13
	σ_{ci} (RL, MPa)		95.74	95.74	95.74	95.74	95.74
UCS (Test, MPa)		93.4	93.4	93.4	93.4	93.4	93.4
σ_c (RL, MPa)			95.74	39.33	18.00	10.24	5.77

Lower Halite

Ref: Nottingham Center for Geomechanics test reports 09/2007 (Job Number: 0907/01)
 and 06/2008 (Job Number: 0608/01)

	Para.	Test	<i>GSI</i>				
			<i>100</i>	<i>84</i>	<i>70</i>	<i>60</i>	<i>50</i>
Rock Mass	Density (g/cm ³)	2.15	2.15	2.15	2.15	2.15	2.15
	Poisson's Ratio	0.39	0.39	0.39	0.39	0.39	0.39
	<i>D</i>		<i>0</i>	<i>0</i>	<i>0</i>	<i>0</i>	<i>0</i>
	<i>m_i (RL)</i>		<i>5.145</i>	<i>5.145</i>	<i>5.145</i>	<i>5.145</i>	<i>5.145</i>
	E (GPa)	1.1	1.09	1.01	0.81	0.57	0.34
	Tensile strength (MPa)	6.45	6.68	2.00	0.70	0.33	0.15
M-C	Cohesion (MPa)		8.55	3.97	2.50	1.96	1.61
	Friction Angle (Degree)		33	31	28	26	23
H-B	<i>m_b</i>		<i>5.145</i>	<i>2.905</i>	<i>1.762</i>	<i>1.233</i>	<i>0.863</i>
	<i>s</i>		<i>1.0000</i>	<i>0.1690</i>	<i>0.0357</i>	<i>0.0117</i>	<i>0.0039</i>
	<i>a</i>		<i>0.500</i>	<i>0.500</i>	<i>0.501</i>	<i>0.503</i>	<i>0.506</i>
	S3cv (MPa)		<i>13</i>	<i>13</i>	<i>13</i>	<i>13</i>	<i>13</i>
	<i>σ_{ci} (RL, MPa)</i>		<i>34.36</i>	<i>34.36</i>	<i>34.36</i>	<i>34.36</i>	<i>34.36</i>
UCS (Test, MPa)		33.6	33.6	33.6	33.6	33.6	33.6
<i>σ_c (RL, MPa)</i>			<i>34.36</i>	<i>14.12</i>	<i>6.46</i>	<i>3.68</i>	<i>2.07</i>

Polyhalite (Low Grade Polyhalite)

Ref: Nottingham Center for Geomechanics test report 06/2008 (Job Number: 0608/01) and Royal School of Mines, Imperial College Laboratory Test Report (Cleveland Potash), July 2000, Lab Reference #812

	Para.	Test	<i>GSI</i>				
			<i>100</i>	<i>84</i>	<i>70</i>	<i>60</i>	<i>50</i>
Rock Mass	Density (g/cm ³)	2.77	2.77	2.77	2.77	2.77	2.77
	Poisson's Ratio	0.27	0.27	0.27	0.27	0.27	0.27
	<i>D</i>		0	0	0	0	0
	<i>m_i (RL)</i>		17.787	17.787	17.787	17.787	17.787
	E (GPa)	55	54.69	50.52	40.30	28.60	16.90
	Tensile strength (MPa)	7.7	7.72	2.31	0.80	0.38	0.18
M-C	Cohesion (MPa)		21.18	10.42	6.96	5.67	4.79
	Friction Angle (Degree)		53	51	48	45	42
H-B	<i>m_b</i>		17.787	10.045	6.092	4.263	2.982
	<i>s</i>		1.0000	0.1690	0.0357	0.0117	0.0039
	<i>a</i>		0.500	0.500	0.501	0.503	0.506
	S3cv (MPa)		13	13	13	13	13
	<i>σ_{ci} (RL, MPa)</i>		137.29	137.29	137.29	137.29	137.29
UCS (Test, MPa)		135.74	135.74	135.74	135.74	135.74	135.74
<i>σ_c (RL, MPa)</i>			137.29	56.4011	25.8139	14.6912	8.26859

Polyhalite Floor Beds (Anhydrite)

Ref: Nottingham Center for Geomechanics test report 06/2008 (Job Number: 0608/01)

	Para.	Test	GSI				
			100	84	70	60	50
Rock Mass	Density (g/cm ³)	2.94	2.94	2.94	2.94	2.94	2.94
	Poisson's Ratio	0.39	0.39	0.39	0.39	0.39	0.39
	<i>D</i>		0	0	0	0	0
	<i>m_f</i> (RL)		12.45	12.45	12.45	12.45	12.45
	E (GPa)	57.3	56.98	52.64	41.99	29.80	17.60
	Tensile strength (MPa)	8.44	8.50	2.54	0.88	0.42	0.20
M-C	Cohesion (MPa)		18.87	9.11	5.97	4.82	4.04
	Friction Angle (Degree)		48	46	42	40	37
H-B	<i>m_b</i>		12.450	7.031	4.264	2.984	2.088
	<i>s</i>		1.0000	0.1690	0.0357	0.0117	0.0039
	<i>a</i>		0.500	0.500	0.501	0.503	0.506
	S3cv (MPa)		13	13	13	13	13
	σ_{ci} (RL, MPa)		105.79	105.79	105.79	105.79	105.79
UCS (Test, MPa)		110.06	110.06	110.06	110.06	110.06	110.06
σ_c (RL, MPa)			105.79	43.46	19.89	11.32	6.37

APPENDIX III:

Laboratory Test Data of Concrete from Boulby Mine

Table 1 Uniaxial compressive strength tests – 1st relining concrete

Sample Ref.	Ave. Length (mm)	Ave. Diameter (mm)	Density (g/cm ³)	Ultimate Compressive Strength (MPa)	Youngs Modulus (GPa)
030210NCG01	99.94	49.37	2.46	96.4	34.1
030210NCG02	100.06	49.42	2.45	97.9	33.1
030210NCG03	100.05	49.42	2.45	83.9	31.5
030210NCG04	100.08	49.44	2.46	97.4	34.0
030210NCG05	100.18	49.38	2.43	109.1	32.5
030210NCG06	99.87	49.44	2.45	91.7	33.6
030210NCG07	100.07	49.38	2.46	88.2	32.8
030210NCG08	100.21	49.42	2.46	92.8	33.6
030210NCG09	100.20	49.40	2.43	81.3	29.1
030210NCG10	100.21	49.36	2.44	95.5	33.0
271109NCG01	100.07	49.40	2.44	94.3	33.3
271109NCG02	100.17	49.28	2.45	84.1	32.0
271109NCG03	100.16	49.35	2.45	91.3	34.4
271109NCG04	100.36	49.32	2.45	86.1	32.2
271109NCG05	100.20	49.29	2.45	92.0	33.4

Table 2 Tensile strength tests – 1st relining concrete

Sample Ref.	Length (mm)	Average Dia. (mm)	Failure Load (kN)	Tensile Strength (MPa)
6	24.34	49.51	9.1	4.81
7	25.13	49.34	11.2	5.75
8	24.98	49.49	13.7	7.05
9	25.03	49.39	11.2	5.59
10	24.96	49.41	8.0	4.13

Table 3 Triaxial compressive strength tests – 1st relining concrete

Sample Ref.	Ave. Length (mm)	Ave. Diameter (mm)	Sample Density (g/cm ³)	Confinement Pressure (MPa)	Comp. Strength (MPa)
141209NCG01	100.24	49.37	2.45	4.97	154.9
141209NCG02	100.16	49.43	2.45	9.94	183.1
141209NCG03	100.25	49.38	2.45	14.92	167.9
141209NCG04	100.37	49.35	2.45	19.89	184.6
141209NCG05	100.12	49.40	2.47	24.87	210.9
141209NCG06	100.03	49.32	2.46	9.95	150.6
050110NCG10	100.22	49.39	2.45	9.95	160.1
180110NCG01	84.07	42.32	2.45	4.96	144.2
180110NCG02	84.24	42.29	2.46	9.94	179.1
180110NCG03	84.19	42.26	2.46	14.92	209.2
180110NCG04	84.20	42.31	2.45	19.90	229.7
180110NCG05	84.02	42.28	2.46	24.88	236.0

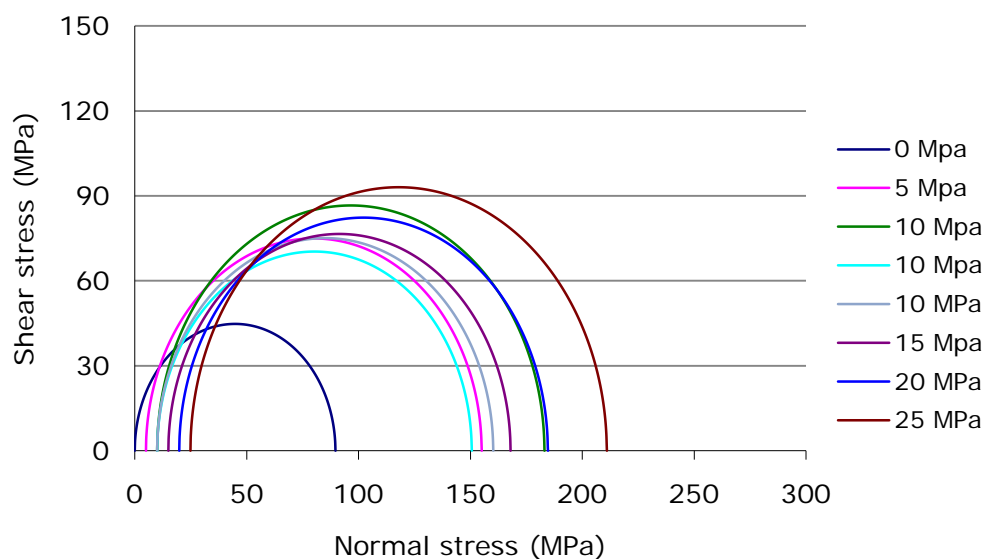


Figure 1 Mohr-Coulomb circles for the concrete used in 1st relining

(Dia. = 49 mm)

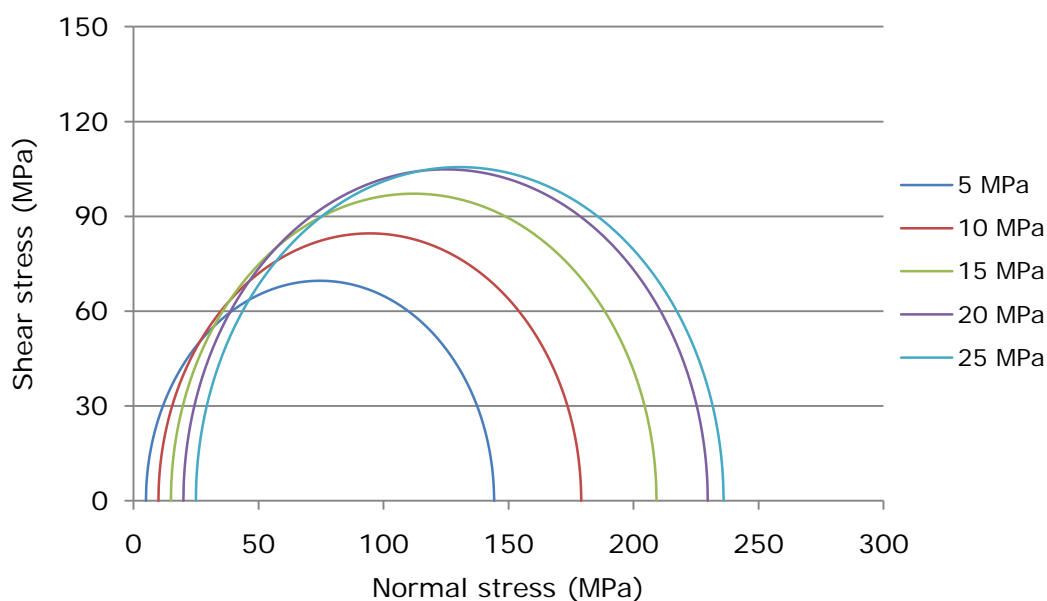


Figure 2 Mohr-Coulomb circles for the concrete used in 1st relining
 (Dia. = 42 mm)

Table 4 Uniaxial compressive strength tests – 2nd relining concrete

Sample Ref.	Ave. Length (mm)	Ave. Diameter (mm)	Sample Density (g/cm ³)	Ultimate Compressive Strength (MPa)	Youngs Modulus (GPa)
101209NCG01	99.44	49.38	2.48	128.1	37.05
101209NCG02	98.70	49.42	2.50	144.5	37.50
101209NCG03	100.21	49.46	2.48	116.5	35.94
101209NCG04	100.09	49.40	2.48	133.1	36.50
101209NCG05	99.18	49.40	2.48	132.0	36.10
030210NCG11	100.30	49.47	2.47	125.5	34.34
030210NCG12	100.23	49.46	2.46	131.6	35.65
030210NCG13	100.15	49.38	2.48	139.5	35.99
030210NCG14	99.10	49.37	2.51	138.4	35.74
030210NCG15	99.97	49.35	2.50	148.8	36.39
030210NCG16	98.98	49.40	2.53	147.1	36.95
030210NCG17	100.13	49.39	2.47	144.0	35.95
030210NCG18	99.08	49.37	2.49	144.4	36.30
030210NCG19	100.06	49.37	2.52	139.0	36.69
030210NCG20	100.13	49.40	2.48	108.2	33.38

Table 5 Tensile strength tests – 2nd relining concrete

Sample Ref.	Length (mm)	Average Dia. (mm)	Failure Load (kN)	Tensile Strength (MPa)
1	25.20	49.44	14.0	7.15
2	25.01	49.43	14.1	7.26
3	25.07	49.40	12.8	6.58
4	25.06	49.40	14.3	7.35
5	25.21	49.43	17.0	8.69

Table 6 Triaxial compressive strength tests – 2nd relining concrete

Sample Ref.	Ave. Length (mm)	Ave. Diameter (mm)	Sample Density (g/cm ³)	Confinement Pressure (MPa)	Comp. Strength (MPa)
141209NCG07	100.11	49.42	2.49	4.96	168.3
141209NCG08	100.12	49.43	2.48	9.94	170.6
141209NCG09	100.01	49.53	2.48	14.92	181.6
141209NCG10	99.72	49.39	2.48	19.90	217.8
141209NCG11	100.06	49.42	2.47	24.88	247.2
180110NCG06	84.15	42.35	2.46	4.96	182.6
180110NCG07	84.05	42.38	2.48	9.94	218.8
180110NCG08	84.15	42.46	2.47	14.91	233.4
180110NCG09	84.04	42.41	2.46	19.89	251.6
180110NCG10	84.04	42.41	2.46	24.87	277.8

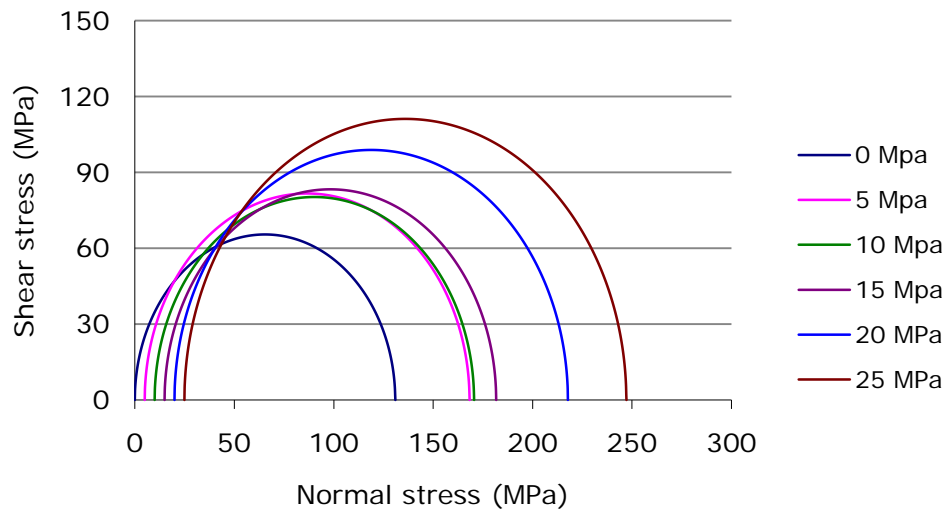


Figure 3 Mohr-Coulomb circles for the concrete used in 2nd relining
(Dia. = 49 mm)

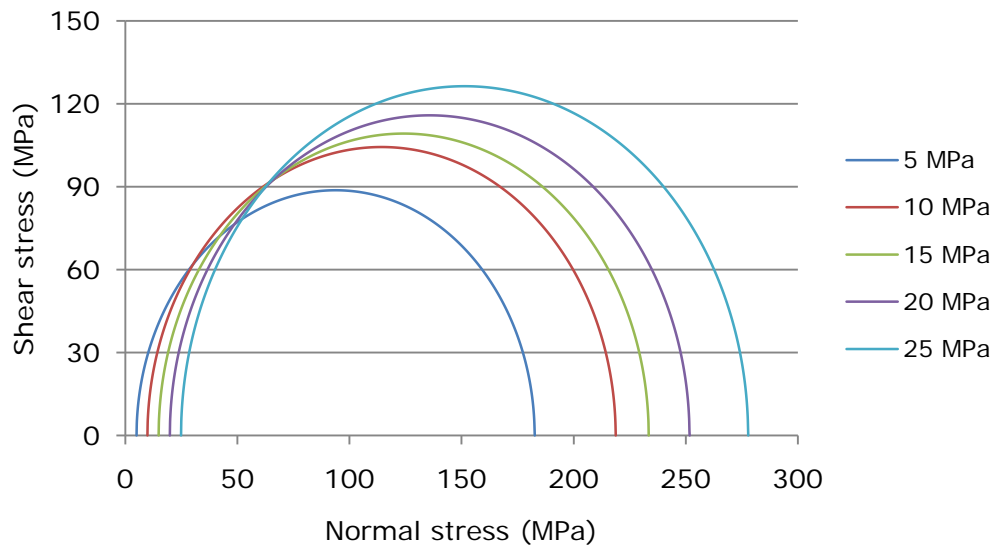


Figure 4 Mohr-Coulomb circles for the concrete used in 2nd relining
(Dia. = 42 mm)

Table 7 Uniaxial compressive strength tests – 3rd relining concrete

Sample Ref.	Ave. Length (mm)	Ave. Diameter (mm)	Sample Density (g/cm ³)	Ultimate Compressive Strength (MPa)	Youngs Modulus (GPa)
270110NCG11	100.17	49.44	2.47	121.8	33.1
270110NCG12	99.89	49.44	2.46	114.2	32.1
270110NCG13	100.02	49.43	2.46	131.2	32.1
170110NCG14	100.10	49.45	2.45	112.1	32.6
030210NCG21	100.28	49.44	2.45	125.3	33.3
030210NCG22	100.15	49.44	2.46	113.1	33.2
030210NCG23	100.37	49.46	2.44	126.3	32.5
030210NCG24	100.34	49.42	2.47	128.9	33.3
030210NCG25	100.23	49.44	2.46	119.7	32.6
030210NCG26	100.19	49.46	2.47	115.0	32.6
030210NCG27	100.31	49.44	2.45	121.9	34.0
030210NCG28	100.16	49.45	2.46	108.1	31.8
030210NCG29	100.28	49.43	2.45	108.0	32.0
030210NCG30	100.14	49.46	2.46	117.2	32.4

Table 8 Tensile strength tests – 3rd relining concrete

Sample Ref.	Length (mm)	Average Dia. (mm)	Failure Load (kN)	Tensile Strength (MPa)
1	25.05	49.59	18.7	9.58
2	25.06	49.41	16.0	8.23
3	25.06	49.43	15.8	8.12
4	25.06	49.40	16.1	8.28
5	25.07	49.46	14.3	7.34

Table 9 Triaxial compressive strength tests – 3rd relining concrete

Sample Ref.	Ave. Length (mm)	Ave. Diameter (mm)	Sample Density (g/cm ³)	Confinement Pressure (MPa)	Comp. Strength (MPa)
120210NCG01	99.98	49.40	2.46	4.97	155.0
120210NCG02	100.05	49.40	2.45	9.95	191.1
120210NCG03	100.11	49.40	2.45	14.93	190.1
120210NCG04	99.87	49.38	2.47	19.91	227.5
120210NCG05	100.02	49.45	2.46	24.89	239.4
120210NCG06	100.10	49.39	2.47	14.93	204.8
280110NCG01	83.98	42.47	2.43	4.96	165.8
280110NCG02	84.20	42.47	2.45	9.94	185.5
280110NCG03	84.47	42.49	2.44	14.92	211.0
280110NCG04	84.13	42.47	2.45	19.90	239.0
280110NCG06	84.14	42.46	2.46	4.96	166.5
280110NCG07	84.14	42.48	2.46	9.94	199.0
280110NCG08	84.09	42.47	2.46	14.92	218.9
280110NCG09	84.16	42.46	2.46	19.90	247.2
280110NCG10	84.03	42.48	2.46	24.89	255.6

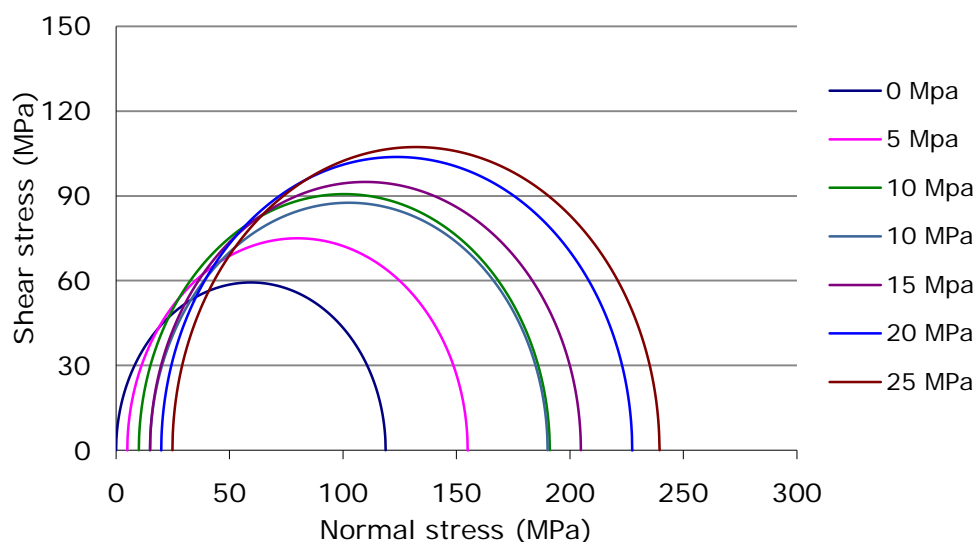


Figure 5 Mohr-Coulomb circles for the concrete used in 3rd relining
 (Dia. = 49 mm)

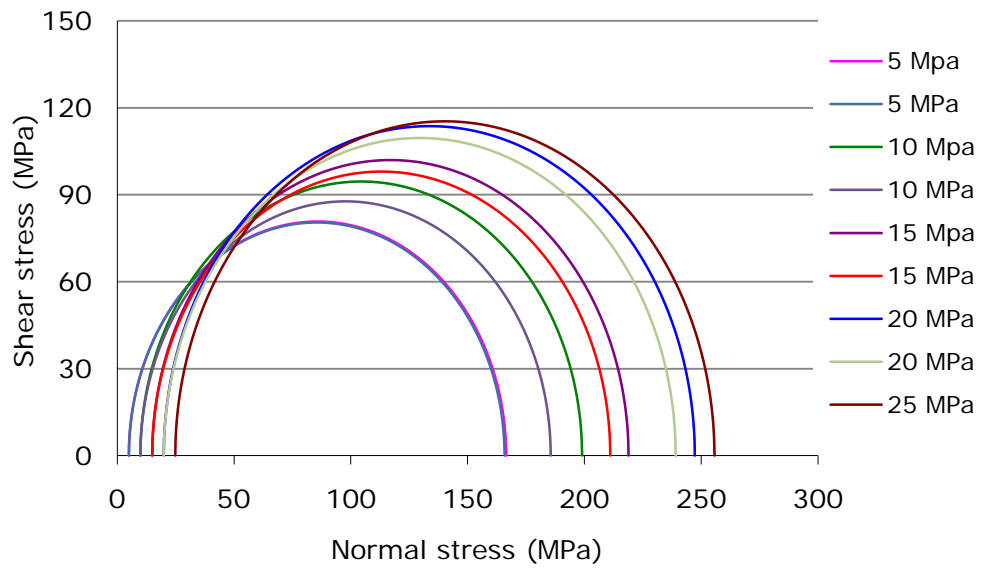


Figure 6 Mohr-Coulomb circles for the concrete used in 3rd relining
 (Dia. = 42 mm)

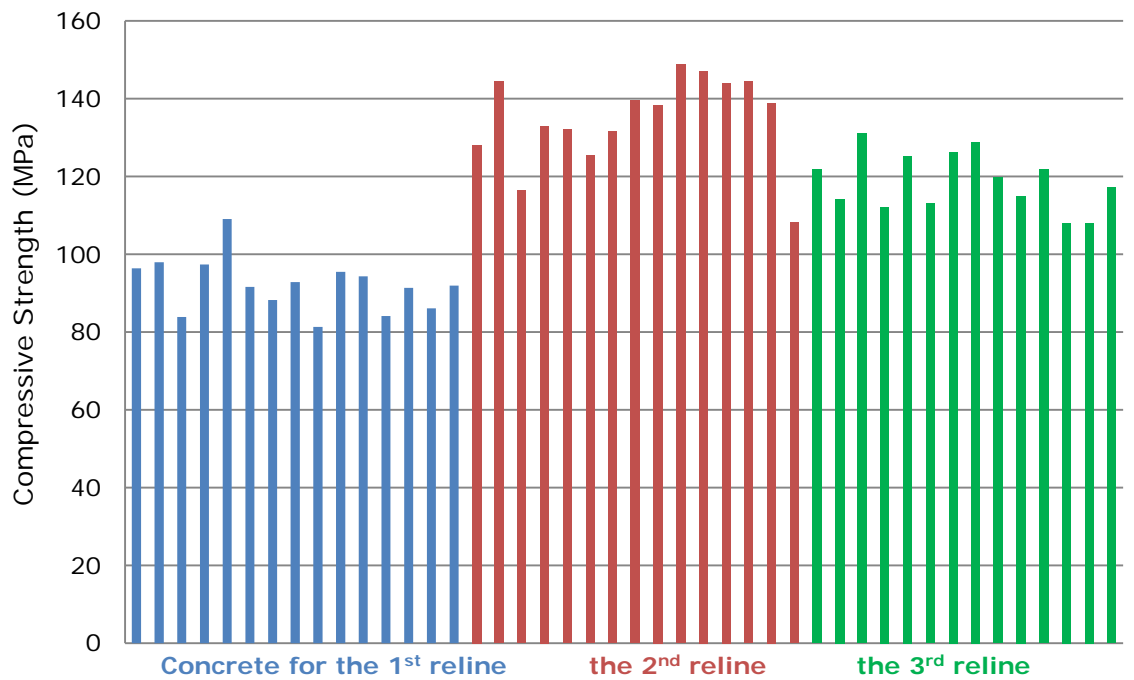


Figure 7 Comparison of the uniaxial compressive strength